Università degli Studi di Torino

Scuola di Dottorato in
Scienze della Natura e Tecnologie Innovative

Dottorato in Scienze Farmaceutiche e Biomolecolari (XXXII ciclo)

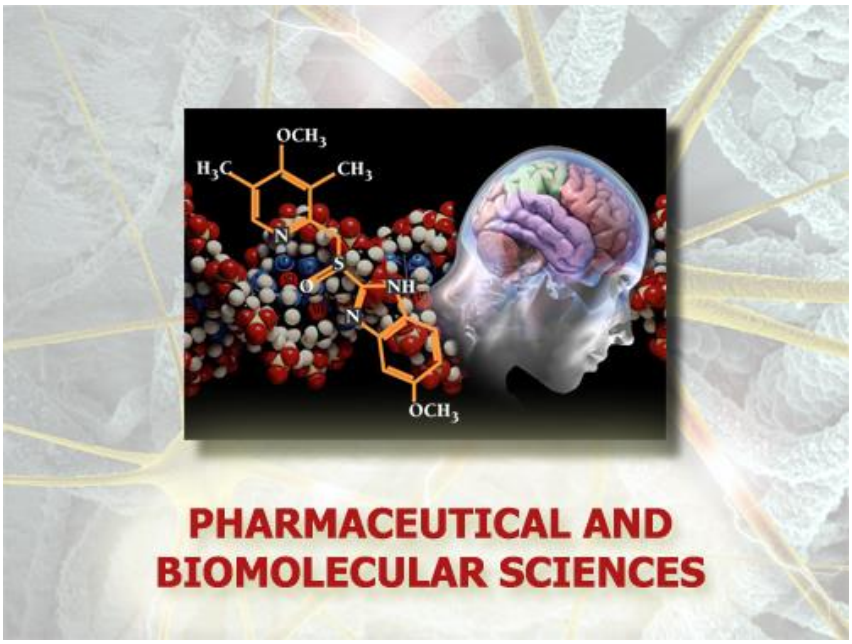

Ultrasound-assisted C=C bond activation

Candidata: Ana Luisa Soutelo Maria

Tutor: Prof. Giancarlo Cravotto
Dr. Jean-Luc Dubois

Università degli Studi di Torino

Dottorato in
Scienze Farmaceutiche e Biomolecolari

Tesi svolta presso il
Dipartimento di Scienza e Tecnologia del Farmaco ed Arkema

CICLO:XXXII

TITOLO DELLA TESI: Ultrasound-assisted C=C bond activation

TESI PRESENTATA DA: Ana Luisa Soutelo Maria

TUTOR(S): Prof. Giancarlo Cravotto and Dr. Jean-Luc Dubois

COORDINATORE DEL DOTTORATO: Prof. Gianmario Martra

ANNI ACCADEMICI: 2017-2019

SETTORE SCIENTIFICO-DISCIPLINARE DI AFFERENZA: CHIM/06

Aknowledgments

First of all I would like to convey my gratefulness to **Dr. Jean-Luc Dubois**, scientific director of Arkema research center. I would like to express my gratitude and cordial thanks for all the supervision and support provided during these 3 years. Thank you very much for **always** be available to explain and to push in the right scientific sense. Having simply an organic background I could expand my knowledge in kinetics and somehow engineering field with our profitable meetings.

I would like to thank as well to **Dr. Jean-Luc Couturier** for receiving me in his team, take care of me helping with all the administration needed inside and even outside of Arkema. My adaptation to France was definitely easier with your help. Thank you for supervising my lab work, help to improve my knowledge and work with helpful discussions. Thank you for always be concerned about my work and for all the support in the COSMIC consortium. As **Dr. Jean-Luc Dubois,** being an extremely busy manager, you always had time for me and my thesis.

Thank you to **Professor Giancarlo Cravotto** for supervising my thesis and for always receive me kindly in your lab during the secondment's time. Thank you for introducing me to the ultrasound technology and the benefits that can afford. I learnt a new world of green technologies in your lab. I appreciated all the support provided during COSMIC and all the concernings with my thesis.

Thank you to **Dr. Jean-François Devaux** for always be available to helpfull discussions and for helping me in my thesis when I needed.

Thank you to **Professor Katia Martina** for the helpful discussions during the secondment's time.

A special thanks to the **COSMIC project** for providing me this award. Thank you to all my "**cosmicologists**" colleagues. It was an enormous pleasure to work with you, to participate in different work/ or not activities. More than "an amazing group of cosmicologists we are an **amazing group of friends**". Thank you all for the support and the amazing scientific or non-scientific discussions that we had. A particular thanks to my Spanish favourite girl **Maria Jesus Moran Plata** for all your help during my thesis. Your friendship was undoubtedly one of the best things I gain from these 3 years adventure.

Un grand merci aux amis du midi, **Fabrice Covolo** (Fafa), **Audrey Martinez**, **Raphael Ecoiffier**, **Emmanuel Chauve**, merci pour être toujours disponible pour moi et pour la votre amitié.

Merci beaucoup **Magali Brebion** pour ton soutien dans et hors labo. J'ai beaucoup appris avec toi, tu étais une formatrice formidable. Merci aussi à **Bruno Palatin**, merci pour ta pacience en me former et pour forcer que j'aprendre le Français ! Merci aussi à **Karine Isaia** pour ton soutien pendant les 3 ans de thése.

Michel Saliba, forcément mon ange gardien depuis que je suis arrivée à Lyon. Merci pour ton incroyable soutien pendant ces 3 ans. Tu es famille.

Ao **pessoal de Algés** e arredores, Gonçalo Moncada, Dantitas, Fafao, Titi, Laminhas, Guedes, Dani e Kika o meu sincero obrigado por estarem sempre presentes mesmo à distância. Obrigada pelas calorosas recepçoes sempre que voltava a Portugal obrigada também pela vossa visita a Lyon quando mais precisava. Um **obrigado** especial ao **Diogo Malaquias,** por me ter apoiado nos momentos mais dificeis destes 3 anos. Obrigado também ao **André Felix** e ao **Tiago Malaquias** por me terem sempre acolhido cada vez que partia para a Bélgica.

Joana Lopes, Jo, obrigada por estes 12 maravilhosos anos de amizade. Obrigada por todo o apoio que me deste durante este periodo ouvindo sempre as minhas reclamacoes e as minhas preocupaçoes (**JULU**).

Mafalda Anjo, Mafi, obrigada pela tua imprescindivel ajuda desde a candidatura até ao final!

Quero agradecer à minha mae, **Ana Paula Barreiros Soutelo**, por sempre acreditar em mim e pelo apoio que me deu desde o inicio até fim.

Last but not least, I would like to thanks to my boyfriend, **Bruno Calado**, the most supportive person of these 3 years abroad, who knows as much as me about this thesis. Thank you for hearing my complains and doubts. Thank you for listening my presentations trainings helping to improve my presenting. **Thank you** for being the first to support my decisions without any kind of criticism.

This study is wholeheartedly dedicated to my mother and boyfriend who have been the source of inspiration and gave me the strength to never give up.

To my mentors Dr. Jean-Luc Dubois, Dr. Jean-Luc Couturier and Prof. Giancarlo Cravotto who guided me for the three years.

Aux techniciens du CRRA pour m'avoir chaleureusement accueilli.

Contents

Abbreviations

Preface

The chemical industry has been an integral part of the global economic landscape for centuries.

In 2013 the European Union chemical industry was responsible for approximately €527 billion in sales revenue, making this one of the most important manufacturing sectors. However, the reality was not so prospering as desired. The trending was not a reflex of the European economy. The European share of the global chemical market decreased from 31% to 17% from 1996 to 2013. The dramatic consequence was the fall of the employments to EU citizens from 1.6 million to 1.2 million in the respective period. The major cause of this decline is associated to the lower-labour-cost markets in the emerging global economies. According to Oxford Economics analysis, the Asia-Pacific chemical industry made the most significant annual contribution to Gross Domestic Product (GDP) and jobs in 2017, 83 million jobs supported against 19 million jobs supported in the EU. To fight this tendency, the development of competitive technologies that deliver performance is vital. Innovation demands the existence of trained scientists and engineers capable and available in the market to design and develop these new technologies.

Process intensification can be the key to gain back EU leadership in the chemical market. The application of novel approaches can help to overcome bottlenecks, such as those imposed by thermodynamics, reaction time and energy consumption, through the combination of processes phenomena into single or fewer process units.

Marie Sklodowska-Curie, born in 1867, was not only a brilliant researcher that worked in the isolation of polonium and on the discovery of the radium, together with her husband and daughter, but also, an exceptional influencer of several scientific and non-scientific actions. Remembered as a remarkable figure in science, her legacy is presented in several institutions and medical centers. Boosted by her heritage, the Marie Sklodowska-Curie Actions (MSCAs) [1] is one of the most prestigious funding programs in the HORIZON 2020. It promotes researcher's education and experience in different working environments while developing knowledge and transferable skills. Since 1994, MSCA's provide grants for all stages of researcher's careers being a promoter of several successful careers and Nobel prizes awards [2].

Horizon 2020 is the "financial instrument implementing the Innovation Union, a Europe 2020 flagship initiative at securing Europe's global competitiveness". The program is foreseen to drive economic growth and create jobs. The main goal is to produce Europe's world-class science removing the barriers to innovation and to facilitate the working exchange between public and private sectors to deliver innovation.

The PhD thesis herein presented is the result of one of the 15 MSCA proposed in HORIZON 2020, the MSC EU-H2020 COSMIC.

COSMIC - Europe on the wave for innovation

The project *European Training Network (ETN) for Continuous Sonication and Microwave Reactors* (COSMIC) (Grant agreement No 721290) [3], was designed with the ambition to revolutionize the chemical process industry through the development of innovative processes already applied such as continuous flow and to present new technologies to the chemical industry as microwaves (MW) and ultrasound (US). The project comprises 4 years (October 2016 to October 2020). COSMIC relayed on the development of specific science and technologic specific objectives such as resource-efficient multiphase reactions in the fields of organic and nanoparticle synthesis, reactors design to efficiently integrate milliflow technologies with US and/or MW-assisted application and finally, knowledge-based assessment and decision methodologies to evaluate and select process-intensification technologies. COSMIC's vision was the combination of these three processes where MW technologies were used as alternative heating sources and US technology used to reduce reaction time and mixing. US technologies have been proved their potential in process intensification such as epoxidation of soybean oil [4], catalyst reactivation [5] or disintegration and oil extraction [6]. On the other hand, MW technology has emerged as a useful methodology to introduce energy in to chemical reactions such as condensation reactions [7], esterifications [8], sensitive reactions like those with organometallic reactants [9] and on solid support synthesis [10]. Continuous technologies would be able to use alternative energy sources to achieve and produce high-value product synthesis.

In the project, the synthesis of nanoparticles and C-H activation were enhanced by MW technology. US promoted the crystallization of zeolites and high value monomers synthesis and the synergistic effect of combined MW-US was tested in copper catalysis.

The COSMIC project jointed the expertise of industrial and academic top scientists to guide and train 15 ESRs (Early Stage Researchers) from different backgrounds and countries. The project aimed to create an international network capable of developing tools for upcoming Europe's future.

Seven countries were unified to produce a successful network. Arkema (Pierre-Bénite and GRL, France), Weber Ultrasonics (Ittersbach, Germany), Microinnova GmbH (Allerheiligen bei Wildon, Austria), Smart Material (Dresden, Germany) and MEAM (Houthalen-Helchteren, Belgium) provided the industrial expertise. KU Leuven (Leuven, Belgium), UCL (London, England), UNITO (Turin, Italy), UCORD (Cordoba, Spain), University of Zaragoza (Zaragossa, Spain) and the University of Göttingen (Göttingen, Germany) were responsible for the academic knowledge.

The PhD thesis presented aimed to a) study the economic evaluation of the industrial process for high-value monomers obtained from oxidative cleavage of unsaturated biosourced fatty compounds, b) to study and propose a process intensification alternative, through cavitation phenomenon's promoted by US technology and c) study the deactivation mechanisms of a hydrogenation Raney®-Nickel catalyst and development of new reactivation processes.

[1] Marie Skłodowska-Curie actions | Horizon 2020, (n.d.). https://ec.europa.eu/programmes/horizon2020/en/h2020-section/marie-sklodowska-curie-actions (accessed January 27, 2020).

[2] Two Nobel Prizes involving MSCA fellows | Marie Skłodowska-Curie Actions, (n.d.). https://ec.europa.eu/research/mariecurieactions/news/two-nobel-prizes-involving-msca-fellows_en (accessed January 27, 2020).

[3] European Training Network for Continuous Sonication and Microwave Reactors, (n.d.). https://cosmic-etn.eu/ (accessed January 27, 2020).

[4] V.P. Chavan, A. V. Patwardhan, P.R. Gogate, Intensification of epoxidation of soybean oil using sonochemical reactors, Chem. Eng. Process. Process Intensif. 54 (2012) 22–28. doi:10.1016/j.cep.2012.01.006.

[5] A. Haghlesan, R. Alizadeh, Reactivation of an industrial spent catalyst as an environmental waste by ultrasound assisted technique for using in styrene production, Chem. Eng. Process. Process Intensif. 110 (2016) 64–72. doi:10.1016/j.cep.2016.09.015.

[6] G. Cravotto, A. Binello, G. Merizzi, M. Avogadro, Improving solvent-free extraction of policosanol from rice bran by high-intensity ultrasound treatment, Eur. J. Lipid Sci. Technol. 106 (2004) 147–151. doi:10.1002/ejlt.200300914.

[7] A. Rayar, M.S.I. Veitía, C. Ferroud, An efficient and selective microwave-assisted Claisen-Schmidt reaction for the synthesis of functionalized benzalacetones, Springerplus. 4 (2015) 8–12. doi:10.1186/s40064-015-0985-8.

[8] A.D.N. De Oliveira, L.R. Da Silva Costa, L.H. De Oliveira Pires, L.A.S. Do Nascimento, R.S. Angélica, C.E.F. Da Costa, J.R. Zamian, G.N. Da Rocha Filho, Microwave-assisted preparation of a new esterification catalyst from wasted flint kaolin, Fuel. 103 (2013) 626–631. doi:10.1016/j.fuel.2012.07.017.

[9] M. Ardon, G. Hogarth, D.T.W. Oscroft, Organometallic chemistry in a conventional microwave oven: The facile synthesis of group 6 carbonyl complexes, J. Organomet. Chem. 689 (2004) 2429–2435. doi:10.1016/j.jorganchem.2004.04.030.

[10] H.P. Narkhede, U.B. More, D.S. Dalal, P.P. Mahulikar, Solid supported synthesis of 2-mercaptobenzimidazole derivatives using microwaves, J. Sci. Ind. Res. (India). 67 (2008) 374–376.

A sweet peek on the thesis

The actual environmental and resources context demand for urgent “invention, design and application of chemical products and processes”.

Oxidative cleavage of fatty acids and derivatives proved to be an attractive way to obtain bifunctional monomers, which can be used for polycondensation reactions to obtain specialty polymers. Hydrogen peroxide proved its efficiency on oxidative cleavage systems, but the kinetics of the catalyzed reactions remains slow. The time-consuming reaction (24h) requires high temperatures (85-95°C) to cleave C-C bonds (347-356 kJ/mole, at 298 K) to recover the monomers. Additionally, several studies highlighted major limitations in mass transfer, leading to undesired by-products and lack of reproducibility at larger scale.

In the last decades, ultrasounds technology has been showing its potential in a variety of catalytic processes. It has been proved that mass transfer, across the phase boundary of multiphasic system, is substantially enhanced through acoustic emulsification.

The PhD thesis herein presented focused on the application of ultrasound in the oxidative cleavage of monounsaturated fatty compounds and in the reactivation of an exhausted catalyst Raney®-Nickel applied in the hydrogenation of monounsaturated fatty nitriles to obtain amino-esters.

The thesis is divided in 4 chapters where 1) the fundamental concepts of oxidative cleavage of fatty acids and last achievements are highlighted. The technology of ultrasound is introduced as a emergent green chemical approach, 2) the economic risk-assessment for an industrial process of oxidative cleavage of monounsaturated long chains to obtain high value monomers, already in operation is presented, 3) the main constrains of operational conditions in the oxidative cleavage process and possible ultrasound application are exposed. Finally, 4) The main deactivation mechanisms of Raney Nickel catalyst in a patented hydrogenation of nitrile monomers process is shown, and a catalyst reactivation process with gain of 100 % catalytic activity is proposed.

As outcome for the thesis three paper were published : “Oxidative cleavage of fatty acid Derivatives for Monomer Synthesis”, “Economic risk assessment using Monte Carlo Simulation for the production of azelaic acid and pelargonic acid from vegetable oils” and “ Regeneration of Raney®-Nickel Catalyst for the synthesis of High-Value Amino-Ester Renewable Monomers”.

Chapter 1. Introduction

1.1 Vegetable Oils

Vegetable oils are oils extracted from the seeds or fruits of specific crops and are often used for food or animal feed. The most significant advantage of these oils is associated to their physicochemical properties, making them and their fatty acids content useful for industrial or non-food applications. These oils are constituted by triacylglycerols (TAG).

Triacylglycerols (TAG)

Nowadays, fatty acids and their chemical derivatives have an important place in almost every phase of modern living. They can be used to add specific qualities in food, pharmaceuticals, cosmetics, plastics, paints, lubricants.

The interest of fatty acids for use in humans quotidian has its origin as early as 2500 BC, were the ancient Babylonians begun to use fatty acids for soap production. Soap industry was established afterward AD 800-900 in Germany and France and greatly expanded until present. Their applications were extended to other markets such as personal care market. Besides their exploitation, it was only in 1818 that the French organic chemist Michel Chevreul elucidated the chemistry of saponification. Chevreul demonstrated that fats consisted of triacylglycerols [1]. Their composition comprises of one molecule trihydric alcohol skeleton (glycerol) esterified with three long-chain fatty acids (**Figure 1-1**).

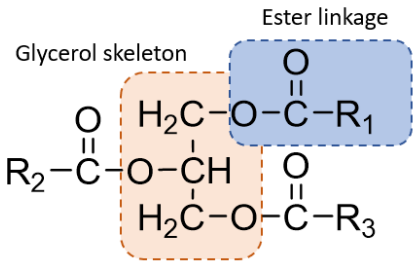

Figure 1-1. Chemical structure of a triacylglycerol.

Fat splitting of triacylglycerols into free fatty acids and glycerol might be one of the most important discoveries in the 19th century. Free fatty acids can be easily obtained by the hydrolysis as discovered by Ernst Twitchell, known as the father of oleochemistry. Twichell [2] worked as a chemist in the Emery candle Company nowadays known as Emery Oleochemicals and discovered

and patented the first splitting process [3], known as Twitchell process, consisted on the application of benzene stearosulphonic acid as a fat-splitting reagent. The era of Oleochemical industry begun resulting in an outstanding fatty acids properties exploitation to generate new molecules such as fatty alcohols, produced by hydrolysis of the wax esters from animal source (whale) or jojoba oil, estolides with hydroxyl or epoxide groups as precursors for use in shampoo and conditioners due to the good moisturizing properties [4] and dimer, trimer or cyclic diesters finding applications in the lubricants industry.

Industrial Oil Crops

Oil crops can be assigned as the symbiosis of the world agriculture to associated industries. Industrial oil crops include oilseeds and perennial plants whose seeds, fruits or mesocarp and nuts are valuable mainly for the edible industrial oils that are extracted from them.

In the last 25 years, it has gained an important place in the world economy. The total area of oil crop cultivation land increased from 160 million in 1980 to 247 million hectares in 2005 [5]. The annual world oil crop production has risen 433 million metric tonnes from 1980 to 2005. Such a remarkable expansion of production is related to the process of concentration on dominant oil crops species. Nowadays, major crop production are Soybean, rapeseed, sunflower and oil palm [6].

Industrial oilseeds are viable feedstock sources to produce polymeric material as those applied in paints, coatings, adhesives foams, etc. Among these industrial oils, biobased feedstock is seen as a replacement of petroleum in the production of such polymers to reduce the environmental impact associated with their origin and increase cost competitiveness. No mining should be involved and the net production of the greenhouse gas, CO_2, should be roughly neutral. Polymers monomers constitution from biosourced oils have their origin in unsaturated fatty acids, obtained from the triacylglycerols. These oils are obtained from the hydrolysis of tallow and fractional distillation of crude tall oil.

Fatty acids

The global fatty acids size was estimated to be worth USD 31.1 billion in 2018 with an estimated growth of 5.2% until 2026 [7].

Free-fatty acids are obtained by the classic and well-established oleochemical transformation from the hydrolysis of the ester functionality of the triglyceride molecule to afford 3 fatty acids molecules. Further transesterification to methyl esters (**Figure 1-2**), opened new market applications.

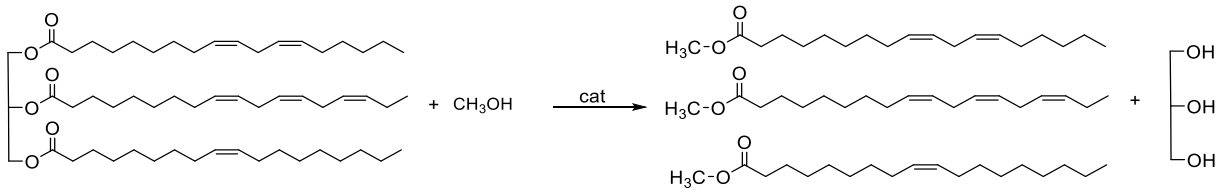

Figure 1-2. Transesterification of triacylglycerol.

Their constitution has a selective role in the choice of market applications. For example, stearic acid, lauric acids and oleic acids are suitable for the cosmetics and toiletries industries [8].

According to the global Fatty Acid Market Size analysis [7], Asia (Malaysia, Indonesia and Philippines) remains till date the most thriving market for fatty acids. Coconut oil and palm kernel oil are example of extraction of vegetable-based raw materials.

As highly functionalized molecules, fatty acids are also valuable renewable building blocks for the synthesis of monomers for specific polymer's properties. The double bond of triacylglycerols can be epoxidized or converted into hydroxyl groups [9,10].

Epoxidized oils are used as secondary plasticizers [11,12], and the hydroxyl-rich oils are used, for example, for polyurethane production [13].

Properties

The two configurations of the double bond, *cis* or *trans*, lead to different properties, such as melting points, which might be important for the different applications.

Cis fatty acids are the most common natural products but are also thermodynamically less stable than *trans* fatty acids. Fatty acids are also classified as monounsaturated fatty acids (MUFAs) and polyunsaturated fatty acids (PUFAs). MUFAs are more appealing to produce high-value monomers because fewer co-products and by-products are formed. In **Table 1-1** it is represented the fatty acids content for different oils (percentage mass-fraction of fatty acids).

	SFA				MUFA			PUFA		Others
Oil	**16:0**	**18:0**	**20:0**	**22:0**	**18:1**	**20:1**	**22:1**	**18:2**	**18:3**	**18:1-OH**
Δ					9	11	13	9, 12	9, 12, 15	9
Rapeseed	4	2			62			22	10	
Crambe	1.8-2.2	0.7			16.5-17.2	3.4-4.7	56.2-62.5	8.7-9.5	4.8-5.2	
Soybean	10	4	0.4	0.4	23	0.3		54	7.5	
Camelina	5.2-7.0	2.2-3.2			14.5-18.5	14.4-17.6	2.4-4.0	14.7-20.4	29.9-35.1	
Castor	1.0-2.0				4.0-9.0					85-90
Linseed	5.5	3.5			17			15	60	
Palm	40.1-47.5		<1.0	<0.6	36-44			6.5-12	<0.5	
Stearin	48.4-73.8	3.9-5.6	0.3-0.6	>0.2	15.6-36			3.2-9.8	0.1-0.6	
Safflower	4.8	1.3			75.3			14.2		

Table 1-1. Δ – carbon number of double bond unsaturation. Fatty acid composition of common edible and non-edible oils extracted from and expressed as percentage mass-fraction of total fatty acids. SFA-Saturated Fatty Acids, MUFA-Monounsaturated Fatty Acids, PUFA-Polyunsaturated Fatty Acids [14].

The growing interest in the use of the fatty acids as monomer precursors is driven not only by their renewability but also because of the polymer technical properties, which are strongly dependent on the carbon length chain [15,16]. Arkema (Colombes, France) is a world leader producer of biobased polymer production, with several brands of polymers for different applications [17,18]. The polyamide Rilsan (PA 11) and Rilsan T (PA 10.10) (**Figure 1-3**) are good examples of biobased polymers produced from castor oil.

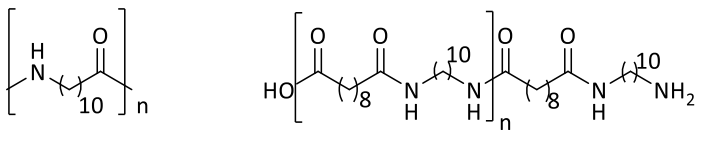

a b

Figure 1-3. Chemical structure of (a) polyamide 11 (Rilsan) and (b) polyamide 10.10 (Rilsan T).

Valuable difunctional molecules that can be produced by oxidative cleavage of fatty acids and derivatives include nonanedioic acid (Azelaic acid - DC9) and 1,11– undecanedicarboxylic acid (Brassylic acid - DC13). However, these molecules have, currently, a limited market application because they must compete with Sebacic acid (DC10) and Dodecanedioic acid (DC12), which are well established in market applications. DC10 is already biobased and made from castor oil [19,20]. DC12 is commonly produced from fossil resources (from a butadiene derivative), but also by fermentation of paraffins (by companies in China and formerly in Japan). Recently the company Verdezyne was building a plant in Malaysia to produce it by fermentation of Dodecanoic acid (Lauric acid - C12:0) ester, but due to a lack of financial resources, the production plant has been halted. DC10 and DC12 [19] have already market applications and would be relevant to produce. Unfortunately, there are no significant sources of fatty acids with a single double bond at the 10th or 12th carbon that would allow a direct oxidative cleavage to these relevant diacids. The other relevant monomers to produce would be the Aminoundecanoic acid (A11) and the Aminododecanoic acid (A12) because they would directly allow the production of polyamides 11 and 12 which are currently on the market. PA11 is produced by Arkema [21], while there are several producers, including Arkema, for PA12 [22]. In addition to these two polyamides that have a current application, it is worth mentioning PA9, which was produced in the past under the name of Pelargon [23,24]. A11 is already bio-based and made from castor oil through a thermal cleavage process. For A12 there have been some attempts to make a monomer by fermentation by Evonik [25] and others. Although there are several options to produce A9 (aminopelargonic acid) from natural resources, the polymer is no longer on the market and it would take much time to reintroduce it. For PA11 and PA12, there are routes through metathesis or hydroformylation which have been investigated, but also through oxidative cleavage [23,26]. For example, the oxidative cleavage of the gondoic nitrile (C20:1, Δ-11) leads to a nitrile-acid intermediate that can be further hydrogenated. Similarly, the oxidative cleavage of the nitrile obtained from the 12-hydroxyoctadecanoic acid, itself made by hydrogenation of (9*Z*,12*R*)-12-Hydroxyoctadec-9-enoic acid (ricinoleic acid C18:1, OH derived from castor oil) leads to nitrile-acid intermediates with 11 and 12 carbons, which can be further hydrogenated to amino acids [27]. Since high purity monomers need to be obtained, the selectivity of the process is of the utmost importance. A good understanding of the reaction mechanism and process conditions is necessary.

1.2 Process intensification: it is time, it is now!

Chemical Industry had a crucial role in the history of human civilization. The first industrial chemical process, the production of sulfuric acid, matches with the birth of the Industrial Revolution dating back to the 18th century. It speeded up that much the society that goods were produced massively, and technologies were developed or highly improved. Commodities arrived to people from every social classes. However, such a "speed of light" grownup and development also brought a very dangerous side-effect. New sources of pollution were introduced. In the middle of the 20th century, the effect of these changes started to be felt in several countries around the world. One of the most known examples is the Great Smog in 1952, where pollutants from factories and home fireplaces mixed with air condensation killed at least 4000 people in London over several days.

The current century has been characterized by the "environmental awareness century". New politics have been implemented and adopted to curb emissions and improve energy efficiency. Greener technologies are highly advertised. The need for the development of processes more sustainable or eco-friendly has never been so vital [28].

Process intensification (PI) is a growing trend in the chemical industry. It arose from the "drastic improvement of equipment and process efficiency" need without compromising the desired output and still have a significant positive impact on the total plant capital and operating costs. [29].

The PI strategy, conceived in 1970s at ICI's New Science laboratory, indicate four main principles that can be classified in two sections.

Improve equipment design in order to overcome limitations of conventional processes, enhancements achieved through: **1)** integration of operations, **2)** integration of functions and **3)** integration or improvement of phenomena/functions limitations occurring in a given conventional operation over **4)** targeted enhancement of a phenomenon of a given operation.

PI dogma includes the perspective of construction of a safer plant, reducing the environmental impact and leading to reductions in carbon emissions.

Intensification needs to simultaneously address four domains: spatial (**STRUCTURE**-structure environment to integrate reaction mixture and create high mass and heat transfer rates), thermodynamics (**ENERGY**- Alternative forms and transfer mechanisms of energy to selective, grandientless and local energy supply), functional (**SYNERGY**- integration of functions steps to

increase the overall efficiency) and temporal (**TIME**- increase energy efficiency along with side reactions minimization) [30].

Process intensification encourages the substitution of the “old” batch industrial thought to a more sustainable continuous process.

Continuous manufacturing offers better mass and heat transfers, which can also have a positive impact on the selectivity. Furthermore, such production line, fully uses equipment units 24/7. For example, dimensioning a batch reactor must consider the reactants dose, heating, cooling, discharge and cleaning. On the other hand, continuous manufacturing has dedicated equipment, which can reduce reaction times and size of the plant (process intensification definition).

Emergent technologies are identified as the master key for an industrial process improvement. These are technical innovations in which technologies from different fie lds are converging and inter-connecting to give a similar goal.

Microwaves (MW) and Ultrasound (US) are examples of emerging technologies. In the thermodynamic domain, MW can be the key to replace conventional conductive-based heating with a “volumetric heating” not being limited by heat transfer surface or heat transfer coefficient [31]. MW heating can be applied in chemical synthesis [32] ; extractions [33] or food processing [34]. US technology finds as well nowadays, a growing place in different market applications.

1.3 Ultrasound – a matter of frequency

Any permanent change in the physicochemical properties and/or form of a material, requires an activation energy. US technology is at the base of sonochemistry. "Ultrasound" is described in physics as acoustic energy with a frequency above human hearing threshold. In the sound spectrum lies in the range from 16 kHz to 200 MHz at different acoustic intensities.

The discovery

The first findings on US were proposed by Lazzaro Spallanzani and Louis Jurine by observing that bats were able to orient themselves in darkness without difficulty. They demonstrated that bats were guided not through eyes but through echo reflection from high frequency inaudible sound. The definition of fundamental physics of sound vibrations (waves), transmission, propagation and rarefaction started to be studied in the later part of the 1800s by Lord Raleigh whose famous treatise "the Theory of sound" describing sound wave as a mathematical equation, foundation of future work in acoustics. In 1826, Jean-Daniel Colladon, a Swiss physicist, used an underwater bell to measure the speed of sound in the water of Geneva's lake. Later in 1880, Marcellin Berthelot [35] proposed for the first time to carry on chemical reactions under: "the energy of ethereal matter, animated by these vibratory and other movements that produce calorific, luminous and electrical phenomena". However, the first ultrasonic source (high frequency) was reported in 1876, by the physiologist Francis Galton who developed the Galton whistle [35]. Four years later, the first piezoelectric disc would change the history of acoustics and open place to the appearance of new scientific domains such as US imaging, sonar, sonochemistry and others.

Piezoelectric effect

Namely called piezoelectricity from the Greek word meaning to press, was firstly discovered in 1880 by Pierre and Jacques Curie. In their findings they observed that an electric charge was generated when a mechanical pressure is exerted on crystalline substances such as the Rochelle salt (sodium potassium tartrate tetrahydrate), quartz (SiO_2) and tourmaline. The charge was directly proportional to the force applied. On the other hand, reverse piezoelectric effect occurs when rapid change of electric potential is applied to the crystal and cause it to vibrate. US transducers contains piezoelectric crystals that expand and contract to interconvert electric and mechanical energy [36].

Ultrasonic waves production

Ultrasonic waves are produced by an ultrasonic frequency generator linked to transducers. The ultrasonic generator converts the frequency and power characteristics of the electrical energy received from the power line as required to operate the ultrasonic transducers.

Different equipment types can be used to produce US energy such as ultrasonic horn, cup horn and tank/bath devices.

The ultrasonic horn transfers the mechanical vibrational energy from the transducer to the medium. The converter converts the high frequency signal into a mechanical vibration in the same frequency (piezoelectric effect).

The sonotrode increases/ decreases amplitude of the mechanical vibration (**Figure 1-4**). The equipment can be coupled/not with a booster that allows to increase the amplitude. The energy is concentrated in a small volume. On the other side, in an ultrasonic tank/bath the energy is spread over a larger volume. In this case cavitation occurs non-conformable and uncontrollably distributed over the tank at low energy intensity (**Figure 1-4**).

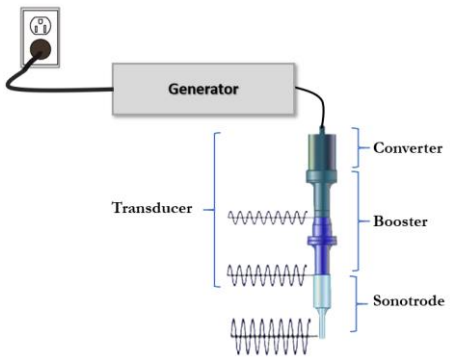

Figure 1-4. Scheme of US system (horn configuration).

Different theories of sonochemistry

In the sonochemistry domain there are three different theories that can explain sonochemical events:

1) **hot-spot theory**

Result of rapid collapse of acoustic cavities in short time (less than 10 µs), with the existence of extremely high heating and cooling rates in the vicinities [37].

2) **electrical theory**

Due to the high temperatures achieved by bubbles implosion (5000 K), a light emission of more than 10^7 photons per flash can be achieved. According to Margulis large electrical field gradients are developed during bubble formation and collapse leading to sonoluminescence [38].

3) **plasma discharge theory**

Le point and Mullie [39], assumed that the cavitation is a fragmentation process due to an intense electrical field instead of a real implosion.

Nowadays only the hot-spot theory is widely accepted.

Bubble collapse

The use of diffused sound energy and/or the use of pressure and kinetic energy of the fluid by concentrating it and delivering it at the actual site of the physicochemical transformation make US technology such an amazing emerging technology. This concentration of energy in liquids can be described as cavitation phenomenon: creation; growth and implosion of bubbles formed when a liquid is subjected to a pressure wave. To achieve acoustic cavitation certain threshold, depending of the liquid used, should be attaint. For example, in water achieving the threshold of 0.5 W/cm^3 at 20 kHz at atmospheric pressure, cavitation occurs.

The sound wave consists of compression and rarefaction cycles.

The definition of cavitation relies on the "fast and strong compression of gas phase in a bubble". The cavities, denominated as cavitation bubbles, are formed and grow in liquid under the oscillatory influence of rarefaction (negative pressure) and compression (positive pressure), zones within a traveling sound wave radiation from a vibrating source or transducer.

Cavitation occurs from the movement of soundwaves radiating away from vibrating source or transducer through a liquid. It occurs when the static pressure is below the liquid's vapor pressure (**Figure 1-5**). The liquid evaporates and the cavitational bubble is formed.

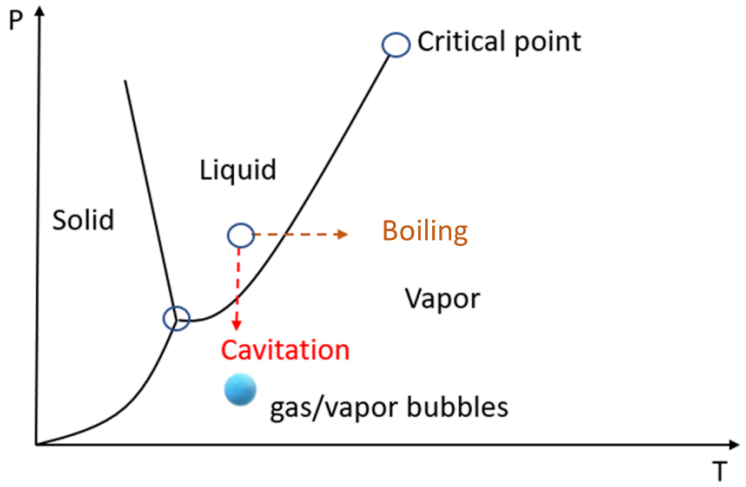

Figure 1-5. Schematic of water phase diagram – cavitation phenomena.

Cavitation bubbles, once formed, either continue to oscillate in a specific time and the degenerate, either, it continues to grow to a size that cannot be sustained and collapses (implode), releasing a shockwave which is formed by the jet from the point of the collapse into the surrounding space. A transient cavitation is formed (**Figure 1-6**).

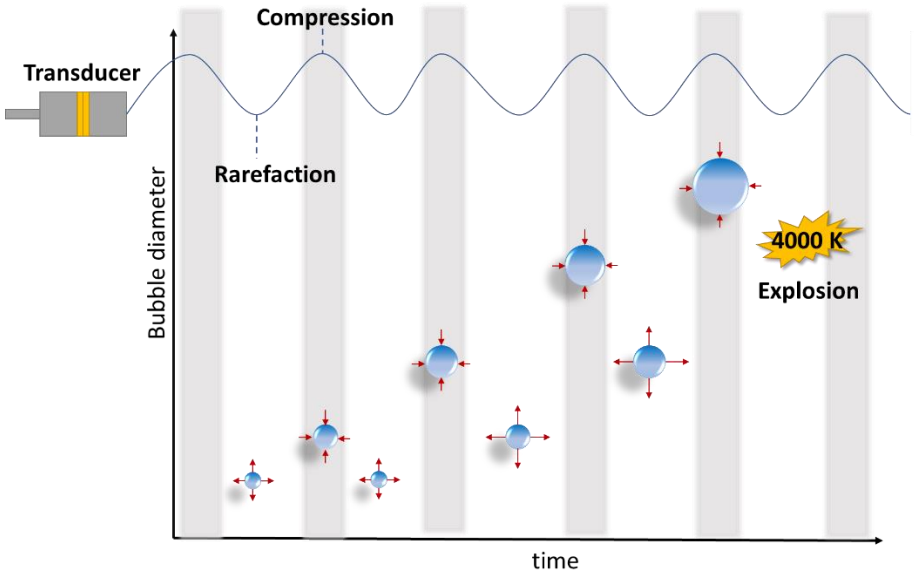

Figure 1-6. Influence of rarefaction and compression zones in the diameter of the cavitation bubble leading to bubble explosion.

The energy which the cavity gains during its growth over terms of microseconds is released during its subsequent implosive collapse in few microseconds. Such fast energy dissipation results into a local high temperature (~14000 K) and high pressures (~1000 atm) as the heat and mass transport processes occur much slowly (milliseconds). The use of these extreme local temperatures, to bring about the desired transformations, is known as cavitational induced transformations.

Cavitation bubbles that only oscillate and do not implode produce an effect called "microstreaming" providing micro-agitation in their immediate vicinity, not providing the intense shockwave associated to the violent collapse of the implosion.

The four basic variables, responsible for changing the dynamics of the cavity and thus the sonochemical transformation are: frequency of irradiation, amplitude, geometric configuration of the reactor and power.

Frequency and bubble size

The frequency (hertz or cycle per second) of an ultrasonic equipment defines its application. This parameter is expressed in kHz or MHz.

US has proven its worth in diagnostics due to its non-destructive nature at low intensities and frequencies from 2 to 18 MHz, avoiding the deleterious effect that X-rays have in living tissues.

Ultrasonic cleaning, from 25 kHz to 1000 kHz, is the most popular application of US in industry. Lower frequencies equipment are used to clean large masses of metal, where ultrasonic erosion is of little consequence (automobile metal parts). Nonetheless, higher frequencies such as from 250 to 1000 kHz are applied in more delicate components like monocrystalline photovoltaic wafers or electronic pieces that can be highly damaged under strong cavitation [40]. Other growing industrial applications are cutting [41], in particular food industry, and welding in automotive and packaging [42].

Frequencies in the range of 20-80 kHz, lead to the formation of more aggressive phenomena such as shockwaves, microjets, micro convection however high frequencies from 150-2000 kHz can favor chemical effects such as radical production, etc.

A described above, the vibrational frequency is generated using either a piezoelectric transducer vibrating at their resonance frequency or using magneto-restrictive transducers.

The power density of the shock wave produced by the implosion of the cavitation bubble is directly related to its size. The higher the cavitation bubble is, the higher will be the power density of the implosion. Size of cavitation is inversely related to frequency [43] (**Equation 1-1**).

$$f_0 = \frac{1}{2\pi}\left(\frac{3\gamma P_\infty}{\rho R_0^2}\right)$$

Equation 1-1. f_0- natural frequency of oscillating bubble, Hz, P_∞-ambient pressure amplitude, $\boldsymbol{\rho}$ – density $Kg.m^{-3}$, R-resonance size the of bubble/cavity at any instance.

The lower the frequency higher will be the compression and rarefaction sound cycle, more time the cavity has to growth. However, fewer cavitation bubbles, each with higher energy, will be

produced. Contrarily, the higher the frequency, lower is the sound cycle, lower is the time of the bubble to grow, and therefore lower will be the cavitation bubble radius. More cavitation bubbles will be produced but with lower energy density. At these frequencies, lower will be the possibility of bubble implosion. In the **Figure 1-7** is possible to observe the type of cavitation bubbles created in ultrasonic baths with two different frequencies (40kHz and 170 kHz).

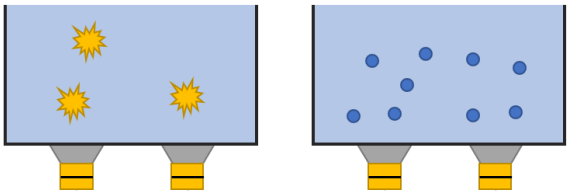

Figure 1-7. Ultrasonic cleaning tanks with 40 kHz and 170 kHz of frequency.

The tank operating at 40 kHz, has three cavitation implosions events each with an energy content of 6 eV for a total of 18 eV overall. The tank on the right, operating at 170 kHz has 9 cavitation events each with an energy content of 2 eV for a total of 18 eV overall. Both tanks have the same overall power, but the physical effects will differ because of their different cavitation characteristics.

In the first case "micro-streaming" resulting from the oscillation of cavitation bubbles that do not implode or the shock waves resulting from the implosion of cavitation bubbles, provide a mixing effect. This mixing action reduces the time for their thorough interaction.

Radical production

In sonochemical reactions there are mainly three reaction sites: interior cavity, gas-liquid interface and bulk liquid (**Figure 1-8**).

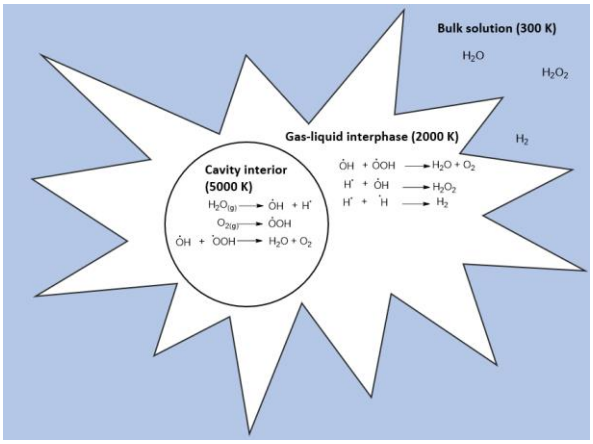

Figure 1-8. Sonochemical reaction zones (adapted from [44]).

Petrier et al. [45], suggested that a high frequency enhances the liquid to the vapor phase OH· radical formation (**Figure 1-9**). These statements are proved thorough the experiments pursued by Somia Haouache et al. [46] in which glucose was obtained by selective depolymerization of cellulose pursued at 525 KHz or even in radical polymerization reactions [47].

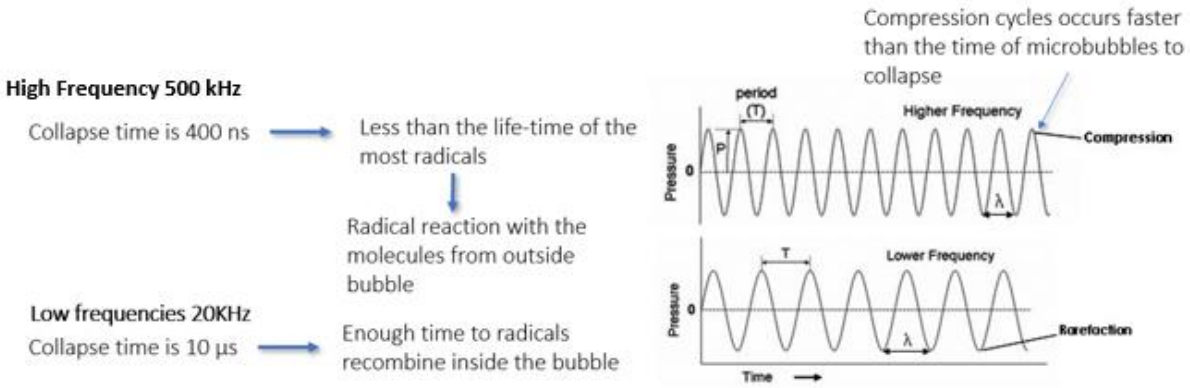

Figure 1-9. Influence of frequency in radical/ not reactions.

Amplitude

Similarly, amplitude also plays an important role in the formation type of cavitation bubbles. Higher the amplitude, higher will be the possibility of the cavity to grow to a higher size (lower negative pressures during the rarefaction cycle) and hence the subsequent collapse is with higher compression ratio and so more severe phenomenon's.

Geometric configuration

The geometric configuration has a major importance in the type of cavitation, repeatability and application purpose.

Sonochemical reactors differ in the number and placement of transducers and on the frequency, power or amplitude parameters.

Ultrasonic horns are typically immersion type of transducers and very high intensities are observed near the horn. The intensity decreases exponentially as one moves away from the horn and vanishes at distance of as low as 2 and 5 cm depending on the maximum power input to the equipment and also to the operating frequency.

Ultrasonic baths, or ultrasonic tanks (**Figure 1-10**) are another common configuration ultrasonic device type. The bottom of the reactor is irradiated with a single or multiple transducer. The active zone is restricted to a vertical plane just above the transducers with a maximum intensity at the center of the transducer. Thus, the area of irradiating surface should be increased (maximum possible) to get better distribution/dissipation of energy in the reactor and maintaining it just above the required cavitational threshold.

Ultrasonic tanks systems are more effective as compared to the ultrasonic horn system in terms of the uniformity of energy distribution and large-scale application (**Figure 1-10**).

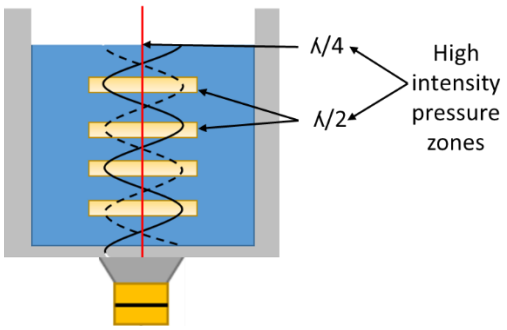

Figure 1-10. Sound wave generation in an ultrasonic cleaning tank.

Scalability

The scale up of horn-type equipment is very difficult as it cannot effectively transmit the acoustic energy into large process fluid volume. Probe-types also suffer from erosion and particles shedding at the delivery tip surface due to high surface intensity (W/m^2), they may also be subject to cavitational blocking (acoustic decoupling), and the larger the transducer displacement (amplitudes) increases stress on the material of construction, resulting in the possibility of stress induced failure. Thus, ultrasonic horn type is commonly recommended for laboratory scale research to obtain parameters design for scale up.

Boundary Layer

The "reach" of the ultrasonic effect near a surface is limited by the boundary layer phenomenon. This phenomenon, caused by friction, limits relative motion of a liquid near a surface with which it is in contact. Since the formation of cavitation bubbles requires the presence of a sound wave (motion), there cannot be a sound wave where there is not enough freedom of motion to allow it to occur. Higher frequency sound waves do not require as much freedom of motion as lower frequency sound waves. Therefore, higher frequency sound waves can penetrate and produce cavitation bubble implosions closer to a surface than can lower frequency sound waves.

Ultrasonic parameters estimation

Nowadays the US technology finds its place in many science and technological applications. Its application depends on different parameters.

Besides, sometimes forgotten the sonochemical system, has a major importance and influence in the chemical process. Before saying that a chemical reaction is improved by the US technology, a rigorous, technical study should be pursued. Reproducibility is difficult to achieve. Different equipments show different results. Several studies in ultrasonic baths suggest that high improvements are obtained in chemical reactions.

The choice of the equipment is dependent on the purpose of US application.

Power

The "nominal electric power" is the power delivered by the generator.

Acoustic power

Above the cavitation threshold, a part of the acoustic energy is converted into heat by adsorption. The acoustic power is though obtained through the mass m (expressed in g) of the irradiated fluid and its specific heat capacity (cp) by the initial temperature rise per unit of time. **(Equation 1-2).**

$$P_{acous} = m\ x\ c_p\ x \left(\frac{dT}{dt}\right)_{t_0}$$

Equation 1-2. Acoustic power. **m:** mass expressed in g, **cp:** heat capacity expressed in $J.g^{-1}.K^{-1}$, **dT/dt:** initial temperature rise per unit of time expressed in $K.s^{-1}$.

The acoustic power is normally reported by unit of volume in $W.L^{-1}$.

Cavitation regions

As result of the intrinsic characteristics of the ultrasonic waves, it is impossible to obtain a homogeneous phenomenon over the entire volume of a liquid. The ultrasonic wave propagates from the transmission source in a cone defined by 90% of the energy propagated in this volume; therefore, the geometry of the reactor is of major importance in ultrasonic irradiation.

Different methods are used to determine the "cavitation zones" in a sonoreactor. For example, in an ultrasonic cleaning tank, the mechanical determination of the active zone is observed by diving vertically and horizontally an aluminium foil (**Figure 1-11**) in the irradiated liquid.

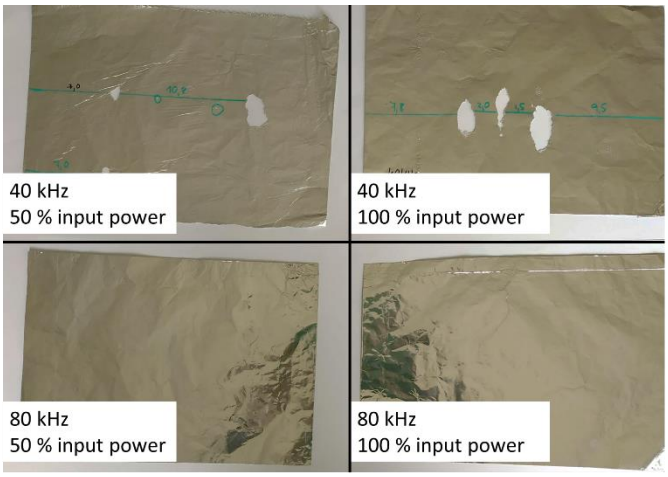

Figure 1-11. Cavitation effect on an aluminium foil at 40 kHz and 80 kHz and at 50 and 100% of input power.

Sonochemistry

Wood and Loomis can be considered even if they were not aware, the fathers of sonochemistry. The results of their published study in 1929 about the progressive destruction of blood corpuscles showed results in emulsion preparation, particle aggregation, acceleration of chemical reactions, crystal segregation and growth and other actions that encouraged the development of sonochemistry [48].

In 1938, Porter and Young reported for the first time the application of US in organic synthesis, proving a chemical acceleration reaction of reduction of benzamide to phenyl isocyanate [49]. Based on Wood and Loomis experiments, in 1932 Oyama (Electronic Engineering, Tohoku Imperial University, Japan) made some important developments in the US physics characterization such as measurements of acoustic pressure and sound coefficient adsorption but also in US-driven emulsification [50].

However, it was only in 1950 that Ostroski and Stambauch obtained a high significant improvement in emulsions preparations, in the reaction rate and in the efficiency of polymerization of styrene under frequencies ranges from 15 to 500 kHz.

In 1950, Noltingk and Neppiras [51] predicted for the first time that a cavitation bubble can achieve 10000 K. The localized voids with extreme hot temperatures, was termed “hot spot”.

In 1982 Makino et al. proved the formation of H and OH radicals in the sonolysis of aqueous solution in an ultrasonic bath of 50 kHz of frequency [52].

Cavitation implosion generates solvent radicals H· and ·OH that recombined can generate H_2O_2 molecules (**Figure 1-12**).

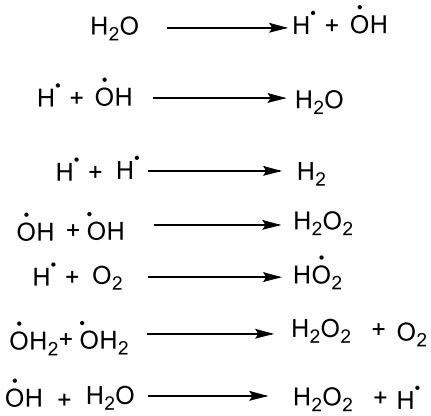

Figure 1-12. Water sonolysis production and recombination of radical species.

On the wave for green chemistry

If we look at the main principles of "green chemistry", we can right away associate it to the main objectives of US application.

- Use of less hazardous chemicals and environmentally friendly solvents.
- Improve selectivity of chemical reactions.
- Minimize energy consumption, lower temperature, and lower pressure.
- Use of renewable feedstock.

In 2006, a review published by Cravotto & and Cintas reported : "The knowledge thus gained confirmed that the bubbles behave as special microreactors in which outcome of the reactions is predictable." [53]. In this sense, new developments in US technologies have urge to fight chemical environmental impact such as the application in the synthesis of fused heterocycles, Diels-Alder cycloaddition of furan dienes in solvent free conditions [54], oxidation reaction such as oxidation of sulphides to sulfoxides under low frequency (22 kHz) and hydrogen peroxide reported by Pandit [55] or biofuel production from non-edible oils [56].

Potential application of sonochemical reactors

Due to the difficulty of repeatability in chemical reactions and up-scaling issues associated with the use of this technology, mainly associated with the unpredictable hot-spot production and localization, the main industrial-scale applications are in the domain of cleaning used for engine parts due to the low cost and efficiency [40] plant extractions (PLAFAR in Romania) and crystallization (Accentus in UK) [57].

1.4 Oxidative cleavage of unsaturated fatty acids[1]

High value monomers can be obtained by oxidative cleavage of the double bond of unsaturated fatty acids. Oxidative scission leads to bifunctional (e.g. diacids) and monofunctional (e.g. monoacid or aldehyde) compounds which serves as intermediates. For example, the reductive ozonolysis of oleic acid/ester leads on one side to nonanal; which can be used in the perfume and fragrance industry; and on the other side to a bifunctional aldehyde-acid/ester which can be used in the polymer industry through reductive amination [27] or hydrogenation [58]. These can also be oxidized to the corresponding acids or hydrogenated to alcohols leading to valuable starting materials for the synthesis of polymers plasticizers. The oxidation of 9-oxononanoic acid leads to azelaic acid (1,9-nonadioic acid), a precursor of plasticizers, lubricants, and polymers like Polyamide-6,9 [59,60]. Respectively, nonanal can be oxidized to pelargonic acid (nonanoic acid) which is used as herbicide [61] or lubricants [59,60] (**Figure 1-13**).

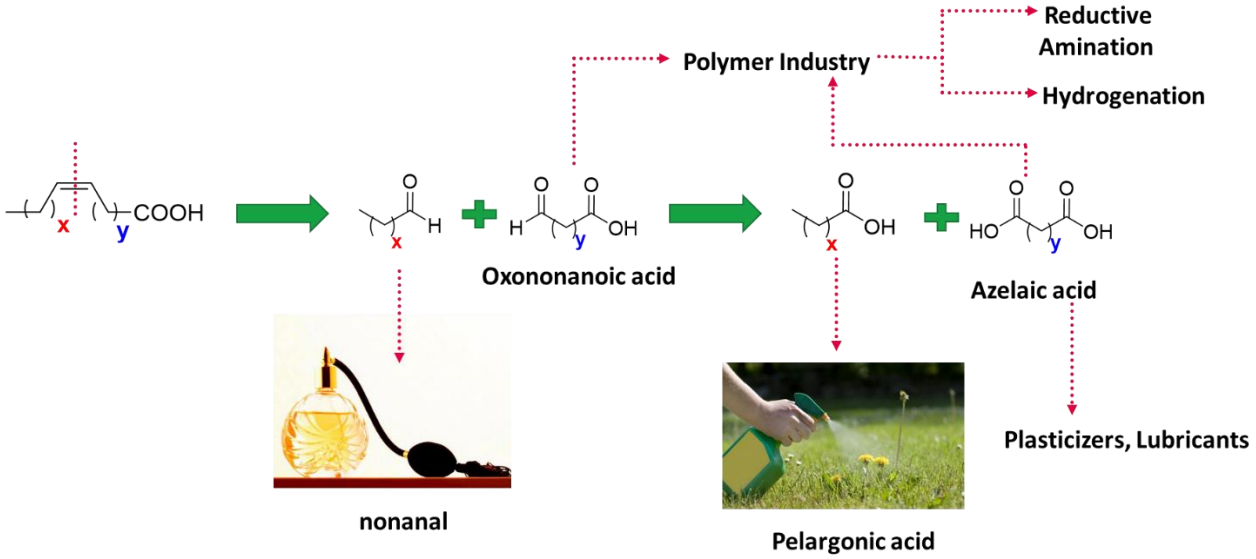

Figure 1-13. Market application of intermediates and products of oxidative cleavage of unsaturated fatty compounds.

Oxidative cleavage of unsaturated fatty acids is mostly accomplished by ozonolysis. Oxidation of the olefins by ozone (O_3) has been proposed as a clean and efficient reaction for use in the production of bio-based aldehydes (reductive ozonolysis) and acid monomers (oxidative

[1] From the publication: Soutelo-Maria, A. L., Dubois, J.L., Couturier, J.L., Cravotto, G., *Oxidative cleavage of fatty acid derivatives for monomer synthesis*, Catalysts, 2018 (10), DOI: 10.3390/catal8100464

ozonolysis). This oxidative cleavage process, the only operational process applied in the chemical industry (P2 Science [62], Emery Oleochemicals [63] and Croda Sipo [64]), presents some disadvantages as high energetic (high electricity consumption) and the need for a special technology for production of ozone (ozone generator) , dilution of the ozone in the feed (1.5-2 wt. % ozone when air is the oxidant), which implies slow reaction kinetics [65]. However, O_2 instead of air can be used and ozone generators are common in paper industry. As alternative, oxidative cleavage using hydrogen peroxide has been studied since 1945 as a potentially cheaper substitute to ozone.

Ozonolysis

Ozone, a colourless gas with the characteristic smell of air after a stormy day, is a well-known oxidant for oxidative cleavage of unsaturated fatty compounds.

Discovered by Harries [66] at the turn of 19th century, oxidative cleavage by ozone became a popular and industrial process to obtain high value monomers from natural sources. The double bond is cleaved quantitatively under extreme mild conditions usually at cryogenic temperatures in dilute solutions in acid / base free conditions. The products of such reaction are aldehydes, ketones, peroxidic derivatives or with oxidative work-up the carboxylic acids.

The mechanism comprises three main steps (1,3-dipolar reactions [2+3]). It starts with a formation of the first intermediate ozonide or molozonide (**Scheme 1-1 step 1**) followed by decomposition of the primary ozonide (first intermediate highly unstable) into carbonyl compound and carbonyl oxide (**Scheme 1-1 step 2**) and finally the addition of the "carbonyl oxide" to the carbonyl compound forming more stable ozonide specie (**Scheme 1-1 step 3**) . In typical process the gas mixture is passed through a solution of the unsaturated compound in methanol or dichloromethane.

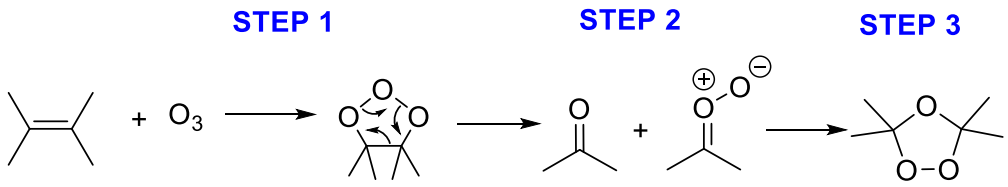

Scheme 1-1. Production of ozonide.

Oxidation of the olefins through ozone has been proposed as a clean efficient reaction for use in the production of bio-based aldehydes, through reductive ozonolysis [62] or carboxylic acids , through oxidative ozonolysis when treated with a mild reducing agent (**Scheme 1-2**).

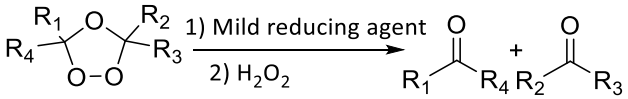

Scheme 1-2. 1) Reductive, 2) oxidative ozonolysis.

Called "Environmentally friendly" reagent forming oxygen as by-product, ozone is known has high atom efficiency oxidant which 66 mol % of the molecule is directly used in the reaction compared to other oxidation systems.

The first intermediate of the reaction besides its high instability is highly energetic (decomposition energy from 200 to 400 kJ/mol). Such intermediate tends to decompose under sudden heat evolution and must be treated under oxidative reductive conditions.

Industrial application

Ozonolysis is nowadays the most popular oxidative cleavage industrial process.

Meanwhile the industrial application of ozone demands several safety precautions. High quality experience with ozone is a critical requirement for its handling in industrial scale.

Koike Kunihiko *et al.* investigated the explosive self-decomposition characteristics of ozone. In their research, they found that the explosion limit for ozone diluted with oxygen at room temperature was 10-11 vol%. At higher volumes an explosive chain decomposition reaction could be caused leading to complete conversion to oxygen in a vessel. Under pressure the limit increases at 100 Tor or less [70].

Hydrogen peroxide

Hydrogen peroxide was discovered in 1818 by the French chemist Louis-Jacques Thenard. This oxidant was firstly produced by treating barium peroxide with nitric acid and improved with the addition of HCl and H_2SO_4 to precipitate the barium sulphate coproduct. However, pure hydrogen peroxide was long believed to be unstable due to the existence of traces of metals after synthesis that catalyzes the hydrogen peroxide decomposition. After 80 years of its discovery, it was obtained for the first time pure, by Richard Wolffenstein through vacuum distillation.

The most known industrial process applied nowadays is the anthraquinone auto-oxidation process developed by BASF in the 1940s. Such process covers the reduction of oxygen with hydrogen production. The anthraquinone, typically 2-ethyl-anthraquinone is hydrogenated to a 2-ethyl-hydroquinone and then reoxidizes back to anthraquinone releasing 1 molecule of hydrogen peroxide. A metal catalyst such as palladium catalyst is used to convert the anthraquinone to hydroquinone followed by autooxidation in air forming hydrogen peroxide **(Figure 1-14**).

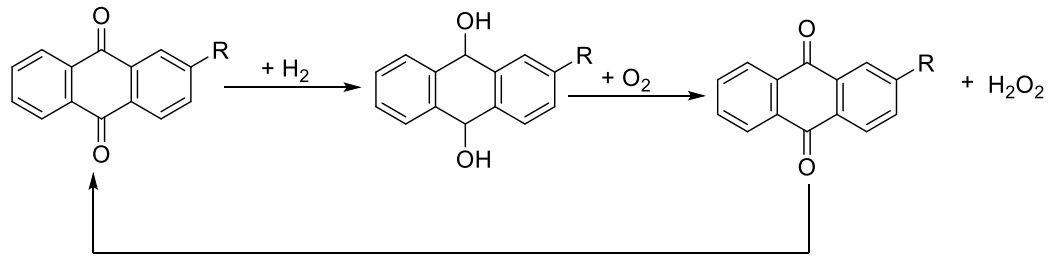

Figure 1-14. Anthraquinone process for Hydrogen peroxide production.

Hydrogen peroxide finds many applications such as chemical synthesis, textile and paper bleaching. The demand for paper and pulp industry leads to an estimated market in 2024 to USD 2.5 Billion. Arkema is among the top three world producers of H_2O_2 with three different brands in the market, ALBONE®, PEROXAL® and VALSTERANE®, with production plants in Asia, Europe and North America [71]. Being a natural metabolite of many organisms, its green nature is associated to its decomposition in only O_2 and H_2O [72]. The content of active oxygen depends on the concentration of H_2O_2 (**Table 1-2**).

Hydrogen peroxide decomposition is quite exothermic ($\Delta H°$= -100.4 kJ/mole), making it a hazardous reagent. Physical properties of H_2O_2 change with the concentration as well the risks associated, for example, the use of highly concentrated aqueous solution (>70 wt. %.) can generate serious hazard problems[73–75].

Property	70 % wt	50 % wt	35 % wt
H_2O_2, g/l	902	597	395
Litres of O_2 at 0 °C / 760 mm Hg released by litre of H_2O_2 at 20 °C	298	197	130
Active O_2 content, mol %	32.8	23.5	16.4
Freezing point, °C	-55	-51	-32
Boiling point at 760 mm Hg, °C	119	114	108
Viscosity, centipoises at 25 °C	1.20	1.17	1.10

Table 1-2. Physical properties of different concentrations of hydrogen peroxide [14].

The fact that the water freezes and evaporates quicker than H_2O_2, promotes the increase of concentration of H_2O_2 in water solution. In this case, the lower the concentration of hydrogen peroxide transported, the lower the transportation hazards [77,78]. However, higher reactivities are achieved with higher concentration of H_2O_2 [23,79,80].

Hydrogen peroxide reacts well with organic compounds. This activation can occur by nucleophilic, electrophilic, radical activation or transition metal activation forming a metal-oxo or metal-peroxo complexes.

The application of this oxidant, from our knowledge, in the epoxidation of α,β unsaturated acids, was initiated by Payne in 1958 [81].

Safety considerations in H_2O_2 manipulation

Attention! Concentrated H_2O_2 it is dangerous! [74,75,82]

Besides its environmentally friendly character, safety should always be taken in account. Decomposition of hydrogen peroxide, as mentioned above, releases heat. In concentrated solutions, the heat raises the temperature of the solution accelerating the decomposition rate. Because of this, stabilizers are added during the manufacture of all grades [83] to inhibit the catalytic decomposition effect of metals and other impurities that may accidentally contaminate the oxidant during shipment, storage, and handling. Still, no additive will prevent decomposition if excessive contamination occurs. In addition, at high H_2O_2 concentrations the mixture with organic compounds might cross the flammability limits. The safety procedures to take in account are:

All containers with H_2O_2 solution must be properly vented, and properly stored away from sources of direct heat and combustible materials.

Adequate ventilation and an enough water supply should be provided for thorough flushing in case of accidental leak on the property or spillage on the worker. Besides H_2O_2 is not considered

an explosive, in contact with organic substances at significant concentrations, and compounds containing catalysts like silver, lead, copper, chromium, mercury and iron oxide rust, rapid decomposition of the oxidant can occur and an explosive pressure rupture of the containing vessel if this is not properly vented.

Reaction Mechanism

Historically the use of H_2O_2 in oxidative cleavage started with studies of hydroxylation of unsaturated fatty acids. The direct conversion of these to the corresponding α,β -glycols was studied in 1949 by Mugdan and Young [9] from *Distillers Company Ltd*, where they found that pertungstic acid catalyzes the addition of 2 hydroxyl groups (-OH) in *R,S* and *S,R* position. The reaction is facilitated by increasing the nucleophilic character of the double bond involving by this, in case of oleic acid, the formation of an epoxide specie as the first intermediate. This reaction was considered by Swern [84] to be an ionic addition reaction followed by the epoxide ring fission by the nucleophilic attack of ^{-}OH group to one electrophilic carbon atom, known as Walden inversion [85], giving place to the isomers *R,S and S,R*-diols formation. Contrary to Mugdan, some authors [86–88] claim that the first step of the reaction, with this kind of catalyst, is non-stereoselective yielding in the first step (I) to epoxide (**2** and **3**), giving place to the racemic mixtures of *syn* diols (**4** and **5**) or *anti*-diols (**6** and **7**) via non-enantioselective hydrolytic cleavage (II). To achieve oxidative cleavage the reaction should proceed by cleavage of C-C bond releasing water (**III**), with formation of corresponding aldehydes (**8** and **9**) and further oxidation to yield carboxylic acids (**IV**) **(Scheme 1-3.).**

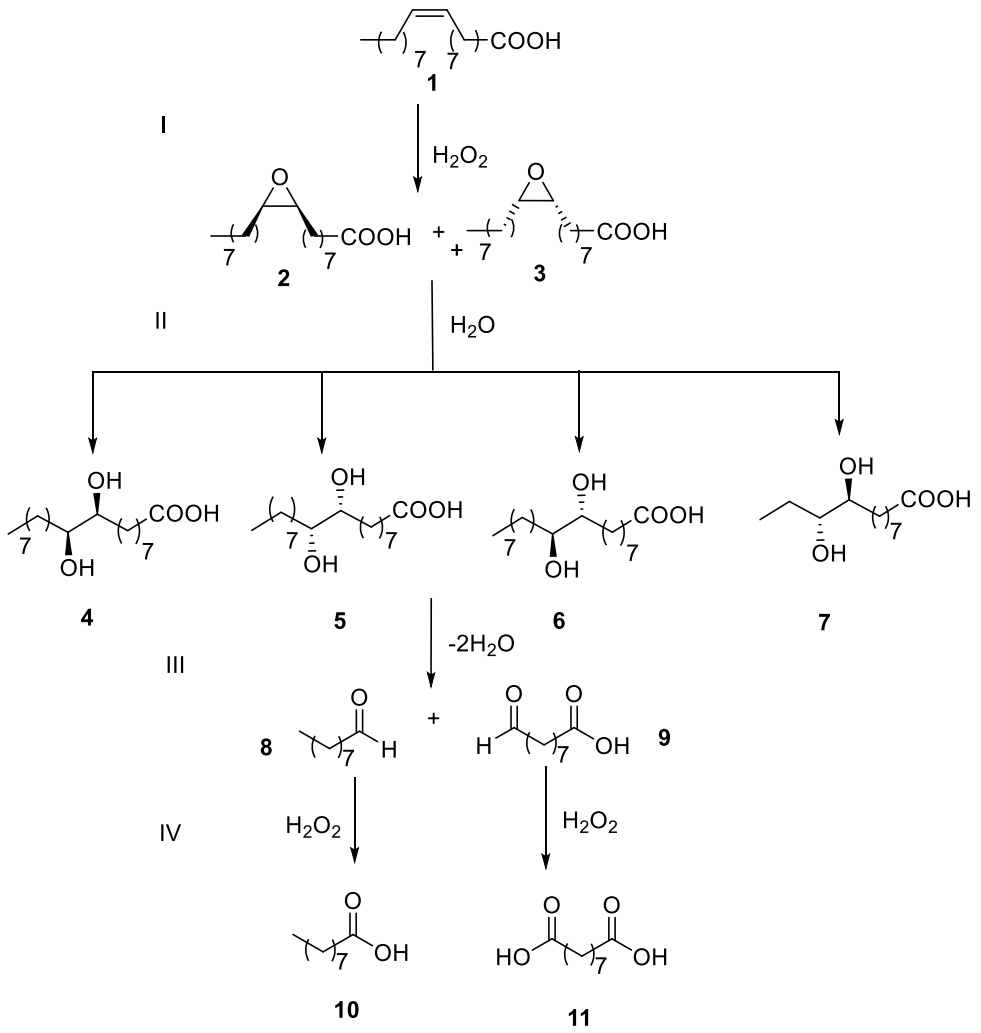

Scheme 1-3. Oxidative cleavage intermediate steps with hydrogen peroxide and tungstic acid.

Catalyst

Many catalysts have been applied in this type of reaction [89–92]. For example, Niobium oxide catalyst has been recently described for the oxidative cleavage of methyl linoleate to obtain aldehydes as a major product. The reaction occurs through a radical mechanism with initial formation of hydroperoxyl radicals (HOO·) formed by the interaction between Nb(V) and H_2O_2. A conjugated hydroperoxide radical is formed, reacting consequently with the molecular oxygen formed by H_2O_2 decomposition in presence of Niobium. The reaction proceeds through a Hock-type rearrangement with water elimination and formation of protonated hemiacetals which fragments to form aldehydes compounds. This radical-type mechanism followed by isomerization and hydroperoxide formation was proposed due to the fact that in tests pursued with methyl oleate and methyl linoleate, only the latter provided significant quantity of aldehydes (40 mol %) [89].

Tungsten-based catalysts are the most common preference in the oxidative cleavage with H_2O_2 studies [93–95].

Tungsten based catalysts

Tungsten as a mineral, was first mentioned in a scientific literature in 1574 as Wolfram. It is recovered from nature as trioxide WO_3 (anhydrous) or $WO_3.nH_2O$ (hydrate) and it exhibits very strong Bronsted acid sites [96,97]. The relatively low point of zero charge (PZC) is the result of its high surface acidity. The oxidation states of tungsten from -2 to +6 leads to several W species which are applied to different reactions, such as tungsten carbide in hydrogenation of olefins [98], tungsten Sulfide (as NiWS) in hydrotreatment/hydrodenitrogenation [99] and tungsten Oxide in acid catalysed reactions such as glycerol dehydration to Acrolein [100].

Based on the experiments of Swern work [84], Luong T. and co-workers [101], reported a new method of preparation of the α,β -glycols by means of a hydrogen peroxide-tungstic acid system at pH=0-1. However, they reported that with the addition of H_2O_2 at concentration below 70 wt. % at 55 °C, the reaction kinetics were extremely low, followed by high exothermic and uncontrollable reaction. The main reaction occurring was the decomposition of H_2O_2.

They assumed that tungstic acid requires a period of preconditioning with aqueous hydrogen peroxide before it can act as a catalyst. The solution of H_2O_2 and tungstic acid was stirred at room temperature for 20 minutes. This can be explained by the fact that in presence of H_2O_2, tungstic acid is oxidized to pertungstic acid, the active intermediate specie to the oxidation process. The work done by Sapunov & Lebedev shows the kinetics and the catalytic mechanism of olefin epoxidation with H_2O_2 in presence of tungsten salts [102]. They demonstrate that the peroxytungstate defines the epoxidation rate. The catalytic specie would be the anion HWO_5^-. The rapid decomposition of H_2O_2, neutralized the active tungsten anion and its activity was substantially reduced.

Luong T. & co-workers hypothesis was that a reaction product was formed with surfactant properties, changing the characteristics of the emulsion and promoting the interaction between oleic acid, hydrogen peroxide and catalyst. If tungstic acid is omitted in the reaction media, no oxidation occurs because decomposition of H_2O_2 is faster than the reaction. They favoured the option of a pre-conditioning hydrogen peroxide-tungstic of 5 h before a 19 h reaction at 55°C, probably leading to the formation of pertungstic acid.

The first intermediate detected from oleic acid was the 9,10-epoxystearic acid (EpSA), with consecutive conversion to *threo*-9,10-dihydroxystearic acid (DHSA). In those studies, it was observed that the rate of oxidation did not accelerate until some accumulation of the DHSA. They found that this specie probably acted as a phase transfer agent in the oleic acid oxidation. This

statement was proved by dissolving 2 wt. % *threo*-DHSA in oleic acid and conducting the oxidation at 55°C. Nevertheless, as the oxidation proceeded, the system became pasty and hardened. By addition of 2.5 mL of water to the solution they achieved for the first-time small quantities of cleavage product [101]. On our side, we confirmed these observations: when the conditions are appropriate to avoid the accumulation of the DHSA as a pasty/solid material, cleavage products are produced [103]

On pre-conditioning with hydrogen peroxide and tungstic acid, a complex A is formed between hydrogen peroxide and tungstic acid proceeding with oxygen transfer to form a polyperoxytungstic acid (B):

$$[H_2WO_4]_n + [H_2O_2]_m \rightleftarrows \underset{\mathbf{A}}{[H_2WO_4]_n.[H_2O_2]_m} \rightleftarrows \underset{\mathbf{B}}{[(H_2WO_5)_m(H_2WO_4)_{n-m}]} + m\,H_2O$$

Two different mechanism were proposed: **1)** When pre-conditioning is not employed: DHSA acid is observed; A complex is formed; and the hydroxyl species facilitates transfer of oxygen from H_2O_2 to the tungsten catalyst and to the double bond through B complex; **2)** When pre-conditioning is used, and hydroxyl intermediate (DHSA) is absent: B is formed being the primary oxidant. After starting the oxidation reaction, some diol intermediate species are formed, and the oxidation proceeds via complex A giving B; while reaction kinetics were obtained with pre-conditioning and DHSA present at the beginning of the reaction. Tungstic acid is not well dissolved in H_2O_2 and it is consistent with our own observations.

Peroxo-tungstate complexes in oxidative cleavage of unsaturated fatty acids

Metal catalyzed oxidations with hydrogen peroxide can be conveniently divided into two categories, involving peroxometal and oxometal species, as the active oxidant [104].

MacKenzie *et al.* [105], applied for the first time a system comprising a cobalt salt instead of tungsten, a portion of DHSA (between 1 mol % and 3 mol %) and using propanol as a solvent. The use of cobalt salts, like cobalt acetate or naphthenate, was guided by the high catalytic activity that remained for long periods of time using oxygen as an oxidant, but also certainly by the lower oxidant cost.

This method is also described by De Vries & Schors [106]. They were able to oxidize α, β-vicinal diols to the corresponding acids, with a combination of H_2O_2 and O_2, using cobalt as a catalyst.

W/Co system

In 1974 *Procter & Gamble* released two patents [107,108] where the oxidative cleavage of vicinal diols was achieved using a combination of tungstic acid and cobalt in the presence of a polar aprotic (dimethylacetamide) solvent and oxygen. They prepared a solution of 70 wt. % H_2O_2 and tungstic acid stirred for 3 h at 35-50 °C and left overnight (the solution passed from yellow to a cloudy-white or grey color). To this, it was added at the beginning a small amount of DHSA, dimethylacetamide, and cobalt. Oxygen was used as a co-oxidant, and the slurry of tungstic acid and hydrogen peroxide was added dropwise over 4h reaction. The reaction temperature rose to a maximum of 100°C.

Following this principle, E. Santacesaria *et al.* [109,110] proposed a reaction in two consecutive steps. The first step is comprised by the reaction between the oleic acid with 60 wt. % H_2O_2, in the presence of tungstic acid to form the α,β-diol species. The second step corresponds to the oxidative cleavage with molecular oxygen, under pressure, of the α,β-diol species, in presence of the *in-situ* formed catalyst, obtained by the reaction between the remaining tungsten catalyst of the first step and the metastable form of cobalt acetate added before the beginning of the second step. The reaction was performed with addition of oxygen, under moderate pressure in autoclave giving place therefore to a triphasic system, gas-liquid-liquid.

In the second step of reaction in presence of O_2 (absence of H_2O_2), the tungstic acid was not active without the addition of cobalt acetate and cobalt acetate was not active alone too – note that in this case there is not enough H_2O_2 to continue the oxidation and that the sole source of oxidant is O_2, which then must interact with the Co moiety. According to the authors by mixing both, a new catalytic species was then formed, which is still not clearly defined.

Cobalt ions can act as well as a templating agent for the formation of polyoxometalate (POM) with a well-defined structure such as Keggin, Dawson or Anderson structures. Anderson structures are easily formed by reacting molybdate, cobalt and hydrogen peroxide. However, these are much less known than tungsten [111].

Santacesaria argued that the activity of this complex catalyst was not due to the original well-structured polyoxometalates (POMs) formed but due to lacunary POMs successively formed in which the cobalt atoms are directly accessible to the reagent and so the tungsten atoms have the capacity to activate the cobalt catalyst. Two different mechanisms were proposed: **1)** direct C-C bond cleavage with formation of an aldehyde group as intermediate with consequent oxidation to

acids; **2)** formation of W-hydroxyketone by initial oxidation of OH group and successive oxidation to acid. The second proposal was supported by the detection of hydroxyketone specie by Gas chromatography (GC-MS). This process has been developed by the bioplastic firm Novamont S.p.A. [80,112,113] and now produced by their joint venture *Matrica*.

W/P system

Heteropoly-acids and anions are those that contain one or two atoms of another element in addition to tungsten, oxygen and hydrogen. It consists of combinations of octahedral WO_6 groups, so that the conversion of WO_4^{2-} into polyanions requires an increase in coordination number. The polymerization of its oxo-ions metal constitution can be related to the metal and oxygen orbitals ability to overlap giving a strong π bonding (M=O). Cotton and Wilkinson [114] state that tungstic acid is polymeric $(H_2WO_4)n$. The lower the pH employed, the higher the aggregation would be expected. This statement was proved by x-ray patterns.

Venturello *et al.* reported the importance of aqueous hydrogen peroxide in conjunction with catalytic amounts of tungstate and phosphate ions, under acidic conditions.

The reaction proceeds via an initial C-H bond fission of the α,β-diol unit to form α-hydroxy ketone followed by oxidative cleavage of the latter yielding aldehydes with further oxidation to obtain carboxylic acids. They supposed that this intermediate probably arises from the decomposition of an adduct formed by interaction of the diol with the anionic tungsten-peroxo species present in the acid solution [115] (**Figure 1-15**).

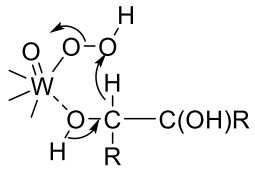

Figure 1-15. Complex formed between the anionic tungsten peroxo specie and the diol intermediate.

Induction time/mass transfer concerns

In 2011, Novamont described in its patent that the oxidative cleavage reaction mechanism of the vicinal diols with oxygen is of a radical type due to the observed reaction acceleration. From their point of view, the reaction showed an induction time in which the hydroxyl radicals started propagating exponentially and uncontrolled leading to a lack of selectivity with the formation of by-products of different chain length [80].

The activity of organometallic complexes of W is found to be limited to homogeneous catalysts in a medium containing H_2O, H_2O_2, catalyst, olefin and the organic solvent. The olefins are in general insoluble in an aqueous phase. The best cleavage results were obtained at concentration of 70 wt. % H_2O_2. Low concentration oxidant solution led to a slow reaction, low productivity of the oxidized products, low conversions and selectivity due to a limited solubility of H_2O_2 in the homogeneous solvent/olefin/ catalyst system.

Aqueous hydrogen peroxide is rapidly decomposed by catalytic metal compounds, reducing the ability of peroxide to proceed oxidation reaction. To avoid faster decomposition, *tert*-butanol can be added, but which can also form *tert*-butyl hydroperoxide. The need for a long induction time described by Venturello suggests the requirement of the use of a new active catalyst, phase transfer catalyst (PTC) to not only solve the dissolution problem but also to stabilize H_2O_2 against decomposition [116].

Phase transfer agent system

MacKenzie [105] did optimize the oxidation of internal olefins. However, in his studies he noticed that by adding small amounts (1-3 mol %) of the intermediate product of the reaction (DHSA), the kinetics of the reaction were improved. Following this studies, Edmund Pultinas *et al.* [107] found also that the fastest rates were obtained with pre-conditioning (H_2O_2 and catalyst) and with hydroxyl intermediate present at the beginning of the reaction, confirming that the hydroxyl intermediate could be acting as a phase transfer agent.

The function of hydroxyl species in accelerating the reactions could be also that of a surfactant, or a complexing agent for the polyperoxy acid acting as a phase transfer catalyst (PTC) allowing higher surface contact between the aqueous phase (H_2O_2 + catalyst) and the organic phase (internal olefin).

Onium salts

According to Bortolini [117], in the presence of hydrogen peroxide, tungstic acids are transformed in the corresponding peroxo-derivatives. In a protic medium, these derivatives are partially dissociated according to the acid-base equilibrium. Neutral and anionic species have different oxidizing characteristics. The former is suitable for oxidizing systems rich in electrons, such as the olefins, transforming them into epoxides and into the hydrolysis product thereof: vicinal diols.

The company *Continental Oil* [118,119] claimed for the first time the application of a quaternary salts in an heterogeneous system.

The Italian company *Montedison S.p.A* [120–122], through extensive studies made by Venturello *et al.* [115,123,124], claims a new method based on a system where the catalytic specie is an onium salt of hetero-pertungstic acid prepared *ex-situ* (**Figure 1-16**) and confirmed by X-Ray crystallography.

$$Q_3\{XO_4[W(O)(O_2)_2]_4\}$$

Figure 1-16. Catalyst I: X represents P or As atoms, n=0, 1 or 2. Q – represents the cation of a quaternary onium salt with the formula $n(C_6H_{17})_3NCH_3^+$. This structure shows 2 peroxo species per tungsten atom.

The reaction is conducted in a biphasic system aqueous/organic in which, the organic phase is constituted by the catalyst I and the olefin and the aqueous phase is comprised of H_2O_2 and water.

Given the lipophilic character of the catalyst and its epoxidizing ability, the epoxidation of the alkene is regarded as the initial stage of the reaction (**epoxidation, Scheme 1-4**). By this, the reaction is believed to involve the formation of a β-hydroxyperoxide alcohol intermediate (**12** and **13**) upon acid hydrolysis (**Scheme 1-4**) of the epoxide formed from the olefin oxidation, at the opposite to the α,β-diol formation shown in **Scheme 1-3**.

This β-hydroxyperoxide alcohol is then oxidized to α-hydroxy ketone (α-ketol) (**14**, **15**) which undergoes through C-C bond fission by hydrogen peroxide, leading to the mono and di-acids. This pathway is denominated as ‘’perhydrolytic’’ (**path 2**) instead of hydrolytic pathway (**path 1**) due to the increase of stability of epoxide with increase of the carbon number. However, **path 1** can also explain the appearance of shorter carboxylic acids obtained in the end of the reaction. This can be due to an over-oxidation of the first products of the oxidative cleavage, the aldehydes **8** and **9**. Once the heteropolymetalate catalyst is put in contact with water in the biphasic system, enough acidity is generated (by phosphotungstic moieties).

Nevertheless, this catalyst (**Figure 1-16**) is important to the epoxide opening by hydrogen peroxide/water, mainly as a Bronsted acid, through the acidic species coming from its partial hydrolytic degradation. Venturello *et al*. alleged that the major route for the two phases oxidation passes through a perhydrolytic pathway, **path 2 (Scheme 1-4.)**.

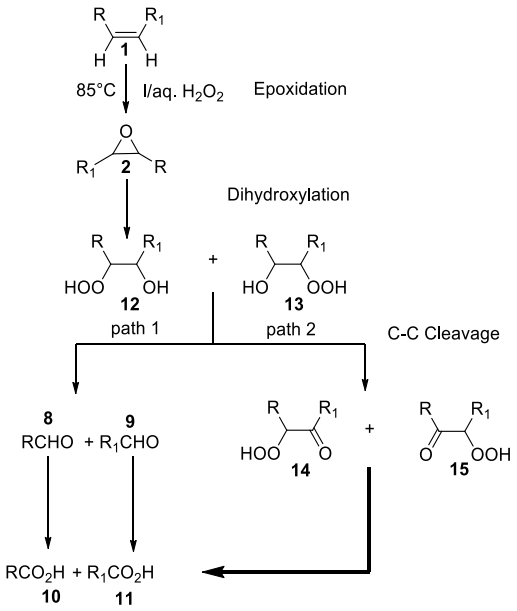

Scheme 1-4. Proposed mechanism according to Venturello et al. studies [125].

Godard *et al.*, based on these studies proposed later a non-stereospecific oxidative cleavage process with the formation of an in-situ catalytic species composed of a peroxo-tungsten complex $Q_3\{PO_2[WO(O_2)_2]_4\}$ as a phase transfer catalyst (PTC) and a co-oxidant in solvent-free conditions. Due to its lipophilic nature, the pyridinium ion can efficiently transfer the peroxo anion, from aqueous phase to the organic phase.

The stoichiometry of the oxidative cleavage requires 4 molar equivalents of hydrogen peroxide, to achieve carboxylic acids, whereas oleic acid generates only 1 molar equivalent of azelaic acid. *DSM* [126] and *Arkema* [23] proposed that the production of azelaic acid can be higher if the starting material is 9-octadecenedioic acid, i.e. a symmetric unsaturated diacid (or derivative), since this generates 2 molar equivalents of azelaic acid for the same amount of hydrogen peroxide, and no side products; thereby contributing to the reduction of the production cost.

In 1993, *Novaol* patented a method of oxidative cleavage, using a solely ionic phase transfer agent Dimethyldioctadecylammonium chloride (Arquad 2HT) [113] in an organic solvent-free conditions. The reaction is performed between 100-104°C for 6h and the yields obtained for pelargonic and monomethyl azelate from methyl oleate are 80 mol % and 77 mol % respectively. The coproducts are not disclosed.

Reaction conditions

pH

Ring opening of epoxy-alkanes fails when carried out in the presence of neutral aqueous hydrogen peroxide only [125].

The pH meter readings in aqueous solution of hydrogen peroxide are lower than the real pH and the difference increases with the increasing addition of H_2O_2. Such behaviour has been linked, by thermodynamic calculations, to the difference in the free energy of solvation of the proton in water and in pure H_2O_2 (about 9 kcal/mole), proton is more firmly bounded to the water. Due to the interaction with H_2O_2 molecules, the apparent acidity of water is increased. The extension of such phenomenon varies with the concentration of H_2O_2 in the aqueous medium [128].

The efficiency of the oxidation is depending on the pH of the reaction. The best results were obtained at pH=3 [124,129,130]. In the Beg and Ahmad [102] kinetic studies with tungsten salt, it was shown that in acid medium an oxyanion is formed as:

$$WO_4^{2-} + H^+ \rightleftharpoons HWO_4^-$$

$$HWO_4^- + H^+ \rightleftharpoons H_2WO_4$$

It was proved that the [HWO_4^-] is maximum at pH = 4.7 but decreases rapidly thereafter. The results of their work demonstrated an intramolecular, concerted mechanism. Despite the lower acidity of the medium, salts of tungstic acid (e.g. Na_2WO_4) intensify epoxidation due to their high stability in water. In this mechanism the electrophilic attack on olefin double bond happens by intramolecular hydrogen bond and the presence of a partial positive charge at peroxide oxygen atom (**Scheme 1-5**).

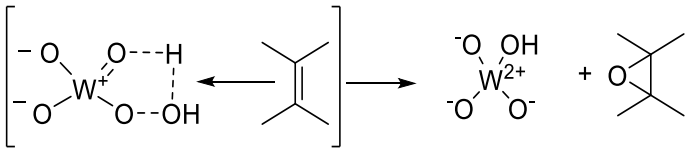

Scheme 1-5. Epoxidation of C=C bond mechanism.

Purification methodology

In Emery's process to isolate the desired mono and di-carboxylic acid, after the ozonolysis reaction, the solution is distilled to provide a first distillate comprising C_2 to C_{22} carboxylic acids. The residue is distilled again to isolate the dicarboxylic acids. To separate the azelaic acid from the impurity acids, liquid-liquid extraction is applied: hot water (between 79-110°C) and a water-immiscible organic aliphatic solvent (like pentane, octane, cyclohexane, etc.) are used. The impurity acids (by-products) that are not soluble in water and remain in the organic phase and are decanted. Azelaic acid as well shorter carbon chains (C_4 and C_8) diacids acids move to the aqueous phase, while

the organic phase retains the monocarboxylic by-products from C_9 to C_{22}. To separate lower chain diacids acids (C_4 to C_8) from the longer chain diacids acids (C_9 or more) crystallization is applied lowering the temperature of the water with different cooling stages from 60 °C to 41 °C, followed by 38 °C and finally 18 °C. The shorter chain di-acids are retained in the mother liquid and removed by filtration. The crystalized azelaic acid-rich stream is then melted and transferred to a distillation unit to separate azelaic acid from higher length diacids. The purified azelaic acid is converted into flakes by cooling below its melting point and then stored [131].

The *Novamont* process (see **Figure 1-17**) differs from the one patented by Emery Oleochemicals. After the reaction, the organic phase contains saturated mono acids and derivatives of saturated carboxylic acids with more than one acid function (diacids) or diacid esters, as well as derivatives of fatty acids present in the starting mixture such as methyl linoleate, methyl stearate and methyl palmitate, and the α,β-diol. The oily phase was dried and degassed and transferred to a distillation column allowing separation of monocarboxylic acid containing the lighter monocarboxylic acids (pelargonic and octanoic acid as main components) from the monomethyl azelate, methyl palmitate, methyl stearate and esters of methyl dihydroxy stearate that were withdrawn from the bottom of the distillation column. This organic phase was then continuously fed to an emulsifier. The emulsion was hydrolysed by feeding it to three consecutive columns filled with acidic ion exchange resin and heated at 100°C for 6h. 4.3 kg of azelaic acid were recovered from 8.5 kg carboxylic acids obtained in the bottom of column **(Figure 1-17)**.

By/Co-products formation

9,10-dihydroxysteraric acid (DHSA)

As described above, the addition of the diol intermediate in small quantities, at the beginning of the reaction, can be a way to accelerate the oxidative cleavage of unsaturated fatty acids. Nevertheless, this method can lead to more by-products formation such as esters and acetals [103]. Some studies describe that from the start of the reaction, a certain amount of cleavage products is already produced. In the acid medium, the diol intermediate called by Catia Bastioli *et al.* [132] as the “reaction foot”, can react with the acids (or aldehydes as observed in our case), already formed, producing esters (or acetals) species.

In its extensive studies [115,120,122,123,125], Venturello *et al.* found a small amount of products with one carbon less than expected (2-5 wt. %). They state that this arises from the cleavage of α-hydroxy aldehyde formed by C-H bond fission of less reactive primary alcohol function

of the starting diol. There have been speculations that these shorter acids could have been produced by isomerization (shift) of the C=C bond in oleic acid, and then cleavage. However, that should lead also to longer chains of the co-products. Since only shorter chains are observed the isomerization hypothesis can be ruled out. Ozonolysis of the starting materials, done in Arkema, also confirmed that the isomerization hypothesis was not relevant. Instead, chain reduction of the cleavage products and intermediates are more probable.

Isomerization

Another hypothesis of by-products origin is the shift of C=C double bond from the 9-10 position to the position 10-11 for example. However, it should be disregarded as in case of oleic acid, although octanoic acid is obtained, sebacic acid (DC10) was never described in the literature nor observed in our experiments.

Shorter chain products – decarboxylation

In processes where no phase transfer catalyst was added, same products with one carbon less [23,127] where quantified at the end of the process. Similarly in a two-step system, W/H_2O_2 followed by Co/O_2, shorter products have been quantified [79,80,132]. The mechanism must then involve a decarboxylation of either the shorter acid/diacid or of the intermediate aldehyde compounds.

Industrial application

To our knowledge, the Italian joint-venture between *Versalis* and *Novamont*, *Matrica,* is the only company to operate the oxidative cleavage of vegetable oils with H_2O_2 producing bio monomers and other products with a plant of 35,000 tons oil/year capacity.

Process Flow-sheet

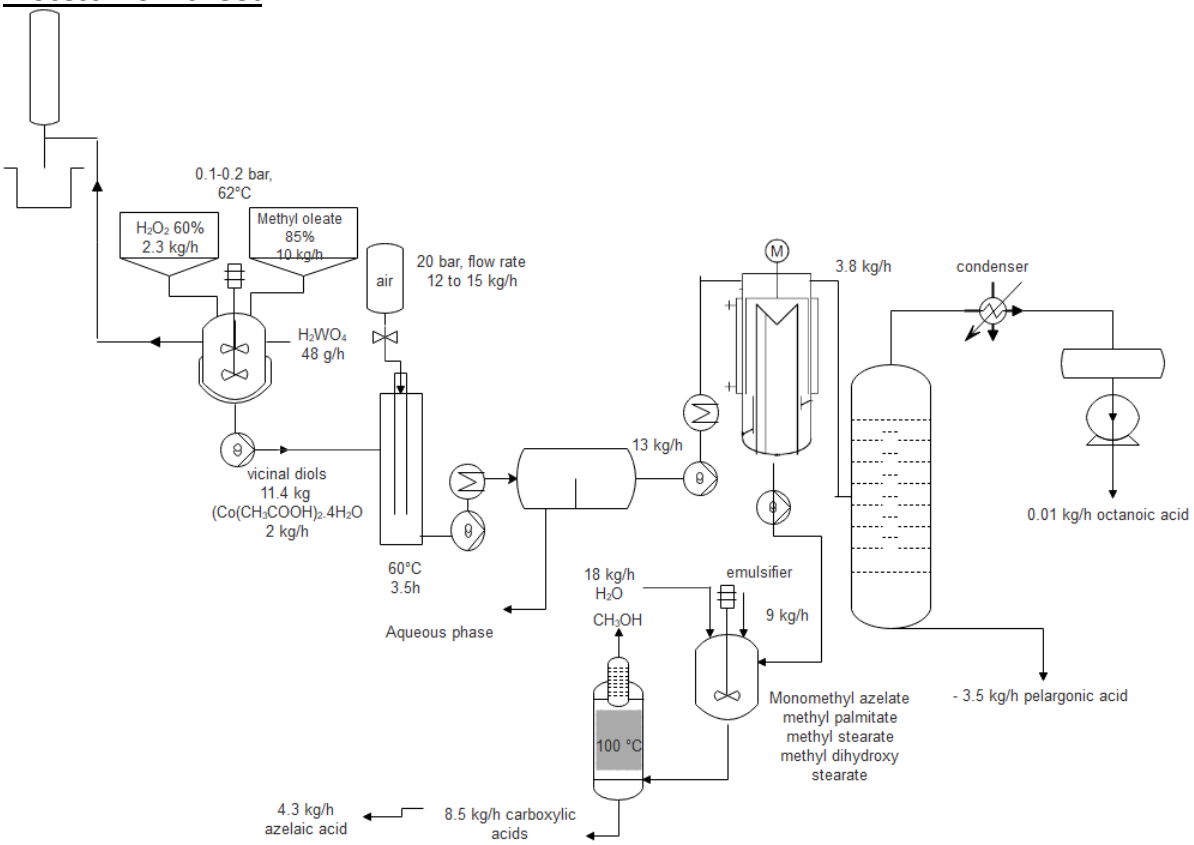

Figure 1-17. Representation of our interpretation about the continuous oxidative cleavage process described in Novamont patents [80,132].

The continuous process and most of the batch academic literature have very different process conditions. In the continuous process, using a stirred tank reactor for the first step reaction, the composition of the reaction medium is equivalent to the composition that comes out of the reactor.

It means that the synthesis is done in a stream rich in diol, while most of the batch reactions studied so far correspond to conditions where the stream is rich in oleic acid/ester at the beginning of the cycle. The same applies to the second stage reaction, where in a continuous mode, with a loop reactor, the composition of the reaction medium is mostly constituted of the cleavage products (pelargonic acid and azelaic acid/ester) in which a minute amount of diol is continuously fed. However, in batch experiment, the reaction starts in a diol rich stream which must dissolve oxygen (or hydrogen peroxide) in order to initiate the cleavage reactions. The difference in reaction medium affects not only the solubility of the oxidants, but also the viscosity, boiling points and many other physic-chemical properties and can favor the formation of side products like the heavy esters of the diol.

Catalyst Recovery

The industrial oxidative cleavage is a continuous process in two consecutive phases. The first stage is the hydroxylation of the monoenoic double bond of oleic acid ester to yield the α,β-diol intermediate, and the subsequent stage the oxidative cleavage of the vicinal diols, obtaining at the end of the reaction a mixture of carboxylic acids. In the first stage a tungsten catalyst is applied while in the oxidation stage a cobalt acetate is used.

The tungsten catalyst is only recovered at the end of the oxidative cleavage stage.

At the end of the reactions the aqueous phase is separated from the organic phase and passed through a cation-exchange resin, fed by gravity, to retain the cobalt ions and to recover tungstic acid, in a concentration of 8000 ppm (kg/mL), and recycled to the first reaction step. The cobalt ions (Co^{2+}) are desorbed from the ion-exchange column and recovered, with a concentration of 9830 ppm (kg/mL) and recycled to the second stage of reaction.

Such a process was developed by the bio-diesel company *Novaol* [134] and optimized by the bioplastic company *Novamont* [135].

1.5 Conclusion and perspectives

The search for a new bio-based raw material represents nowadays the biggest economic impact to different industrial sectors. Materials from renewable resources are being proved to be able to fulfil the chemical industry needs at lower costs.

Currently, plant oils represent an important role to produce these specialty materials. Apart from the renewability aspect, this feedstock has an enormous synthetic potential. The fatty acids constituents of oils have physical and chemical properties that allow the formation of suitable monomers for different applications. Among these fatty acids, the double bond present in the Monounsaturated Fatty Acids (MUFAs) make them the ideal starting material to produce specialty polyamides. These specialty monomers can be obtained by oxidative cleavage of the C=C bond present in the MFAs.

The existence of by/co-products suggest the co-existence of different by-side reactions such as decarboxylation (shorter carbon chain) but also acetalization and esterification (high molecular weight products), related to the starting material impurities and to the presence of α, β-diol intermediate in the reaction media. The high industrial interest demands for an economic risk assessment to evaluate the economic impact of the process and the influence of the starting material purity.

On **chapter 2** it is described an economic risk assessment of an active industrial process for the production of high value monomers obtained through oxidative cleavage which shows the impact on the oil choice on the by-products formation and operational cost. The relevant process economic impact stimulates the research in this field in the search of new technologies. Among them, acoustic cavitation appears as an interesting emerging technology [53-55,136]. In the last decades, ultrasound technology has been showing its potential in a variety of catalytic processes. It has been proved that mass transfer, across the phase boundary of multiphasic system, is substantially enhanced through acoustic emulsification. In this sense on **chapter 3**, the aim of our work was to exploit sonochemical methods to overcome mass transfer and time-consuming of conventional oxidative cleavage reaction in functionalized MUFAs, particularly in oleonitrile to afford nitrile monomers, percursors of aminoacids monomers of PA9. Finally, on **chapter 4**, we studied the hydrogenation of a monounsaturated nitrile ester to afford amino-esters also monomers of PA9. The catalyst deactivation was studied and new reactivation methods, including ultrasonic treatment where proposed.

1.6 References

[1] E. Chevreul, Recherches chimiques sur les corps gras d'origine animale, Chez Levrault, 1823.
[2] H.E. Howe, Industrial and Engineering Chemistry, Ind. Eng. Chem. 32 (1940) 1413–1414. doi:10.1021/ie50371a001.
[3] M.E. Bowden, J.K. Smith, C.H. Foundation, American Chemical Enterprise: A Perspective on 100 Years of Innovation to Commemora te the Centennial of the Society of Chemical Industry (American Section), fouth ed. Chemical Heritage Foundation, 1994.
[4] T.A. Isbell, Chemistry and physical properties of estolides, Grasas y Aceites. 62 (2011) 8–20. doi:10.3989/gya/010810.
[5] J. Vollmann, I. Rajcan, Oil Crops, Springer New York, 2009.
[6] S.K. Gupta, Technological innovations in major world oil crops, volume 1, Technol. Innov. Major World Oil Crop. Vol. 1 Breed. 1 (2012) 1–405. doi:10.1007/978-1-4614-0356-2.
[7] Global Fatty Acid Market Size, Share - Industry Trend Report 2019-2026, (https://www.polarismarketresearch.com/industry-analysis/fatty-acid-market (accessed February 3, 2020).
[8] V. Mank, T. Polonska, Use of natural oils as bioactive ingredients of cosmetic products, Ukr. Food J. 5 (2016) 281–289. doi:10.24263/2304-974x-2016-5-2-7.
[9] M. Mugdan, D. P. Young, Catalytic Hydroxylation of unsaturated compounds, J. Am. Oil Chem. Soc. (1949) 2988–3000. doi:10.1039/JRD9490002988.
[10] L. Rios, D. Echeverri, F. Cardeño, Hydroxylation of vegetable oils using acidic resins as catalysts, Ind. Crops Prod. 43 (2013) 183–187. doi:10.1016/j.indcrop.2012.07.035.
[11] R.P. Wool, Polymers and composite resins from plant oils. Academia Press, 2005, pp. 56-113.
[12] Q. Fu, Y. Long, Y. Gao, Y. Ling, H. Qian, F. Wang, X. Zhu, Synthesis and properties of castor oil based plasticizers, RSC Adv. 9 (2019) 10049–10057. doi:10.1039/c8ra10288k.
[13] P. Alagi, Y.J. Choi, S.C. Hong, Preparation of vegetable oil-based polyols with controlled hydroxyl functionalities for thermoplastic polyurethane, Eur. Polym. J. 78 (2016) 46–60. doi:10.1016/j.eurpolymj.2016.03.003.
[14] J. Beare-Rogers, A. Dieffenbacher, J. V Holm, International Union of Pure and applied chemistry joint commitee of international union of nutrition Sciences and IUPAC commision on Food*Lexicon of Lipid nutrition(IUPAC Technical Report), 2001.
[15] S.S. Narine, X. Kong, Vegetable Oils in Production of Polymers and Plastics, Bailey's Ind. Oil Fat Prod. (2005) 279–306. doi:10.1002/047167849X.bio047.
[16] D.G. Hayes, M.J. Dumont, Polymeric products derived from industrial oils for paints, coatings, and other applications, AOCS Press., 2016. doi:10.1016/B978-1-893997-98-1.00003-8.
[17] Rilsan® Polyamide Family, https://www.arkema.com/en/products/product-finder/range-viewer/Rilsan-Polyamide-Family/ (accessed August 21, 2018).
[18] Technical Polymers-Arkema.com. https://www.arkema.com/en/products/product-finder/range-viewer/Rilsan-polyamide-Family/ (accessed on 21 August 2018).
[19] P. Perret, From castor oil to Specialty Polyamides: the success of the diversification, 2014.
[20] Oleris® Sebacic acid - Biobased carboxylic acid directyl processed from castor oil.https://www.arkema.com/en/products/product-finder/product-viewer/Oleris-Bio-BasedbrSebacic-acid/ (accessed on February 3, 2020).
[21] J.-F Devaux, G., Lê, B. Pees, Application of eco-profile methodology to polyamide 11. (report)
[22] Rilsamid® Polyamide 12. https://www.arkema.com/en/products/product-finder/product-viewer/Rilsamid-Polyamide-12-Resin/ (accessed April 13,2019).
[23] J. Dubois, Method for Synthesising 9-Aminononanoic Acid or Esters Thereof from Natural Unsaturated Fatty Acids. European Patent 2,307,353 (B1), 29 August 2012.
[24] W.J. Roff, J.R. Scott, Fibres, Films, Plastics and Rubbers: A Handbook of Common Polymers, Elsevier Science, 2013.
[25] An alternative raw material for polyamide 12: Evonik is operating a pilot plant for bio-based ω-amino lauric acid, https://corporate.evonik.com/en/Pages/article.aspx?articleId=100566 (accessed September 17, 2019).
[26] B. Markush, J.-L. Couturier, J. Dubois, Process for producing nitrile-fatty acid compounds, U.S. patent 2013/0345388 (A1), 26 December 2013.
[27] K. Louis, E. Beauchene, L. Vivier, J.L. Dubois, K.D.O. Vigier, P.Y. Pouilloux, Reductive Amination of Aldehyde Ester from Veg etable Oils to Produce Amino Ester in the Presence of Anhydrous Ammonia, ChemistrySelect. 1 (2016) 2004–2008. doi:10.1002/slct.201600571.
[28] K. Boodhoo, A. Harvey, Process Intensification Technologies for Green Chemistry: Engineering Solutions for Sustainable Chemical Processing, Wiley, 2013.
[29] T. Van Gerven, A. Stankiewicz, 2009-VanGervenStankiewicz-Structure, Energy, Synergy, Time.pdf, (2009) 2465–2474.
[30] A. Stankiewicz, T. Van Gerven, G. Stefanidis, The Fundamentals of Process Intensification, Wiley, 2019.
[31] G.D. Stefanidis, A.N. Muñoz, G.S.J. Sturm, A. Stankiewicz, A helicopter view of microwave application to chemical processes: Reactions, separations, and equipment concepts, Rev. Chem. Eng. 30 (2014) 233–259. doi:10.1515/revce-2013-0033.
[32] Z.L. Wu, B. Ondruschka, G. Cravotto, Degradation of phenol under combined irradiation of microwaves and ultrasound, Environ. Sci. Technol. (2008). doi:10.1021/es8013375.
[33] G. Cravotto, A. Binello, G. Merizzi, M. Avogadro, Improving solvent-free extraction of policosanol from rice bran by high-intensity ultrasound treatment, Eur. J. Lipid Sci. Technol. 106 (2004) 147–151. doi:10.1002/ejlt.200300914.
[34] S. Chandrasekaran, S. Ramanathan, T. Basak, Microwave food processing-A review, Food Res. Int. 52 (2013) 243–261. doi:10.1016/j.foodres.2013.02.033.
[35] M. Ashokkumar, F. Cavalieri, F. Chemat, K. Okitsu, A. Sambandam, K. Yasui, B. Zisu, Handbook of ultrasonics and sonochemistry, Handb. Ultrason. Sonochemistry. (2016) 1–1487. doi:10.1007/978-981-287-278-4.
[36] P.G. Newman, G.S. Rozycki, The history of ultrasound, Surg. Clin. North Am. (1998). doi:10.1016/S0039-6109(05)70308-X.
[37] E.B. Flint, K.S. Suslick, The temperature of cavitation, Science (80-.). 253 (1991) 1397–1399. doi:10.1126/science.253.5026.1397.
[38] M.A. Margulis, Fundamental aspects of sonochemistry, Ultrasonics. 30 (1992) 152–155. doi:10.1016/0041-624X(92)90065-T.
[39] T. Lepoint, F. Mullie, What exactly is cavitation chemistry?, Ultrason. - Sonochemistry. 1 (1994) 13–22. doi:10.1016/1350-4177(94)90020-5.
[40] Cleaning - Weber Ultrasonics. https://www.weber-ultrasonics.com/en/schweissen/ (accessed January 22, 2018).
[41] Cutting - Weber Ultrasonics. https://www.weber-ultrasonics.com/en/cutting/ (accessed February 8, 2020).

[42] Welding - Weber Ultrasonics. https://www.weber-ultrasonics.com/en/welding/ (accessed February 8, 2020).

[43] B. Avvaru, A.B. Pandit, Oscillating bubble concentration and its size distribution using acoustic emission spectra, Ultrason. Sonochem. 16 (2009) 105–115. doi:10.1016/j.ultsonch.2008.07.003.

[44] P. Chowdhury, T. Viraraghavan, Sonochemical degradation of chlorinated organic compounds, phenolic compounds and organic dyes - A review, Sci. Total Environ. 407 (2009) 2474–2492. doi:10.1016/j.scitotenv.2008.12.031.

[45] C. Pétrier, M.F. Lamy, A. Francony, A. Benahcene, B. David, V. Renaudin, N. Gondrexon, Sonochemical degradation of phenol in dilute aqueous solutions: Comparison of the reaction rates at 20 and 487 kHz, J. Phys. Chem. 98 (1994) 10514–10520. doi:10.1021/j100092a021.

[46] E. Article, P.N. Amaniampong, M.G. Fernandez, Selective radical depolymerization of cellulose to glucose induced by high frequency ultrasound†, Chem. Sci. (2020). doi:10.1039/d0sc00020e.

[47] T.G. McKenzie, F. Karimi, M. Ashokkumar, G.G. Qiao, Ultrasound and Sonochemistry for Radical Polymerization: Sound Synthesis, Chem. - A Eur. J. 25 (2019) 5372–5388. doi:10.1002/chem.201803771.

[48] E.N. Harvey, A.L. Loomis, High frequency sound waves of small intensity and their biological effects, Nature. 121 (1928) 622–624. doi:10.1038/121622a0.

[49] C.A. Komar, J. Pasini, U.S.B. of Mines, Ultrasonic Phenomena and Methods of Measurement: A Bibliography, U.S. Department of the Interior, Bureau of Mines, 1963.

[50] N. Maropis, J.B. Jones, C.D. Twardowski, A. Incorporated, U.S.A.E.C.N.Y.O. Office, Investigation of Ultrasonic Potentialities in Fluid Flow Promotion, Aeroprojects Incorporated, 1958.

[51] E.A. Neppiras, B.E. Noltingk, Cavitation Produced by Ultrasonics: Theoretical Conditions for the Onset of Cavitation, Proc. Phys. Soc. Sect. B. 64 (1951) 1032–1038. doi:10.1088/0370-1301/64/12/302.

[52] K. Makino, M.M. Mossoba, P. Riesz, Chemical effects of ultrasound on aqueous solutions. Formation of hydroxyl radicals and hydrogen atoms, J. Phys. Chem. 87 (1983) 1369–1377. doi:10.1021/j100231a020.

[53] G. Cravotto, P. Cintas, Power ultrasound in organic synthesis: moving cavitational chemistry from academia to innovative and large-scale applications, Chem. Soc. Rev. 35 (2006) 180–196. doi:10.1039/B503848K.

[54] K. Wei, H.T. Gao, W.D.Z. Li, Facile synthesis of oxabicyclic alkenes by ultrasonication-promoted Diels-Alder cycloaddition of furano Dienes, J. Org. Chem. 69 (2004) 5763–5765. doi:10.1021/jo049210a.

[55] N.N. Mahamuni, P.R. Gogate, A.B. Pandit, Ultrasound-accelerated green and selective oxidation of sulfides to sulfoxides, Ind. Eng. Chem. Res. 45 (2006) 8829–8836. doi:10.1021/ie061006l.

[56] G. Kumar, D. Kumar, R. Johari, Time reducing process for biofuel production from non edible oil assisted by ultrasonication, Ultrason. Sonochem. 21 (2014) 1618–1623. doi:10.1016/j.ultsonch.2014.04.004.

[57] G. Ruecroft, D. Hipkiss, T. Ly, N. Maxted, P.W. Cains, Sonocrystallization: The use of ultrasound for improved industrial crystallization, Org. Process Res. Dev. 9 (2005) 923–932. doi:10.1021/op050109x.

[58] K. Louis, L. Vivier, J.M. Clacens, M. Brandhorst, J.L. Dubois, K. De Oliveira Vigier, Y. Pouilloux, Sustainable route to methyl-9-hydroxononanoate (polymer precursor) by oxidative cleavage of fatty acid methyl ester from rapeseed oil, Green Chem. 16 (2014) 96–101. doi:10.1039/c3gc41491d.

[59] Bio-Lubricants | Natural-based Lubricants | Emery Oleochemicals, (2018). https://www.emeryoleo.com/Bio-Lubricants.php (accessed September 14, 2018).

[60] Matrìca | Products | Intermediates | Pelargonic acid, (2018). http://www.matrica.it/pelargonic-acid.asp?ver=en#.W3KgIOgzZPY (accessed August 14, 2018).

[61] L.R. Pokhrel, I. Karsai, Long-term sub-lethal effects of low concentration commercial herbicide (glyphosate/pelargonic acid) formulation in Bryophyllum pinnatum, Sci. Total Environ. 538 (2015) 279–287. doi:10.1016/J.SCITOTENV.2015.08.052.

[62] P. Foley, Y. Yang, Ozonolysis operations for generation of reduced and/or oxidized product streams, U.S. patent 2014/9,035,091 (B2), 30 January 2014.

[63] C.G. Goebel, A.C. Brown, H.F. Oehischlaeger, R.P. Rolfes. Method of Making Oleic Acid. U.S; Patent 2,813,113 (A1), 12 November 1957.

[64] J., Zhu; J., Du; X. ,Xie. Method for producing nonandioic acid, pelargonic acid by ozonization-oxidative decomposition of oleic acid, CN patent 101,244,998 (B1) 14 September 2011.

[65] B. Zaldman, A. Kisilev, Y. Sasson, N. Garti, Double bond oxidation of unsaturated fatty acids, J. Am. Oil Chem. Soc. 65 (1988) 611–615. doi:10.1007/BF02540689.

[66] C. Harries, Ueber die Einwirkung des Ozons auf organische Verbindungen, Justus Liebig's Ann. Der Chemie. 343 (1905) 311–344. doi:10.1002/jlac.19053430209.

[67] Bio-Lubricants Product, 2013. https://www.emeryoleo.com/content/Emery_BL_brochure.pdf (accessed August 14, 2018).

[68] Where We Operate | Croda, (2019). https://www.croda.com/en-gb/about-us/where-we-operate (accessed April 14, 2019).

[69] P2 Science |, (2019). https://p2science.com/ (accessed April 14, 2019).

[70] K. Koike, M. Nifuku, K. Izumi, S. Nakamura, S. Fujiwara, S. Horiguchi, Explosion properties of highly concentrated ozone gas, in: J. Loss Prev. Process Ind., 2005. doi:10.1016/j.jlp.2005.07.020.

[71] EPA, Hydrogen peroxide, 2017. http://www.epa.govt.nz/search-databases/Pages/ccid-details.aspx?SubstanceID=1778.

[72] A. Goti, F. Cardona, Hydrogen Peroxide in Green Oxidation Reactions: Recent Catalytic Processes, Green Chem. React. 53 (2013) 191–212. doi:10.1007/978-1-4020-8457-7_9.

[73] Explosion and fire in a hydrogen peroxide plant – La référence du retour d'expérience sur accidents technologiques. https://www.aria.developpement-durable.gouv.fr/fiche_detaillee/3536_en/?lang=en (accessed September 9, 2018).

[74] Explosion sur un équipement de stérilisation dans une usine agroalimentaire – La référence du retour d'expérience sur accidents technologiques. https://www.aria.developpement-durable.gouv.fr/accident/48973/ (accessed August 26, 2018).

[75] Explosion dans une usine agroalimentaire de produits laitiers. – La référence du retour d'expérience sur accidents technologiques. https://www.aria.developpement-durable.gouv.fr/accident/46398/ (accessed August 26, 2018).

[76] A. Inc, Hydrogen Peroxide. http://americas.brightenyourfuture.com/export/sites/byf-americas/.content/medias/downloads/literature/hydrogen-peroxide-brochure.pdf (accessed September 14, 2018).

[77] R I D Convention concerning International Carriage by Rail (COTIF) Appendix C-Regulations concerning the International Carriage of Dangerous Goods by Rail (RID). http://otif.org/fileadmin/new/3-Reference-Text/3B-RID/RID_2017_E.pdf (accessed August 14, 2018).

[78] Background to Regulations and Guidance. http://hsa.ie/eng/Your_Industry/ADR_-_Carriage_of_Dangerous_Goods_by_Road/ADR_Files/Guidance_on_the_appointment_of_a_dangerous_goods_safety_adviser.pdf (accessed August 14, 2018).

[79] C., Bastioli; G., Borsotti, A. Merlin; T., Milizia. Process for the Catalytic Cleavage of Vgetable Oils. U.S. Patent 8,222,438 (B2), 20 November

2008.
[80] A. Bieser, G. Borsottu, A. Ferrari, A. Pirocco, Continuous process for the production of derivatives of saturated carboxylic acids, U.S. Patent 8,846,962 (B2), 30 September 2014.
[81] G.B. Payne, P.H. Williams, Reactions of Hydrogen Peroxide. IV. Sodium Tungstate Catalyzed Epoxidation of α,β-Unsaturated Acids, J. Org. Chem. 24 (1959) 54–55. doi:10.1021/jo01083a017.
[82] Feu de poubelle dans une centrale nucléaire – La référence du retour d'expérience sur accidents technologiques. https://www.aria.developpement-durable.gouv.fr/accident/50397/ (accessed August 26, 2018).
[83] A. Inc, Hydrogen Peroxide Brochure - Arkema Inc. http://americas.brightenyourfuture.com/export/sites/byf-americas/.content/medias/downloads/literature/hydrogen-peroxide-brochure.pdf (accessed September 9, 2018).
[84] D. Swern, Electronic Interpretation of the Reaction of Olefins with Organic Per-Acids, J. Am. Chem. Soc. 69 (1947) 1692–1698. doi:10.1021/ja01199a037.
[85] Z. Wang, Walden Inversion, in: Compr. Org. Name React. Reagents, 2010: pp. 2937–2941. doi:10.1002/9780470638859.conrr656.
[86] R. Noyori, M. Aoki, K. Sato, Green oxidation with aqueous hydrogen peroxide, Chem. Commun. (2003). doi:10.1039/b303160h.
[87] E. Antonelli, R. D'Aloisio, M. Gambaro, T. Fiorani, C. Venturello, Efficient oxidative cleavage of olefins to carboxylic acids with hydrogen peroxide catalyzed by methyltrioctylammonium tetrakis(oxodiperoxotungsto)phosphate(3-) under two-phase conditions. Synthetic aspects and investigation of the reaction course, J. Org. Chem. (1998). doi:10.1021/jo980481t.
[88] R. Kadyrov, D. Hackenberger, Oxidative Cleavage of Long Chain Olefins to Carboxylic Acids with Hydrogen Peroxide, Top. Catal. 57 (2014) 1366–1371. doi:10.1007/s11244-014-0304-6.
[89] C. Paraguassú Cecchi, D. Cesarín-Sobrinho, A. Buarque Ferreira, J. Netto-Ferreira, New Insights on the Oxidation of Unsaturated Fatty Acid Methyl Esters Catalyzed by Niobium(V) Oxide. A Study of the Catalyst Surface Reactivity, Catalysts. 8 (2018) 6. doi:10.3390/catal8010006.
[90] S. Rup, M. Sindt, N. Oget, Catalytic oxidative cleavage of olefins by RuO4 organic solvent-free under ultrasonic irradiation, Tetrahedron Lett. (2010). doi:10.1016/j.tetlet.2010.04.040.
[91] B. Hajra, N. Sultana, C. Guria, A.K. Pathak, V.K. Saxena, Liquid Phase Selective Catalytic Oxidation of Oleic Acid to Azelaic Acid Using Air and Transition Metal Acetate Bromide Complex, JAOCS, J. Am. Oil Chem. Soc. 94 (2017) 1463–1480. doi:10.1007/s11746-017-3048-1.
[92] X. Li, P. Jiang, Z. Wang, Y. Huang, Phosphotungstate-Based Ionic Silica Nanoparticles Network for Alkenes Epoxidation, Catalysts. 6 (2015) 2. doi:10.3390/catal6010002.
[93] V. Benessere, M.E. Cucciolito, A. De Santis, M. Di Serio, R. Esposito, F. Ruffo, R. Turco, Sustainable Process for Production of Azelaic Acid Through Oxidative Cleavage of Oleic Acid, JAOCS, J. Am. Oil Chem. Soc. 92 (2015) 1701–1707. doi:10.1007/s11746-015-2727-z.
[94] H. Noureddini, M. Kanabur, H. Noureddini, Liquid-Phase Catalytic Oxidation of Unsaturated Fatty Acids, (1999). http://digitalcommons.unl.edu/chemeng_biomaterials.
[95] Zillillah, T.A. Ngu, Z. Li, Phosphotungstic acid-functionalized magnetic nanoparticles as an efficient and recyclable catalyst for the one-pot production of biodiesel from grease via esterification and transesterification, Green Chem. (2014). doi:10.1039/c3gc41379a.
[96] E. Lassner, W.D. Schubert, Tungsten: Properties, Chemistry, Technology of the Element, Alloys, and Chemical Compounds, Springer US, 2012.
[97] K. Tanabe, Chapter 3 - Determination of Basic Properties on Solid Surfaces, in: K. Tanabe (Ed.), Solid Acids and Bases, Academic Press, 1970: pp. 35–44. doi:https://doi.org/10.1016/B978-0-12-683250-1.50007-9.
[98] C. Moreno-Castilla, M.A. Alvarez-Merino, F. Carrasco-Marín, J.L.G.G. Fierro, Tungsten and tungsten carbide supported on activated carbon: Surface structures and performance for ethylene hydrogenation, Langmuir. 17 (2001) 1752–1756. doi:10.1021/la001367k.
[99] O.Y. Gutiérrez, S. Singh, E. Schachtl, J. Kim, E. Kondratieva, J. Hein, J.A. Lercher, Effects of the Support on the Performance and Promotion of (Ni)MoS2 Catalysts for Simultaneous Hydrodenitrogenation and Hydrodesulfurization. Effects of the Support on the Performance and Promotion of (Ni)MoS2 Catalysts for Simultaneous Hydrodenitrogenati, ACS Catal. 4 (2014) 1487–1499. doi:10.1021/cs500034d.
[100] J. Dubois, W. Duquenne Chrostophe, Holderich, J. Kervennal, Procede de deshydratation du glycerol en acrolene, 2882053, 2005.
[101] T. Luong, H. Schriftman, D. Swern, Direct Hydroxylation of Fats and Derivatives with Hydrogen Peroxide Tungstic Acid System a, J. Am. Oil Chem. Soc. 40 (1966) 316–320.
[102] B. Assaz, I. Ahmad, Kinetics and Mechanism of the Epoxidation of Allyl Alcohol with Aqueous Hydrogen Peroxide Catalyzed by Tungstic Acid, J. Am. Chem. Soc. 82 (1960) 1267–1277. doi:10.1021/ja01491a001.
[103] A. Soutelo-Maria, J.-L. Dubois, J.-Ll. Couturier, G. Cravotto, (To be published).
[104] H. Wójtowicz, Synthetic utility of metal catalyzed hydrogen peroxide oxidation of C - H , C - C and C = C bonds in alkanes , arenes and alkenes : Recent advances, Arkivoc. (2017) 12–58. doi:10.3998/ark.5550190.p009.578.
[105] J.R. Mackenzie, N.J. Morristown, S. Chester, J. Morgan, Oxidation of fatty acids, U.S. Patent 2,820,046 (A1), 14 January 1958.
[106] G. De Vries, A. Schors, Oxygenation of Organic Compounds - A Novel Oxidative Cleavage of 1,2-Diols, Tetrahedron Lett. 9 (1968), pp. 9–10.
[107] E. Pultinas, J. Cincinnati, R. D., Oxidation of vicinal glycols in the presence of organic peroxides and cobaltous compounds, U.S. Patent 3,711,523 (A1), 17 December 1973.
[108] E. Pultinas, Preparaton of carboxylic acids by the oxidation of vicinal glycols, U.S. Patent 3,855,257 (A1),23 June 1974.
[109] E. Santacesaria, A. Sorrentino, F. Rainone, M. Di Serio, F. Speranza, Oxidative Cleavage of the Double Bond of Monoenic Fatty Chains in Two Steps: A New Promising Route to Azelaic Acid and Other Industrial Products, Ind. Eng. Chem. Res. 39 (2000) 2766–2771. doi:10.1021/ie990920u.
[110] E. Santacesaria, M. Ambrosio, A. Sorrentino, R. Tesser, M. Di Serio, Double bond oxidative cleavage of monoenic fatty chains, Catal. Today. 79–80 (2003) 59–65. doi:10.1016/S0920-5861(03)00045-2.
[111] W.C. Cheng, C.J. Pereira, Preparation of cobalt-molybdenum hydrotreating catalysts usinghydrogen peroxide stabilization, Appl. Catal. (1987). doi:10.1016/S0166-9834(00)83065-1.
[112] A. Bieser, G. Borsotti, F. Digioia, Continuous process for the production of the carboxilic acids, U.S. Patent 9,272,975 (B2), 1 March 2016.
[113] A. Gardano, M. Foa, Process for the preparation of carboxylic acids and esters thereof by oxidative cleavage of unsaturated fatty acids and esters thereof, 0666838 B1, 1994.
[114] F. Cotton, G. Wilkinson, The elements of the Second and Third Transition Series. In Advanced Inorganic Chemistry, 6th ed., Noida, Inda, 2007.
[115] C. Venturello, M. Ricci, Oxidative Cleavage of 1,2-Diols to Carboxylic Acids by Hydrogen Peroxide, J. Org. Chem. 51 (1986) 1599–1602. doi:10.1021/jo00359a042.
[116] C.M. Starks, Phase-transfer catalysis. I. Heterogeneous reactions involving anion transfer by quaternary ammonium and phosphonium salts, J. Am. Chem. Soc. 93 (1971) 195–199. doi:10.1021/ja00730a033.
[117] O. Bortolini, G. Amato, A. Arcoria, F.P. Ballistreri, G.A. Tomaselli, V. Conte, F. Di Furia, G. Modena, G. Valle, Oxidations withperoxotungsten

complexes: rates and mechanism of stoichiometric olefin epoxidations, J. Mol. Catal. 37 (1986) 165–175. doi:10.1016/0304-5102(86)85006-4.
[118] C.M. Starks, Phase-Transfer Catalysis. I. Heterogeneous Reactions Involving Anion Transfer by Quaternary Ammonium and Phosphonium Salts, J. Am. Chem. Soc. 93 (1971) 195–199. doi:10.1021/ja00730a033.
[119] D.R. Napier, C.M. Starks, Phase transfer catalysis of heteroneneous reactions by quaternay salts, 3992432, 1975. doi:10.1016/j.(73).
[120] C. Venturello, ; Rino D'aloisio, M. Ricci, Peroxide Compositions Based on Tungsten and Phosphorus or arsenic, and Processes and Uses Relative Thereto. U.S;; Patent 4,595,671 (A1), 17 June 1986.
[121] C. Venturello, R. D'Aloisio, M. Ricci, Process for Preparing Carboxylic Acids from Olefins or Vicinal Dihydroxi Compounds. EP Patent 122,804 (A1), 24 October 1984.
[122] C. Venturello, M.Gambaro, Process for the preparation of vicinal diols soluble in water. U.S. patent 4,562,299, 31 December 1985.
[123] C. Venturello, R. D'Aloisio, Quaternary ammonium tetrakis(diperoxotungsto)phosphates(3-) as a new class of catalysts for efficient alkene epoxidation with hydrogen peroxide, J. Org. Chem. 53 (1988) 1553–1557. doi:10.1021/jo00242a041.
[124] E. Antonelli, R. D'Aloisio, M. Gambaro, T. Fiorani, C. Venturello, Efficient Oxidative Cleavage of Olefins to Carboxylic Acids with Hydrogen Peroxide Catalyzed by Methyltrioctylammonium Tetrakis(oxodiperoxotungsto)phosphate(3−) under Two-Phase Conditions. Synthetic Aspects and Investigation of the Reaction Course, J. Org. Chem. 63 (1998) 7190–7206. doi:10.1021/jo980481t.
[125] E. Antonelli, R. D'Aloisio, M. Gambaro, T. Fiorani, C. Venturello, Efficient Oxidative Cleavage of Olefins to Carboxylic Acids with Hydrogen Peroxide Catalyzed by Methyltrioctylammonium Tetrakis(oxodiperoxotungsto)phosphate(3−) under Two-Phase Conditions. Synthetic Aspects and Investigation of the Reaction Course, J. Org. 63 (1998) 7190–7206. doi:10.1021/jo980481t.
[126] H. Dekker, Process for the Preparation of Azelaic Acid from 9-Octadecenedioic Acid. WO Patent 2013/092353(A1), 27 June 2013
[127] M., Brandhorst; J.L. , Dubois. Procede de Coupure de Chaines Grasses Insaturees. EP Patent 2,785,676 (B1), 28 October 2015
[128] A.G. Mitchell, W.F.K. Wynnejones, Thermodynamic and Other Properties of Solutions Involving Hydrogen Bonding, Discuss. Faraday Soc. 33 (1953) 161–168. doi:10.1039/df9531500161.
[129] C. Venturello, R. D'Aloisio, Quaternary Ammonium Tetrakis(diperoxotungsto)phosphates(3-) as a New Class of Catalysts for Efficient Alkene Epoxidation with Hydrogen Peroxide, J. Org. Chem. (1988). doi:10.1021/jo00242a041.
[130] A. Godard, P. De Caro, S. Thiebaud-Roux, E. Vedrenne, Z. Mouloungui, New Environmentally Friendly Oxidative Scission of Oleic Acid into Azelaic Acid and Pelargonic Acid, J. Am. Oil Chem. Soc. 90 (2013) 133–140. doi:10.1007/s11746-012-2134-7.
[131] T.C., Walker; S.W., Turner; J.W. , Landwehr; D.S. , da Rosa; Durchholz, M.E. Method of Purifying a Dicarboxylic Acid. U.S. Patent 9,248,381 (B2), 2 February 2016.
[132] C. Bastioli, T. Milizia, B. Giampero, Process for the production of derivatives of saturated carboxylic acid, U.S. Patent 7,812,186 (B2), 12 October 2010.
[133] A. ,Gardano; S., Strologo; M.Foa, Process for Recovering Cobalt and Tungsten from Reaction Liquors. U.S. Patent 5,599,514 (A), 4 February 1997.
[134] G., Borsotti; F., Digioia, Process for the Recovery of Cobalt and Tungstic Acid and/or Its Derivatives from Aqueous Solution. PCT Patent Application WO 2016/116479 Al, 28 July 2016.
[135] R. Singla, F. Grieser, M. Ashokkumar, Kinetics and Mechanism for the Sonochemical Degradation of a Nonionic Surfactant, J. Phys. Chem. A. 113 (2009) 2865–2872. doi:10.1021/jp808968e.
[136] L. Rinaldi, Z. Wu, S. Giovando, M. Bracco, D. Crudo, V. Bosco, G. Cravotto, Oxidative polymerization of waste cooking oil with air under hydrodynamic cavitation, Green Process Synth. 6 (2017) 425–432. doi:10.1515/gps-2016-014

Chapter 2. conomic Risk Assessment using Monte Carlo Simulation for the production of azelaic acid and pelargonic acid from vegetable oils[2]

[2] From the publication : De Leon Izeppi, G. A., Dubois, J.L., Balle, A., Soutelo-Maria, A.L., *Economic Risk Assessement Using Monte Carlo Simulation For the Production of Azelaic Acid and Pelargonic acid from Vegetable oils*. (doi.org/10.1016/j.indcrop.2020.112411)

2.1 Introduction

The discovery of petroleum in the 19th century had a tremendous impact on our society. It has become the main source of energy and raw materials for the industry. Nevertheless, it is a non-renewable material, its use has a negative effect on climate change and its decline will have a great impact on our way of living.

As a result, the interest in sources that could substitute fossil carbon/petroleum has increased.

Nonetheless, this decision cannot be made in a short period of time considering that manufacturing plants are planned to run for years and the adoption of new products can take more than 20 years [1].

Unlike petroleum, vegetable oils are renewable and their use in the chemical industry is not a novel topic. Vegetable oils can be subdivided in edible and non-edible oils. Non-edible oils have fatty acid profiles that can be useful for industrial applications. Linseed [2] and castor oils [1] are grown because of their unique chemical properties, important for the chemical industry [3]. They have been used for non-edible purposes like paints [4], plastics agrochemicals [5] and as lubricants [6]. The popularity of renewable fuels has resulted in a significant investment of public and private capital for the development of non-edible alternative crops.

Industrial vegetable oils have gained also interest in the polymer industry due to their attractive fatty acid composition used as renewable building blocks precursors. Arkema (Colombes, France) has 4 production plant-based factories distributed in France (2 factories), the United States (1 factory) and China (1 factory). Several of these compounds are already being used as raw materials to produce more complex end products in commercial applications. The company is well known for the production of 11-aminoundecanoic acid, from the oil of castor bean, for the specialty polyamides (PA) production of Rilsan®, Pebax® and Rnew® polymer ranges. Arkema is also a world-leading supplier of sebacic acid (DC10) and the derivative diamine (DA10) renewable monomers of PA6,10 (Rilsan® S) and PA 10,10 (Rilsan® T).

The increase in the demand of renewable monomers production requires effective production processes. Among the industrial processes to obtain renewable monomers, the oxidative cleavage of unsaturated fatty acids has been considered as a greener alternative to achieve these renewable monomers. Valuable difunctional monomers such as azelaic acid are being already produced by this process by Emery, Croda Sipo and more recently Matrica S.p.A. [7]. Other

renewable monomers have been under investigations lately, such as the production of dodecanedioic acid (DDDA, or DC12) by Verdezyne, through fermentation of Lauric acid ester, but the company has not been able to complete its demonstration plant. Recently, Evonik communicated on the production of Amino Dodecanoic acid ester also through fermentation of Lauric acid ester, but the product does not seem to be on the market yet.

Regardless of the high interest in renewable products, an economic risk assessment is necessary to evaluate each project, to identify the impact of the vegetable oil choice and to identify the impact of the technology.

2.2 Materials and methods

2.2.1 Net present Value (NPV)

The decision to make an investment relies on the profitability of the project. There are several methodologies to evaluate projects and select the one which generates the biggest economic benefit, which helps management to decide which project receives funding. These types of methodologies can also be used as filters in the early stages of a project. These methodologies can be payout period plus interest (POP), Net Present Value (NPV) and discounted cash flow (DCFROR), between others [8,9].

One of the most used methodologies is the NPV or sometimes called the net present worth (NPW) [8]. The NPV is the sum of the yearly cash flow in present value terms and it can be described with the **Equation 2-1**.

$$NPV = \sum_{t=0}^{n} \frac{OCF}{(1+i)^t}$$

Equation 2-1. Net Present Value (NPV). t: year, n: number of years that the project is operational, i: discount rate and OCF: annual cash flow.

If the NPV is higher than 0 it means that the project generates a return rate higher than the discount rate [8].

The discount rate might be defined based on specific targets and/or the interest for borrowing money. For instance, a discount rate equal to the interest of borrowing money would be required to generate a positive NPV to make a profit.

Additionally, the NPV can be used to compare two or more projects and the project with the highest NPV would generate the highest return rate (if all projects use the same discount rate).

The annual operational cash flow can be determined with **Equation 2-2.**

$$OCF=ANP+D$$

Equation 2-2. Annual operational cash flow. **ANP:** Annual Net Profit and D: depreciation.

The ANP can be determined with **Equation 2-3** and **Equation 2-4.**

$$ANP=AP*(1-TR) \quad if \quad AP>0$$

Equation 2-3. Annual Net profit calculation if the annual profit is positive. **AP:** Annual Profit, **TR:** tax rate.

$$ANP=AP*1 \quad if \quad AP<0$$

Equation 2-4. Annual Net profit calculation if the annual profit is negative. **AP:** Annual Profit, **TR:** tax rate.

$$AP=Sales-Expenses-D$$

Equation 2-5. Sales: annual sales generated from the sales of the products, **Expenses:** annual expenses of the plant**.**

In the present case study, the following items were considered as expenses:

- Catalysts
- Labour costs
- Utilities
- Maintenance and repairs
- Operating supplies
- Property taxes
- Financing interest
- Insurance
- Rent
- Royalties
- Distribution and selling
- Research and development
- Monte Carlo Simulation

Typically, economic considerations are done using a deterministic approach. This type of approach consists of input and output variables which are constant in time. In other words, once

the variables and their values have been fixed, the result or outcome will remain constant. This type of analysis is simple and a good starting point for any analysis, but it deviates from reality by not considering uncertainty and fluctuations over time. In addition, the set of data selected can severely affect the result while not representing the reality or a high probability of occurrence.

Certain methods exist in order to evaluate the impact of uncertainty, such as sensitivity analysis. This type of analysis measures the impact of uncertainty, but it does not define the probability of happening.

Monte-Carlo method, on the other hand, is a stochastic method (non-deterministic). On this method, the variable inputs come from probabilistic distributions instead of single or fixed values. This approach leads to output variables with its own probabilistic distributions and allows to evaluate the probability of certain results as can be seen in **Figure 2-1.**

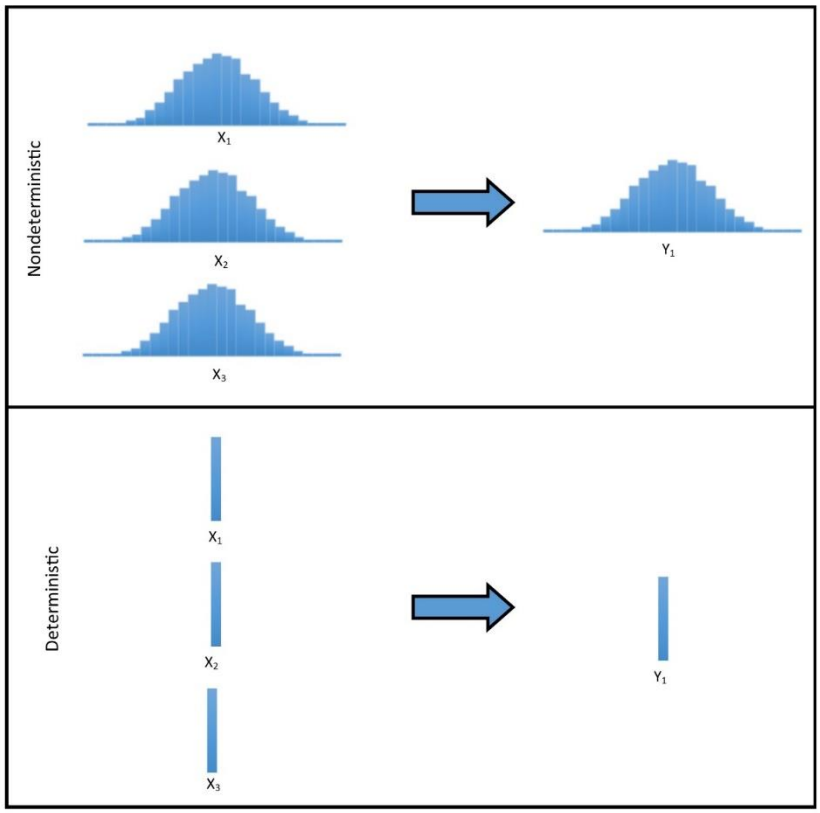

Figure 2-1. Comparison of a deterministic and non-deterministic approach for data analysis.

The Monte Carlo method consists of simple steps:

- Definition of the probabilistic distribution of the variables.
- Generation of the correlation between variables to shorten distribution of output variables.
- Generation of a series of values based on the probabilistic distribution.
- Generation of the deterministic output for each of the series of values generated.

- Analysis of all of the deterministic values.
- Chemical Process (**Supplementary data S 1.1**).

2.2.2 *Industrial process / Benchmark*

The industrial production of bi-functional monomers such as azelaic acid through ozonolysis is accomplished since the beginning of XXth century by the oleochemical company Emery Oleochemicals with a plant in the USA [10]and Croda Sipo [11] with a plant in China. More recently P2 Science [12] has invested also in the production of the monomer azelaic acid through ozone application. However, this process presents some disadvantages such as high energy and technologic demand to produce ozone and some potential risks associated with ozone utilization.

The application of hydrogen peroxide as the oxidant of this reaction has been industrialized by the Italian company Matrica S.p.A (joint venture between ENI and Novamont S.p.A). Matrica S.p.A invested in a processing facility in Porto Torres [13]. The investment was divided into three phases and during phase 1, a plant capable of producing azelaic and pelargonic acid was installed. The maximum capacity of the plant has been stated to be between 32,000 - 40,000 tons by different sources. The products include azelaic acid, carboxylic acids for esterification and for the market, glycerol and other secondary products with high boiling points. Based on the publicly released information by Matrica the general mass balance of the plant can be seen in **Figure 2-2**.

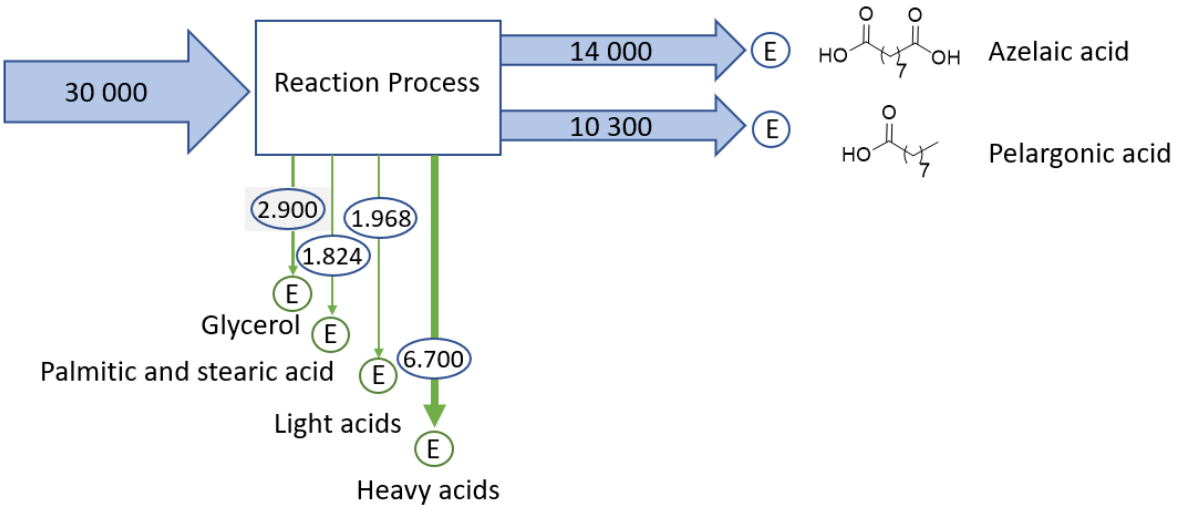

Figure 2-2. General mass balance described in the integrated environmental authorization from the plant installed at Porto Torres **[14] E-** exit**.**

The reported process used high oleic acid sunflower, although Novamont and Matrica communicate a lot on the use of Cardoon oil. Nevertheless, other sources of vegetable oils could be used but different end products and byproducts are to be expected.

The industrial process patented by Novamont S.p.A. [15] has already been described before and it is used as the basis for the case study (**Chapter 1**). The process described in the patents of Novamont S.p.A has been adapted to close the mass balance and can be observed in **Figure 2-3**.

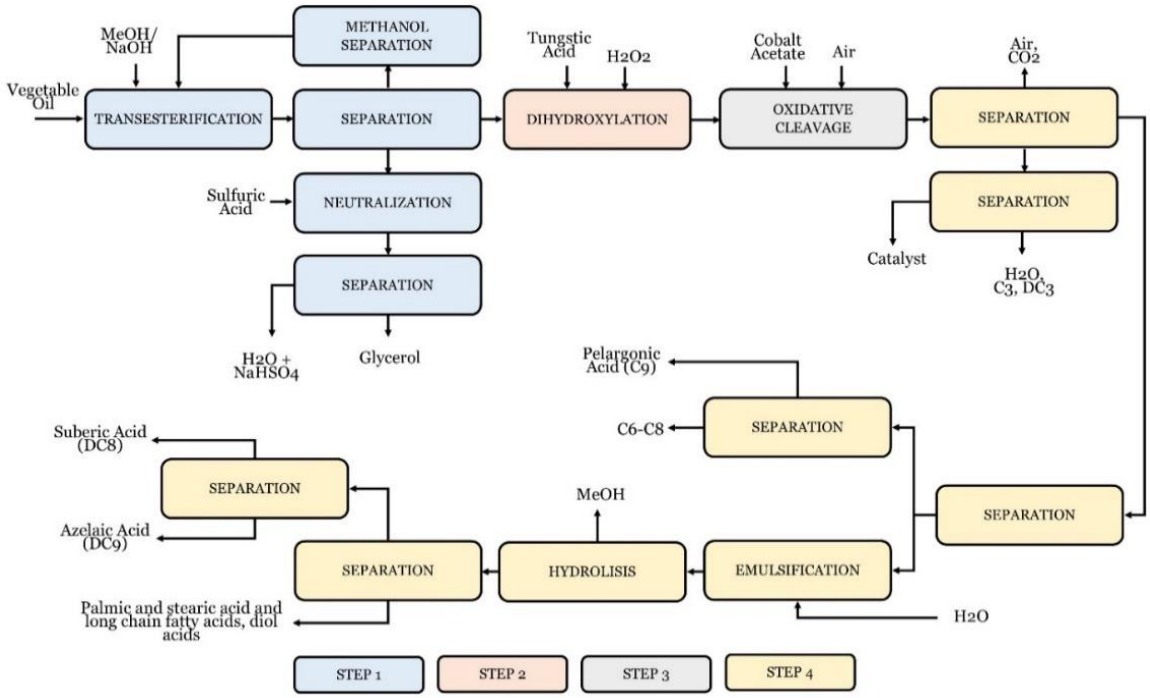

Figure 2-3. The chemical process for the production of azelaic and pelargonic acid from vegetable oils – Although diol esters are produced in the process, in order to simplify the analysis they have been omitted in the mass balance, which would mean that they are recycled in the process at the step 3.

The process covers 4 main steps. In **step 1**, the transesterification of the triglycerides with methanol and an inorganic base occurs to obtain the fatty acids methyl esters (FAME) and glycerol. Crude glycerol is extracted from the reaction medium. **Step 2**, dihydroxylation, comprises the oxidation of the double bond with H_2O_2 and tungsten catalyst into the formation of methyl dihydroxy-stearate intermediates. **Step 3** involves the C-C oxidative cleavage of the intermediate formed in **step 2**. The reaction proceeds under 20 bars of industrial air (containing about 21 % oxygen) – this pressure is referred as Pmax later in the study. Finally, **step 4** constitutes the purification process. After oxidative cleavage, the organic phase contains mono and dicarboxylic acids and the derivatives of the fatty acids present initially in **step 2** such as methyl stearate, palmitate and still the remaining diol intermediate. The pelargonic acid (C9) and the lighter monocarboxylic acids (C6-C8) can be recovered with a distillation column. The monomethyl azelate, methyl palmitate, methyl stearate and the esters of methyl dihydroxy-stearate recovered from the

bottom of the distillation column are continuously feed into a reactor with an emulsifier and then hydrolysed into three consecutive columns filled with acid ion exchange resin. The azelaic acid is separated by crystallization from the heavier saturated fatty acids palmitic and stearic [7]. Products obtained with one carbon less such as acid C8 (octanoic acid) and dicarboxylic acid DC8 (suberic acid) are the result of the decarboxylation of pelargonic acid and azelaic acid, a side-reaction (loss of selectivity) of the process.

2.2.3 Raw materials

2.2.3.1 Vegetable oils

Vegetable oils are the main raw material and they represent the major expense. Vegetable oils are triglycerides **Figure 2-4**. Where R1, R2, and R3 represent three different or identical fatty acids.

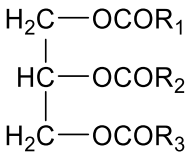

Figure 2-4. Structure of a triglyceride. R1, R2, R3 – un/saturated fatty acids constitution.

The composition of the fatty acids depends on the type of oil as described in the introduction. At the same time, each fatty acid can lead to different renewable products.

2.2.3.2 *Others*

Other raw materials in the analysis include hydrogen peroxide which is used for the dihydroxylation reaction. Methanol, which is used in the transesterification process, is recovered at the end of the process through the hydrolysis of the methyl esters. Tungstic acid and cobalt acetate are the catalysts used to carry out the oxidative scission of fatty acids and to a lower extent sodium hydroxide and sulfuric acid are used in the transesterification process.

2.2.3.3 *Oxidative cleavage / Main reaction*

These renewable products can be obtained through different reactions depending on the chemical structure of the vegetable oils. The total number of carbons, the presence of double bonds, ester linkages or hydroxyl groups in the chemical structure will determine the type of reaction and the type of products that can be produced.

Furthermore, vegetable oils do not contain only one fatty acid but several of them. These different compounds lead to several coproducts and byproducts during the reaction, which added to reactions yields lower than 100%, demands several separation and isolation steps to obtain products with high purity needed for commercial and industrial applications such as polymers.

The main reaction which is considered in this case study is the oxidative cleavage of unsaturated fatty acids. Oxidative scission of the double bonds present in the fatty acids can be accomplished using ozone as an oxidant (ozonolysis) or through the use of hydrogen peroxide and a tungsten-based catalyst. The expected products without considering side reactions are shown in **Table 2-1**.

Saturated fatty acids are not expected to react during the process such as palmitic acid (C16:0) and stearic acid (C18:0), therefore they are recovered at the end of the process.

Fatty acid	Carbon number, n: carbon number insaturation	Azelaic acid (DC9)	Pelargonic acid (C9:0)	Palmitic acid (C16:0)	Steraic acid (C18:0)	Others saturated (C20:0/C22:0)	Heptanoic acid (C7:0)	Caproic acid (C6:0)	Malonic acid (DC3)	Propionic acid (C3:0)
Oleic acid	C18:1 n-9	1	1	0	0	0	0	0	0	0
Linoleic acid	C18:2 n-9,12	1	0	0	0	0	0	1	1	0
alpha-Linolenic acid	C18:3 n-9,12,15	1	0	0	0	0	0	0	2	1
Palmitoleic acid	C16:1	1	0	0	0	0	1	0	0	0
Palmitic acid	C16:0	0	0	1	0	0	0	0	0	0
Stearic acid	C18:0	0	0	0	1	0	0	0	0	0
Others saturated	C20:0 / C22:0	0	0	0	0	1	0	0	0	0

Table 2-1. Number of moles of products/ building blocks obtained from the oxidative cleavage per mole of fatty acid.

As we can observe in **Table 2-1** the production of azelaic acid and pelargonic acid is highly dependent on the oil composition. The larger the content of C18:2 and C18:3, the lower the production of pelargonic acid. Higher content of C16:0, C18:0 or other high molecular weight saturated fatty acids, reflects lower production of pelargonic acid and azelaic acid as there are no double bonds to oxidize. The production of these high-value monomers relies on the selection of the most appropriate vegetable oil.

2.2.4 Products

Azelaic acid and Pelargonic acid have the highest market price and are therefore considered as the main products of the process.

2.2.4.1 *Azelaic acid*

One of the main products of this case study is azelaic acid (DC9). DC9 is a linear saturated dicarboxylic acid with 9 carbons and the following formula $HOOC(CH_2)_7COOH$. This bi-functional monomer is a biobased product and it is highly appreciated for its physicochemical properties in the cosmetic and pharmaceuticals [16], electronics [17], lubricants, plasticizers and in the polymer industry to form the Nylon-6,9 [18]. Azelaic acid can be obtained by the oxidative cleavage of oleic acid, linoleic acid, and α-linoleic acid along with different by-products depending on the number of unsaturation of the fatty acid precursor.

In some cases, raw materials can be replaced by cheaper sources, which indirectly correlates the market prices of raw materials through competition and it can be used to predict the future prices of the raw materials. Nevertheless, in some cases, the substitution of raw materials can be performed in limited cases due to physicochemical properties, which is the case of sebacic acid (DC10).

Sebacic acid (DC10) is a dicarboxylic acid, $HOOC(CH_2)_8COOH$, with a strong presence in several industries. This renewable monomer is produced industrially from ricinoleic acid, obtained from castor seeds, and besides its similar structure to azelaic acid, it has different physicochemical properties, which makes azelaic acid more convenient in certain applications like lubricants as a result of a lower melting point as seen in **Table 2-2**. As it is possible to observe, there is a periodicity in melting points for the different dicarboxylic acids. This periodicity leads to DC7, DC9 and DC11 having a similar melting point compared to DC8 and DC10 which have much higher melting points. Recently the price of sebacic acid has been increasing due to Asian political-economic constraints related to the closure of several plants during winter times given past preference to coal burn for energy production, contributing so to air pollution [19]. As a result, the sebacic acid supply became tight and the price increased to around 5,000 $/ton. The same constraint does not apply to azelaic acid, which is produced in China but also in the US, while most of the sebacic acid worldwide is produced in China (with some production in India and recently in Oman).

Azelaic acid, although less pure than sebacic acid, has a market at a higher price today, but also a much lower market share. Sebacic acid world production might reach 100 kt/year by 2024 and the market size was above 300m USD in 2016 [19]. On the other hand, azelaic acid had a market

size of 94m USD in 2017 and expected to reach 140m by 2025 ("Global Azelaic Acid Market Growth Opportunity," 2019). It is reasonable to think that in the past also there was a price differential and that azelaic niche markets allowed it to survive even when sebacic acid was cheaper.

Sebacic acid is correlated to the price of castor oil. But azelaic acid should depend for example on animal fat, vegetable oils (US source) or palm oil (Asian source). However, its market value is so high that it decorrelates from the oil source. Castor has been historically about twice the price of palm oil, so indirectly there is a kind of correlation between azelaic acid and castor oil.

Dicarboxylic acid	Number of carbons	Melting point (°C)	molecular weight (g/mol)	Density (g/mL)
Pimelic acid (DC7)	7	106	160.17	1.28
Suberic acid (DC8)	8	144.0	174.20	1.27
Azelaic acid (DC9)	9	106.5	188.22	1.225
Sebacic acid (DC10)	10	130.8	202.25	1.208
Undecanedioic acid (DC11)	11	108-110	216.28	0.89

Table 2-2. Physical properties of some dicarboxylic acids (Haynes, 2015).

2.2.4.2 *Pelargonic acid*

Pelargonic, a carboxylic acid with 9 carbons and chemical formula $HOOC(CH_2)_7CH_3$, is the second main product of this case study. This monofunctional carboxylic acid can be obtained by the oxidative cleavage of oleic acid, gondoic acid and erucic acid along different byproducts depending on the precursor unsaturated fatty acid used. In 1995 the Mycogen Corporation introduced pelargonic acid in the pesticides market with the brand name Scythe® and since then has being used as a natural herbicide [20]. Alike azelaic acid, the replacement of pelargonic acid depends on the physicochemical properties of the acids as seen in **Table 2-3**.

Monocarboxylic acid	Number of carbons	Melting point (°C)	Boiling Point (°C)	Molecular weight (g/mol)	Density (g/ml)
Enanthic acid (C7)	7	-7.5	223	130.19	0.92
Caprylic acid (C8)	8	16.3	239	144.21	0.91
Pelargonic acid (C9)	9	12.3	254.5	158.24	0.91
Capric acid (C10)	10	31.5	268.7	172.27	0.99
Undecanoic acid (C11)	11	28.6	280.0	186.30	0.891

Table 2-3. Physical properties of some carboxylic acids [21].

2.2.4.3 *Others*

Other products from the reaction, which have a lower market price include glycerol. Glycerol market price has dropped since the expansion of biodiesel, where glycerol is a byproduct and the supply is much greater than the demand. Additionally, long-chain saturated fatty acids would be produced.

Other products might have a lower number of carbons due to undesired decarboxylation, which reduces the yield and efficiency of the process (non-selective reaction).

2.2.4.4 *Mass balance*

Based on the chemical process described in **Figure 2-3**, the required amount of raw materials and end-products are determined for the following vegetable oils and are shown in **Table 2-4**. The mass balance was based with the next two vegetable oils:

- High oleic sunflower (C18:1 = 85%, C18:2 = 5%, C16:0 = 4%, C18:0 = 6%)
- Palm oil (C18:1 = 40.5%, C18:2 = 10%, C18:3 = 0.2%, C16:0 = 44%, C18:0 = 4%)

		High Oleic Sunflower Oil processing plant	Palm Oil processing plant
Raw Materials / catalysts	Vegetable oil	21.8	38.7
	H_2O_2 pure	3.02	3.45
	Tungstic acid	0.089	0.102
	Cobalt acetate	0.065	0.075
	Methanol	0	0
Products / byproducts	Azelaic acid (DC9)	10.0	10.0
	Suberic acid (DC8)	2.31	2.31
	Caproic acid (C6)	0.431	1.53
	Heptanoic (C7)	0	0
	Caprylic acid (C8)	1.81	1.53
	Pelargonic acid (C9)	7.94	6.71
	Palmitic acid (C16:0)	0.833	16.3
	Stearic acid (C18:0)	1.25	1.48
	Arachidic acid (C20:0)	0	0.480
	Glycerol	2.27	4.19
	Propionic acid (C3), Malonic acid (DC3)	0.387	1.45

Table 2-4. Mass balance to produce 10000 ton of azelaic acid per year (x 10^3 ton/year).

The following assumptions were made for the mass balance:

- A concentration of 0.51 mmol of tungstic acid and 0.29 mmol of cobalt acetate was used according to the number of C=C bonds (double bonds) in the oil composition.
- Due to the high solubility of DC3 and C3 in water, it was assumed that they are not recovered and end up as wastes.
- The oxidative cleavage reaction has an efficiency of 80% for the production of azelaic acid and pelargonic acid. The side products of this reaction consist of CO_2, octanoic or caprylic acid (C8) and octanedioic or suberic acid (DC8). That means we assume that 80 wt % is C9 and the rest is CO_2 and C8. The decarboxylation reaction is a serious drawback of the process as it makes the final purification of the products more complex and could impede the valorisation of the diacid as a high purity monomer. The following assumptions were took in account:
  - Other products have a yield of 100%.
  - Separation efficiency is 100%.
  - Transesterification reaction had a yield of 100%.
  - Methanol recovery was assumed to be 100% .

As seen in **Table 2-4,** two plants with a yearly production of 10 kton of azelaic (DC9) and 7-8 kton of pelargonic acid (C9) per year are compared. Lower C9 is assumed for the case of Palm Oil due to different ratio (PuFA/MuFA). It is also seen that the total the plant capacity (vegetable oil to be processed) which uses high oleic sunflower oil (H.O.S.O) is half of the plant that uses palm oil (22k ton/year vs 39k ton/year). In other words, due to the composition of fatty acids in high oleic sunflower oil, less raw material is required to obtain the same amount of the desired products (DC9, C9).

2.3 Results

2.3.1 Economic analysis

2.3.1.1 *Products and raw materials price distributions*

The goal in this section is to identify the prices distribution, based on the historical data, corrected for inflation. The price distribution was fitted with several statistical laws (Normal, Log-Normal, Gamma and Weibull) and the best fit was identified. The distribution then reflects geo-climatic or geopolitical parameters that affect the market prices.

Furthermore, it was determined if the past events that affected the prices have the same probability to occur in the future and to decide if the same laws of distribution should apply, estimate the mean and the other statistical parameters.

After each distribution was fitted, the future distribution of the prices was estimated based on the past and our own experience. Both the fitted distribution based on the historical price of two raw materials and the future distribution are shown in **Figure 2-5** and **Figure 2-6**. The fitted distribution for the other raw material produced such as H_2O_2 and Methanol can be found in **Supplementary Data S.1.2-S.1.6**.

High Oleic Sunflower Oil	Palm Oil
5% to 95% probability range: [507, 1535] US$/ton Distribution type: Log-Normal mean:6.8, σ:0.34	5% to 95% probability range: [268, 1245] US$/ton Distribution type: Gamma, K:5, Θ:136

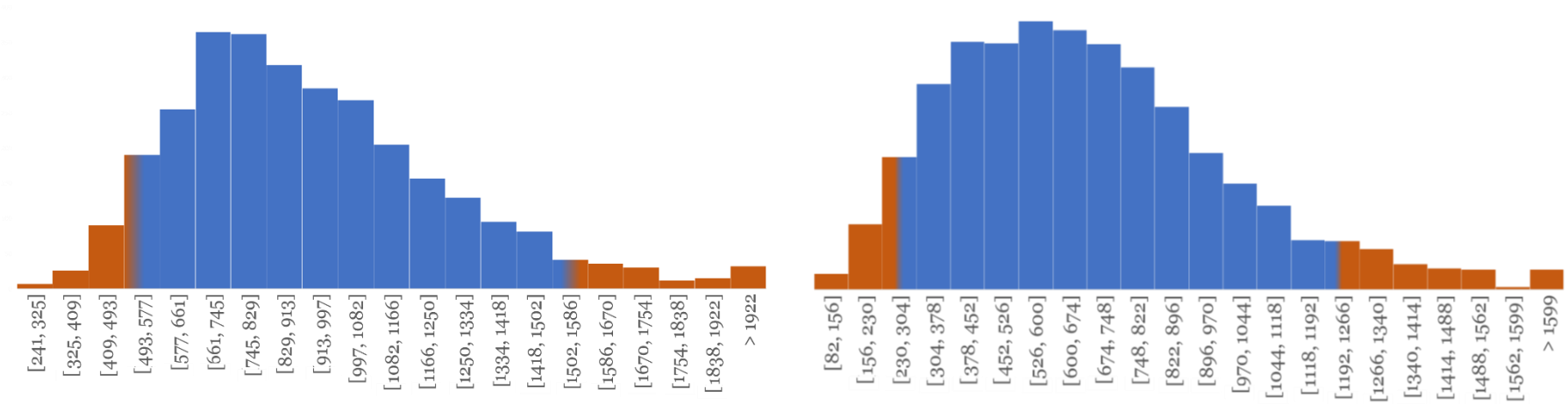

Figure 2-5. Fitted price distribution of raw materials (historical data) taking into consideration inflation [22,23].

High Oleic Sunflower Oil	Palm Oil
5% to 95% probability range: [762,1058] US$/ton Distribution type: Log-Normal mean:6.8, σ:0.1	5% to 95% probability range: [428,743] US$/ton Distribution type: Gamma, K:36, Θ:16

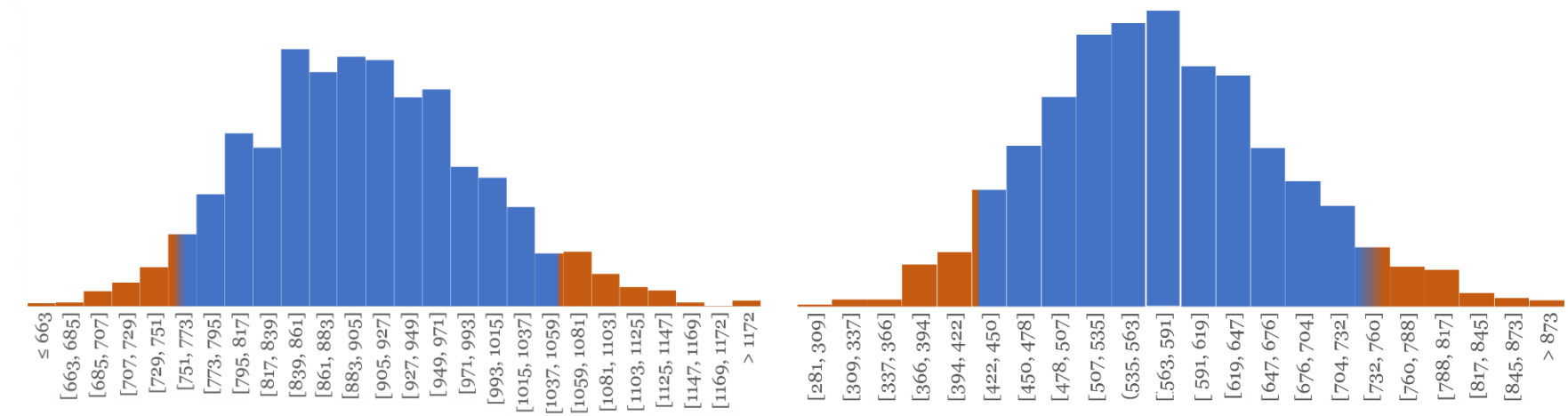

Figure 2-6. Fitted future price distribution of raw materials based on historical prices and assuming ranges for the future.

2.3.2 *Correlation matrix*

In addition, a correlation matrix was prepared and the correlation factor between each of the parameters was estimated. In other words, the dependency between the prices of each of the variables (raw materials prices and products) was determined. The main purpose is to sharpen the distribution of the final output, by restricting the range in which the individual distributions are allowed in the Monte Carlo Simulation.

The historical data were analysed to determine correlation coefficients between them. A matrix of correlation coefficients was generated. On a case by case basis, the correlation coefficient was adjusted to reflect the expected value for the future. The adjusted value took into consideration if the values which shown some correlation is due to casualty or if there is a true dependence between the values. For instance, methanol and azelaic acid are two different products for different markets and the new plant will not have an impact on the price of methanol. On the contrary, if the demand for acid C9 increases, it could be expected that the price of C8 would increase due to a direct substitution in some applications. When no correlation coefficient was available from historical data, a value was generated by expert judgement. Then random values were generated with the assigned distribution laws, and the data are multiplied by a Cholesky matrix generated from the correlation matrix in order to create correlations between the data. The generated correlation matrixes can be found in the supplementary information (**Supplementary Data S.1.1)**.

2.3.3 *Capital costs*

Capital costs are the expenditures needed to design and build a chemical plant. These expenses are fixed costs and represent the highest investment before the start-up of the plant. The determination of capital costs depends on the degree of the project definition. The Association for the Advancement of Cost Engineering (AACE) categorizes cost estimation in 5 classes with different ranges of accuracies, as seen in **Table 2-5**.

Class	Degree of projection definition	Usage	methodology	accuracy
5	0 – 2%	Conceptual screening	Capacity factored or parametric models	Low: -20 to – 50% High: +30 – +100%
4	1 – 15%	Study of feasibility	Equipment factored or parametric models	Low: -15 to – 30% High: +20 – +50%
3	10 – 40%	Budget authorization or control	Semi-detailed unit costs	Low: -10 to – 20% High: +10 – +30%
2	30 – 70%	Budget control	Detailed unit costs	Low: -5 to – 15% High: +5 – +20%
1	70 – 100%	Construction	Detailed unit costs	Low: -3 to – 10% High: +3 – +15%

Table 2-5. Cost estimation classification matrix [24].

Several correlations have been proposed in the literature for cost estimations at the early stages of a project. Some of these correlations were made by Wilson, Taylor, Bridgewater, Klumpar, Petley, and Lange, between others [24]. These correlations vary on the information required to estimate the total capital costs and it is possible to achieve Class 5 and Class 4 level of accuracy with these methods.

Due to simplicity and limited information about the plant, the correlation based on the work of Petley was used in the Monte Carlo simulation, found as one of the best identified by Mirela Tsakgari [24]. The correlation was attained with fuzzy matching using different processes [25]. The original correlation by Petley is described in **Equation 2-6.**

$$Capital\ Cost\ (1988) = 55882Q^{\,0.44}N^{0.486}{T_{max}}^{0.038}{P_{max}}^{-0.02}{F_m}^{0.341}$$

Equation 2-6. Capital Cost. **Q:** capacity in tonnes/year, $\mathbf{T_{max}}$**:** maximum temperature of the process in kelvin, $\mathbf{P_{max}}$**:** maximum pressure in bars, **N:** number of functional units, F_m: factor for the material of construction.

The Capital Cost is the total expenses of the processing facilities in US dollars in 1988.

The correlation proposed by Petley is not a grass-root investment but rather only the cost of the processing facilities is considered. Additionally, the estimation is based on prices from 1988 and the location of the plant is different than the one assumed here. The correlation was updated to current prices 2018 by taking consideration of the inflation in 30 years. The inflation factor can be estimated with the Chemical Engineering Plant Cost Indexes (CEPCI). These factors are dimensional numbers used to bring up-to-date data from a different period by considering inflation through time. The CEPCI for 1988 was 342.5 and the CEPCI for 2018 is 603.1 [26]. It has been estimated that the total Outside Battery Limits (OSBL) investment is between 24-50% of the processing facilities [9]. For this case study, it was assumed that a factor of 40% would be used. Additionally, it was assumed that the plant would be built in France and the appropriate relocation factor was used.

Bearing in mind the uncertainty of the original equation and the additional factors used, the final uncertainty of the method is further increased. It has been stated that big projects are usually underestimated, and under-budgeted and real cost estimations can be represented by a log-normal distribution [27]. Therefore, in the present analysis, it was assumed that capital investment had log-normal distribution and the following probabilities were used: P10, P90 values of -20% and +120 %, which the fitting used gave -26% and +118% respectively.

The following assumptions were taken to estimate the capital cost of the project:

- Number of steps: 15
- Maximum temperature (Tmax): 473.15 K
- Maximum pressure (Pmax): 20 bar of Air, during the oxidative cleavage step
- Desired output: 10,000 ton/year of azelaic acid (total capacity of the plant is dependent on the oil type as seen in **Table 2-5**)
- Fm: 1.5
- Location Factor: 1.05 (Plant located in France)

Based on the previous information, the initial estimated cost of the processing facilities for the production plant that process palm oil is equal to 58 million $, which increases up to 81 million $ once the outside battery limits are considered. Contrary, the estimated cost of a plant that uses high oleic sunflower oil is equal to 45 million $ and 63 million $ with the outside battery limits. Additionally, once taken into consideration the uncertainty of the estimation, the log-normal distribution and the probabilities used, the average capital investment increases to 83 million $ for the high oleic sunflower plant and 106 million $ for the palm oil plant.

The use of "higher" quality raw material with "better" composition for the production of azelaic acid and pelargonic acid reduces the total capital investment costs by more than 25% (25 million $). Nevertheless, it should be also considered that the price of raw materials during the total operation of the plant are much higher. The annual purchase for both vegetable oils are around 20 million $ (average value) in a period of 10 years these costs would increase up to 200 million $ (10 year operation time and not considering inflation and price variation over time) just for the vegetable oil in any case analysed.

Additional assumptions

- The following assumptions were used in the simulation:
- Utility costs would be 10% of the total cost of the raw materials (the detailed energy demand is unknown at the moment)
- A total of 5 operators/shift and 5 shifts per day are needed
- The average labour cost of one operator is 60,000 $/y, giving a total of 3.6m $/y for the labour costs (LC). These costs are deterministic.

Additionally, the following costs were determined using factors:

- Operating supervision: 18% of LC
- Laboratory charges: 18% of LC
- Plant overhead: 60% of LC
- Administration 20% of LC

The following costs were determined based on the total capital costs (TCC) and are therefore stochastic values:

- Maintenance and repairs: 2% of TCC
- Operating supplies: 1% of TCC
- Property taxes: 2% of TCC
- Insurance:2% of TCC

The following costs were determined based on the total product sales (TPS):

- Royalties: 3% of TPS
- Distribution and selling: 10% of TPS
- Research and development: 5% of TPS
- Waste treatment was not considered in the analysis
- The discount rate was assumed to be 10%
- Tax rate equal to 35%

The initial capital investment would be done in two years and 2/3 of the investment would be performed in the first year (year 0 in the NPV)

The plant would achieve a 50% capacity in year 3% capacity in year 4% capacity in year 4 and full capacity in year 5.

2.4 Discussion

2.4.1 Monte-Carlo Simulation

A Monte Carlo simulation was performed for both palm oil and high oleic sunflower oil including the revenues and expenses previously described. A total of 3,000 iterations were used to simulate the potential outcomes of the analysis.

The average cumulative cash flow of both vegetable oils is shown in **Figure 2-7.** The initial investment of palm oil is 25% higher than the initial investment of high oleic sunflower oil. The main difference is due to the amount of oil needed to process annually. In other words, in order to achieve the same yearly throughput of azelaic acid, the plant that processes palm oil must have a capacity twice bigger compared to a plant that processes high oleic sunflower oil. The same outcome would be expected if a higher selectivity would be achieved using other technologies (smaller capacity) . Therefore, new processing technologies could reduce the amount of raw materials needed by having a higher selectivity (lower OPEX) and at the same time reduce the size of the plant (lower CAPEX). This outcome could be used for future research areas, in which the use of non-conventional processes could increase the economic success of the plant only if the selectivity of the process is increased. Additionally, if two vegetable oils have identical selectivity, it should not be assumed that the cheapest raw material would be the best performing. A raw material with a higher price, but also with a better fatty acid profile can lead to higher profits.

Other areas of technological improvement rely on the number of processing steps. In the scenario evaluated, it was assumed that a transesterification reaction was needed before performing the scission of the fatty acids. It would be more convenient from an investment and operational perspective, if the conversion of fatty acids into esters was not performed and that the reaction would be carried out directly on the oil leading to the removal of several steps reducing though the capital cost. Furthermore, fewer side-products of low value might be preferable.

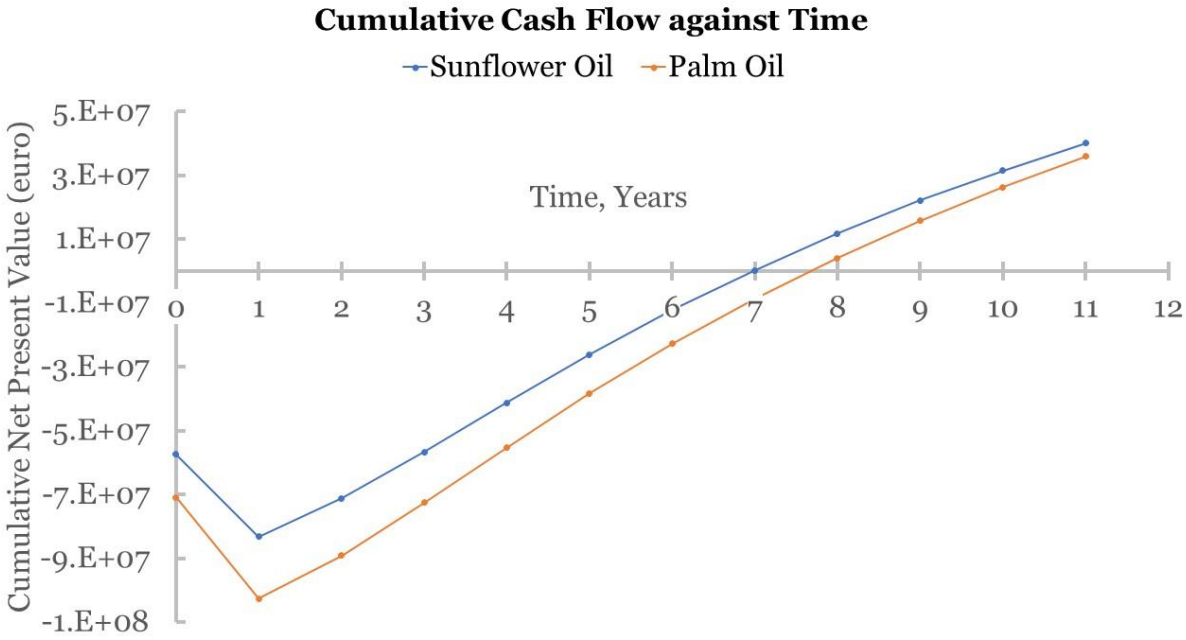

Figure 2-7. Average Cumulative Cash Flow of Monte Carlo Simulation.

Lower initial investment also reduces the payback time of the plant. In the case studies, a total of 7 years would be required to recover the investment using high oleic sunflower oil vs 8 years with palm oil **Figure 2-7.** Even though on a period higher than 20 years, the cumulative cash flow of the palm oil might be higher than the high oleic sunflower oil-based. As the future is unpredictable, an investor takes into account the risks taken initially and so, the shorter the payback time the more convincing is the investment on such a project. Additionally, the cumulative probability distribution of the NPV for both vegetable oils was generated, and it is shown in **Figure 2-8**. There are 90% probabilities of making a better profit (NPV>0) than the Internal Rate of Return (IRR) with high oleic sunflower oil vs 85% with palm oil under the current scenarios evaluated.

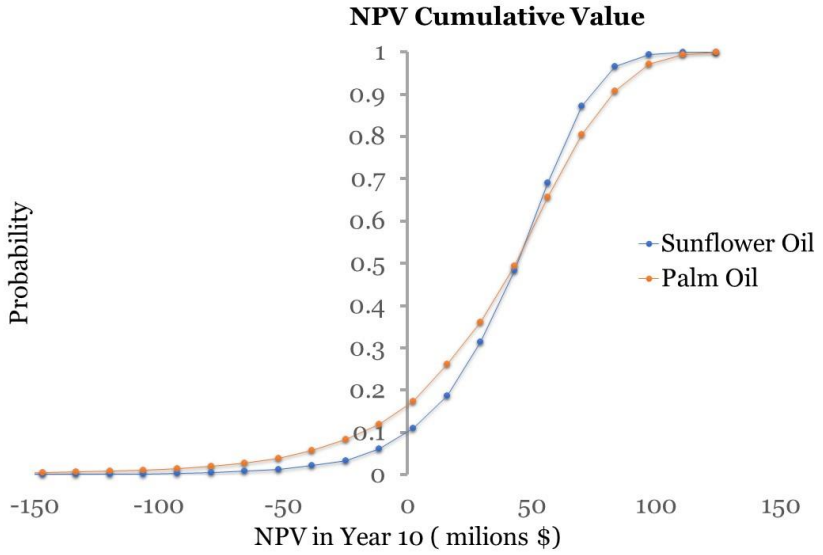

Figure 2-8. NPV Cumulative value.

Lastly, a sensitivity analysis was performed to measure the impact of uncertainty in each of the parameters analysed. The sensitivity analysis is represented with a tornado plot and can be seen in **Figure 2-9**. Through the analysis, the lower 5% and highest 95% percentile of each of the values was evaluated.

The tornado plot **Figure 2-9** clearly shows that the most impacting uncertainty variables are the azelaic acid and pelargonic acid. Moreover, capital costs and vegetable oil had also a major impact on the uncertainty of NPV. In other words, in order to improve the NPV and probability distribution, the first focus should be on increasing the production of azelaic acid and pelargonic acid by improving selectivity. Additionally, the initial capital investment could be reduced by improving efficiency with new processing technologies and/or using raw materials with a different fatty acid composition. Cost information in **Supplementary Data S.1.3**.

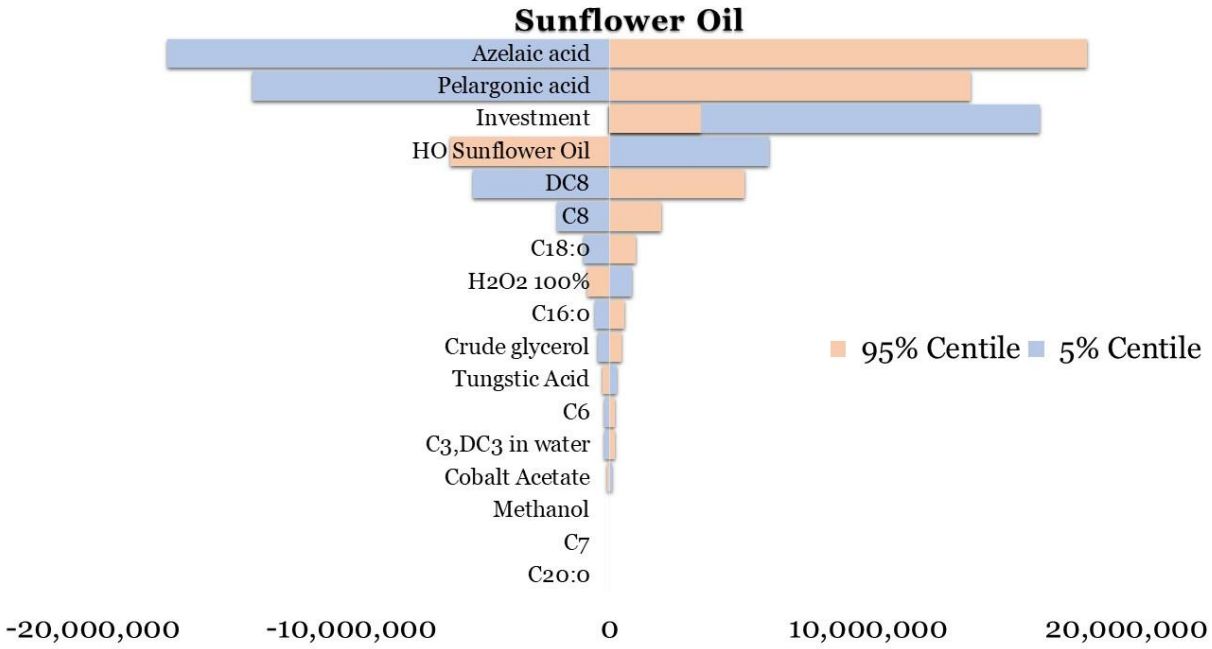

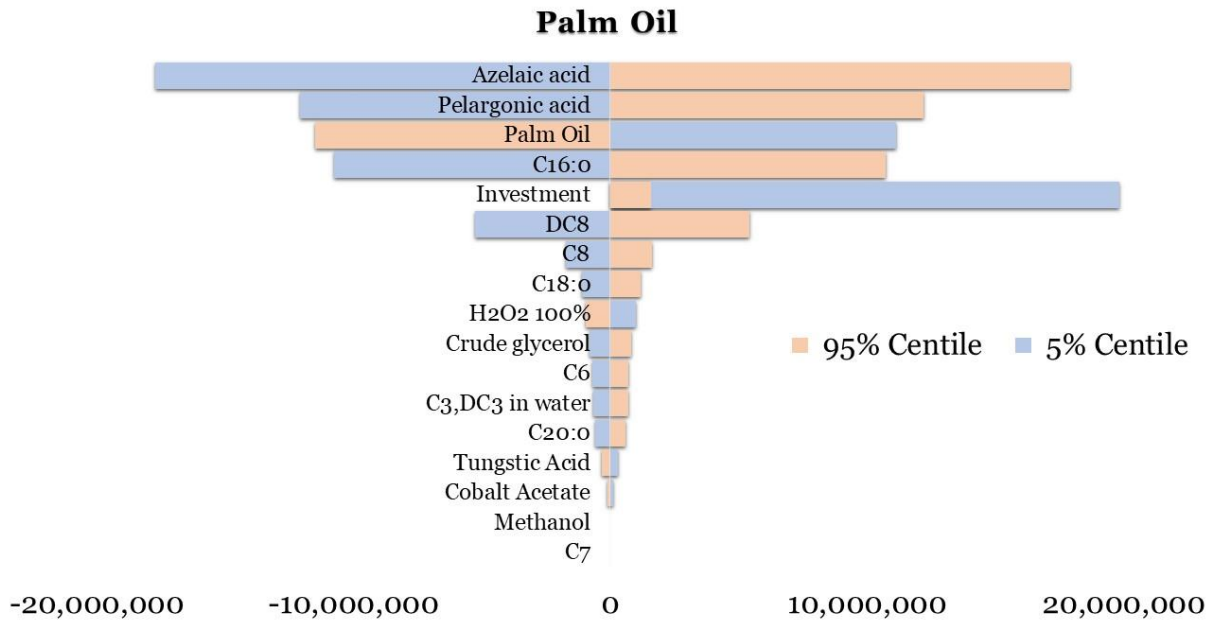

Figure 2-9. Tornado plot for the production of azelaic acid from high oleic sunflower oil and palm oil.

2.5 Conclusions

Two stochastic models were used to assess the economic feasibility of the production of azelaic acid and pelargonic acid from vegetable oils. The case study is also used as a tool to focus on research and development needs and the potential benefits of new technologies (process intensification and continuous manufacturing).

In the analysis, the composition of high oleic sunflower oil allows to produce almost twice as much azelaic acid (most valuable product) per ton of vegetable oil. Therefore, by using high oleic sunflower oil, the initial capital investment is drastically reduced and the probability of generating a profit is increased, assuming that both plants have the same process selectivity. Based on the present study, future research should focus on improving the selectivity of the reaction as the first filter to improve CAPEX and OPEX. The second filter should focus on the selection of the best performing vegetable oils depending on the fatty acid content to improve the ratio benefits vs costs. Moreover, the ideal solution should focus on maximizing the selection of lower quality oils (cheaper oils), but it would be affected by the formation of a high number of side products of low value. In the cases here exploited, although High Oleic Sunflower Oil was about 50 % more expensive than Palm Oil, it leads to higher profit. For specialty chemicals, the fatty acid profile and the value generated by coproducts, has a high impact on the selection of the right feedstock at the right price.

Other alternatives, to improve the profitability and payback time of the project, could be retrofitting an old biodiesel plant to reduce the initial capital investment or the purchase of FAMEs, to avoid the transesterification step and reduce the number of processing steps (5 process units removed) and likewise the capital investment. Ultrasound technology appears to be an essential key to overcome the need for high amount of raw materials needed and to overcome mass transfer issues associated to biphasic system as described in the following chapter. Therefore, in the next chapter we describe the exploitation of ultrasound application in the oxidative cleavage of monounsaturated compounds to obtain high value products for the chemical industry.

2.6 References

[1] J.-L. Dubois, Arkema's Integrated Plant-Based Factories, Chem. Fuels from Bio-Based Build. Blocks. (2016) 535–548. doi:10.1002/9783527698202.ch20.

[2] M. Zuk, D. Richter, J. Matuła, J. Szopa, Linseed, the multipurpose plant, Ind. Crops Prod. 75 (2015) 165–177. doi:10.1016/j.indcrop.2015.05.005.

[3] A.E. Atabani, A.S. Silitonga, H.C. Ong, T.M.I. Mahlia, H.H. Masjuki, I.A. Badruddin, H. Fayaz, Non-edible vegetable oils: A critical evaluation of oil extraction, fatty acid compositions, biodiesel production, characteristics, engine performance and emissions production, Renew. Sustain. Energy Rev. 18 (2013) 211–245. doi:10.1016/j.rser.2012.10.013.

[4] Sarbio®, (2019). https://emea.sartomer.com/en/products/sarbio-emea/?_ga=2.245545668.1397572268.1555250356-725160408.1534235200 (accessed April 14, 2019).

[5] EU Pesticides database - European Commission, (2019). http://ec.europa.eu/food/plant/pesticides/eu-pesticides-database/public/?event=activesubstance.detail&language=EN&selectedID=1634 (accessed April 14, 2019).

[6] N.J. Fox, G.W. Stachowiak, Vegetable oil-based lubricants-A review of oxidation, Tribol. Int. (2007). doi:10.1016/j.triboint.2006.10.001.

[7] A. Soutelo-Maria, J.-L. Dubois, J.-L. Couturier, G. Cravotto, Oxidative Cleavage of Fatty Acid Derivatives for Monomer Synthesis, Catalysts. 8 (2018) 464. doi:10.3390/catal8100464.

[8] D.W. Green, R.H. Perry, Perry's Chemical Engineers' Handbook, Eighth Edition, McGraw-Hill Education, 2007.

[9] M.S. Peters, K.D. Timmerhaus, R.E. West, Plant Design and Economics for Chemical Engineers, Third edition, McGraw-Hill Education, 2003.

[10] Bio-Lubricants | Natural-based Lubricants | Emery Oleochemicals, (2018). https://www.emeryoleo.com/Bio-Lubricants.php (accessed September 14, 2018).

[11] Where We Operate | Croda, (2019). https://www.croda.com/en-gb/about-us/where-we-operate (accessed April 14, 2019).

[12] P. Foley, Y. Yang, Ozonolysis operations for generation of reduced and/or oxidized product streams, US patent 2014/0031584 (A1), 30 January 2014.

[13] Novamont S.p.A. - Chimica Vivente per la Qualità della Vita, (2019). https://www.novamont.com/ (accessed April 14, 2019).

[14] A. Bieser, G. Borsotti, F. Digioia, Continuous process for the production of the carboxilic acids, 2017.

[15] A. Bieser, Borsott, G. I, F. Digioia, A. Ferrari, A. Pirocco, Continuous process of oxidative cleavage of vegetable oils, n.d.

[16] Capchem, (2019). http://www.corum.com.tw/products_more.php?c=2&v=4&d=8 (accessed April 14, 2019).

[17] J. Kawakami, M. Sakakura, Electrolyte For eletrolytic Capacitor, European patent 2 555 213, (B1) 27 December 2017.

[18] Q.A. Acton, Dicarboxylic Acids—Advances in Research and Application: 2013 Edition, ScholarlyEditions, 2013.

[19] Chemical Industry Impacted by Chinese EPA Crackdown - Chemceed, (2019). https://www.chemceed.com/industry-news/chemical-industry-impacted-chinese-epa-crackdown/ (accessed August 16, 2019).

[20] D.C. Washington, M. Jacob, S. Moore, Scythe Herbicide, 2014. http://www.epa.gov (accessed August 17, 2019).

[21] W.M. Haynes, CRC Handbook of Chemistry and Physics, 96th Edition, CRC Press, 2015.

[22] Palm oil - Monthly Price - Commodity Prices - Price Charts, Data, and News - IndexMundi, (2019). https://www.indexmundi.com/commodities/?commodity=palm-oil&months=60 (accessed August 17, 2019).

[23] Sunflower oil - Monthly Price - Commodity Prices - Price Charts, Data, and News - IndexMundi, (2019). https://www.indexmundi.com/commodities/?commodity=sunflower-oil&months=60 (accessed August 17, 2019).

[24] M. Tsagkari, J.-L. Couturier, A. Kokossis, J.-L. Dubois, Early-Stage Capital Cost Estimation of Biorefinery Processes: A Comparative Study of Heuristic Techniques., ChemSusChem. 9 (2016) 2284–97. doi:10.1002/cssc.201600309.

[25] G.J. Petley, A method for estimating the capital cost of chemical process plants : fuzzy matching, PhD Thesis, Loughborough University (UK), 1997.

[26] W.M. Vatavuk, Updating the CE plant cost index, Chem. Eng. 109 (2002) 62–70.

[27] J.K. Hollmann, Estimate accuracy: Dealing with reality, https://www.validest.com/index_htm_files/Hollmann_Accuracy.pdf (accessed August 17, 2019).

Chapter 3. Ultrasound-assisted oxidative cleavage of unsaturated fatty compound

3.1 Introduction

The **Chapter 2** describes the application of new bio-based raw material to fulfil the chemical industry needs at lower costs. The fatty acids constituents of oils have physical and chemical properties that allows the formation of suitable monomers for different applications. Among these fatty acids, the double bond present in the Mono Unsaturated Fatty Acids (MUFAs) makes them the ideal starting material for the production of specialty monomers as mentioned in the previous chapter.

Relevant monomers are Aminoundecanoic acid (A11) and Aminododecanoic acid (A12) the perfect building blocks to produce specialty polyamides.

3.1.1 Arkema and the Polyamide 11

The polyamide 11 is synthesized from castor oil, an important feedstock deeply demanded in chemical industry due to the short-term renewability by nature. The fact that ricin oleic acid represents 90% of oil constitution, make it attractive for the synthesis of high value monomers.

To synthesize the PA 11, methyl ricinoleate is produced from castor oil by methanolysis (transesterification with methanol), followed by pyrolysis of the methyl ricinoleate at 500°C to obtain methyl undecylenic acid and form heptaldehyde which, find its application in fragrances and cosmetics. Undecylenic acid is obtained through the hydrolysis of methyl undecylenate. Finally, the latter is treated with hydrogen bromide (HBr) followed by aqueous ammonia to obtain the 11-ω-aminoundecanoic acid which is used as monomer precursor of PA 11.

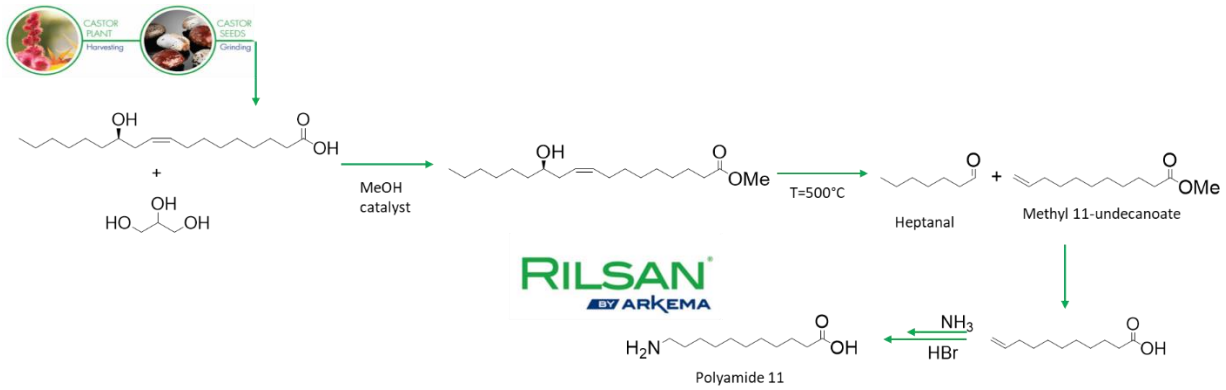

Figure 3-1. Synthesis of Polyamide 11.

In order to reduce the CAPEX of the process, Arkema has proposed two different ways to synthesize the PA 11 through metathesis (fewer steps) or by oxidative cleavage using H_2O_2 as

oxidant. In the first case an amino-ester monomer is obtained through cross metathesis (see **Chapter 4**) and in the second case, an amino-acid monomer is obtained by oxidative cleavage under solvent-free conditions (**Scheme 3-1**).

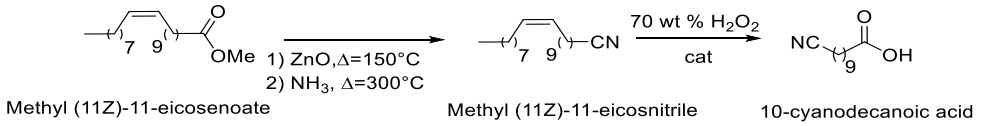

Scheme 3-1. Synthesis of the amino-acid monomer for the PA11 production from oxidative cleavage of Methyl (11Z)-11-icosenoate.

In this sense, Arkema (France) selected the unsaturated fatty nitriles as precursors of a new synthetic route to obtain the polyamide 11 (PA11) and the polyamide 12 (PA12) using H_2O_2 in a solventless multiphasic system[1]. Markush Brandhorst and Jean-Luc Dubois proposed in 2015 the obtention of amino-acid monomers from ricinoleic acid (**Scheme 3-2**).

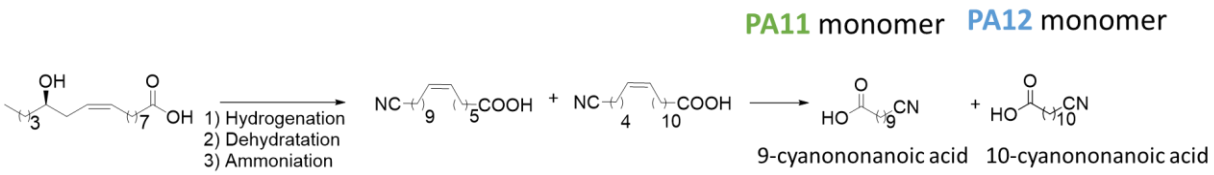

Scheme 3-2. Obtention of PA 11 and PA 12 monomers from oxidative cleavage of ricin oleic acid [1].

However, the solventless multiphasic system requires a phase transfer agent (emulsifier) to overcome mass transfer limitations. Also, the formation of undesired by-products and lack of reaction reproducibility, make the system not suitable for industrial up-scale application. In addition, the time-consuming reaction (i.e. 24h) requires high temperatures (85-95°C) to cleave the C-C bond (347-356 kJ/mole, at 398 K) to obtain the desirable monomers.

As discussed in **Chapter 2,** process intensification can be the key solution to find a faster and affordable process to produce these monomers. To overcome the obstacles, imposed by conventional systems, the ultrasound technology appears to be the ideal solution. In a biphasic system a continuous phase is produced by ultrasound irradiation, i.e. tiny droplets of one liquid (dispersed phase) are scattered into the other liquid. When the pressure of amplitude of the applied sound source reaches a certain minimum (cavitation threshold) cavitation occurs, and when this minimum is reached, the process of emulsification initiates.

3.1.2 Oleonitrile

Oleonitrile is a monounsaturated fatty nitrile obtained by condensation of oleic acid with ammonia by the same process as represented in **Scheme 3-2**. Its most known application is related to the reduction of the nitrile function to afford oleylamine or stearylamine, highly used as surfactant or surfactant precursor and more recently applied in the synthesis of nanoparticles. Some studies have been focus on the application of oleylamine as a capping agent of nanocatalysts applied in the oxidative cleavage of oleic acid [2]. The synergic effect of surfactant allied to the nanocatalyst can prevent the aggregation of particles, key-factor for the reduction of the of the catalyst activity.

On the other hand, from oleonitrile is also possible, by oxidative cleavage of the double bond in C9 and C10, to afford the precursor aminoacid monomer of PA9, the 8-cyanooctanoic acid.

3.1.2.1 *Oleonitrile reaction mechanism*

The oxidative cleavage of oleonitrile undergoes through several intermediate steps.

The first step of the reaction is the oxidation of the C=C in C9 and C10 of oleonitrile (**1**) to form the epoxide specie (**2**). The epoxide intermediate is hydrolyzed forming the intermediate diol (**3**) with concomitant C-C oxidative cleavage affording the aldehydes (**4** and **5**) and finally, by oxidation, the corresponding carboxylic acids (**6** and **7** - **Scheme 3-3**).

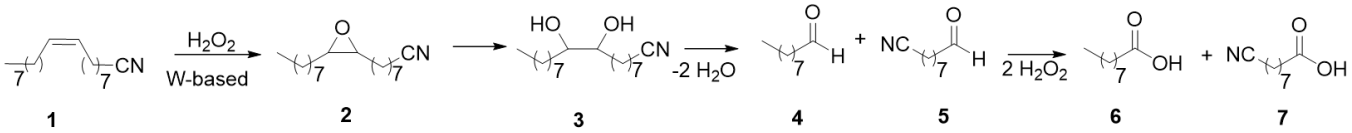

Scheme 3-3. Oxidative cleavage of oleonitrile.

3.1.3 Ultrasound in oxidative cleavage of unsaturated fatty compounds

Sandrine Rup *et al.* [3], demonstrated the obtention of 81 mol % azelaic acid and 97 mol % yield pelargonic acid under ultrasonic radiation (sonotrode 130 W, 20 KHz), in presence of RuO_4 catalyst and a phase transfer agent, Aliquat® 336 in a binary heterogeneous solvent system H_2O/ MeCN and $NaIO_4$ as co-oxidant. In their experiments they highlight the reduction of reaction time from 3h in conventional stirring to 30 minutes by ultrasonic mixing. They found as well that also in an organic-free solvent conditions (water) azelaic acid was obtained with 62 mol % yield [4,5]. Likewise, they observed the formation of a di-ketone intermediate specie. The same system was adapted to other olefin types (**Scheme 3-4** and **Table 3-1**).

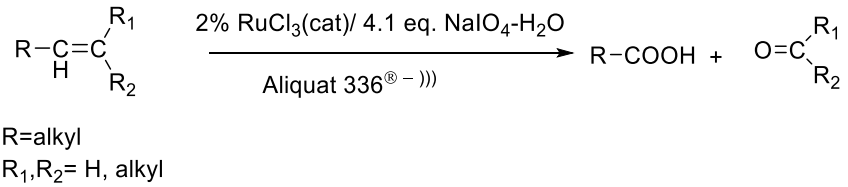

Scheme 3-4. Olefin oxidative cleavage by $Ru/NaIO_4$ – 2% Aliquat ® 336 in water under sonication [5] .

Entry	Reactant	Product	Reaction time	Yield mol %
1	1-decen	Pelargonic acid	30	76
2	1-methylcyclohexene	6-oxoheptanoic acid	15	74
3	cyclohexene	Adipic acid	20	81
5	10-undecenoic acid	Sebacic acid	45	85
6	Oleic acid	Azelaic acid Pelargonic acid	480	62 98

Table 3-1. Olefin oxidative cleavage yield products by $Ru/NaIO_4$ – 2% Aliquat ® 336 in water under sonication [5] .

3.1.3.1 *Ultrasound and phase transfer catalyst*

Some researches support that a combination of phase transfer agent and ultrasound is the ideal setup for the formation of emulsions and reaction rate improvement. In such cases, the phase transfer catalyst initiates the reaction by the transfer of species across the interface and by the ultrasound phenomenon's such as micro-jets, the surface contact area between the liquid phase and the aqueous phase is increased [6].

Maw-Ling Wang et Venugopal Rajendran proposed the application of ultrasound to improve the epoxidation of 1,7-octadiene using 28 kHz and 200 W input power along with phosphotungstic acid ($H_3PW_{12}O_{40}$), hydrogen peroxide and Aliquat 336® (trioctylmethylammonium chloride), in a liquid-liquid phase transfer catalyst (LLPTC) biphasic system.

The cavitation bubble collapse near the liquid-liquid interface, promoted by ultrasounds, disrupts the interphase and impels jets of one liquid into the other, forming fine emulsions and leading to a dramatic increase across the interfacial contact area, where transfer of species can take place.

In this chapter we discuss the study of oxidative cleavage of mono-unsaturated fatty compounds in biphasic conditions, with higher focus on the oxidative cleavage of oleonitrile to afford 8-cyanooctanoic acid, a precursor of PA9. We discuss the application of ultrasound in different systems (batch and continuous) to reduce the reaction time, the emulsifier (phase transfer agent) content, increase the selectivity of the reaction and achieve higher monomer quality.

The major reaction concerns never described in literature, are also highlighted, as for, the importance of the diol intermediate solubility and physical state in the reaction's progress.

The role of the functional group, in the success of the oxidative cleavage process, is also emphasized, as well, the decomposition of hydrogen peroxide giving some key answers to the lower monomer yields obtained after reaction.

3.2 Materials and Methods

3.2.1 General Data

Chemical Reactants

All commercially available reagents and solvents were used without previous purification. Oleic acid 90% and 84% were purchase from Merck-Sigma Aldrich and Fluka™. Methyl oleate 98%, 1-decen (99%), 10-undecenoic acid and methyl decanoate (98%) were purchase from Merck-Sigma Aldrich. Oleonitrile (75%) and the (Z)-octadec-11-ene-1-nitrile (Z)-octadec-11-ene-1-nitrile (86%), were produced in the R&D laboratories of Arkema Rhône-Alpes Research Center France (CRRA). The solvents, methanol and ethyl acetate were purchase from Merck-Sigma Aldrich. Hydrogen peroxide 35 and 70 weight % was produced in the Hydrogen Peroxide plant of Arkema Jarrie (France). Aliquat 336® and the hexadecylpiridinium bromide and chloride were purchase from Merck-Sigma Aldrich and Alfa Aesar. Permanganate potassium (99%) was purchase from Carlo Erba.

3.2.2 Instrumentation and acquisition parameters

3.2.2.1 Chromatographic analysis

Gas chromatography was performed using a gas chromatograph 7890B Series GC System Agilent equipped with a flame ionisation detector and an autosampler. 1 µL aliquot of the samples was injected. The retention gap was attached to a 30 m x 0.250 mm ID column filled with a 0.250 µm film thickness HP-5 ms stationary phase. The initial oven temperature was set at 60 °C for 2min and increased to 280°C °C at a rate of 15 °C/min. The injector and detector temperatures were set at 280 °C and 320 °C, respectively. Helium was used as the carrier gas for the mobile phase at a flow control from 3.5 mL for 8 minutes and increased to 6.0 mL/min with a rate of 0.25 mL/min/min and hold time of 22 minutes. The column was backflushed at 320 °C for a total of 4 void volumes after every run to prevent the appearance of ghost peaks from previous runs.

GC/MS analysis were performed in a GC Agilent 6890 (Agilent technologies, Santa Clara, CA, USA) coupled with a mass detector Agilent Network 5973, using a 30 m capillary column, i.d. of 0.25 mm and 0.25 µm of film thickness HP-5 5% Phenyl Methyl Siloxane stationary phase. The initial oven temperature of 60 °C was increased to 165 °C at a rate of 15 °C/min, then to 200 °C at a rate of 4 °C/min until 200°C and finally increased to 300 °C at a rate of 25 °C/min with a hold time of 10 minutes. The injector and detector temperatures were set at 250°C and 280 °C, respectively.

Helium was used as the carrier gas for the mobile phase with a flow of 1.3 mL/min. The column was backflushed at 300 °C for a total of 3 void volumes after every run to prevent the appearance of ghost peaks from previous runs.

a) Determination of conversion rate of unsaturated fatty compounds (C_{UFC})

The conversion of the unsaturated fatty compounds (UFCs) and the yield of the oxidative cleavage products was obtained through the peak areas from the samples analyzed by Gas Chromatography with flame ionisation detector (GC-FID). The saturated fatty compounds such as palmitic (C16:0) and stearic (C18:0) compounds do not react in the oxidant system and do not influence the conversion of the monounsaturated fatty compound. However, stearic compounds (C18:0) were took in account as internal standard in order to obtain a more accurate quantification.

$$C_{UFC} = \frac{\frac{A^{i}_{UFC(C18:1)}}{A^{i}_{SFC(C18:0)}} - \frac{A^{f}_{UFC(C18:1)}}{A^{f}_{SFC(C18:0)}}}{A^{i}_{UFC(C18:0)}} x100$$

Equation 3-1. Conversion of Unsaturated fatty compound in the oxidative cleavage reaction. $\boldsymbol{A^{i}_{UFC(C18:1)}}$: peak area of the monounsaturated fatty compound in t=0. $\boldsymbol{A^{f}_{UFC(C18:1)}}$: peak area of the monounsaturated fatty compound $C_{18:1}$ in the end of the reaction. $\boldsymbol{A^{i}_{SFC(C18:0)}}$: Peak area of saturated fatty compound $C_{18:0}$ at t=0. $\boldsymbol{A^{f}_{SFC(C18:0)}}$: Peak area of saturated fatty compound C_{180} at the end of reaction.

b) Oxidative cleavage yield products

The yield of the oxidative cleavage products was calculated from Internal Standard Calibration methodology which compare the instrument response from the target compounds in the sample to the responses of the reference standards added to the sample extracted before injection. In our studies we added hexanoic acid as internal standard.

$$RF = \frac{A_{IS}\, x\, m_{SC}}{m_{IS}\, x\, A_{SC}}$$

Equation 3-2. RF: Response factor, $\boldsymbol{A_{IS}}$: Peak area of internal standard, $\boldsymbol{m_{IS}}$ **:** mass of internal standard. $\boldsymbol{m_{SC}}$: mass of specific compound of interest and $\boldsymbol{A_{SC}}$: Peak area of specific compound of interest.

The mass of the products can be obtained from the calibration curve:

$$m_{SC} = RFx\left(\frac{A_{SC}}{A_{IS}} + b\right) x\, m_{IS}$$

Equation 3-3. Quantification of specific compound of interest. $\boldsymbol{m_{SC}}$: mass of oxidative cleavage product. $\boldsymbol{m_{IS}}$: mass of internal standard.

c) Kinetic studies evaluation:

The species in the reaction media were quantified according to the relative peak area detected by GC-FID. The stereonitrile (NC18:0) and the methyl stearate (C18:0) present in the reactants oleonitrile and oleic acid respectively were assumed as internal standard.

The pentadecanoic acid was used as internal standard in the oxidative cleavage of 1-decen, 1-decenoic acid and methyl 1-decenoate.

$$specie\ relative\ peak\ area\ = \frac{A^{t=n}_{UFC(C18:1)}}{A^{t=n}_{SFC(C18:0)}}$$

Equation 3-4. Relative peak area of specie analysed. $\boldsymbol{A^{t=n}_{UFC(C18:1)}}$: peak area of the monounsaturated fatty compound $C_{18:1}$ in time n. $\boldsymbol{A^{t}_{SFC(C18:0)}}$: Peak area of saturated fatty compound $C_{18:0}$.

3.2.2.2 *Nuclear Magnetic Resonance (NMR)*

^{1}H-RMN and ^{13}C-RMN spectra were recorded in $CDCl_3$ or d6-DMSO (Euriso-Top, Saint Aubin, France) NMR spectra were recorded with a Bruker 300 Avance (300 MHz and 75 MHz for ^{1}H and ^{13}C, respectively) at 25 °C. Chemical shifts were calibrated to the residual proton and carbon resonances of the solvent; $CDCl_3$ (δH = 7.26, δC = 77.16) and DMSO (^{1}H=2.54, ^{13}C=40.45 ppm).

3.2.2.3 *Infra-Red Spectroscopy*

Infrared spectrum was traced on a spectrophotometer Perkin Elmer model Spectrum 1000 FT-IR. The samples were analyzed in NaCl pellets.

3.2.2.4 *Viscosity measurements*

An Brokfield viscometer (model DV-III + Rheometer V5.0 LV External Control) was used to measure the viscosity of oleic acid 85% and oleonitrile 78% at 25°C and 60°C. Samples (8 mL) were injected in a Spindle (SC4-18) and the viscometer automatically calculated the kinematic viscosity ($mPa.s^{-1}$). All measurements were made in triplicate and the average results are reported.

3.2.2.5 *Melting points*

The melting points were measured in a Stuart SMP 20 devices.

3.2.3 Ultrasonic devices

3.2.1.2 *Ultrasonic tank reactor*

The ultrasonic tank system consisted in an ultrasonic stainless steel tank (9.3 cm x 28cm x 20cm), lent by Weber Ultrasonics ™, with two SONOPLATE® devices, connected with two different ultrasonic generators (MG Multi resonance frequencies in the range 40-120 kHz and one with fix frequency at 25 kHz) both with a maximum of output power of 200 W.

3.2.1.3 *Cup-horn sonoreactor*

The ultrasonic cup-horn system was made up of a jacketed stainless-steel reaction cell (internal diameter x height: 119 x 140 mm) equipped with a piezoelectric ceramic set at the bottom of the jacketed chemical reactor. The low frequency transducer consisted of a resonance frequency of 22 kHz and Input power of 200 W (Synaptec, Lewennes, France). Cooling was carried out by water circulation.

3.2.1.4 *Titanium horn sonoreactor*

The ultrasonic horn reactor system was constituted by a piezoelectric transducer with resonance frequency of 20.1 kHz connected with an ultrasonic generator (Nautilus) with an output power of 100 W. (In presence of 25 mL deionized water and sonication time of 15 minutes (by pulse): $P_{acoust.\ vol}$ = 1.05 W/mL^{-1} for P_{ele} = 20 W).

3.2.1.5 *High speed mixer*

The HSM (Magic Lab, by IKA Germany) is modular laboratory system especially designed for mixing. The system configuration is composed by three rotors with orifice dimensions of 170 mm x 270 mm x 235 mm. The configuration of the system includes a cooling system to disperse the heat released, generated by the rotors and the operating unit, and control the operating parameters such as temperature, rotor speed (14600 rpm) and rotation time (3000-26000 rpm).

3.2.1.6 *Ultrasonic System for flow apparatus*

The ultrasonic system was composed by a sonotrode with diameter of 18 mm (T18 HT HP) constituted by titanium, aluminium and vanadium: TA6V ELI, a piezoelectric transducer with fix frequency at 25 kHz and an ultrasonic cell (18 mL) jacketed stainless steel (Synetude, Cogni, France). The piezoelectric transducer, with a resonance frequency of 20 kHz, was cooled down with industrial air and the ultrasonic cell with water circulation at 25°C. A generator (230 V 50/60 Hz 800W) was

used to supply energy to the low frequency transducer (In presence of 18 mL deionized water and sonication time of 6 minutes: $P_{acoust.\ vol} = 0.35\ W/mL^{-1}$ for $P_{ele} = 6.28\ W$).

3.2.1.7 *Calorimetric measurements*

Acoustic Power of ultrasonic tank reactor was determined in deionized water using calorimetry for 10 minutes irradiation and 5 minutes cooling under silent conditions according to the procedure described by Margulis [7,8]. The temperature was measured by a Thermocouple Probe Temperature sensor type K coupled to a digital temperature controller.

3.2.1.8 *Hydrogen peroxide quantification*

The content of hydrogen peroxide in the reactant's solution prepared and its decomposition over the reaction time was quantified by the permanganate potassium titration method. A 100 µL sample of aqueous solution was diluted in 10 mL of deionized water and 15 mL of 35% w/v H_2SO_4. While stirring the aqueous solution was titrated with potassium permanganate (0.05 mol/L) until achieved a persistent pink coloration. The experiment was replicated 3x under identical conditions.

3.2.2 Oxidative cleavage of mono-unsaturated long-chain compounds

3.2.2.1 *Silent conditions*

3.2.2.1.1 General procedure for oxidative cleavage of monounsaturated long-chain compounds in absence of phase transfer agent (24h reaction time) solvent-free conditions

a) In-situ catalyst

A 250 cm^3 double-jacket reactor is charged with the unsaturated fatty compound (**Table 3-2**) and the tungsten-based catalyst (**Table 3-3**). The reaction media is stirred at 1000 rpm and heated to 70°C. This temperature was thermostatically controlled by circulation of water. The reactor was continuously and dropwise feed with hydrogen peroxide 35 to 70 wt % (6 eq.), by a peristaltic pump. After one hour, an air flow rate of 400 mL/min was circulated in the reaction mixture via a Teflon tube. At the same time, the valve on the "Dean-Stark" was opened in order to collect the water present in the reaction mixture obtained due to degradation of H_2O_2. Hydrogen peroxide was added dropwise for a total time of 5h and the reaction stopped after 24h. The aqueous phase was separated from the organic phase. The organic phase was washed with demineralized water several times until the weight % of H_2O_2 measured was lower than 0.2 wt %. The organic phase was then concentrated under reduced pressure. The organic phase and remaining products were analyzed and quantified (internal standard method) by GC-FID.

Substrate	mmol	g
Oleonitrile (77 %)	293	100.38
Oleic acid (95%)	342	101.2

Table 3-2. Monounsaturated compound reactor loading.

Catalyst	mmol	g	Eq.
H_2WO_4	5.84	1.46	2 %
$H_3PW_{12}O_{40}$	5.72	16.48	2 %

Table 3-3. W-based catalyst reactor loading. Eq.: mol catalyst/mol monounsaturated fatty compound. **Eq**.=mol catalyst/mol monounsaturated compound.

b) Catalyst dissolved in the oxidant mixture

The tungsten-based catalyst (2 eq.%) (**Table 3-3**) was dissolved in an aqueous solution of 35 to 70 wt % hydrogen peroxide (6 eq.) and stirred at room temperature for 30 minutes (oxidant solution). The monounsaturated fatty compound was charged in a 250 cm^3 double jacket. The reaction media was stirred at 1000 rpm and heated to 70°C. This temperature was maintained thermostatically controlled by circulation of water. The reactor was continuously drop wisely fed with the oxidant solution, by a peristaltic pump. After one hour, an air flow rate of 400 mL/min was circulated in the reaction mixture via a Teflon tube. Hydrogen peroxide was added dropwise for a total time of 6h and the reaction stopped after 24h. The aqueous phase was separated from the organic phase. The organic phase was washed with demineralized water several times until the weight % of H_2O_2 measured was lower than 0.2 wt %. The organic phase was then concentrated under reduced pressure. The organic phase and the remaining products were analysed and quantified (internal standard method) by GC-FID.

3.2.2.1.2 General procedure for oxidative cleavage of monounsaturated long-chain compounds in presence of a phase transfer agent (24h reaction time)

The tungsten-based catalyst (2 eq. %) **(Table 3-3)** was dissolved in an aqueous solution of hydrogen peroxide (6 eq.), stirred at room temperature for 30 minutes (oxidant solution). The monounsaturated fatty compound (**Table 3-4**) and the phase transfer agent, were charged in a 250 cm^3 double jacket. The reaction was followed with the same protocol applied in **3.2.2.1.1b)**. Extraction of the organic phase and compounds quantification and identification were followed as described in **3.2.2.1.1b)**.

Substrate	mmoles	g
Oleonitrile (77 %)	293	100.38
Oleic acid (95%)	342	101.2
Methyl oleate (99%)	334	100.5
(Z)-octadec-11-ene-1-nitrile		
(Z)-octadec-11-ene-1-nitrile	260	80
(86%)		
Decen-1-ene (98%)	18.9	26.5
Methyl decanoate (99%)	377	70.38
10-undecenoic acid (98%)	378	69.92

Table 3-4. Monounsaturated compound reactor loading.

Phase transfer agent	mmoles	g
Aliquat 336®	5.6	2.32
$C_{21}H_{38}ClN.\ xH_2O$	5.8	1.94
$C_{21}H_{38}BrN.\ xH_2O$	5.7	2.19

Table 3-5. Phase-transfer agent tested in the catalytic system.

3.2.2.1.3 *General procedure for oxidative cleavage of monounsaturated fatty compounds in presence of phase transfer agent (5h reaction time)*

The phosphotungstic acid (5.72 mmol, 2 eq. %) was dissolved in an aqueous solution of 35 or 70 wt% hydrogen peroxide (6 eq.), stirred at room temperature for 30 minutes (oxidant solution). The monounsaturated fatty compound (**Table 3-6**) and the phase transfer agent were charged in a 250 cm^3 double jacket. The reaction media was stirred at 1000 rpm and heated to 60°C. This temperature was maintained constant and thermostatically controlled by circulation of water. The reactor was continuously and dropwise feed with the pre-mixed solution of the tungsten-based catalyst dissolved in hydrogen peroxide by a peristaltic pump for 2h. The aqueous phase was separated from the organic phase. The organic phase was washed with demineralized water several times until the weight % of H_2O_2 measured was lower than 0.2 wt %. The organic phase was then concentrated under reduced pressure. The organic phase and remaining products were analysed and quantified (internal standard method) by GC-FID.

Substrate	mmoles	g
(Z)-octadec-9-enenitrile (77 %)	293	100.38
cis-9-octadecenoic acid (95%)	342	101.2
Methyl cis-9-octadecenoate (99%)	334	100.5
(Z)-octadec-11-ene-1-nitrile (Z)-octadec-11-ene-1-nitrile (86%)	260	80
Decen-1-ene (98%)	18.9	26.5

Table 3-6. Monounsaturated compound reactor loading.

Phase transfer agent	moles	g	Eq.
Aliquat 336®	5.84 mmoles	1.460	2 %
$C_{21}H_{38}BrN.xH_2O$	5.5 mmoles	1.035	2 %

Table 3-7. Phase transfer agent reactor loading. Eq: mol catalyst/mol monounsaturated fatty substrate. Eq.: mol PTA/mol monounsaturated fatty compound.

3.2.2.1.4 General procedure for oxidative cleavage of monounsaturated long-chain compounds in organic solvent without phase transfer agent (24h reaction time)

Phosphotungstic acid (3.11 mmol, 2 eq. %) was dissolved in hydrogen peroxide 35 wt % (6 eq.) and stirred at room temperature for 30 minutes.

The monounsaturated fatty compounds (**Table 3-8**) and the organic solvent (**Table** 3-9**)** were charged in a 250 cm^3 double jacket pyrex reactor. The reaction media was stirred at 1000 rpm and heated to 60°C. This temperature was maintained constant and thermostatically controlled by water circulation. The reactor was continuously fed and dropwise with a pre-mixed oxidant solution by a peristaltic pump for 6h. The aqueous layer was separated from the organic phase. The latter was washed with deionized water several times until the weight % of H_2O_2 measured was lower than 0.2 wt %. The organic phase was then concentrated under reduced pressure. Organic phase and remaining products were analysed and quantified (internal standard method) by GC-FID.

Substrate	mmol	g
cis-9-octadecenoic acid (95%)	137	40.78
1-Decene (98%)	378	53

Table 3-8. Monounsaturated fatty compound reactor loading.

Solvent	mmol	g	Eq.
2-methylpropan-2-ol	137	40.78	2
undec-10-enoic acid (98%)	378	70.38	2

Table 3-9. Solvent reactor loading. Eq: mol reactant/mol monounsaturated fatty substrate.

3.2.2.2 *Oxidative cleavage of unsaturated fatty compounds under ultrasonic conditions – Indirect sonication (ultrasonic tank)*

3.2.2.2.1 Oxidative cleavage of unsaturated fatty compounds in the absence of phase transfer agent

Into a 50 mL 3-neck round bottom flask, the monounsaturated fatty compound (**Table 3-10**) was added and sonicated for 10 minutes. A mixture of the tungsten-based catalyst (**Table 3-11**) and 35 wt % H_2O_2 (266 mmoles, 6eq.), previously mixed for 30 minutes at room temperature, was added drop wisely for 2 h to the reaction mixture. The biphasic system was subject to a 25 or 120 kHz ultrasonic irradiation and input power of 200 W, for 5h at 54°C. After reaction the aqueous phase was separated from the organic phase. During the reaction samples were taken and quenched with deionized water and the organic phase decanted followed by analysis by gas-chromatography (GC-FID) with flame ionisation. In order to avoid the existence of residual H_2O_2, the organic phase was extracted with H_2O deionized (3 x 10 mL). The presence of residual H_2O_2 in the water solution extraction fractions was quantified by permanganate titration method. After the content of H_2O_2 detected was lower than 0.2 wt% detected the organic phase was concentrated under reduced pressure. The organic phase was analysed by GC-FID for quantification by internal standard method (hexanoic acid used as internal standard).

Substrate	mmoles	g
(Z)-octadec-9-enenitrile (77 %)	44.3	15.18
cis-9-octadecenoic acid (95%)	54	15.2
Methyl cis-9-octadecenoate (99%)	33.7	11.53

Table 3-10. Monounsaturated long-chain compound reactor loading.

Catalyst	mmoles	g	Eq.
H_2WO_4	0.9	0.24	2 %
	10	2.40	20 %
$H_3PW_{12}O_{40}$	0.9	2.49	2 %

Table 3-11. W-based catalyst reactor loading. Eq: mol catalyst/mol monounsaturated fatty substrate.

3.2.2.2.2 General procedure for oxidative cleavage of monounsaturated fatty compounds in the presence of phase transfer agent

The unsaturated fatty compounds and the tungsten-based catalyst were added with the same procedure as **3.2.2.1.2.** with the phase transfer agent (**Table 3-7**). The reaction was followed with the same protocol applied in **3.2.2.1.2..** Extraction of the organic phase and compounds quantification and identification were followed as described in **3.2.2.1.2.**

3.2.2.3 *Oxidative cleavage of unsaturated fatty compounds under ultrasonic conditions – direct sonication (ultrasonic sonotrode)*

3.2.2.3.1 General procedure for oxidative cleavage of monounsaturated fatty compounds in absence of phase transfer agent

The reactants were introduced into a 3-neck round bottomed flask (**Table 3-12**) in the same procedure as described in **3.2.2.1.3**. The biphasic system was sonicated at 20 kHz and input power of 100W, to direct ultrasonic irradiation for 5h. In order to cool the reaction system, the flask was immersed in an ice bath. Reaction temperature rose from 35°C to 60°C in 5h reaction time. In the

reaction work-up the aqueous layer was separated from the organic phase. During the reaction, samples were taken and quenched with deionized water and the decanted organic phase was concentrated and analysed by GC-FID. In order to get rid from residual H_2O_2, the organic phase was extracted with deionized H_2O (3 x 10 mL). The presence of residual H_2O_2 in the water solution extraction fractions was quantified by permanganate titration method. Once H_2O_2 content was lower than 0.2 wt% the organic phase was concentrated under reduced pressure. The organic phase was analysed by GC-FID for quantification by internal standard method (hexanoic acid used as internal standard).

Substrate	mmol	g
(Z)-octadec-9-enenitrile (77 %)	42	14.41
cis-9-octadecenoic acid (95%)	54.17	18

Table 3-12. Monounsaturated fatty compound reactor loading.

Catalyst	moles	g	Eq.
H_2WO_4	0.84 mmoles	0.28	2 %
	11.56 mmoles	2.86	20 %
$H_3PW_{12}O_{40}$	1 mmoles	2.85	2 %

Table 3-13. W-based catalyst reactor loading. Eq: mol catalyst/mol monounsaturated fatty substrate.

Note: The characterisation of products and by/co-products were determined by GC/MS and the yields were determined by internal standard method as previously described considering the same response factor for the aldehydes.

3.2.2.3.2 General procedure for oxidative cleavage of monounsaturated fatty compounds in presence of phase transfer agent

The reactants were introduced into a 3-neck round bottomed flask in the same procedure as described in **3.2.2.1.2.** At the end of the reaction the organic layer and aqueous phase were treated and analysed as described in **3.2.2.1.2.** .

Note: The characterisation of the products and by/co-products was carried out by GC/MS and the yield were determined by internal standard method as described previously considering the same response factor for the aldehydes.

Substrate	mmol	g
(Z)-octadec-9-enenitrile (77 %)	43.71	15
cis-9-octadecenoic acid (95%)	52.98	17.6

Table 3-14. Monounsaturated fatty compound reactor loading.

3.2.2.3.3 Oxidative cleavage of unsaturated fatty compounds under direct sonication (ultrasonic sonotrode) with pre-emulsification

The phosphotungstic acid (1.9% mol eq.,1 mmol) was dissolved in 35 wt% H_2O_2 and stirred at room temperature for 30 minutes. The oxidant solution was added dropwise to a dispersor IKA®magic LAB® filled with the monounsaturated fatty compound **(Table 3-15**). The mixture was stirred at 1600 rpm.min^{-1} for 1h. Temperature rose from 27 to 70°C. After 2h the reaction media was sonicated at 29 kHz with the ultrasound horn for 3h.

Substrate	mmol	g
(Z)-octadec-9-enenitrile (77 %)	42	14.41
cis-9-octadecenoic acid (95%)	54.17	18

Table 3-15. Monounsaturated fatty compound reactor loading.

3.2.2.3.4 Oxidative cleavage of unsaturated fatty compounds under direct sonication (Cup Horn)

The reactants were introduced into the cup horn in the same procedure as described in **3.2.2.2.1**. The reaction mixture was sonicated under 24 kHz and 200W of input power for 5h. The exothermic reaction was controlled with a cooling system filled with water in the double-jacket reactor. At the end of the reaction the organic phase and aqueous phase were treated and analysed as described in **3.2.2.2.1.**

3.2.2.4 *Oxidative cleavage of oleonitrile under continuous ultrasonic system*

The tungsten-based catalyst (2 eq.%) was dissolved in an aqueous solution of hydrogen peroxide (6 eq, 1.07 moles), solution stirred at room temperature for 30 minutes (oxidant solution). The oleonitrile (214 mmoles, 56.4g) was charged in a 250 cm^3 double jacket reactor. The reaction media was stirred at 1000 rpm and heated to 60°C. The reactor was continuously and drop wisely fed with the oxidant solution, by a peristaltic pump for 2h. After 2h reaction in the stirrer tank reactor (**STR1**), the reaction media was pumped by a piston pump with a flow of 18 mL/min to the ultrasound reactor and the reaction mixture was sonicated at 20.3 kHz (50% or 100% Amplitude) ultrasonic irradiation for a contact time of 1 minute. After sonication the reaction mixture was collected in a second stirred tank reactor (**STR2**) cooled at room temperature in order to collect samples after ultrasound irradiation. After the reaction mixture was completed recovered in **STR2**, was drained to the **STR1** at 60°C and pumped to a new cycle to the ultrasonic system (**Figure 3-2**). After 6 cycles, the aqueous phase was separated from the organic phase by decantation. The organic phase was washed with demineralized water several times until the weight % of H_2O_2 measured was lower than 0.2 wt %. The organic layer was then concentrated under reduced pressure. The organic phase and the remaining products were analysed and quantified (internal standard method) by GC-FID.

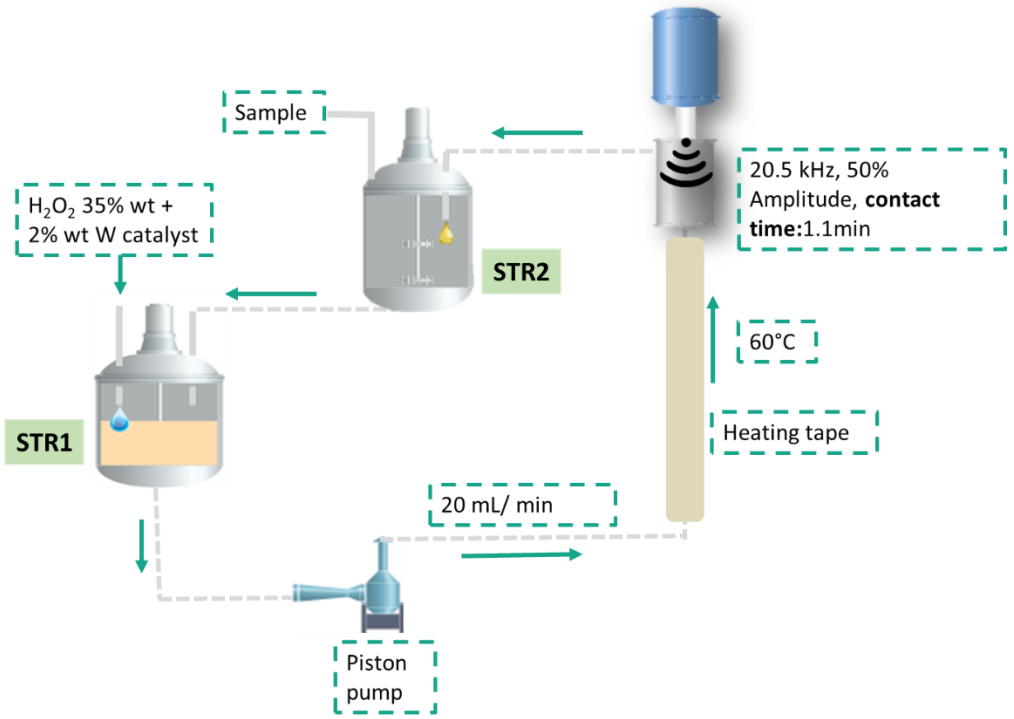

Figure 3-2. Continuous ultrasonic system.

3.2.3 Products characterization

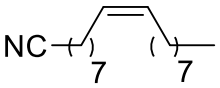

Z-octadec-9-enenitrile ($C_{18}H_{33}N$) (75%): ^{1}H NMR (δ ppm, CDCl3, 400 MHz,298 K): δ: 5.28 (m, 2H, CH=CH_2), 2.27 (t, J = 6 Hz, 2H, CH_2CN), 2.11 (m, 4H, CH_2CH=CH), 1.95 (m, 2H, CH_2CH_2CN), 1.59 (m, 2H, $CH_2CH_2CH_2$CN), 1.35–1.20 (m,CH_2 chain), 0.87 (t, J = 6 Hz, 3H, CH_3CH_2) ppm.

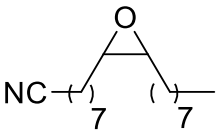

8-(3-octyloxiran-2-yl)octanenitrile ($C_{18}H_{33}NO$):

m/z: M^+ 280, 155 ($C_{10}H_{19}O^+$), 134 ($C_9H_{15}N^+$), 55.

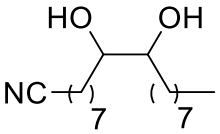

9,10-dihydroxyoctadecanenitrile ($C_{18}H_{35}NO_2$)*:

m/z (di-TMS derivative): 226 ($C_{12}H_{24}NOSi^+$) , 215 ($C_{12}H_{27}OSi^+$), 73.

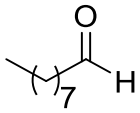

Nonanal ($C_9H_{18}O$)*:

m/z: 114 ($C_8H_{15}^+$) 98 ($C_7H_{15}^+$), 70 ($C_5H_{11}^+$), 57 ($C_3H_5O^+$)

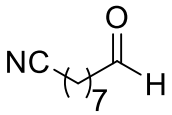

10-oxodecanenitrile ($C_9H_{15}NO$):

m/z:: M^+ 209, 124 ($C_8H_{15}^+$), 110 ($C_7H_{12}N^+$), 82 ($C_5H_8N^+$), 41($C_2H_8N^+$).

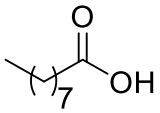

Pelargonic acid ($C_9H_{18}O_2$):

m/z (di-TMS derivative): M^+ 230, 215 ($C_{11}H_{23}O_2Si^+$), 117 ($C_4H_9O_2Si^+$).

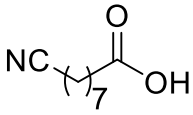

8-cyanooctanoic acid ($C_9H_{15}NO_2$)*:

m/z (di-TMS derivative): 226 ($C_{11}H_{20}NO_2Si^+$), 117 ($C_4H_9O_2Si^+$).

Note: *- The molecular ion for the respectives molecules was not detected due to the detection mode used in the analytic method. However, the fragmentation patterns sustain the identification of the compounds.

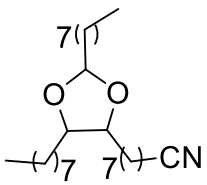

8-(2,5-dioctyl-1,3-dioxolan-4-yl)octanenitrile ($C_{27}H_{51}NO_2$)*:

m/z (di-TMS derivative): M^+420, 308 ($C_{19}H_{34}NO_2^+$)

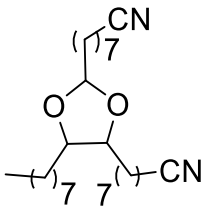

8-(2,5-dioctyl-1,3-dioxolan-4-yl)dioctanenitrile ($C_{27}H_{51}N_2O_2$)*:

m/z (di-TMS derivative): M^+431, 308 ($C_{19}H_{34}NO_2^+$), 280 ($C_{18}H_{33}NO^+$).

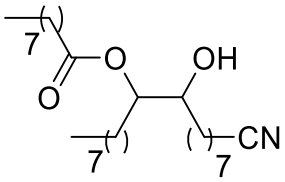

1-cyano-8-hydroxyheptadecan-9-yl nonanoate ($C_{27}H_{51}NO_3$)*:

m/z (di-TMS derivative): 385 ($C_{22}H_{45}O_3Si^+$), 228 ($C_{13}H_{28}OSi^+$),215 ($C_{12}H_{27}OSi^+$).

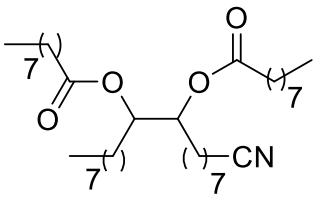

1-cyanoheptadecane-8,9-diyl dinonanoate ($C_{36}H_{67}NO_4$)*:

m/z (di-TMS derivative): 420 ($C_{27}H_{50}NO_2^+$), 308.

3.3 Results and Discussion

3.3.1 Reaction parameters choice

The catalytic system was based on different parameters such as reduction of reaction time and oxidant concentration in order to apply to this system, the ultrasound technology in safe conditions. Firstly, reaction parameters in solvent-free and silent conditions were optimized based on the previous conditions described by Markush *et all.* [1] .

3.3.2 Optimization of conventional reaction conditions

Herein it is aimed to describe the oxidative cleavage of oleonitrile and oleic acid optimization study in conventional conditions (silent conditions).

Reaction's mass transfer challenges and difficult reaction heating control are described. The discovery of the importance of the 9,10-dihydroxystearic acid/nitrile intermediate in the rate of the reaction and in the formation of new high molecular weight molecules is a crucial key-factor that has been missing in the oxidative cleavage experiments described in the existent literature.

The influence of the catalyst (tungsten based), phase transfer agent and hydrogen peroxide concentration in the oxidative cleavage of oleonitrile, in particular, was studied.

3.3.2.1 *Mixing speed*

The effect of varying stirring speed on the rate of the epoxidation of oleonitrile (**Scheme 3-5**) was studied in the range of 500 to 1500 rpm. The reaction conditions applied were the addition of an oxidant mixture comprised by 2% eq. (mol cat/mol oleonitrile) and 1 eq. of 70 wt % H_2O_2 added drop wisely for 1 hour (**Scheme 3-5**) .

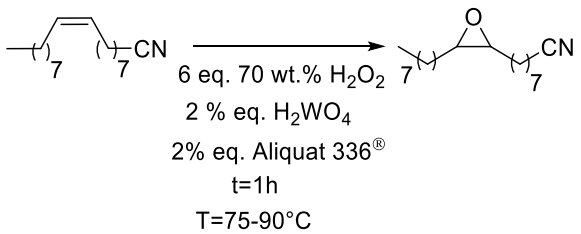

Scheme 3-5. Epoxidation of oleonitrile.

As shown in **Figure 3-3,** no improvement in the reaction rate was observed with the different stirring speeds tested. At these stirring agitations, mass transfer effects are, to all intents and purposes, removed. The graph also shows that the reaction rate is relatively slow compared to the mass

transfer rate. The results indicate that the chemical reaction is a rate determining step. Therefore, to avoid any mass transfer effect and due to the slightly higher oleonitrile conversion results obtained with the 1000 rpm stirring speed was chosen for the oxidative cleavage experiments.

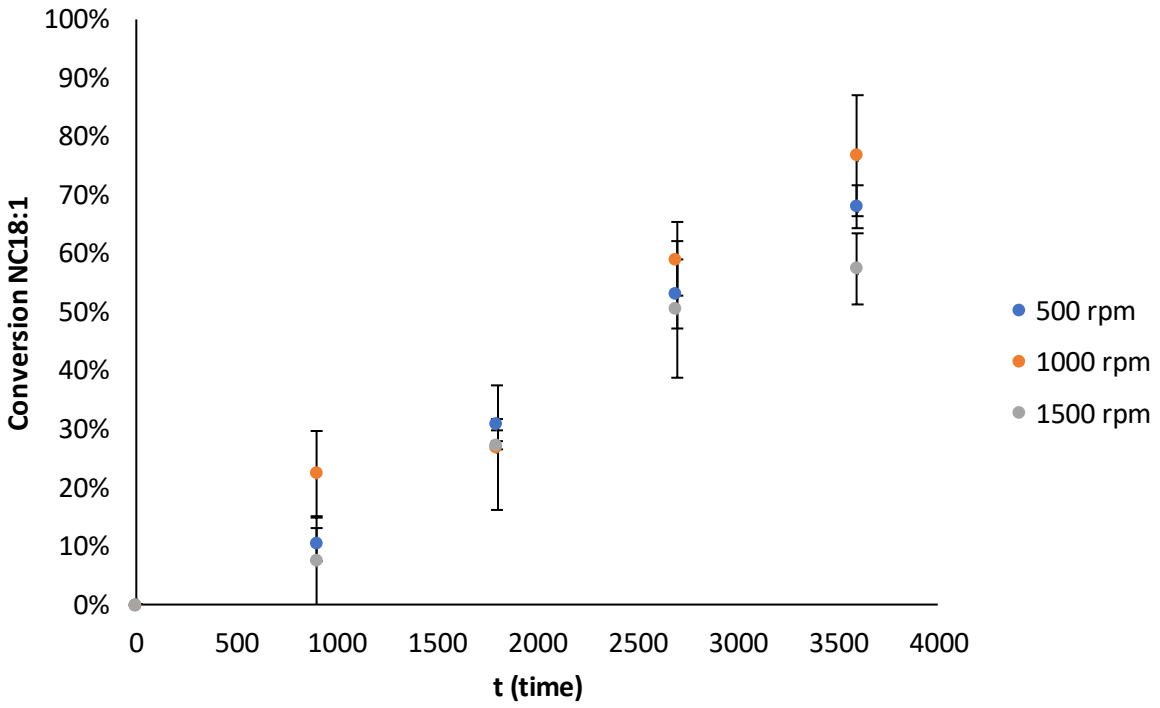

Figure 3-3. Conversion of oleonitrile in the first hour of oxidant addition at different rpm. Reaction conditions: Oleonitrile, 2 eq % H_2WO_4, 1 eq. 70 wt.% H_2O_2. Eq.: mol reactant/mol oleonitrile.

3.3.2.2 *Oxidant mixture flow addition*

The experiments were pursued in the conditions where the catalyst, tungstic acid (2 eq. %), was previously dissolved in a solution of 6 eq. 35 wt % H_2O_2.

The graph from **Figure 3-4** represents the consumption of oleonitrile in 1h with different oxidant mixture flow additions 0.305 mL/min and 0.917 mL/min (3.5×10^{-3} mol/min and 1.1×10^{-2} mol/min of 35 wt% H_2O_2 respectively) in the reaction media. As it is possible to observe, the consumption of oleonitrile increases with the stoichiometric amount (**eq:** mole ratio H_2O_2/C=C) of H_2O_2 added in the same period. The reaction rate is determined by the H_2O_2 addition in the reaction media where no mass transfer limitation should occur in this biphasic system in the first 1h.

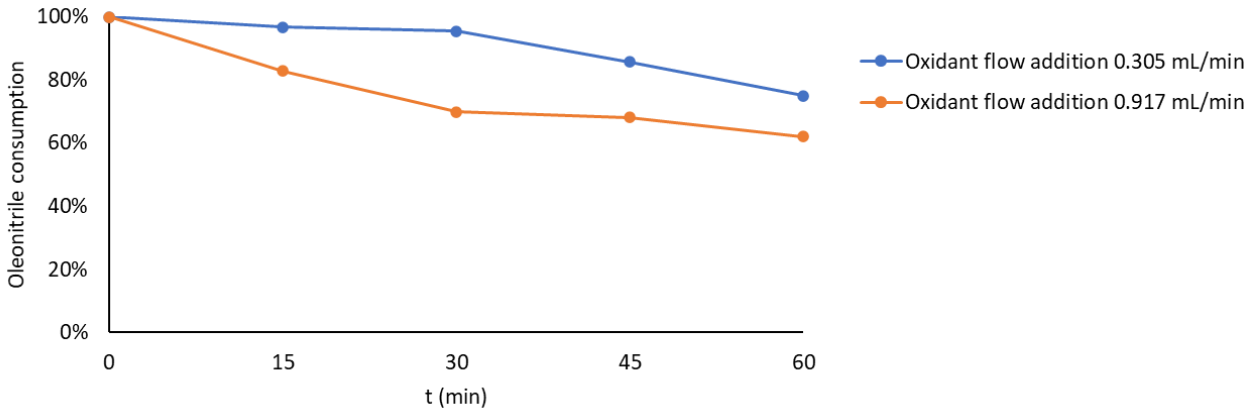

Figure 3-4. Consumption of oleonitrile in the first hour of oxidant addition at different oxidant solution rate. Reaction conditions: Oleonitrile 75% purity, 2 mol % eq. H_2WO_4 (dissolved in 6 mol eq. 35 wt% H_2O_2) at 90°C and stirred at 1000 rpm for 1h.

On **Figure 3-5.**, it is represented the Residual NC18:1 measured in function of the solution 35 wt% H_2O_2 equivalents (mol H_2O_2/ mol NC18:1) added. After the addition of one equivalent of H_2O_2 there was supposed to form already the epoxide specie and after 3 equivalents the final oxidative cleavage products. However, with one equivalent only 30% of oleonitrile is converted.

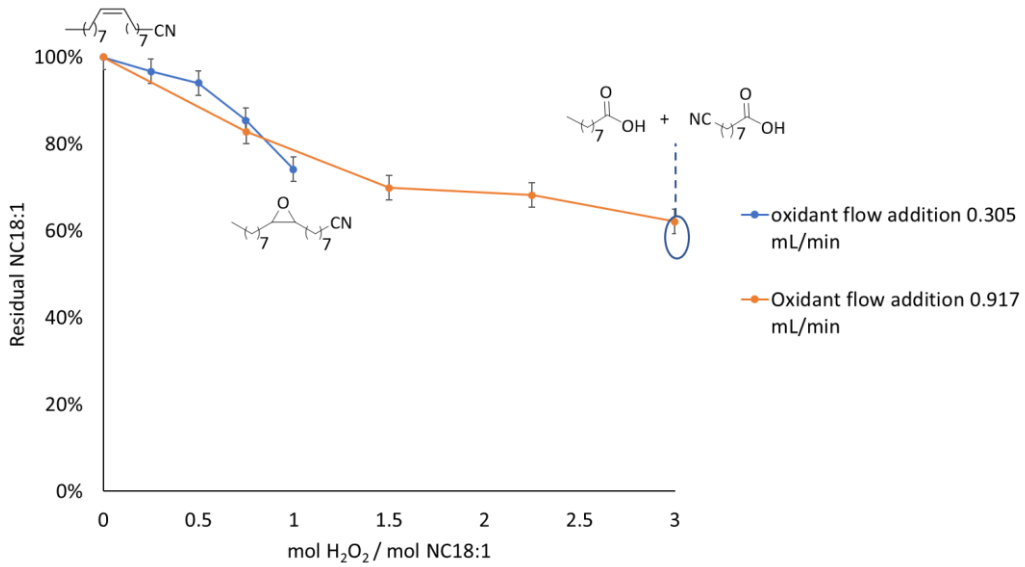

Figure 3-5. Consumption of oleonitrile in the first hour of oxidant addition at different oxidant solution rate. Reaction conditions: Oleonitrile 75% purity, 2 mol % eq. H_2WO_4 (dissolved in 6 mol eq. 35 wt% H_2O_2) at 90°C and stirred at 1000 rpm for 1h, values corrected to STD= +- 3%.

From the graph is also possible to observe tendency for the overlapping of the two curves, which shows that the reaction is not dependent on the quantity of H_2O_2 that is added in the reaction medium but on the catalyst quantity that is present in the reaction medium. In the beginning of the reaction the H_2O_2 added is quickly consumed. However, the reaction is still slow since the concentration of the catalyst is low in the first minutes. The conversion of oleonitrile is though

proportionally dependent on the amount of the catalytic specie present in the reaction media and not in the amount of 35 wt% H_2O_2 present in the medium.

3.3.2.3 *Oxidant concentration*

In this study the catalyst was dissolved previously in the H_2O_2 solution forming the oxidant solution in order to form ex-situ the catalytic specie peroxotungstate. The oxidant solution was added dropwise in the reaction media with a flow of 0.917 mL/min.

The consumption of oleonitrile over time at different H_2O_2 concentrations is represented in the graph from **Figure 3-6**. In the first minutes, while H_2O_2 is added to the reaction media, it is consumed, the concentration of H_2O_2 has no influence in the consumption of oleonitrile contrarly of the influence of the catalyst concentration. In the graph represented it is possible to observe that the conversion of oleonitrile depends on time. Also, once H_2O_2 accumulates in the reaction media (after 360 sec), higher the concentration of H_2O_2 and higher the catalyst concentration in the reaction media, higher will be the consumption of oleonitrile over time. The reaction speed is highly dependent on the concentration of the catalytic specie in the reaction media.

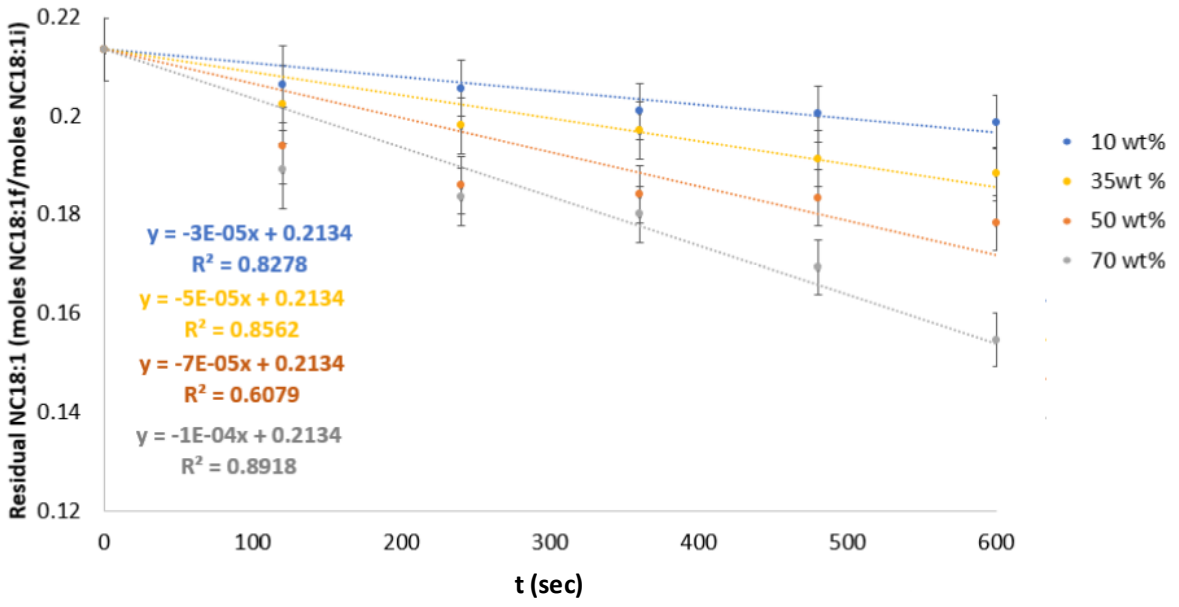

Figure 3-6. Residual moles of oleonitrile in the first 10 minutes of oxidant addition at 10, 35, 50, 70 wt % H_2O_2. Reaction conditions: 2 mol % H_2WO_4 / mol oleonitrile, T: 90°C, reaction time: 10 minutes, flow addition: 0.917 mL/min.

The graph from **Figure 3-7** represents the variation of residual moles of oleonitrile in the reaction media number by the number of moles of H_2O_2 added at different H_2O_2 concentrations with the same flow (0.917 mL/min). The graph shows that the conversion is almost not influenced by changing the amount of hydrogen peroxide in the reaction media.

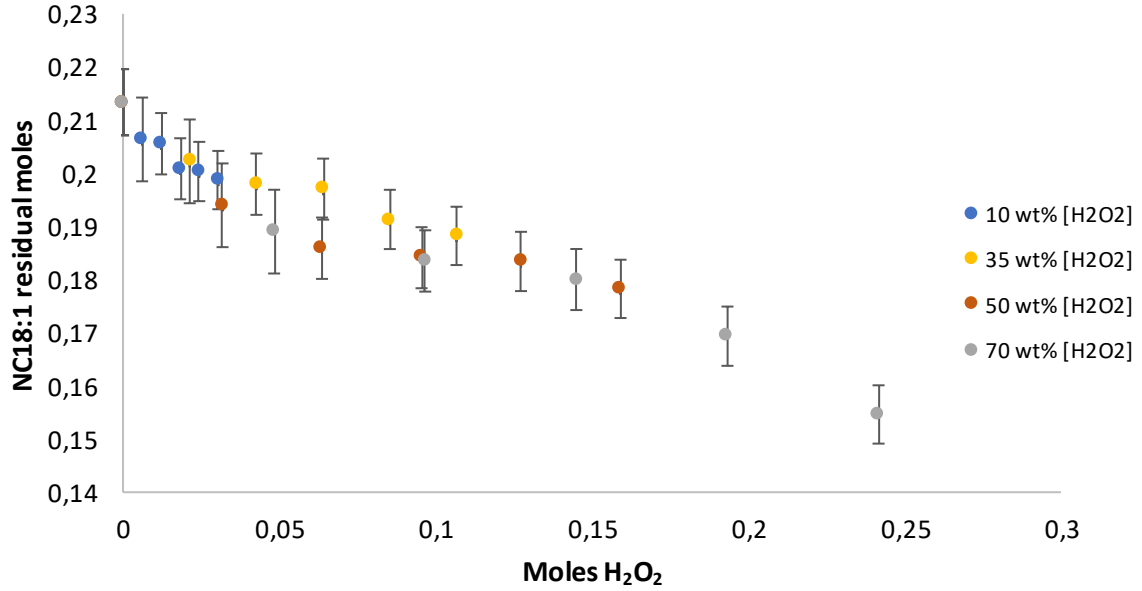

Figure 3-7. Residual moles of oleonitrile over the number of moles of H_2O_2 of oxidant addition at 10, 35, 50, 70 wt % H_2O_2. Reaction conditions: 2 eq % H_2WO_4 (mol H_2WO_4/ mol oleonitrile), T: 90°C, reaction time: 10 minutes, flow addition: 0.917 mL/min.

These results sustain the fact that the consumption of oleonitrile is proportionally dependent on catalyst loading and not on the H_2O_2 flow addition.

The key determining step is though the formation of the active catalytic specie peroxotungstate ($H_2W(On)O_4$). Higher concentration of H_2O_2 higher will be the solubility of the catalyst in the oxidant solution and lower the volume of aqueous phase in the reaction media. The active specie will have higher contact with the organic phase and more easily will be reactivated in the concentrated H_2O_2 aqueous phase (**Figure 3-8**).

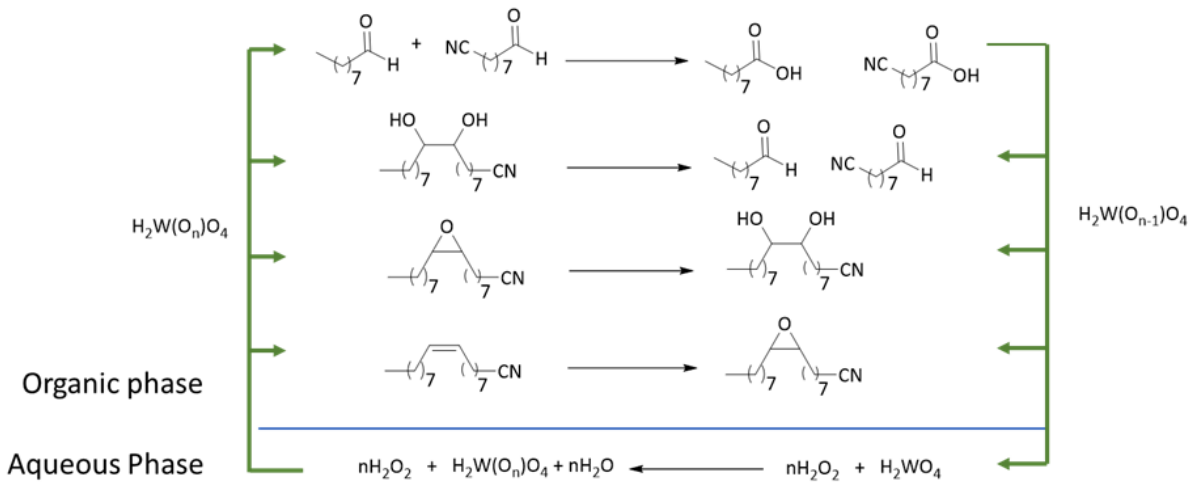

Figure 3-8. Biphasic system of oxidative cleavage of oleonitrile.

3.3.2.4 *Tungsten-based catalyst influence*

3.3.2.4.1 Catalyst pre-conditioning

As referred in chapter one, tungsten-based catalysts are found to be the perfect catalysts for oxidation reactions as shown by several authors [9–11] . Hajime Suzuki et al. found in their experiments that H_2WO_4 can stably oxidize water to O_2 rather than its dihydrate specie H_4WO_5 or WO_3. They proved that the higher tilt angle affords greater overlap between W-5d band and O-2p orbitals which might explain it success in oxidation reactions in H_2O_2 solutions [12].

As described in **chapter 1**, the pre-conditioning of hydrogen peroxide with the tungsten-based catalyst is essential to form the catalytic specie for the oxidation reaction.

In **Figure 3-9**. it is represented the oxidative cleavage yield % by 2 eq.% tungstic acid addition in-situ (not dissolved in the hydrogen peroxide) and pre-condition (pre-dissolution in H_2O_2). In presence of a phase transfer agent it was obtained an improvement of 10% monomer yield, when the catalyst was pre-dissolved in the hydrogen peroxide solution, compared with the addition of the tungstic acid in the beggining of the reaction (*in-situ*) (**Figure 3-9**).

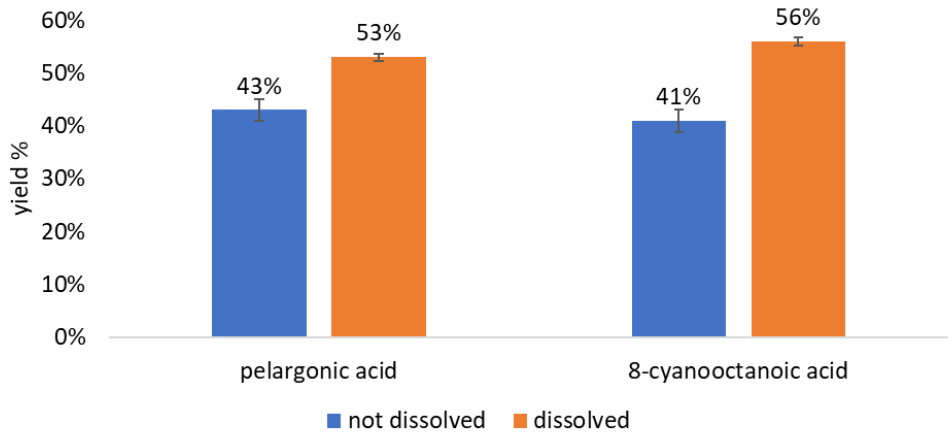

Figure 3-9. Pelargonic acid and 8-cyanooctanoic acid yields obtained by/not previous dissolution of the catalyst in the H_2O_2. Reaction conditions: Oleonitrile, 2 % eq. H_2WO_4 / mol oleonitrile, 6 eq. H_2O_2 , 24h, T:90°C. Eq.: mol substrate/mol oleonitrile.

For the oxidative cleavage of monounsaturated compounds, we tested two different tungsten-based catalysts, tungstic acid (H_2WO_4) and a Keggin type polyoxometalate phosphotungstic acid ($H_3PW_{12}O_{40}$) in the oxidative cleavage of oleic acid and oleonitrile. The catalyst was previously dissolved in the 70 wt. % H_2O_2 and stirred for 30 minutes before addition in the reaction media.

Phosphotungstic acid has 10 x O/mole and 11 x more W/mole than tungstic acid. It is a strong Bronsted acid, pKa =-13, and the Keggin anions have three types of outer oxygen atoms as a potential protonation centers: terminal oxygens M=O and two types of bridging oxygens M-O-M, edge sharing and corner sharing. Contrarily to tungstic acid, phosphotungstic acid is easily soluble in H_2O_2 aqueous. As mentioned in **Chapter 1**, Venturello , Antonelli [13,14] and Goddard [15] mentioned the perfect synergy between the phosphotungstic acid, and the phase transfer agent catalytic specie formed such as ($Q_3PO_2[WO(O_2)_2]_4$), sinthesized ex-situ (Venturello) and in-situ (Goddard), in the oxidative cleavage of oleic acid affording 82 and 86 % yield of azelaic acid and pelargonic acid.

However, in our experiments with oleonitrile as a substrate, lower yield was obtained when phosphotungstic was applied (**Table 3-16**).

Substrate	Catalyst	pelargonic acid (%)	8-cyanooctanoic acid (%)
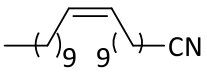	2 eq % H_2WO_4	53	56
	2 eq% $H_3PW_{12}O_{40}$	28.3	22.7

Table 3-16. Influence of the tungsten-based catalyst on the yield products of oxidative cleavage of oleonitrile. Reaction conditions: Oleonitrile, 2 % eq. W catalyst/mol oleonitrile, 6 eq. H_2O_2, 24h, T:90°C. Eq.: mol substrate/mol oleonitrile. Eq.: mol catalyst/mol oleonitrile.

In the first hour of addition of the oxidant mixture with phosphotungstic acid in the reaction media, high exotherm temperature was observed. The temperature rose in 10 minutes from 70 to 95°C and the reaction medium presented an orange coloration. The application of 70 wt% H_2O_2 might be too aggressive and once the oxidant mixture was added to the reaction media that contained the phase transfer agent, might promote the formation of an inactive specie.

It is generally accepted that the active specie is the peroxophosphotungstate trianion (PPW^{3-}) [14] as for example $(PO_4[W(O)(O_2)_2]_4)^{3-}$, obtained by dissolution of H_2O_2 with phosphotungstic acid ($H_3PW_{12}O_{40}$). However, as demonstrated by Luis de la Garza et *al.* [16] at high concentration of H_2O_2 solution, the full oxidation of $PW_4O_{24}^{3-}$ specie and the formation of WO_6^{2-}can occur. This anion can also partially bind to the phase transfer agent and co-precipitate as $[Q^{2+}]_2[WO_6^{2-}]$ yielding an orange product that proved also to be inactive in their experiments in the epoxidation of methyl oleate [16]. Thus, the orange color can be also related to the decomposition of the phase transfer agent, as for example, the formation of Br_2 or Cl_2 species.

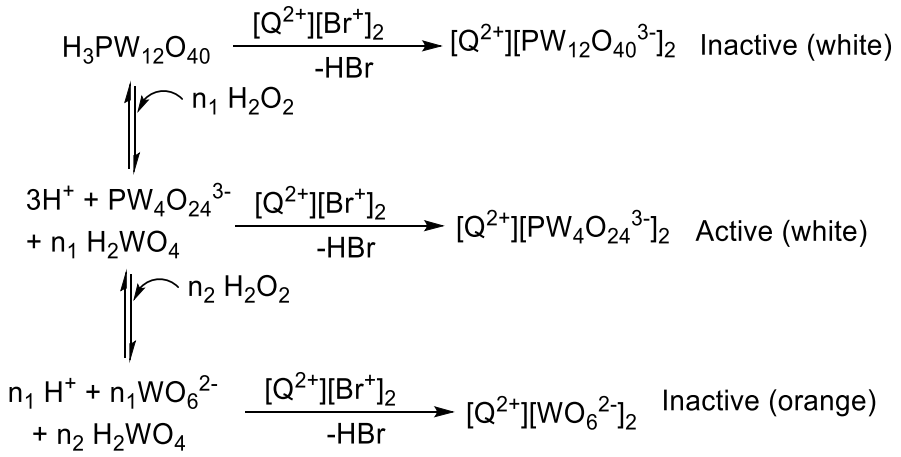

Scheme 3-6. Sequential oxidation of phosphotungstic acid by hydrogen peroxide and potential pairing with the phase transfer agent Q^{2+}. (Scheme adapted from Luis Garza et *al.* publication [16]).

We studied the influence of the catalyst concentration in the consumption of oleonitrile in the first hour of reaction.

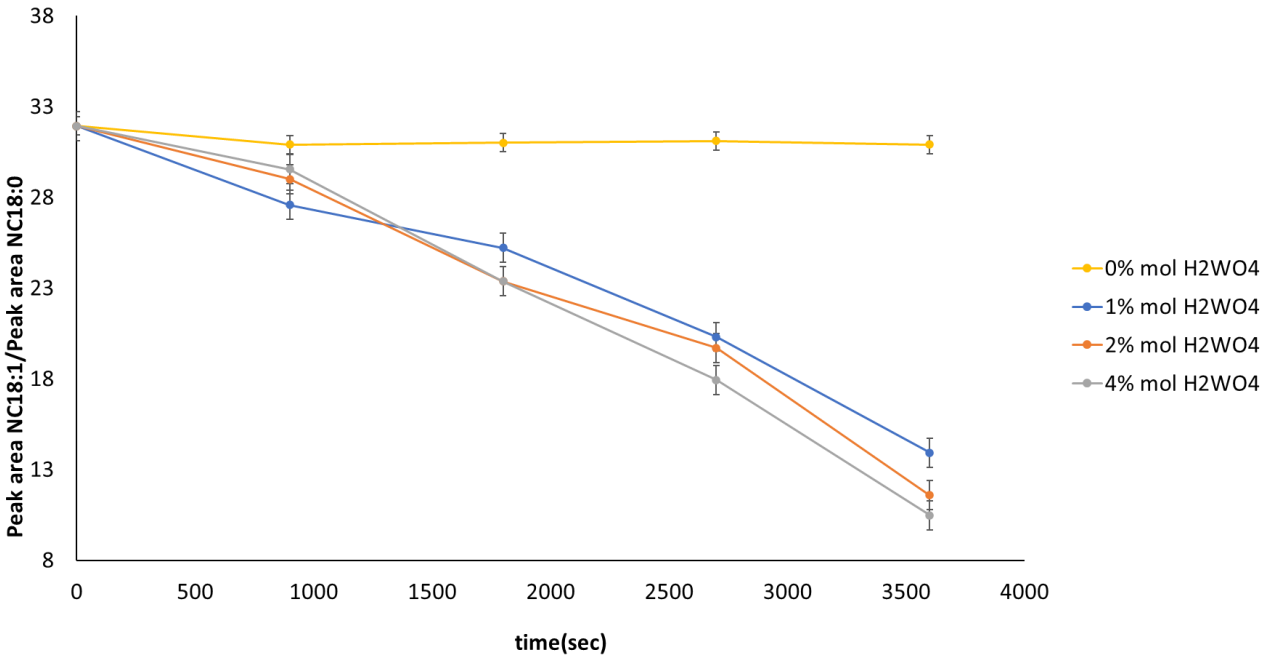

Figure 3-10. Influence of catalyst concentration in the consumption of oleonitrile in the first hour of reaction. **Eq**: mol catalyst/mol oleonitrile.

No substantial improvement was observed at higher (4 eq. %) H_2WO_4 loading.

3.3.2.5 *Type of Monounsaturate substrate*

The oxidative cleavage of monounsaturated compounds with different functional groups were tested in the reaction conditions of dissolution of tungstic acid in 70 wt% H_2O_2 and addition dropwise for 6h with a total of reaction of 24h (**Table 3-17**).

Substrate	product	Yield (%)
Oleonitrile (75% purity)	Pelargonic acid	53
	8-cyanooctanoic acid	56
Oleic acid (98% purity)	Pelargonic acid	46
	Azelaic acid	45
(Z)-octadec-11-enenitrile	11-cyanodecanoic acid	45
	Heptanoic acid	46
(Z)-octadec-12-enenitrile	11-cyanodecanoic acid	30
	Hexanoic acid	44
Methyl oleate (98% purity)	Pelargonic acid	69
	methylazelate	53
1-decen (98% purity)	Pelargonic acid	60

Table 3-17. Oxidative cleavage products yield for oleonitrile, oleic acid, (Z)-octadec-11-enenitrile, (Z)-octadec-12-enenitrile, methyl oleoate and 1-decen. Reaction conditions: Oleonitrile, 2 eq.% H_2WO_4, 6 eq. 70 wt% H_2O_2, 24h, T:90℃. Eq: mol catalyst/mol oleonitrile.

No significant difference was observed in the yields of the oxidative cleavage products of oleonitrile, oleic acid, (Z)-octadec-11-enenitrile and (Z)-octadec-12-enenitrile and 1-decen. However, higher yield (69% pelargonic acid and 53% methylazelate) was obtained in the oxidative cleavage of methyl oleate (**Table 3-17**).

3.3.2.6 *By-products obtained by isomerisation*

The possibility of isomerization of the double bond, during oxidative cleavage process of methyl oleate, was sustained by the presence of octanoic acid (1) and the C10 ester acid (2) in the final product. The presence of acid heptanoic (3) and the ester acid C11 (4) could indicate the oxidative cleavage of the isomerized double bond in the position C12 and C13 of methyl linoleic present in the starting material (2% chromatographic peak area) **(Figure 3-11)**.

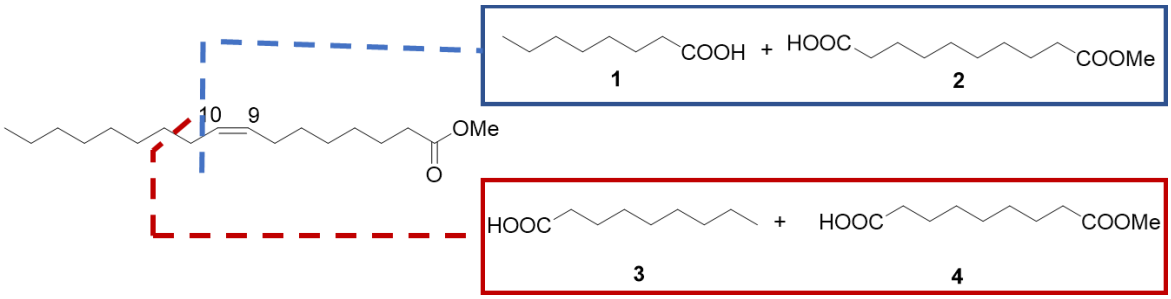

Figure 3-11. Products obtain by oxidative cleavage of methyl oleate and the product result of isomerization of methyl oleate.

The isomerization could occur from tungsten oxalate complex with the intermediary epoxide as it is suggested by some authors [14,17].

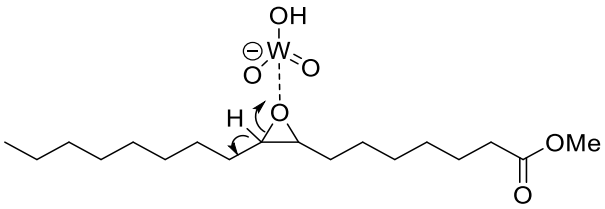

Figure 3-12. Possible cause of isomerization of double bond from C9-C10 to C10-C11.

After reaction the hydrolysed product of methyl azelate, azelaic acid, and methyl sebacate, sebacic acid, were identified by GC-FID.

3.3.2.7 *PTA influence*

Oil-water biphasic-systems often needs the use of a third component with hydrophobic and hydrophilic characteristics. Phase transfer agent (PTA) or Phase Transfer Catalyst (PTC), if it determines the reaction rate, in catalytic amounts, can improve the rate of heterogeneous reactions. Their application includes two fundamental processes: transport of the anion to the inorganic layer by using an onium counter ion. Phase transfer agents reduce the interfacial tension between the two liquids increasing the interface area, allowing higher contact between the two liquid, forming a stable emulsion. Usually, these types of catalysts are comprised by quaternary ammonium salts. Ideally, the PTA is in the interphase of the biphasic system allows the transfer of the oxidant in the aqueous phase to the organic phase through the formation of one ion pair sufficiently lipophilic. The anion is though transfer to the organic phase with the organic substrate. In biphasic systems such as the oxidative cleavage of unsaturated fats with hydrogen peroxide, quaternary ammonium salts are often applied. Their ability to form essentially non solvated

electrically neutral lipophilic ion-pairs with the anionic species, make them suitable for application in water-oil systems. As mentioned on **chapter 1**, Venturello was a pioneer in the application of quaternary ammonium salts in the oxidative cleavage of unsaturated compounds.

In the oxidative cleavage study of internal monounsaturated compounds three different quaternary ammonium salts were tested as phase transfer agents: the Aliquat 336® (**Figure 3-13 i**) and the cetyl pyridinium bromide or chloride (**Figure 3-13 ii and iii)**.

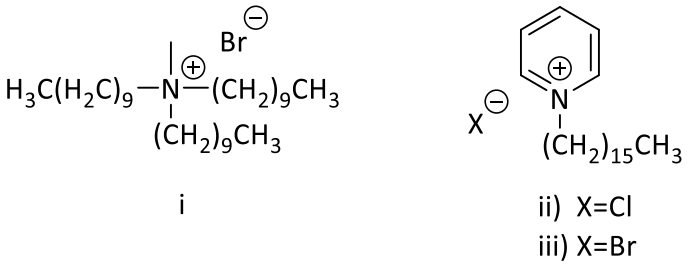

i ii) X=Cl iii) X=Br

Figure 3-13. Phase transfer agents used in the oxidative cleavage of unsaturated compounds. i) Aliquat 336® and Cetylpiridinium i) chloride or ii) bromide.

Substrate	Experiment	PTA	Yield 1 %	Yield 2 %
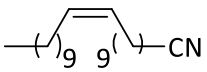	1	-	25.7	26
	2	i	53	56
	3	ii	48	42
	4	iii	47	46
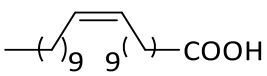	5	-	10	8
	6	i	56.8	51

Table 3-18. Influence of PTA in the oxidative cleavage of oleonitrile and oleic acid products yield.

The products yield **was significantly improved** in the presence of a phase transfer agent. However, no significant difference was observed when tested different PTAs in the catalytic system. (**Table 3-18**).

On his studies, Venturello proposed the formation of a peroxo catalyst formed with the tungsten-based catalyst applied. The existence of a peroxo complex facilitates the transfer of the oxygen from the aqueous phase (H_2O_2) to the organic phase. However, in this publication the peroxo-complexes are produced *ex-situ* [13]. As mentioned before Godard et al. proposed the formation of *in-situ* catalytic specie which reacts with the olefin giving place to an epoxide specie followed by diol formation and concomitant cleavage of C-C bond giving place to aldehyde products and carboxylic acid from the oxidation of aldehydes.

3.3.2.8 *Reaction mechanism in presence/absence of a phase transfer agent*

The oxidative cleavage of oleonitrile was controlled by samples withdrawn periodically from the reactor and put into the test vial containing 1 mL of deionised water in order to quench the reaction. The organic layer was decanted and analysed by GC-FID.

In the absence of phase transfer agent the oxidative cleavage of oleonitrile proceeds through epoxidation of C-C double bond in C_9 and C_{10} (**2**), followed by the epoxide's ring-opening reaction via hydrolysis producing the diol specie **3**, C-C cleavage affording the aldehydes **4** and **5** and concomitant oxidation leading to the carboxylic acids **6** and **7** (**Scheme 3-7**). However, in presence of a phase transfer agent, no diol (**3**) intermediate was detected in the samples analysed during the reaction time.

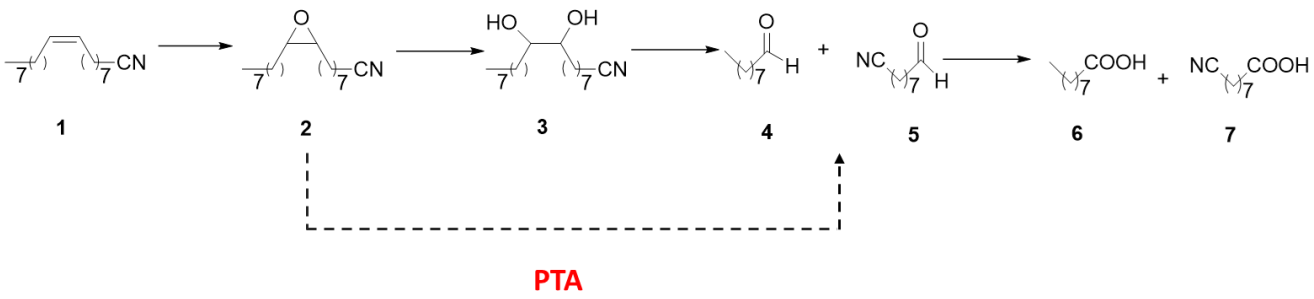

Scheme 3-7. Oleonitrile oxidative cleavage in presence/not of a phase transfer agent. **1:** oleonitrile, **2:** 8- (3-octyloxiran-2-yl) octanenitrile (epoxide intermediate), **3:** 9,10-dihydroxyoctadecanenitrile, **4:** nonanal, **5:** 8-oxononanenitrile , **6:** pelargonic acid, **7:** 8-cyanooctanoic acid. Reaction conditions: Oleonitrile, 2 eq. % H_2WO_4, 6 eq. 35 wt % H_2O_2, 24h, T:90°C, 2 eq.% cetylpiridinium bromide (when applicable).

The absence of the diol specie peak (no peak detected in the GC-FID analysis) can be an indication that a high molecular weight complex, such as acetal or esters not detected by the chromatographic method are formed. Another possibility is the fact that during the treatment of the sample a specie formed between the peroxo-quaternary ammonium complex and the diol intermediate (**Figure 3-14**) is formed and, during the samples treatment it migrates to the aqueous phase not being detected in the analysis of the organic phase.

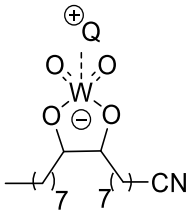

Figure 3-14. Possible intermediate specie formed in presence of PTA. Q^+=$C_{25}H_{54}ClN$, $C_{21}H_{38}BrN.H_2O$, $C_{21}H_{38}ClN.H_2O$.

The reaction was also slower in presence of a phase transfer agent (**Figure 3-15**).

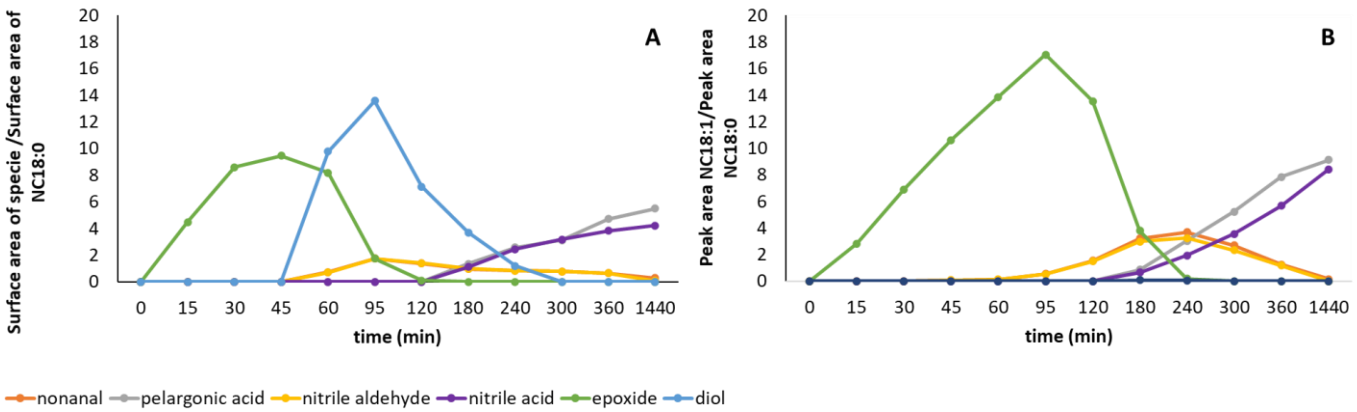

Figure 3-15. Intermediate and product species formed during the oxidative cleavage of oleonitrile with 2% mol H_2WO_4, 6 eq. H_2O_2, not (**A**) or in presence of 2 eq. % Aliquat 336® (**B**).

3.3.2.9 *Mass balance Study*

The quantification of the oxidative cleavage products after reaction was done by the internal standard calibration methodology through GC-FID analysis. However, the products quantified by this method does not fulfil the mass balance of the reaction. This can be the result of significant loses during the extraction procedure after reaction. In **Figure 3-16**, it is described the mass balance of the oxidative cleavage of oleic acid.

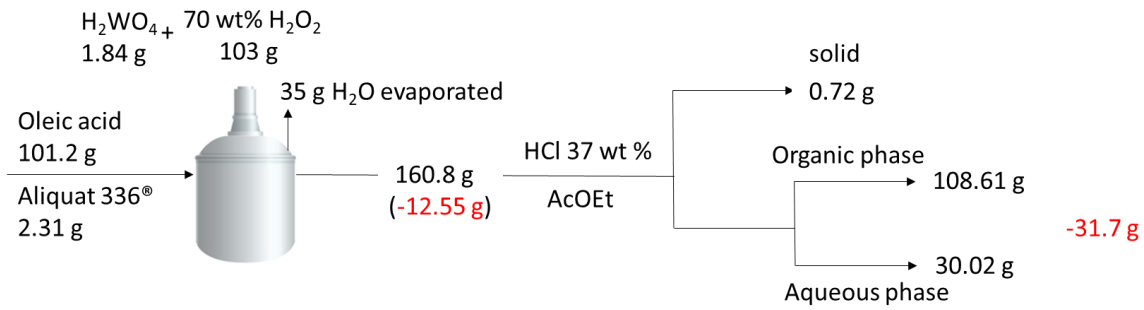

Figure 3-16. Mass balance of oxidative cleavage of oleonitrile. Reaction conditions: Oleonitrile, 2 mol % H_2WO_4, 6 eq. H_2O_2, 24h, T:90°C.

From the internal standard calibration methodology through GC-FID analysis, the total mass quantified in the reaction is 92.89 g. The difference between the quantified mass of the organic phase in the end of the process and the quantified mass in the calibration methodology applied, demonstrate that approximately 16 g of products are not detected by the analysis methodology applied (**Table 3-19**).

Azelaic acid (g)	Pelargonic acid (g)	Nonanal (g)	Oxopelargonic acid (g)	Stearic acid (g)	Palmitic acid (g)	High MW (g)	Total mass (g)	Missing mass (g)
41.47	42.23	1.15	1.38	1.64	0.27	4.75	92.89	16

Table 3-19. Quantification of oxidative cleavage products, saturated fatty compounds that did not reacted during the reaction and high molecular weight molecules identified by GC-FID.

3.3.2.10 *Reaction conditions optimization for application in ultrasound system*

In order to apply the ultrasound technology to the oxidative cleavage system, the same was optimized at lower hydrogen peroxide concentrations, based on the experiments of Godard et al. [18].Godard et *al.* proposed a 5h reaction system using phosphotungstic acid 2 eq.% (dissolved in the oxidant mixture) and cetylpiridium bromide 5.5 eq.% as a phase transfer agent to achieve 81.5 mol % yield of azelaic acid (**2**) and 86.1 mol % yield of pelargonic acid (**1**). However, on their studies they describe a methodology where a solution of 2 eq.% $H_3PW_{12}O_{40}$ dissolved in 6 eq. of 35 wt% H_2O_2, is added over only 5 minutes at 60°C [18]. Such experiment might work at low product quantities, but in up-scale conditions can be highly dangerous. We adapted the conditions described in their work to higher reactant mass. However, after only 2 minutes of oxidant solution addition the temperature rose from 60°C to 105°C and the reaction needed to be stopped in order to not overcome the limits of flammability. In order to work in safer conditions, we adapted the reaction system to 2h addition of the oxidant solution in the reaction media (**Scheme 3-8** and **Table 3-20**).

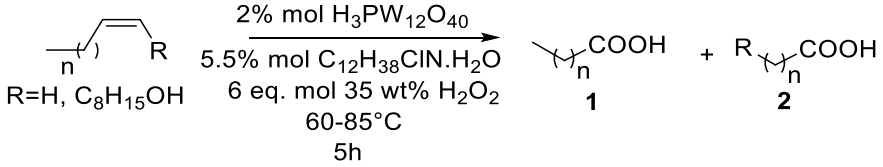

Scheme 3-8. Oxidative cleavage of monounsaturated compounds based on Goddard reaction conditions [18].

Experiment	Substrate	1 (%)	2 (%)
i	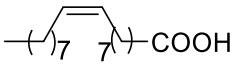 **1**	55.5	62.1
ii	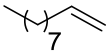 **2**	-	39
iii	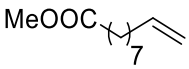 **3**	-	12.5
iv	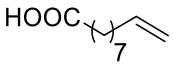 **4**	-	34.3
v	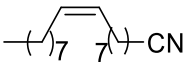 **5**	37	35

Table 3-20. Oxidative cleavage of monounsaturated fatty compounds. **1 –** oleic acid, **2 –** 1-decen, **3 –** methyl – 9-decenoate, **4 –** 9-decenoic acid and **5 -** oleonitrile. Reaction conditions: 2 eq.% $H_3PW_{12}O_{40}$; 6 eq. H_2O_2 35 wt%, 5.5 eq. % cetylpiridinium bromide, 5h reaction time. In case of terminal olefins the formic acid was not detected by GC-FID. **Eq:** mol reactant/mol oleonitrile.

Higher oxidative cleavage products yields in terminal olefins would be expected in comparison to internal olefins as it the case of oleic acid. However, in such reaction conditions lower yield was obtained in terminal olefins (from 39-12.5%, cleavage products). In case of iii the hydrolysis product of the ester function (azelaic acid) was also obtained. Due to the acidity of the reaction media pH =1.0 , the hydrolysis of the ester function of iii is promoted.

3.3.3 US-Assisted oxidative cleavage of unsaturated fatty compounds

3.3.3.1 *Indirect sonication*

The use of a phase transfer agent can represent an important impact in the process industrialization cost. Some studies support the use of ultrasound to enhance the emulsification of a biphasic system. Darya Radziuk *et al.* [19] demonstrated that mass transfer across the phase boundary is substantially enhanced through acoustic emulsification. Polymers in the aqueous phase in presence of ultrasound are known to undergo emulsion polymerization, in which the diameter of droplets is initially a function of the amount of shear forces [20] . In order to increase the mass transfer in the reaction media, reduce the reaction time and avoid the use of a phase transfer agent, we decided to apply the ultrasound technology to, attain the threshold of cavitation and create perfect emulsions and increase the surface contact area between the two phases of the heterogenous system.

In order to study the effect of ultrasounds in the oxidative cleavage of unsaturated fatty compounds and determine the best frequency to apply, we started the experiments in an ultrasonic cleaning tank lent by Weber Ultrasonics AG.

3.3.3.2 *Ultrasonic frequency*

The first strategy was to find the best frequency to apply in the oxidative system. The reaction was tested at 25 kHz (low frequencies) and 120 kHz (high frequencies) in presence of H_2WO_4 and in presence of $H_3PW_{12}O_{40}$ (**Figure 3-17**).

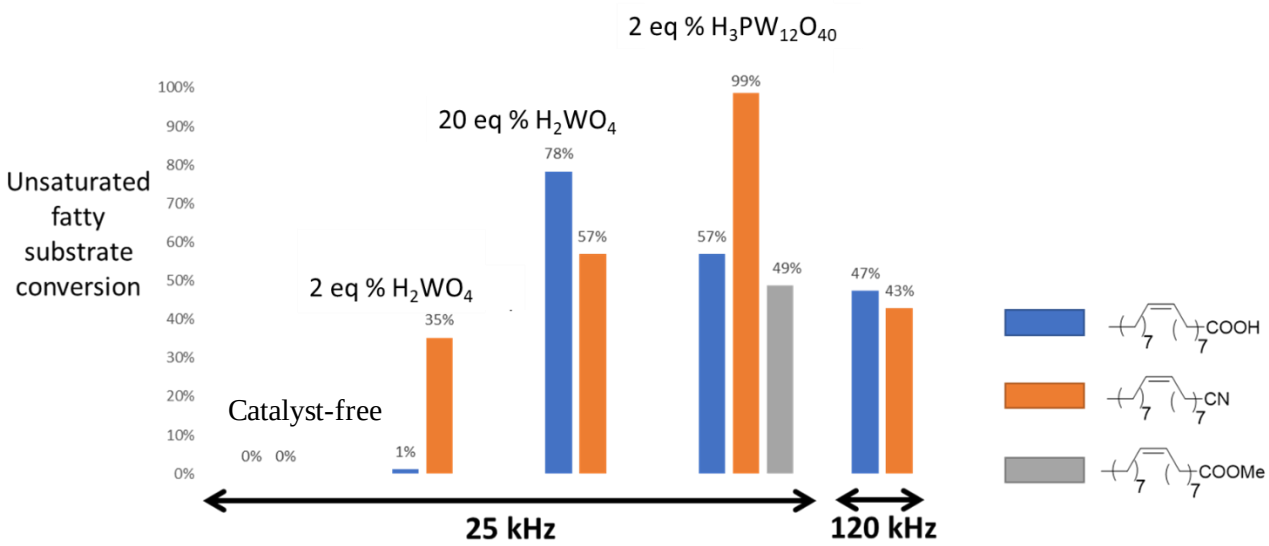

Figure 3-17. Catalyst and ultrasonic frequency conversion on the unsaturated fatty substrate conversion. **Catalyst free:** Unsaturated fatty substrate, 6 eq. mol H_2O_2.

Lower frequencies led to higher conversion of the monounsaturated fatty substrates tested.

The experiments pursued with phosphotungstic acid afforded higher conversion of oleonitrile even when 20 mol % of H_2WO_4 was used **(Figure 3-17)**.

In case of oleic acid after 240 minutes the reaction was stopped due to the formation of a white agglomeration (**Figure 3-18**).

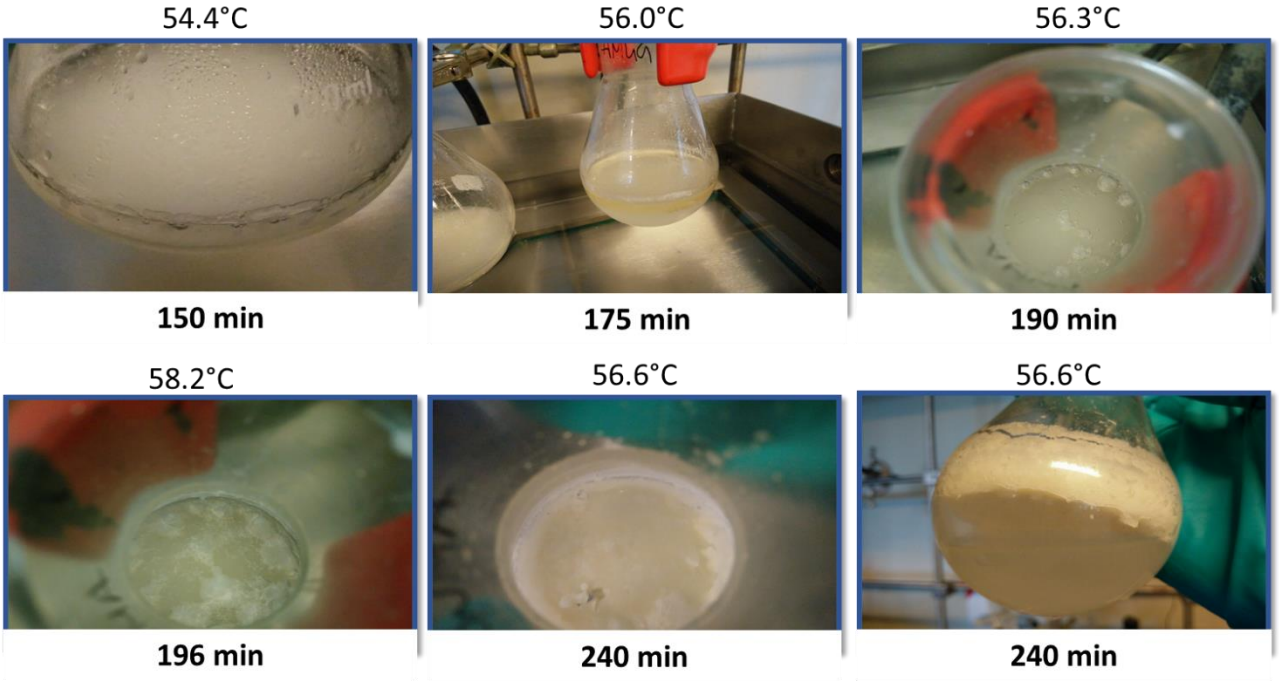

Figure 3-18. White agglomeration formation.

This phenomenon can be related to physical and chemical phenomena.

1) **"Breaking emulsion" (physical phenomenon)**

The physical phenomenon can be related to the phenomenon of flocculation or breaking combined with coalescence.

Firstly, the small spheres of oil stick together to form clumps or flocks which act as larger drops. Secondly the breaking phenomenon due to coalescence and creaming combined result in completely separation of oil from water so that it floats at the top in a single, continuous layer. This phenomenon's it is called "breaking emulsion". However, to reverse the process emulsions must be remade which requires high energy (**Figure 3-19**).

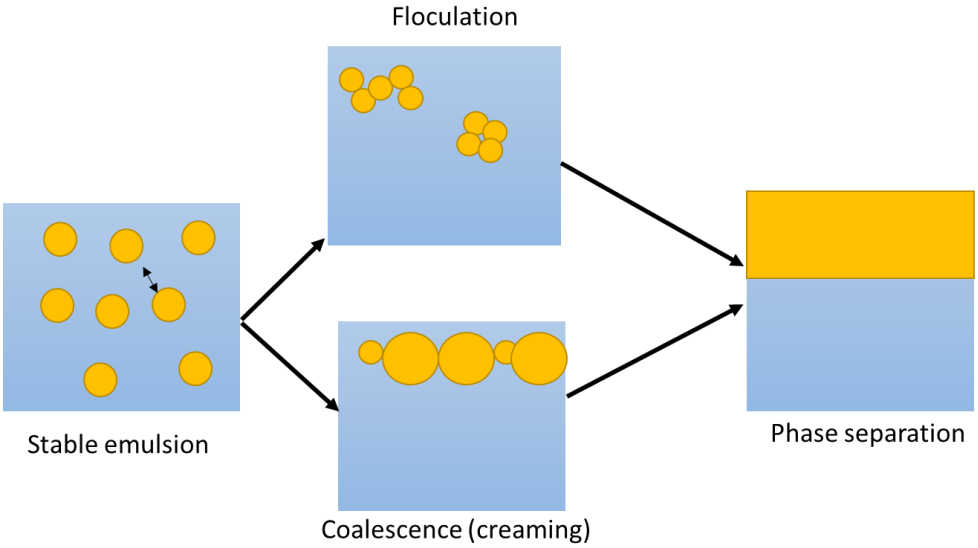

Figure 3-19. Aggregation of oil particles in oil-in-water system resulting in the emulsion breaking.

The explanation for the fact that under 120 kHz such phenomenon's does not occurs is related to the fact that at high frequencies the cavitation bubble size is reduced contrarily in case of low frequencies.

2) Formation of high molecular weight molecules (chemical phenomena)

A second hypothesis relies on the catalyst applied once with 2 eq. % H_2WO_4 this phenomenon does not occur. However, once we equal the number of oxygens as in phosphotungstic acid pursing the experiment at 20% mol H_2WO_4, the same agglomeration is obtained. Such can be related to the fact that once the catalyst is more reactive (11 x W/mol and 36 x O/mol more than tungstic acid) the production of higher molecular weight molecules such as acetals or esters from reaction between the 10-dihydroxystearic acid with the oxidative cleavage products such as aldehydes or mono and dicarboxylic acid, is favoured. Once the reaction temperature is below the melting point of these species, the same accumulates in the reaction media creating a solid thick layer and the reaction is stopped (**Figure 3-20**).

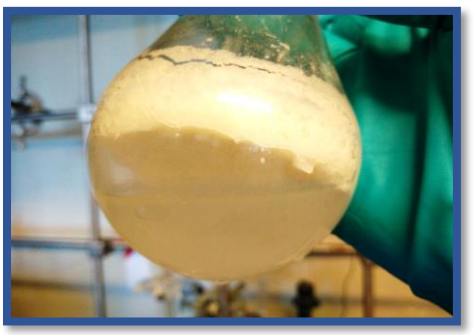

Figure 3-20. White agglomeration formed at 240 min in the oxidative cleavage of oleic acid. Reaction conditions: H_2O_2 35 wt %, 2 mol % $H_3PW_{12}O_{40}$ or 20 mol % H_2WO_4. Melting point: 80-98°C.

3.3.3.3 *Phase transfer agent*

Some researchers argue that the effect of ultrasound is enhanced in presence of an emulsifier [4,21]. In our experiments, we tested the cetylpiridinium bromide as emulsifier test.

The oxidative cleavage products were only obtained in presence of a phase transfer agent (**Table 3-21**).

		)))		Silent conditions	
Substrate	**PTA**	**Yield 1 (%)**	**Yield 2 (%)**	**Yield 1 (%)**	**Yield 2 (%)**
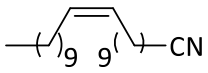	-	-	-	-	-
	Cetylpiridinium bromide	14	18	0-4	0-4
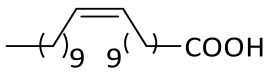	-	-	-	-	-
	Cetylpiridinium bromide	19	24 %	0-4	0-4

Table 3-21. Oxidative cleavage products of oleonitrile and oleic acid in/not presence of an emulsifier. Reaction conditions: H_2O_2 35wt %, 2 mol % $H_3PW_{12}O_4$, 2 mol % Cetylpiridinium Bromide (when applicable), 54°C, 5h in silent conditions and under sonication at 25 kHz, 0.024 $W.mL^{-1}$ (input power of 100W, 60.19 W taking in account the cp of H_2O) .

Figure 3-21. Reaction media in presence/absence of Cetylpiridinium bromide.

The acoustic power calculated, 0.024 $W.mL^{-1}$, is the acoustic power that is absorbed in the water of the ultrasonic tank by mL of water. Once, the reaction takes place in a glass flask the acoustic power in the reaction media should be much lower once it can occur phenomena of sound reflection in the glass, and the sound absorption can also be influenced by the thickness of the flask.

For this reason, the level of reproducibility of the chemical synthesis in indirect sonication conditions, is low.

3.3.3.4 *Indirect sonication versus direct sonication*

Besides the enthusiastic results obtained when compared to the same conditions with a stirrer tank reactor at lower temperatures than applied conventionally, yields obtained in the order of 20% are not satisfactory. In indirect sonication, the ultrasonic wave needs to cross the liquid inside the ultrasonic device and then cross the wall of the sample container. Therefore, ultrasonic intensity inside the sample container is reduced. Direct sonication obtained by using ultrasonic probe allows much higher ultrasound intensity to the medium once it is in direct contact.

The results obtained for the oxidative cleavage system are presented in **Table 3-22.** In our experiments we needed to reduce the quantity of phase transfer agent when applied the cup-horn and the sonotrode. Using higher than 2 eq% of PTA, respecting to the substrate, promoted a substantial foam which was difficult to control.

The highest oxidative cleavage yield products were obtained when the reaction was subjected to sonotrode at 25 kHz in the absence of the emulsifier. This might be related to the fact that with phase transfer agent the foam, produced due to the local high intensity supplied by the ultrasonic horn, is formed hindering the dispersion of sound waves in the reaction media preventing the reaction to occur.

Apparatus	PTA	nonanal	Nitrile aldehyde	Pelargonic acid	8-cyanooctanoic acid
Conventional	-	-	-	-	-
(54°C)	5 eq. %	-	-	0-4%	0-4%
Conventional	-	-	-	-	-
(85°C)	2 eq.%	-	-	37%	35%
Ultrasonic tank	-	-	-	-	-
(54-57°C)	5 eq.%	-	-	14 %	18 %
Cup-horn	-	-	-	-	-
60°C	2 eq.%	5%	7%	-	10%
Sonotrode	-	20%	25%	40%	45%
50-64°C	2 eq. %	4%	5%	14%	10%

Table 3-22. Oxidative cleavage of oleonitrile products yield obtained in the different equipments tested. Reaction conditions: 6 eq. H_2O_2 35wt %, 2 eq. % $H_3PW_{12}O_{40}$, 2 eq. % Cetylpiridinium Bromide (when applicable), 5h reaction time. Eq.: mol reactant/ mol oleonitrile.

3.3.3.5 *Emulsion formation before sonication*

Ultrasound wave propagation is affected as mentioned before by the viscosity of the medium. In that sense, we used the Dispersor IKA® magic LAB in order to create the perfect emulsion system and overcome the increase of viscosity when formation of the diol intermediate. However the oxidative cleavage yield products attaint was lower than in the sole application of the ultrasonic probe.

Apparatus	PTA	nonanal	Nitrile aldehyde	Pelargonic acid	8-cyanooctanoic acid
Sonoprobe	-	20%	25%	40%	45%
50-64°C	2 mol %	4%	5%	14%	10%
IKA ® magic LAB	-	15%	14%	33%	32%
+ Sonoprobe	2 mol %	23%	19%	4%	5%
50-64°C	2 mol %	4%	5%	14%	10%

Table 3-23. Oxidative cleavage of oleonitrile yield products obtained in absence and formation of a pre-emulsion before sonication.

3.3.3.6 *H_2O_2 decomposition*

Direct sonication represents higher energy delivered to the medium but has also an important constraint, the fact that the metal of the sonotrode is in contact with the liquid. In contact with titanium (metal of the sonotrode tested), H_2O_2 may decompose and the efficiency of the catalytic system would be reduced. Another reason is the formation of hot spots when cavitation bubbles which generates high local (not measured) temperatures might allow faster decomposition of H_2O_2.

In order to test the possible application of the catalytic system by direct sonication, we measured the decomposition of H_2O_2 in presence and absence of phosphotungstic catalyst for 5h. The decomposition of H_2O_2 over the oxidative cleavage of oleonitrile and oleic acid was also measured, leading to interesting results (**Figure 3-22**).

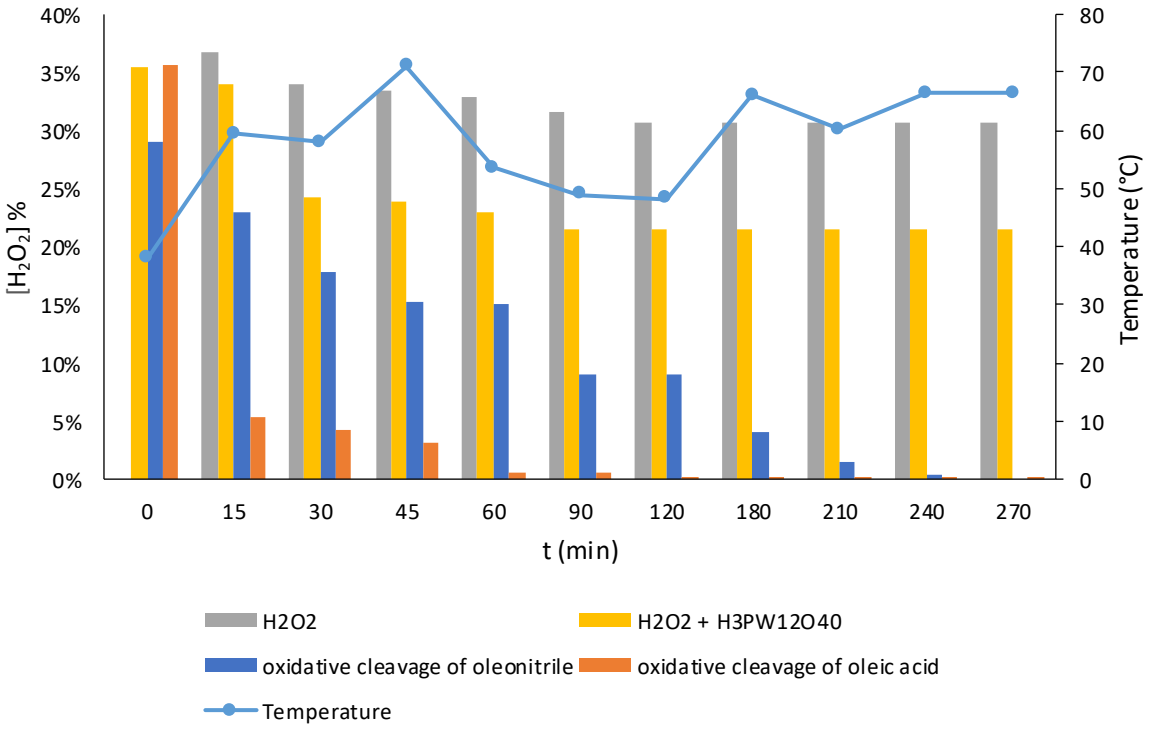

Figure 3-22. Decomposition of H_2O_2 during the oxidative cleavage of oleonitrile and oleic acid.

In **Figure 3-22**, the decomposition of H_2O_2 over the 5h of sonication was lower than 6%. In presence of phosphotungstic acid the H_2O_2 concentration at the end of the reaction time was 14 wt%.

However, the decomposition was faster in presence of oleic acid (decrease of 20 wt% after only 15 minutes) than in presence of oleonitrile.

The result obtained can be an indication that as soon as pelargonic acid and azelaic acid are produced, the decomposition of H_2O_2 is favored instead of the oxidative cleavage of the monounsaturated substrate.

3.3.3.7 *Viscosity of oil*

In sonication, the energy transmitted per unit medium area is known as the intensity and proportional to the square of the amplitude (I x A^2). This means that the amplitude of ultrasound waves impacts the intensity of cavitation by determining the number of bubbles that implode per unit of time. Thus, during intense cavitation, extreme temperatures and pressures can be produced inside the collapsing bubbles and cause the molecules present within the bubbles to decompose severely. In **Equation 3-5** it is described the influence of the viscosity in the intensity of sound propagation in medium.

$$I = \frac{P_{amax}}{2\rho V}$$

Equation 3-5. Amplitude intensity of ultrasound. $\boldsymbol{P_{amax}}$: maximum pressure amplitude of the wave, $\boldsymbol{\rho}$: the density of the medium and **V**: the velocity of the sound in the medium.

The liquid viscosity is therefore an important physical parameter that impacts the energy dissipated by the cavitation bubbles and therefore, affects the wave attenuation and the shape of the acoustic field [22]. At 21°C the viscosity of oleonitrile is 22 x lower than oleic acid and at 60°C is 3x lower (**Table 3-24**).

Substrate	21°C	60°C
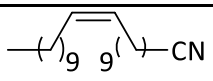	9.32 mPa	3.36 mPa
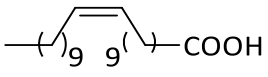	31.55 mPa	9.55 mPa

Table 3-24. Viscosity of oleonitrile and oleic acid at 21°C and 60°C.

The formation of new high molecular weight compounds introduces new forces of interaction between the molecules, increasing the viscosity of the medium and thus prevent the relative motion of the fluid.

3.3.3.8 *By-products formation*

Under direct sonication, with an ultrasonic horn at 25 kHz frequencies (100 W input power), the oxidative cleavage of oleonitrile was faster compared to conventional conditions (stirrer tank reactor). Already after only 15 minutes the aldehydes start to be produced (**Figure 3-23**). However, a new intermediate specie was detected, already supposed in the literature but never detected in our experiments in conventional synthesis.

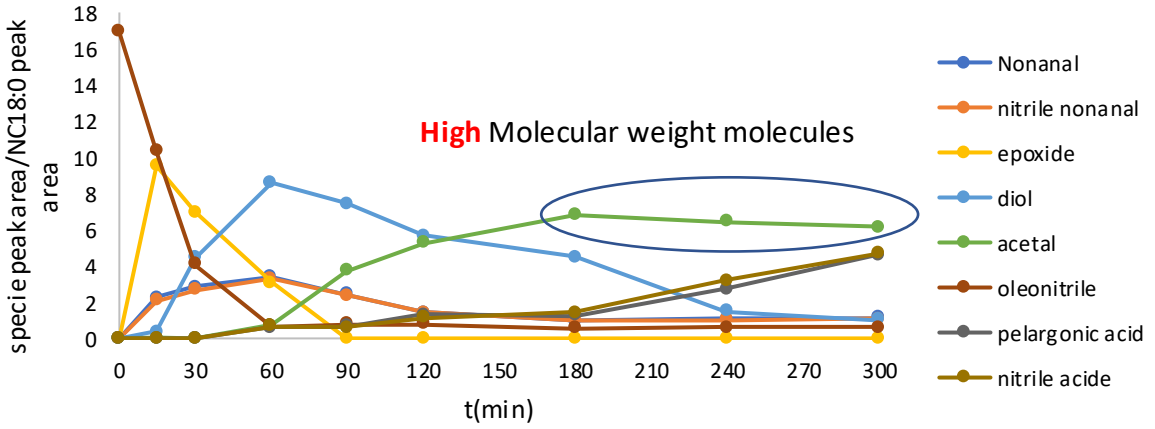

Figure 3-23. Oxidative cleavage on oleonitrile reaction progression. Reaction conditions: oleonitrile, 6 eq.35 wt% H_2O_2 and 2 mol% $H_3PW_{12}O_{40}$.45-60°C, 25 kHz, 100 W input power for 5h.

In GC/MS analysis 2 peaks were observed in the range of retention time of 39.42 to 39.86 minutes identified as di-ketones (**Figure 3-24**). The beta-fragmentation of diketone *cis* and *trans* was identified in the mass spectrum of the two different peaks. Such suggests a new pathway mechanistic when applied high intensity ultrasound.

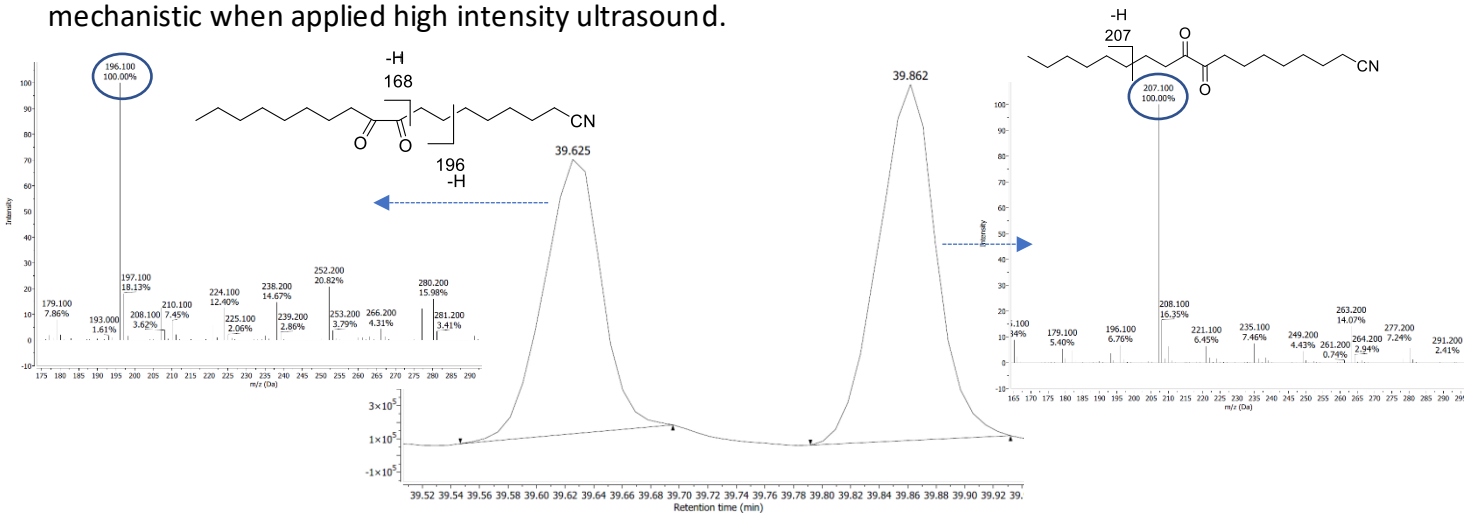

Figure 3-24. Chromatogram and mass spectrum of cis/trans diketone intermediate specie.

Therefore, we can conclude that ultrasounds not only catalyse the oxidative cleavage reaction but also the ketonization of the diol intermediate (20 % in GC-FID peak areas).

Estolides and acetals species from the oxidative cleavage of oleonitrile were identified by ^{1}H-NMR and GC-MS.

Once the first oxidative cleavage products, aldehydes, start to be formed, and the diol intermediate is still present in the reaction media; the acidic medium conditions, pH=1, catalyses the acetalization and ketonisation (when ultrasounds are applied) of diol intermediate species (**Scheme 3-9**).

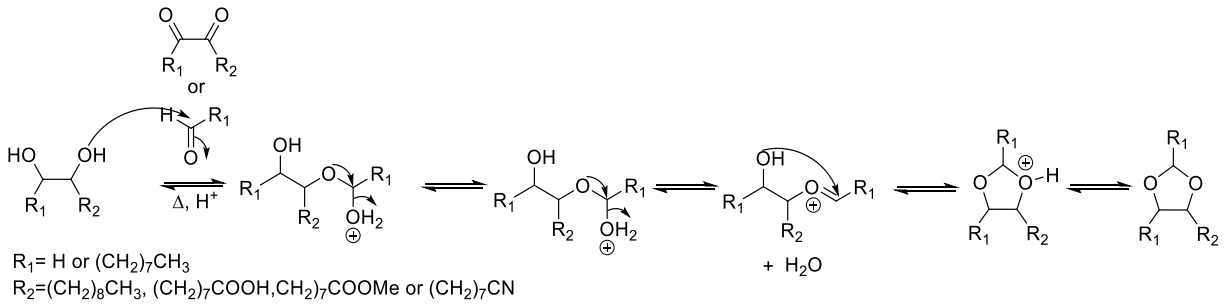

Scheme 3-9. Acetalization of diol intermediate formed.

Also, in the oxidative cleavage of oleonitrile, we were able to identify by GC-MS, the acetals formed with different carbon chain lengths (**Figure 3-25**). This result can be explained by the loss of a carbon through Bayer-Villiger oxidation.

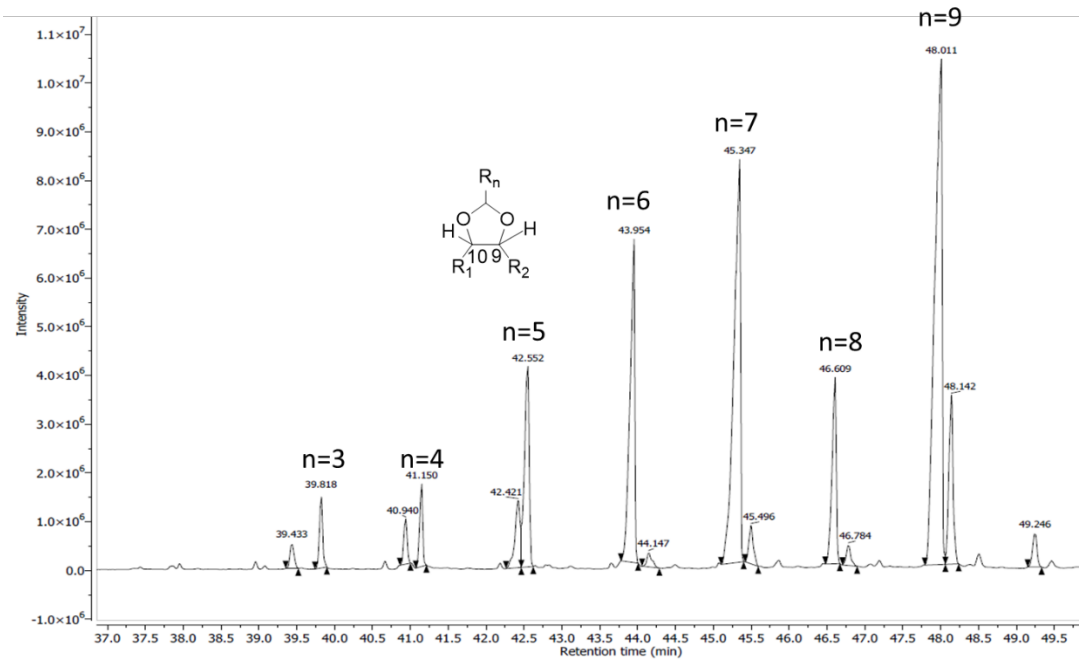

Figure 3-25. GC-MS spectrum of intermediate acetal specie with different carbon chain lengths.

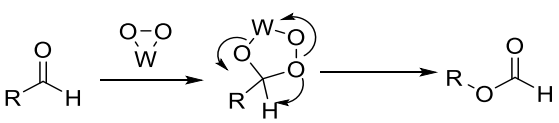

Scheme 3-10. Bayer-Villiger oxidation.

Through successive alcohol oxidations and concomitant Bayer-Villiger oxidation, the species with one carbon less can be formed.

The estolides and acetals species from oleic acid, 1-decene, decen-(1)-oic acid and decen-(1)-oate were only identified on the analysis of the crude mixture in ^{1}H-NRM and ^{13}C-NMR spectroscopy (**Figure 3-26**).

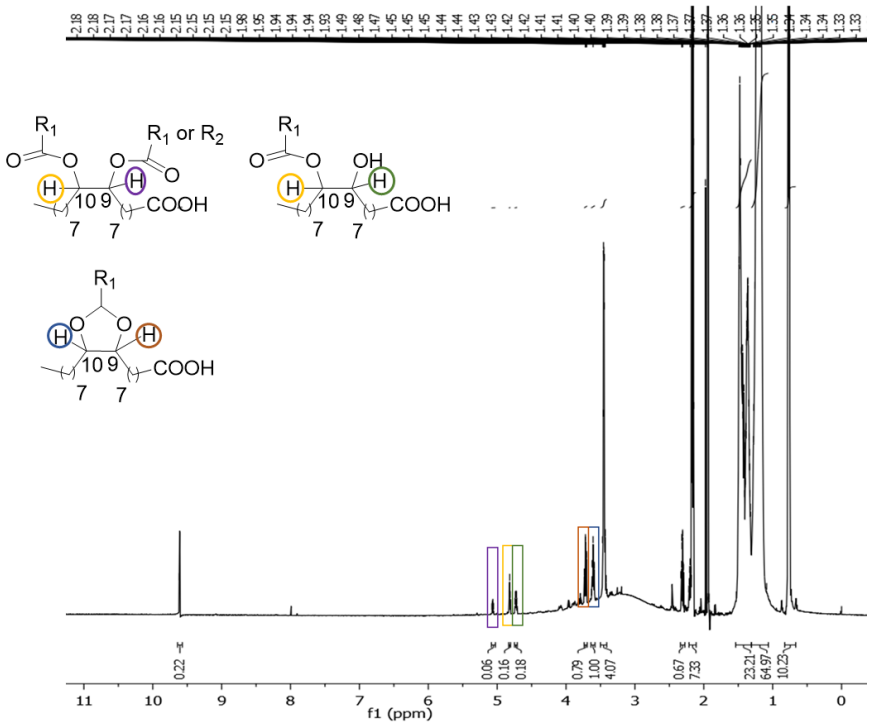

Figure 3-26. ^{1}H-RMN crude organic phase from oxidative cleavage of oleic acid.

3.3.4 Reaction mechanism (some considerations)

The studies pursued on the oxidative cleavage of unsaturated fatty compounds in presence of a catalytic system H_2O_2/ H_2WO_4 or $H_3PW_{12}O_{40}$, demonstrated that the reaction in acidic conditions and in presence of ultrasounds may generate different mechanistic pathways, producing higher molecular weight molecules which can be an important constraint in the reaction proceeds and consequently restrict the obtention of higher monomer yields.

Beyond the oxidative cleavage of oleonitrile, these intermediates were never identified in the chromatographic method applied. Their discovery explains the mass not quantified by the chromatographic method missing in the mass balance of the reaction.

The oxidative cleavage of unsaturated fatty compounds with H_2O_2 was extensively studied by different authors [14,23]. The most widely accepted is the reaction mechanism proposed by Noyori et al [23], which includes the epoxidation of C-C double bond of the monounsaturated

compound, giving the peroxidic character of the catalyst, epoxide (**2**) hydrolysis to afford 1,2-diol (**4**) intermediate and oxidation of 1,2 diol affording the first oxidative cleavage products, the aldehydes (**5** and **6**), and finally, through Bayer-Villiger oxidation to produce the final carboxylic acid (**7** and **8**) products (**pathway a**, **Scheme 3-11**). However, in the literature fewer are the authors that highlight the formation and importance of by-products as well the different mechanistic pathways.

In our experiments we observed, only in the experiments carried by sonication, the formation of an intermediate di-ketone (**pathway b**, **Scheme 3-11**).

Antonelli et al. [14] suggested, as mentioned in chapter one, the formation of an hydroperoxide specie which, by thermal decomposition, would afford the di-ketone intermediate also detected in our experiments under sonication. In 1921, Sharpless did also already mentioned the production of diketones oxidised by $KMNO_4$ and later Lee *et al.* [24] suggested that the dione takes place via an abstraction of hydrogen atom in analogy with the oxidation of alcohols (**Scheme 3-12**). In their application of ultrasounds in a binary heterogeneous mixture, for the scission of monoenic fatty acids, Rup *et al.* [4] also describes the existence of this intermediate when a ruthenium catalyst is applied in the system.

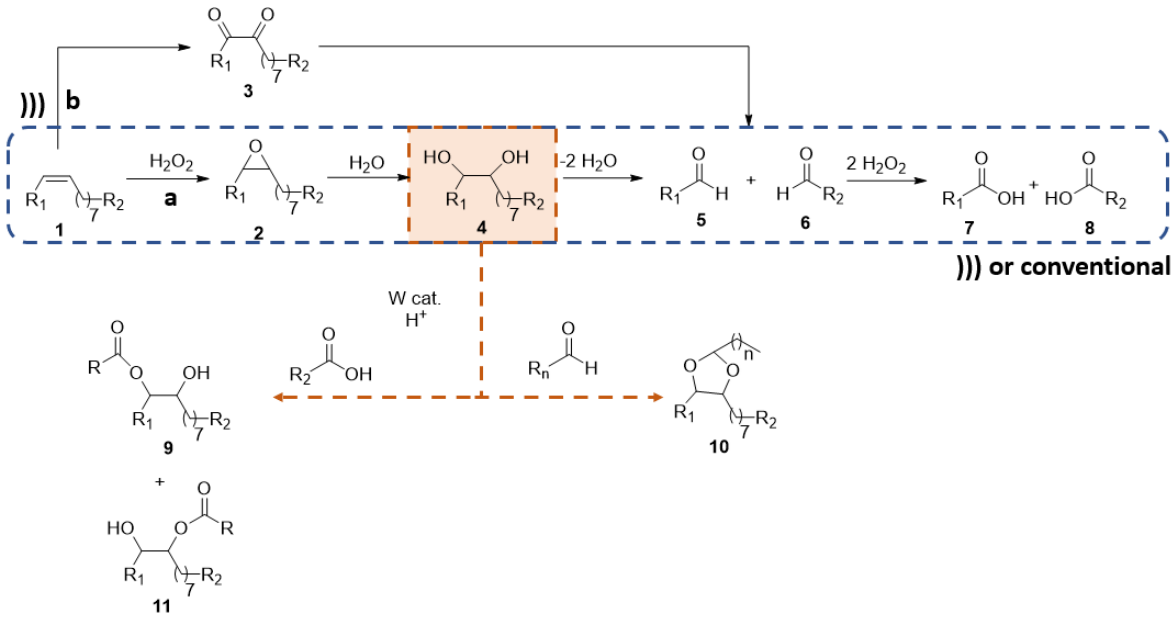

Scheme 3-11. Oxidative cleavage mechanism and by-products formation according to our experiments under sonication and in silent conditions.

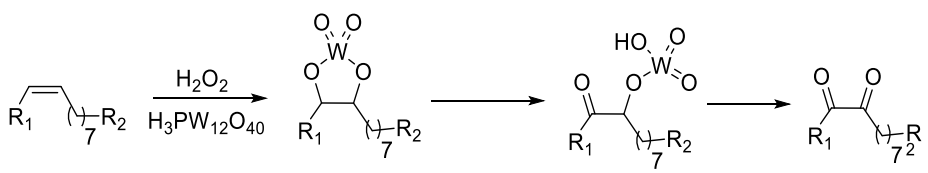

Scheme 3-12. Possible mechanism to the formation of di-ketone intermediate based in literature [5].

3.3.5 Solvent influence

We studied the oxidative cleavage of oleic acid and 1-decen in solvent conditions. We used *tert*-butanol, highly described in the literature as radical scavenger and octanoic acid. In case of 1-decen we tested pelargonic acid and decanenitrile as the reaction solvent (**Scheme 3-13**).

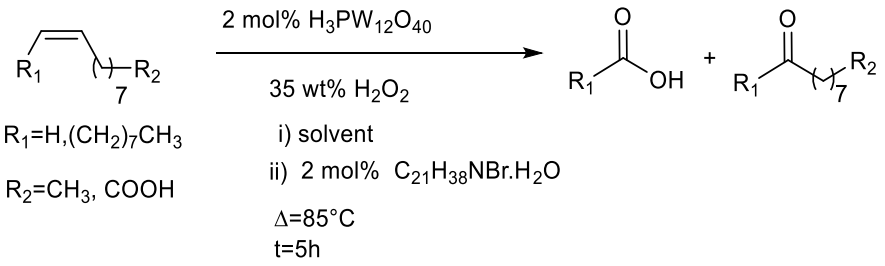

Scheme 3-13. Oxidative cleavage of oleic acid or 1-decen. Reaction conditions: Oleonitrile, 2 eq% H_2WO_4, 6 eq. H_2O_2, 24h, T:90°C i) solvent tert-butanol, octanoic acid, pelargonic acid or decanenitrile ii) 2 eq % cetylpiridinium bromide solvent-free. Eq: mol reactant/mol monounsaturated compound.

Surprisingly in presence of octanoic acid, pelargonic acid and decanenitrile, the conversion of oleic acid and 1-decen was low. Through the quantification of H_2O_2 during the reaction time we observed a decrease of 20 wt% already in the first minutes of reaction.

With the results obtained we can assume that the decomposition of hydrogen peroxide is favored when substrate with acid function are present in the reaction media. Such result shows that this might be not the best system to produce high % of monomers in industrial scale once when the pelargonic acid is produced during the reaction, the decomposition of H_2O_2 is favored instead of the oxidative cleavage (**Table 3-25** and **Table 3-26**).

Solvent	PA (%)	AA (%)	Conversion (%)
tert-butanol	20	23	100
Octanoic acid	0	0	10
Solvent-free conditions	55.5	62.1	100

Table 3-25. Pelargonic acid and azelaic acid yield obtained in the oxidative cleavage of oleic acid in solvent and solvent-free conditions. Reaction conditions: oleic acid, 2 eq% $H_3PW_{12}O_{40}$, 6eq. H_2O_2, 2eq % cetylpiridinium bromide (in solvent-free conditions), 2 eq. mol solvent to oleic acid (no PTA added). Eq.: mol reactant/mol monounsaturated fatty acid.

solvent	PA (%)	Conversion (%)
Decanenitrile	0	0
Pelargonic acid	0	0
Solvent-free	35	100

Table 3-26. Pelargonic acid yield obtained in the oxidative cleavage of 1-decen in solvent and solvent-free conditions. Reaction conditions: oleic acid, 2 eq% $H_3PW_{12}O_{40}$, 6eq. H2O2, 2eq% cetylpiridinium bromide (in solvent-free conditions), 2 eq. mol solvent to oleic acid (no PTA added). Eq.: mol substrate/mol monounsaturated fatty compound.

3.3.6 Continuous system

Overall, the oxidative cleavage of oleonitrile under sonication afforded satisfactory results at lower temperature than applied in conventional batch methodology and in the absence of a phase transfer agent, in that sense, we decided to study the viability of the catalytic system in a continuous flow apparatus (**Figure 3-27**) under sonication.

We built the apparatus in a semi-continuous system where, firstly a stirrer tank reactor (**STR1**) was charged with oleonitrile and continuously fed dropwise with an oxidant mixture comprises of 35 wt% H_2O_2 and a tungsten-based catalyst for 2h. The reaction media was heated at 90°C for these two hours. After the end of addition of the oxidant solution the reaction media was

pumped through the ultrasound reactor with a flow of 10 or 20 mL/min and finally collected in a second stirrer tank reactor (**STR2** cooled at 35°C) to control the reaction after sonication. We tested the influence of ultrasonic amplitude, contact time and temperature of the medium before sonication in the reaction proceedings (**Figure 3-27**).

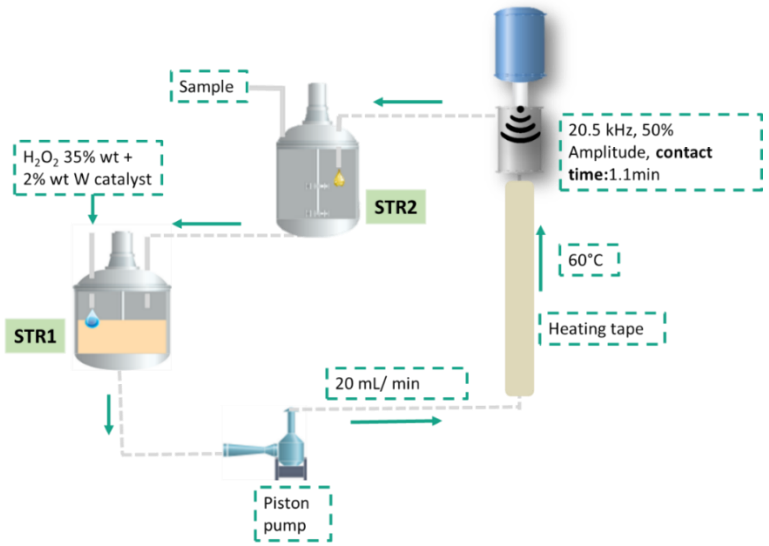

Figure 3-27. Oxidative cleavage continuous flow system.

After 2h in **STR1** we cooled down the reaction media until 35°C in order to avoid any reaction in the circuit from the **STR1** to the ultrasonic system. We proceeded for a total of 5 cycles (**Figure 3-28**). We observed an increase of temperature (14°C approximately) of the reaction media associated with the application of ultrasounds.

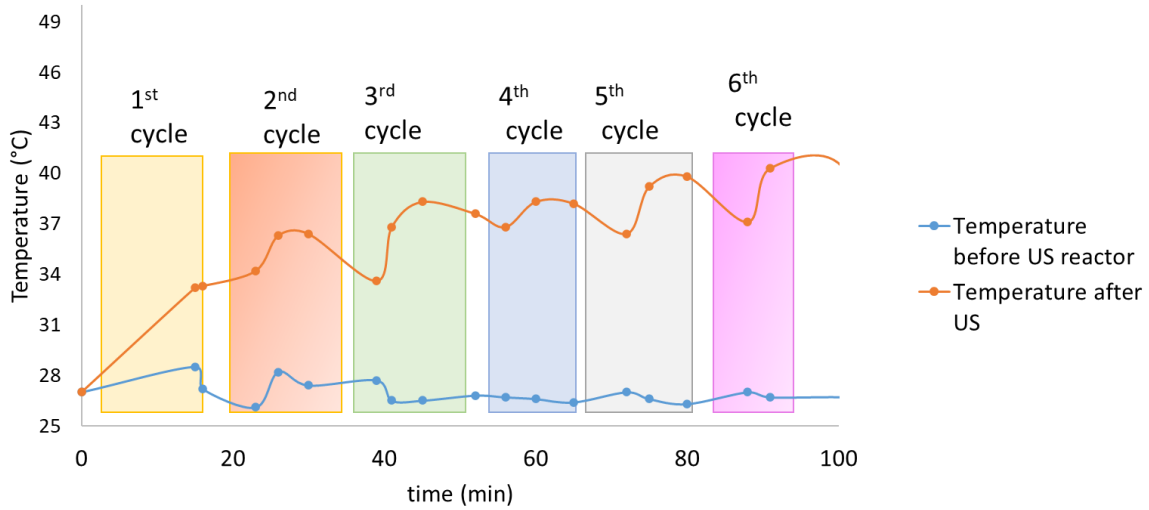

Figure 3-28. Temperature variation before and after sonication.

With the increase of the liquid temperature to 72°C, before sonication, a substantial improvement was observed in the kinetic of reaction (**Figure 3-29**).

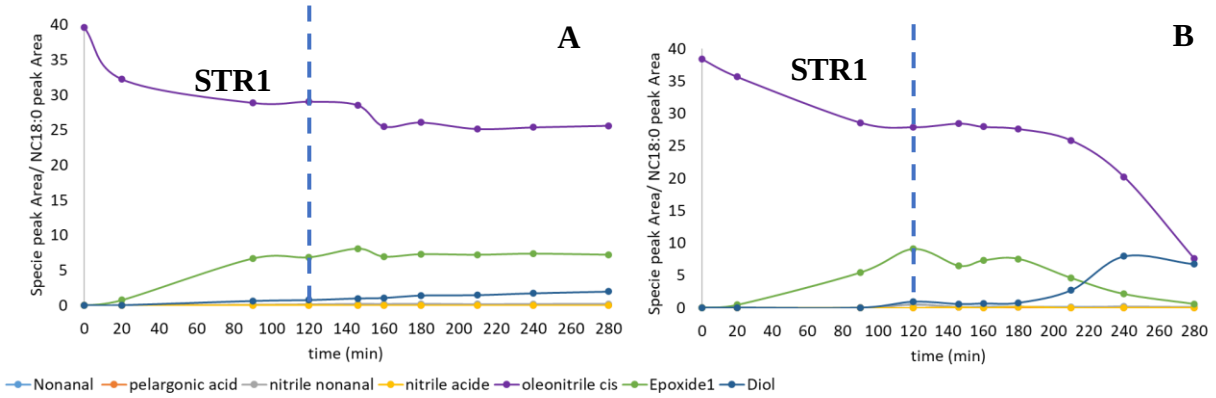

Figure 3-29. Oxidative cleavage of oleonitrile reaction profile. A- liquid at 35°C before sonication, B-liquid at 70°C before sonication.

3.3.6.1 *Ultrasonic amplitude and contact time variation in flow conditions*

We studied the influence of variation of amplitude in conversion of oleonitrile. We observed an improvement of 12% and 15% oleonitrile at 50W and 100W compared with 5% obtained in silent conditions. However, only 1-2% improvement on the conversion of oleonitrile was obtained by increasing the ultrasonic contact time from 0.9 to 1.8 minutes and at different amplitudes (**Table 3-27**).

trial	time	Amplitude	Flow (mL/min)	% ON conversion	% 120-1ST cycle
1	120[1]	Silent	20	68	5
	135[2]			73	
2	120[1]	50%		45	11
	135[2]			56	
3	120[1]	Silent		62	4
	135[2]			66	
4	120[1]	100%		63	12
	135[2]			75	
5	120[1]	Silence	10	46	3
	155[2]			49	
6	120[1]	100%		45	15
	155[2]			60	

Table 3-27. Conversion of oleonitrile before and after one catalytic cycle in silent conditions and with a total sonication of 0.9 to 1.8 minutes and input power amplitude of 50% (50 W) and 100% (100 W). [1]- Reaction time in STR1, [2]- Reaction time after 1 cycle.

By comparing the conversion obtained, after 5h in silent conditions, we can assume that the ultrasound technology does have a positive impact in the conversion of oleonitrile, once in 6 minutes of total sonication time and at lower temperatures than in batch conditions, we were able to obtain similar conversion (75%) as in conventional conditions at 90°C using a stirred tank reactor with mechanical agitation (**Table 3-28**).

System	Temperature	ON conversion	Nitrile aldehyde	nonanal	Pelargonic acid	Nitrile acid
Batch reactor (mechanical agitation)	90°C	98 %	31 %	28 %	18 %	15 %
Continuous sonication system	70°C	90 %	28 %	29 %	4 %	5 %

Table 3-28. Batch mechanical agitation vs Continuous sonication system**.**

Nonetheless, the results obtained does not sustain the applicability of ultrasound in an industrial process for the oxidative cleavage with the catalytic system described.

3.4 Conclusion

It has been proved that mass transfer across the phase boundary of a multiphasic system is substantially enhanced through acoustic emulsification. The aim of our work was to exploit sonochemical methods to overcome mass transfer and time limitation of conventional oxidative cleavage reaction in monounsaturated MUFAs and derivatives.

Significant results were obtained with an ultrasonic horn, working at frequency of 25 kHz and 100W of input power. With this system we were able to reduce **1)** the reaction time from 24h to 5h, **2)** the concentration of H_2O_2 from 70% to 35%, **3)** reduce the working temperature from 90°C to 60°C but also **4)** to achieve the desirable monomers in the absence of an emulsifier. The oxidative cleavage products of oleonitrile were obtained at similar monomer yields of 40% (pelargonic acid) and 45% (8-cyanooctanoic acid) than in batch conditions at 90°C and 24h reaction time in presence of a PTA. However, the monomer yield attaint was not satisfactory.

With our experiments we discovered that the acidity of the medium due to the catalyst applied and the constitution of the monounsaturated fatty compound enhances the decomposition of H_2O_2 instead of the oxidative cleavage itself. Also, can generate higher molecular weight molecules, which viscosity hampers the mass transfer in the reaction medium. However, the formation of high MW molecules can be valorised. The same reaction system can be optimized to

be foccus on the production of high molecular weight acetals which can be isolated and hidrolysed to obtain the aldehydes intermediates which are much more valuable than the carboxylic acids. On the other hand to afford the carboxylic acids, a system in two steps would be preferred. Firstly, the synthesis of the diol intermediate, secondly increase of pH in reaction medium and concomitant oxidative cleavage with other oxidant than hydrogen peroxide, such as oxygen.

3.5 References

[1] B. Markush, J.-L. Couturier, J. Dubois, Process for producing nitrile-fatty acid compounds, U.S. patent 2013/0345388 (A1), 26 December 2013.

[2] A. Enferadi Kerenkan, F. Béland, T.O. Do, Chemically catalyzed oxidative cleavage of unsaturated fatty acids and their derivatives into valuable products for industrial applications: A review and perspective, Catal. Sci. Technol. 6 (2016) 971–987. doi:10.1039/c5cy01118c.

[3] S. Rup, M. Sindt, N. Oget, Catalytic oxidative cleavage of olefins by RuO4 organic solvent-free under ultrasonic irradiation, Tetrahedron Lett. 51 (2010) 3123–3126. doi:10.1016/j.tetlet.2010.04.040.

[4] S. Rup, F. Zimmermann, E. Meux, M. Schneider, M. Sindt, N. Oget, The ultrasound-assisted oxidative scission of monoenic fatty acids by ruthenium tetroxide catalysis: Influence of the mixture of solvents, Ultrason. Sonochem. (2009). doi:10.1016/j.ultsonch.2008.08.003.

[5] S. Rup, M. Sindt, N. Oget, Catalytic oxidative cleavage of olefins by RuO4 organic solvent-free under ultrasonic irradiation, Tetrahedron Lett. (2010). doi:10.1016/j.tetlet.2010.04.040.

[6] S.G. Gaikwad, A.B. Pandit, Ultrasound emulsification: Effect of ultrasonic and physicochemical properties on dispersed phase volume and droplet size, Ultrason. Sonochem. 15 (2008) 554–563. doi:10.1016/j.ultsonch.2007.06.011.

[7] M.A. Margulis, Fundamental aspects of sonochemistry, Ultrasonics. 30 (1992) 152–155. doi:10.1016/0041-624X(92)90065-T.

[8] M.A. Margulis, I.M. Margulis, Calorimetric method for measurement of acoustic power absorbed in a volume of a liquid, in: Ultrason. Sonochem., 2003: pp. 343–345. doi:10.1016/S1350-4177(03)00100-7.

[9] Y. Ishii, K. Yamawaki, T. Ura, H. Yamada, T. Yoshida, M. Ogawa, Hydrogen peroxide oxidation catalyzed by heteropoly acids combined with cetylpyridinium chloride. Epoxidation of olefins and allylic alcohols, ketonization of alcohols and diols, and oxidative cleavage of 1,2-diols and olefins, J. Org. Chem. 53 (1988) 3587–3593. doi:10.1021/jo00250a032.

[10] D.C. Duncan, R.C. Chambers, E. Hecht, C.L. Hill, Mechanism and Dynamics in the H3[PW12O40]-Catalyzed Selective Epoxidation of Terminal Olefins by H2O2. Formation, Reactivity, and Stability of {PO4[WO(O2)2]4}3-, J. Am. Chem. Soc. 117 (1995) 681–691. doi:10.1021/ja00107a012.

[11] Y. Yoshimura, Y. Ogasawara, K. Suzuki, K. Yamaguchi, N. Mizuno, "release and catch" catalysis by tungstate species for the oxidative cleavage of olefins, Catal. Sci. Technol. 7 (2017) 1662–1670. doi:10.1039/c7cy00062f.

[12] H. Suzuki, O. Tomita, M. Higashi, R. Abe, Tungstic acids H2WO4 and H4WO5 as stable photocatalysts for water oxidation under visible light, (2017) 10280–10288. doi:10.1039/c7ta01228d.

[13] C. Venturello, R. D'Aloisio, M. Ricci, Peroxide Composition Based on Tungsten and Phosphorus or Arsenic, and Processes and US ES Relative thereto, U.S. patent 4595 671 (A) , 17 Jun 1986.

[14] E. Antonelli, R. D'Aloisio, M. Gambaro, T. Fiorani, C. Venturello, Efficient oxidative cleavage of olefins to carboxylic acids with hydrogen peroxide catalyzed by methyltrioctylammonium tetrakis(oxodiperoxotungsto)phosphate(3-) under two-phase conditions. Synthetic aspects and investigation of the reaction course, J. Org. Chem. (1998). doi:10.1021/jo980481t.

[15] A. Godard, P. De Caro, E. Vedrenne, Z. Mouloungui, S. Thiebaud-Roux, From crops to products for crops: preserving the ecosystem through the use of bio-based molecules; From crops to products for crops: preserving the ecosystem through the use of bio-based molecules, Publ. by EDP Sci. 23 (2016). doi:10.1051/ocl/2016037.

[16] L.C. de la Garza, K. De Oliveira Vigier, G. Chatel, A. Moores, Amphiphilic dipyridinium-phosphotungstate as an efficient and recyclable catalyst for triphasic fatty ester epoxidation and oxidative cleavage with hydrogen peroxide, Green Chem. 19 (2017) 2855–2862. doi:10.1039/C7GC00298J.

[17] C. Venturello, M. Ricci, Oxidative cleavage of 1,2-diols to carboxylic acids by hydrogen peroxide, J. Org. Chem. 51 (1986) 1599–1602. doi:10.1021/jo00359a042.

[18] A. Godard, P. De Caro, E. Vedrenne, Z. Mouloungui, S. Thiebaud-Roux, From crops to products for crops: preserving the ecosystem through the use of bio-based molecules, Publ. by EDP Sci. 23 (2016) 1–12. doi:10.1051/ocl/2016037.

[19] D. Radziuk, H. Möhwald, Ultrasonically treated liquid interfaces for progress in cleaning and separation processes, Phys. Chem. Chem. Phys. 18 (2016) 21–46. doi:10.1039/C5CP05142H.

[20] M.A. Bradley, S.W. Prescott, H.A.S. Schoonbrood, K. Landfester, F. Grieser, Miniemulsion Copolymerization of Methyl Methacrylate and Butyl Acrylate by Ultrasonic Initiation, Macromolecules. 38 (2005) 6346–6351. doi:10.1021/ma0473622.

[21] M.L. Wang, V. Rajendran, Ultrasound assisted phase-transfer catalytic epoxidation of 1,7-octadiene - A kinetic study, Ultrason. Sonochem. 14 (2007) 46–54. doi:10.1016/j.ultsonch.2006.01.007.

[22] V. Salinas, Y. Vargas, O. Louisnard, L. Gaete, Influence of the liquid viscosity on the formation of bubble structures in a 20 kHz field, Ultrason. Sonochem. 22 (2015) 227–234. doi:10.1016/j.ultsonch.2014.07.007.

[23] R. Noyori, M. Aoki, K. Sato, Green oxidation with aqueous hydrogen peroxide, Chem. Commun. (2003) 1977. doi:10.1039/b303160h.

[24] D.G. Lee, V.S. Chang, Oxidation of Hydrocarbons. 8. Use of Dimethyl Polyethylene Glycol as a Phase Transfer Agent for the Oxidation of Alkenes by Potassium Permanganate, J. Org. Chem. 43 (1978) 1532–1536. doi:10.1021/jo00402a009.

Chapter 4. Raney-Nickel catalyst recycling for the obtention of high-value amino-ester monomer

4.1 Introduction

Amino compounds find applications in several different markets. Compounds with amine substituents can be used in resins [1], rubbers [2], dyes[3], in the pharmaceutical industry as analgesics like Morphine [4] and emulsifiers[5]. An example is the dodecylamine and octadecylamine, readily available and cheap, prepared on a large scale from nitriles of fatty acids (lauric and stearic).

The nucleophilic nature of amines confers high reactivity, making them of crucial interest in the polymer industry. Along with amino acids, diamines from renewable sources are potential polymers building blocks.

The synthesis of diamine building blocks is mostly accomplished by the efficient heterogeneous catalytic hydrogenation of nitrile compounds extremely reported in several publications [6–8].

The most known application of diamine monomer is the production of Nylon 6,6 trough adiponitrile hydrogenation obtained from adipic acid with approximately 1.5 million tons/year **(Scheme 4-1).**

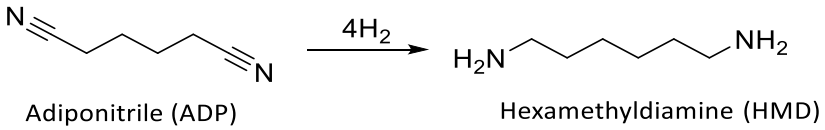

Adiponitrile (ADP) Hexamethyldiamine (HMD)

Scheme 4-1. Adiponitrile hydrogenation reaction.

Hydrogenations of nitriles are usually performed in the liquid phase at high temperatures and high hydrogen pressures in presence of heterogeneous transition metal catalysts.

On the paper, the hydrogenation of nitriles to amines is barely simple **(Scheme 4-2)**:

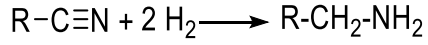

Scheme 4-2. Reduction of nitrile to amine by hydrogenation.

However, the experimental reality is highly more complex. The selectivity of the reaction can be extremely affected and limited by the possibility of by/co-products formation.

Starting with Sabatier and Senderens [9], the chemical principles and mechanisms of hydrogenation of nitriles has been investigated by many authors [10–12]. In the Sabatier's and Senderens's studies of alkylnitriles hydrogenation and on Mignonac [11] studies of aromatic nitriles hydrogenation both agree in the existence of an intermediate imine. Mignonac, supported this

statement by the identification of the hydrobenzamide (**3**) which he suggested that would be a product of three molecules of benzaldehyde imine (**2**) and concomitant obtention of secondary imine (**4**) and benzylamine (**5**) through hydrogenolysis (**Scheme 4-3**).

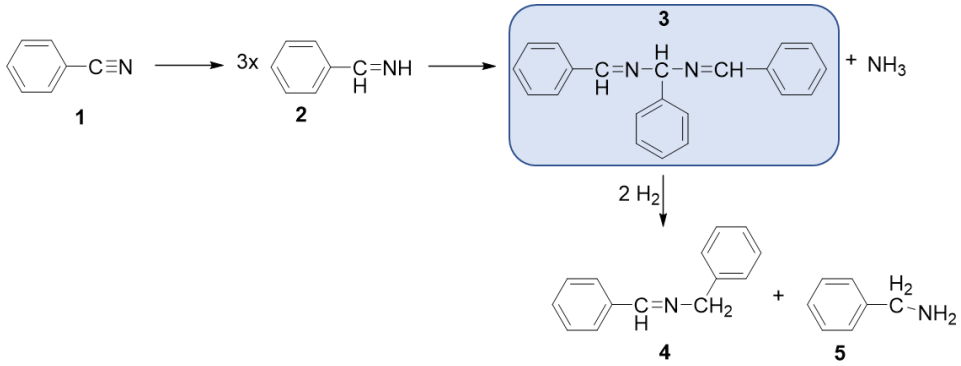

Scheme 4-3. Hydrogenation of benzene nitrile with di-imine intermediate formation (**3**).

Reaction complete mechanism was firstly proposed by von Braun et al [13] and later modified by Greenfield [10].

Greenfield [10] studied different catalysts transition metals based such as Co, Ni, Pt, Pd, Rh and Ru in the hydrogenation of butyronitrile to amines in methanol solution. The higher yields of butylamine were found in the experiments where Ni or Co catalysts were used yielding, without any alkaline additive, 81 and 79 % of primary amine, respectively. In these experiments, it was found that by adding ammonia in the reaction media, the ratio of primary to secondary amine significantly increased in the case of Ni and Ru based catalysts obtaining the yields of 97 and 89 %, respectively.

Good results were also achieved with other alkaline additives such as NaOH and sodium carbonate. However, it was observed that the reaction rate was highly reduced, even when low concentrations were applied (**Table 4-1**).

Alkaline additive	Time (hr)	mole yield nitrile (%)	mole yield $BuNH_2$ (%)	mole yield Bu_2NH (%)	mole yield Bu_3N (%)
-	0.8	-	81	16	-
NH_3	0.7	-	96.5	3.5	-
Na_2CO_3	2	-	92	8	-
NaOH	6.3	-	91	9	-

Table 4-1. Hydrogenation of butyronitrile to obtain butylamine. Ni catalysts 50% Ni on kieselguhr, Girdler G-49B, 125℃, Methanol as a solvent [10].

On the other side, catalysts platinum and palladium-based proved their efficiency for tertiary amine formation in water solution and the presence of ammonia.

More recently, researchers have sought to develop metal-supported catalysts without the presence of any additive. Segobia et al. [14] argue that the addition of ammonia affords concerns regarding the corrosion and additional costs of separation or disposal thereof. They reported the use of supported catalysts based in Ni, Co, and Ru in SiO_2 in the absence of alkaline additives in the hydrogenation of unsaturated cinnamonitrile.

4.1.1 Nickel – Devil's Copper

Firstly discovered by Cronstedt in 1751 [15], Nickel found application in catalysis, as aluminium nickel, ammonium nickel hydrates, nickel halides, nickel metals and Raney® Nickel catalysts.

Reduction reactions can be traced back to Wilde's hydrogenation of acetylene into ethylene and ethane in 1874. However, it was only in 1899, after the discovery of $Ni(CO_4)$ complexes by Mond in 1888 [16], that Sabatier and Senderens established for the first time nickel-based hydrogenation, converting unsaturated organic molecules into corresponding saturated compounds by passing the vapor of organic molecules and hydrogen over hot, finely divided nickel [9]. The organo-nickel chemistry Era had begun.

Nickel-based catalysts have proven their effectiveness in several types of reactions, including cross-couplings [17], methanations [18,19], nucleophilic allylations [20], oligomerisations [21,22], hydrodeoxygenations [23] and hydrogenation processes [24].

4.1.1.1 *Raney catalysts*

Raney catalysts are widely used in the industry due to their high activity, technological ability and relatively low cost. Traditionally they are made by leaching of a non-noble component pyrometallurgical alloys (PM).

Hydrogenation reactions can be pursued using heterogeneous Raney® nickel catalyst, which is the most popular catalyst in the field. Invented by Murray Raney in 1927 [25], the catalyst is prepared by leaching a doped Ni and Al alloy with a sodium hydroxide solution.

Raney®-nickel catalysts, also known as sponge Nickel, have magnetic properties [26]. These catalysts are designated in forms W1 to W8. The differences in these catalysts are the varied activities that they show, which are the result of different preparation methods; alloy composition, NaOH concentration, the temperature at which the alloy is added to the basic solution, the temperature and duration of alloy digestion after addition to the base, and finally the method used to wash the catalyst from the sodium aluminate and excess base [27]. Type W6 [28] is the most active catalyst and has several well-known advantages, including high activity and selectivity, but its poor stability and short lifetime mean that catalyst replacement is required, which entails high costs and environmental impact.

This method includes the cast of a Nickel and aluminium ingot of 50:50 wt% composition with a subsequent crush to a fine particle size of the order of 50-100 µm. The Ni-Al powder is consequently leached using aqueous sodium hydroxide solution to remove the aluminium (caustic leaching) **Scheme 4-4** [29].

$$2(Ni-Al)_{(s)} + 2OH^-_{(aq)} + 6H_2O_{(l)} \rightarrow 2\,Ni_{(s)} + 2Al(OH)^-_{4(aq)} + 3H_{2(g)}$$

Scheme 4-4. Nickel aluminium leaching.

4.1.1.2 *Applications*

Nickel sponge type catalysts are used to the obtention of high-value monomers such as adipic acid through benzene reduction, performed in the slurry phase, to obtain cyclohexane, which is subsequently oxidised to adipic acid [30] or sorbitol also produced via the catalytic hydrogenation of glucose over Raney®-nickel catalysts [31]. Another example of products that are obtained using this catalyst can be found in di-amine monomers, which are produced via the reduction of di-nitriles, such as in the reduction of adiponitrile to hexamethylenediamine [6]. A further example is the use of this catalyst in the preparation of amino-ester monomers, such as methyl 11-aminoundecanoate, from 10-cyanodecenoate [32]. Methyl 11-aminoundecanoate is the alternative monomer used for the production of polyamide 11 (Rilsan ®) [33].

4.1.1.3 *Advantages*

Due to its high specific surface area (BET) (varying from 20 to 100 m^2), Raney Nickel is extremely reactive. Its production has low cost compared with precious metal catalysts and it is easily removed from the product due to its high density (8.9 x 10^3 $kg.m^{-3}$) and ability to customize composition and add promoters.

4.1.1.4 *Disadvantages*

Powdered Raney Nickel cannot be applied in fixed-bed reactors and after the reaction must be separated from the reaction medium by costly sedimentation and/or filtration. Therefore, a variety of processes for preparing fitted items to be performed as fixed-bed catalysts have been disclosed such as the preparation of granulated catalysts prepared by crushing the alloy to the required size range with concomitant catalyst reactivation or the preparation of extruded Raney-Nickel catalysts by the addition of other metals such as Cu and/or Cr [34].

Nowadays an increased number of researchers have devoted their work in the production of Raney Nickel properly shaped, to be adapted to fix-bed reactors. The research is focused in the activation of the superficial layer of granular Raney alloys by adding different substances into catalyst alloy [35] or even by adding polyamides, such as PA 6, to support the catalyst, as it is described in the Haibin Jiang et al [36] work.

Raney Nickel catalytic activity is hard to control and during its application it is inevitable that degradation of catalyst occurs, Al_2O_3 is released and its acidity can lead to side reactions.

4.1.1.5 *Deactivation mechanisms*

The low stability and catalyst lifetime are compensated by the outstanding properties of Raney-Nickel, such as high activity and selectivity.

Catalyst deactivation is a pervasive issue resulting in the loss of catalytic reaction rate, loss of catalytic activity, and selectivity over time. Industrially such a phenomenon can represent a cost of billions of dollars per year as it demands catalyst replacement and process shutdown.

Deactivation is caused by several factors: chemical (poisoning, vapor compound formation accompanied by transport, and vapor-solid and/or solid-solid reactions); mechanical (fouling and attrition/crushing); thermal (thermal degradation); and sintering (agglomeration of metal particles). Regarding to Raney-Nickel catalysts it is for example known that a catalyst in the W5 form can lose its activity after about a week of storage in ethanol, due to the formation of acetaldehyde, which poisons the catalyst [27].

In nitrile hydrogenations, Raney®-nickel deactivation is caused by chemisorption through multiple bonds and π-back bonding.

4.1.1.6 *Reactivation mechanisms*

As mentioned before, Raney-Nickel catalysts can be one of the costly ingredients in the chemical process where is applied. The industrial requirement is that the catalyst should be reactivated after deactivation to recover its capabilities to a significant level. Meanwhile its reactivation it is not always equal depending upon a multitude of factors, such as, the nature of the contaminants and present level of hydrogenation capability of the catalyst. Generally, the process of reactivation involves a loss of 5 to 40% of the material due to the removal of oxidized Nickel and contaminants/residues of reactants.

The most common procedures for exhausted (inactive) Raney®-nickel recycling include acidic treatment (acetic acid at 20-50°C) or treatment with non-oxidising aqueous alkaline solution (NaOH at 40-150°C). More recently, Haoliang Ping *et al.*, have proposed a regeneration method that involves coke elimination with water, from 300°C to 450°C, for a catalyst that is deactivated during the dehydrogenation of cyclohexane.

4.2 Aim of the work

In 2014 the team of Johan Bidange, Jean-Luc Dubois and Jean-Luc Couturier et al; studied the production of methyl-10-cyanodecenoate by ruthenium catalysed ethenolysis of oleonitrile affording 9-decenitrile [37–40]. Arkema has being investigating, in the past years, the obtention of unsaturated products by cross metathesis [41]. In this study, the 10-cyanodecenoate was obtained from cross metathesis of methyl-9-decenoate with acrylonitrile. Below we describe the different process steps for the production of methyl -11-amino-undecanoate, an alternative monomer to synthesize the Polyamide 11 (**Figure 4-1**).

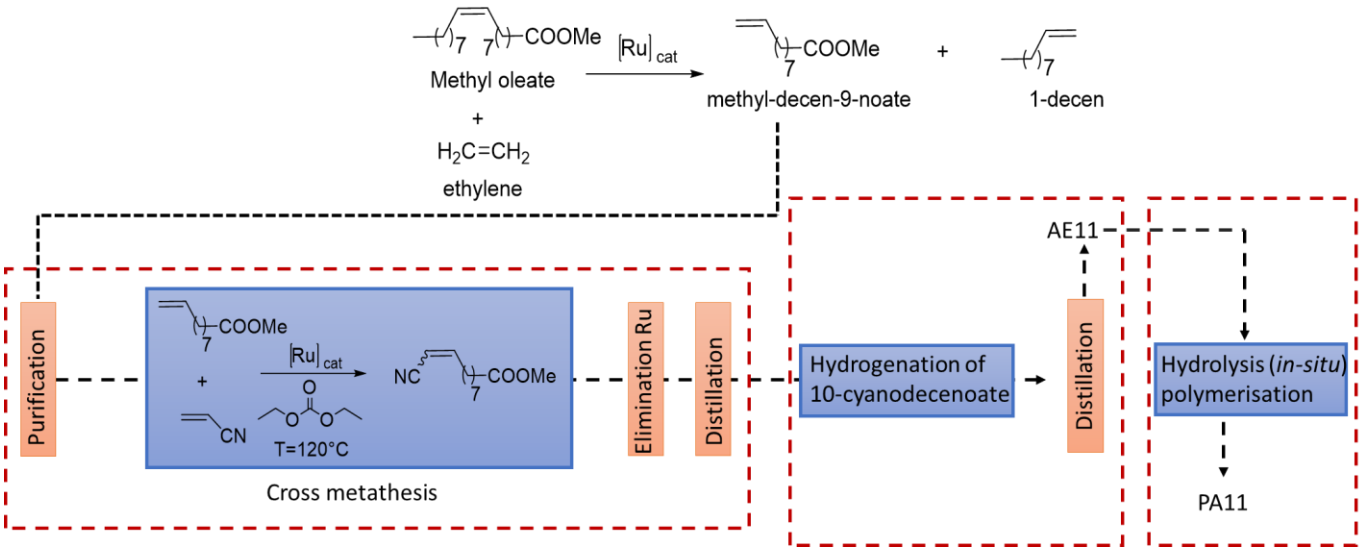

Figure 4-1. Production of PA11.

In previous work, the synthesis of amino-esters from nitrile-esters was tested with different catalysts such as Ru, Co, Nickel and Raney-Nickel catalysts [42].

The main objective of our work was to study the deactivation and reactivation mechanism of a commercial Raney-Nickel catalyst, as it deactivates faster in the hydrogenation of 10-cyanodecenoate. Herein we describe the efficiency of three different Raney-Nickel reactivation procedures: solvent wash, sonication or under hot hydrogen and its application in the

hydrogenation of methyl (9Z)-10-cyano-9-decenoate (UNE11) to produce methyl-aminoundecanoate (AE11).

The main purpose of the work was to study the catalyst reactivation and its deactivation mechanisms; however, herein, we also propose a kinetic model based on data from the experiments pursued to obtain the highest catalyst deactivation. To more accurate kinetic study, more precise experiments should be produced.

4.2.1 Safety consideration

Caution!!

Particular attention must be paid when handling Raney®-nickel because it is self-heating and spontaneously ignites upon contact with air (pyrophoric nature). This phenomenon is caused by the high dispersion and strong lattice distortion of Raney®-nickel. Moreover, the hydrogen that is contained within, and its consequent gas desorption, can lead to self-ignition. For these reasons, contact with air must be prevented by keeping the catalyst wet within liquids, such as water.

Raney®-nickel should **NEVER** be thrown into a waste receptacle, and always deposited in special waste disposal equipment.

4.3 Materials and Methods

Chemical Reactants

The solvents, methanol, toluene and methylcyclohexane, were purchased from Merck-Sigma Aldrich and VWR chemicals. Methyl (*9Z*)-10-cyano-9-decenoate 98% was produced in the R&D laboratories of Arkema Rhône-Alpes Research Center - France (CRRA). The Commercial catalyst Raney®-nickel 4200 (W.R. Grace and Co. Raney®) was used, as a slurry in H_2O, as the heterogeneous catalyst for the synthesis of amino ester monomers.

4.3.1 Instrumentation and acquisition parameters

Chromatographic analysis

Gas chromatography was performed using a gas chromatograph 6890 Series GC System Agilent equipped with a flame ionisation detector and an autosampler. 1 µL aliquots of the samples were injected. The retention gap was attached to a 30 m x 0.530 mm ID column filled with a 1.0 µm film thickness Rtx®- 200 stationary phase. The initial oven temperature of 60 °C was increased to 165 °C at a rate of 15 °C/min, then to 200 °C at a rate of 4 °C/min and then finally increased to 300 °C at a rate of 25 °C/min. The injector and detector temperatures were set at 230 °C and 320 °C, respectively. Helium was used as the carrier gas for the mobile phase at a flow control from 3.5 mL for 8 minutes and increased to 6.0 mL/min with a rate of 0.25 mL/min/min and hold time of 22 minutes. The column was backflushed at 320 °C for a total of 4 void volumes after every run to prevent the appearance of ghost peaks from previous runs.

The peak area % of AE11 specie was assigned with an uncertainty of +/- 4 % (2*RSD=2σ). The same relative standard deviation was assumed for the other products.

Fourier Transformed Infrared (FTIR) spectra were recorded in transmission mode at a resolution of 2.0 cm^{-1} and by acquiring 60 scans on a Perkin-Elmer 2000 spectrometer (equipped with a MCT detector).

GC/MS analysis were performed in a GC Agilent 6890 (Agilent technologies, Santa Clara, CA, USA) accoupled with a mass detector Agilent Network 5973, using a 30 m capillary column, i.d. of 0.25 mm and 0.25 µm of film thickness HP-5 5% Phenyl Methyl Siloxane stationary phase. The initial oven temperature of 60 °C was increased to 165 °C at a rate of 15 °C/min, then to 200 °C at a rate of 4 °C/min until 200°C and then finally increased to 300 °C at a rate of 25 °C/min with a hold time of 10 minutes. The injector and detector temperatures were set at 250°C and 280 °C, respectively.

Helium was used as the carrier gas for the mobile phase with a flow of 1.3 mL/min. The column was backflushed at 300 °C for a total of 3 void volumes after every run to prevent the appearance of ghost peaks from previous runs.

FTIR Measurements on Raney Nickel catalyst

The samples in the form of powders suspended in H_2O were deposited by dropping the solution directly on a **KBr pellet** that was fixed in a cell allowing thermal treatments in controlled atmosphere and spectrum scanning at controlled temperature (from 90 K up to RT). The cell was connected with a vacuum line.

The samples were outgassed at room temperature for 10 minutes to remove water and then cooled at 90 K under outgassing before CO adsorption at low temperature. The spectrum of the sample before the inlet of the probe was used as background for each spectrum of adsorbed CO.

ICP/MS analysis

Micro-analysis was performed using ICP MS ICAP Qc thermo with S10 auto sampler. The samples were digested with a solution of chloridric acid and nitric acid in the proportion of 4:1. The internal standard solutions of Ni and Al were prepared from 5µg/l – 10 µg/l – 20 µg/l and 50 µ/l.

4.3.2 Hydrogenation of methyl 10-cyanodecenoate (UNE11)

The hydrogenation of UNE11 was performed in a 300 cm^3 stirred batch reactor. The temperature was controlled automatically by heat exchange via the wall and a cooling coil. The reaction media was agitated by a gas-inducing Rushton turbine. The autoclave was also linked to a vent line, which can sustain pressure at 0-200 bar, and itself connected to a Yokogawa recorder and a manometer.

4.3.3 *Treatment of Raney®-nickel catalyst*

Commercial Raney®-nickel is usually stored in water in order to minimise surface oxidation and delay the catalyst-aging process. The extraction of the water that remains in the catalyst entails washing with methanol (3 x 10 mL), followed by 3 x 10 mL of the chosen solvent. We considered the catalyst weight to be constituted by those of the final washing solvent and the catalyst itself in 50 wt% in solvent (estimated).

4.3.4 *Reaction setup*

The operating conditions used in the various experiments are reported in **Table 4-2**. Solvent, catalyst and (9Z)-10-cyano-9-decenoate were poured into the reactor to a maximum volume of 180 cm3, and gaseous ammonia was then added. The reaction was carried out at constant pressure, in the 40-60 bar range, by manual hydrogen feed regulation. The temperature was set to 90°C. Hydrogen consumption lasted 3h (**Table 4-2**).

Stirrer speed (tr/mn)	**1000-1500**
UNE11 concentration (*wt* % to solvent)	30, 40 and 50
Solvent	Toluene or Methylcyclohexane
Temperature (°C / K)	90 °C (363 K)
Reaction time (min)	120-180
Catalyst loading (dry eq. *wt* % related to UNE11)	2, 5, 10 and 20 wt %
NH_3 (equivalents to UNE11)	0.9 to1.15

Table 4-2. Hydrogenation of (*9Z*)-10-cyano-9-decenoate to methyl-11-amino-undecanoate reaction conditions.

4.3.5 *Ultrasound reactivation set-up*

The catalyst reactivation experiments under sonication were performed in a round bottom flask placed in an ultrasonic cleaning tank with ultrasonic mono-frequency module generator at 25 kHz and multi-frequency module generator at 40, 80, 120 kHz (SONIC DIGITAL MULTI). Cavitation density changes with the position in the tank. In order to precisely locate the flask where the highest energy density and cavitation distribution would be applied, we used an aluminium foil to determine

the right position for a more efficient sonication. Cavitation phenomenon's more aggressive, higher energy density, such as jetting cavitation can be observed by the appearance of holes in the foil sheet.

The reaction species were identified and quantified (peak areas %) by gas chromatography with flame ionisation detection (FID). Reaction samples were prepared at a concentration of 66 µL/mg in $CHCl_3$.

4.3.6 Instrumentation and acquisition parameters

Chromatographic analysis

Gas chromatography was performed using a gas chromatograph 6890 Series GC System Agilent equipped with a flame ionisation detector and an autosampler. 1 µL aliquots of the samples were injected. The retention gap was attached to a 30 m x 0.530 mm ID column filled with a 1.0 µm film thickness Rtx®- 200 stationary phase. The initial oven temperature of 60 °C was increased to 165 °C at a rate of 15 °C/min, then to 200 °C at a rate of 4 °C/min and then finally increased to 300 °C at a rate of 25 °C/min. The injector and detector temperatures were set at 230 °C and 320 °C, respectively. Helium was used as the carrier gas for the mobile phase at a flow control from 3.5 mL for 8 minutes and increased to 6.0 mL/min with a rate of 0.25 mL/min/min and hold time of 22 minutes. The column was backflushed at 320 °C for a total of 4 void volumes after every run to prevent the appearance of ghost peaks from previous runs.

The peak area % of AE11 specie was assigned with an uncertainty of +/- 4 % (2*RSD=2σ). The same relative standard deviation was assumed for the other products.

Fourier Transformed Infrared (FTIR) spectra were recorded in transmission mode at a resolution of 2.0 cm^{-1} and by acquiring 60 scans on a Perkin-Elmer 2000 spectrometer (equipped with a MCT detector).

GC/MS analysis were performed in a GC Agilent 6890 (Agilent technologies, Santa Clara, CA, USA) accoupled with a mass detector Agilent Network 5973, using a 30 m capillary column, i.d. of 0.25 mm and 0.25 µm of film thickness HP-5 5% Phenyl Methyl Siloxane stationary phase. The initial oven temperature of 60 °C was increased to 165 °C at a rate of 15 °C/min, then to 200 °C at a rate of 4 °C/min until 200°C and then finally increased to 300 °C at a rate of 25 °C/min with a hold time of 10 minutes. The injector and detector temperatures were set at 250°C and 280 °C, respectively.

Helium was used as the carrier gas for the mobile phase with a flow of 1.3 mL/min. The column was backflushed at 300 °C for a total of 3 void volumes after every run to prevent the appearance of ghost peaks from previous runs.

FTIR Measurements on Raney Nickel catalyst

The samples in the form of powders suspended in H_2O were deposited by dropping the solution directly on a **KBr pellet** that was fixed in a cell allowing thermal treatments in controlled atmosphere and spectrum scanning at controlled temperature (from 90 K up to RT). The cell was connected with a vacuum line.

The samples were outgassed at room temperature for 10 minutes to remove water and then cooled at 90 K under outgassing before CO adsorption at low temperature. The spectrum of the sample before the inlet of the probe was used as background for each spectrum of adsorbed CO.

ICP/MS analysis

Micro-analysis was performed using ICP MS ICAP Qc thermo with S10 auto sampler. The samples were digested with a solution of chloridric acid and nitric acid in the proportion of 4:1. The internal standard solutions of Ni and Al were prepared from 5µg/l – 10 µg/l – 20 µg/l and 50 µ/l.

4.3.7 Reaction Repeatability

A relative standard deviation (RSD) value of 4.2% for the two essays after catalyst reactivation under H_2 pressure at 200°C proves the repeatability of the reaction.

As mentioned before, in the sample analysis after 1 cycle reaction we detected the dimer specie. However, after catalyst reactivation under hydrogen atmosphere the species AE11, SNE11 and methyl-undecanote and I_2 were detected in the solvent solution. This can be an indication that after one reaction cycle polymeric species are adsorbed to the catalyst peak blocking the cavities of the catalyst.

Once the catalyst is exposed to hydrogen atmosphere at high temperature the hydrogenolysis of the polymeric species can occur. The catalyst cavity is no more blocked and the species that were adsorbed in the cavity desorb and once the reactivation time is too low (1h) to proceed to the hydrogenation of these compounds, those are detected in the solvent after reactivation (**Table 4-3**).

Trial	AE11 %	$\bar{X}$	S^2	S_w	2 × RSD (2 sigma)
1	90.2				
2	88.2	90.1	3.7	1.9	4.2%
3	92				

Table 4-3. Repeatability experiments tests.

4.3.8 Products characterisation

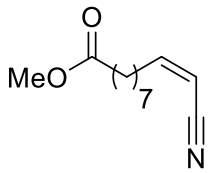

Methyl(Z)-10-cyano-9-decenoate (UNE11) ($C_{11}H_{16}NO_2$)

m/z: 178, 150, 136, 182.

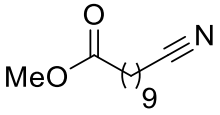

Methyl 10-cyanodecanoate (SNE11) ($C_{11}H_{18}NO_2$):

m/z: 180, 98, 74.

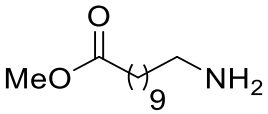

Methyl 11-aminoundecanoate (SNE11) ($C_{11}H_{20}NO_2$):

m/z: 185, 142, 30.

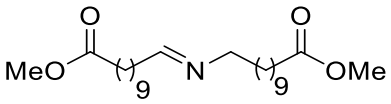

methyl (E)-9-((9-methoxy-9-oxononyl)imino)nonanoate(I_2) ($C_{22}H_{39}NO_4$):

m/z: 380, 268.

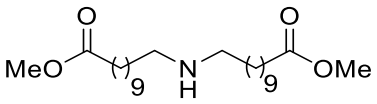

dimethyl 9,9'-azanediyldinonanoate (A_2) ($C_{22}H_{40}NO_4$):

m/z: 382, 228.

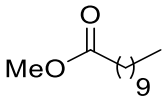

Methyl undecanoate ($C_{11}H_{21}NO_2$):

m/z: 169, 157,143,87,74.

4.4 Results and Discussion[3]

The hydrogenation of (9Z)-10-cyano-9-decenoate (UNE11) to methyl-11-amino-undecanoate (AE11) occurs over two steps. Firstly, the double bond at C9 and C10 is reduced, followed by the reduction of nitrile group to amine (**Scheme 4-5**).

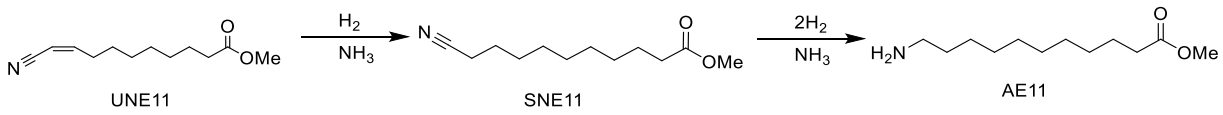

Scheme 4-5 . Hydrogenation of (*9Z*)-10-cyano-9-decenoate (UNE11) to methyl-11-amino-undecanoate (AE11).

According to literature on the hydrogenation of nitrile compounds [43,44], the production of amines from the reduction of nitrile compounds occurs via the formation of a primary imine, an extremely reactive intermediate, which, besides the formation of the desired amine, can lead to the

[3] From the publication Soutelo-Maria, A. L., Dubois, J.L., Couturier, J.L., Cravotto, G., Regeneration of Raney®-Nickel Catalyst for the Synthesis of High-Value Amino-Ester Renewable Monomers (doi.org/10.3390/catal10020229)

formation of side-products, including secondary imines (more stable). A number of varying reaction conditions were considered, as were the deactivation mechanisms of the Raney®-nickel catalyst.

4.4.1 Reaction conditions

4.4.1.1 *Reaction time*

As depicted in **Table 4-4**, the highest production of AE11 was obtained after 180 minutes of reaction time. The presence of the saturated nitrile ester (SNE11) (62%) after 120 min shows that the hydrogenation of the nitrile function is the rate limiting step. This is in accordance with the studies performed by Kukula and Koprivova [43], on the hydrogenation of *cis*-2-pentenenitrile. The reaction rate of the double bond from *cis*-2-pentenenitrile to valeronitrile was the same as that for valeronitrile to pentylamine. They concluded that the double bond of *cis*-2-pentenitrile was hydrogenated while the molecule was adsorbed into the active sites of the catalyst by the nitrile function [43] . The reduction of nitrile was also much slower using the doped Raney®-nickel catalyst, which showed higher reactivity for the reduction of C=C double bond than for the reduction of $C \equiv N$ (nitrile). Other causes for the high reactivity of the C=C bond are its proximity to the nitrile function and the *cis* conformation of the molecule (**Table 4-4**).

trials	t (min)	H_2 bar	NH_3/UNE11 (mol/mol)	AE11 %	UNE11 %	SNE11 %	I_2 %	A_2 %	Dimer %
1	180	60	1.15	92	-	3.0	0.09	4.44	-
2	120	60	1.15	36	-	62	0.28	0.27	0.02

Table 4-4. Influence of reaction time on the hydrogenation of UNE11. 60 bar H_2 atmosphere, 1 eq. NH_3 (1 equivalent mol of NH_3 to UNE11), 10 wt % Raney®-Nickel (wt % to UNE11) reaction time: 180 min (trial 1), 120 min (trial 2). **AE11:** methyl-11-aminoundecanoate, **UNE11:** (9Z)-10-cyano-9-decenoate, **SNE11:** methyl-10-cyanodecanoate. **I_2:** Secondary imine, **A_2**: Secondary amine, **Dimer:** dimer of the amino-ester. (See **Scheme 4-6** for molecular structure). Percentages of the reaction species were measured by GC-FID relative peak area.

The deactivation % (loss of AE11 yield) was calculated using the difference between the GC peak area % of AE11 formation when the catalyst (cycle 1) was used for the first time and the % peak area of AE11 formation in a second cycle (cycle 2) of hydrogenation (**Equation 4-1**).

$$Catalyst\ Deactivation\ \% = (conv\ 1 - conv\ 2)\ x\ 100$$

Equation 4-1. Conv1: Conversion UNE11 to AE11 obtained in the 1st cycle, **Conv2:** Conversion UNE11 to AE11 obtained in the 2nd cycle. Deactivation of catalyst between the hydrogenation cycles.

Compared to the experiments carried out at 40 bar H_2 (67% AE11 peak area obtained), working at higher hydrogen pressure (60 bar) led to higher AE11 production (91%). However, higher pressure caused higher catalyst deactivation. Secondary amine (A_2) formation in the experiments performed at 60 bar (**Table 4-5**) was higher (4.4%) than at 40 bar of pressure (0.25%).

Trials	H_2 bar	NH_3/UNE11 (mol/mol)	AE11 %	UNE11 %	SNE11 %	I_2 %	A_2 %	Dimer %	Deactivation (%)
1	40	1.00	67	-	30	0.66	0.25	0.03	-
2	40	1.00	41	-	57	0.38	0.39	0.03	26
3	60	1.05	91	-	11	0.09	4.44	-	-
4	60	1.10	47	-	50	0.19	0.91	-	44

Table 4-5. Influence of H_2 pressure. Trial 1 and 3: first cycle catalyst hydrogenation of UNE11 at 40 and 60 bar H_2 atmosphere. Trials 2 and 4: Second cycle catalyst hydrogenation of UNE11 at 40 and 60 bar H_2 atmosphere without any type of reactivation. **AE11:** methyl-11-aminoundecanoate, **UNE11:** (9Z)-10-cyano-9-decenoate, **SNE11:** methyl-10-cyanodecanoate. **I_2:** Secondary imine, **A_2**: Secondary amine, **Dimer:** dimer of the amino-ester. (See **Scheme 4-6.** Hydrogenation of UNE11 to AE11 and corresponding side-reactions. Formation of a secondary amine and tertiary amine: (a) via condensation between two primary imines; (b) via condensation amine-imine. Dimer formation (c) via condensation of two AE11 molecules. UNE11: (9Z)-10-cyano-9-decenoate, SNE11: methyl-10-cyanodecanoate, AE11: methyl-11-aminoundecanoate, I2: secondary imine, A2: secondary amine, Dimer: dimer of the AE11. Mechanism based on Krupka and Pasek's publication [21].for molecular structure). Percentages of the reaction species were measured by GC-FID relative peak area.

These results suggest that the catalyst deactivation mechanism is related to the adsorption of the secondary (A_2) and tertiary (A_3) amines onto the catalyst surface, and that the active sites are blocked by steric hindrance. In further investigation, it would be possible to isolate a secondary/tertiary amine larger amount and use it to pre-treat a fresh catalyst in order to validate this hypothesis. The formation of a secondary imine (I_2) can be explained by the nucleophilic addition of the primary amine (AE11) to the α-carbon of the aldimine intermediate (pathway b) or via imine–

imine nucleophilic addition (pathway a). The secondary amine (A_2) can be obtained via the hydrogenolysis of the diamine intermediate or hydrogenation of secondary imine (I_2), which is formed through loss of ammonia of secondary diamine. (**Scheme 4-6**).

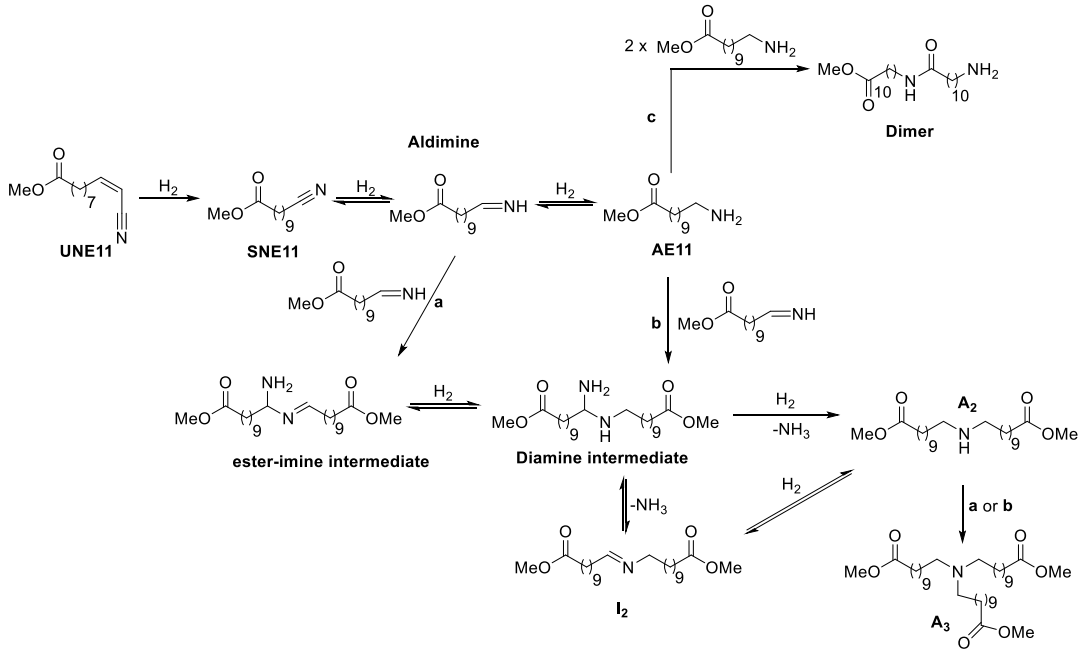

Scheme 4-6. Hydrogenation of UNE11 to AE11 and corresponding side-reactions. Formation of a secondary amine and tertiary amine: (a) via condensation between two primary imines; (b) via condensation amine-imine. Dimer formation (c) via condensation of two AE11 molecules. UNE11: (9*Z*)-10-cyano-9-decenoate, SNE11: methyl-10-cyanodecanoate, AE11: methyl-11-aminoundecanoate, I_2: secondary imine, A_2: secondary amine, Dimer: dimer of the AE11. Mechanism based on Krupka and Pasek's publication [21].

Dimers from condensation of 2 molecules of AE11 were also detected by GC-MS proving the co-formation of oligomers during the reaction. In fatty nitrile and dinitrile hydrogenation, Raney catalysts are usually used, but the Raney-Nickel deactivation is slow compared to present case. Therefore, it is likely that the ester function plays an important role in the catalyst deactivation. The detection of oligomers with amide function proves that the oligomers also contribute to catalyst deactivation by physical deposition (**Figure 4-2**).

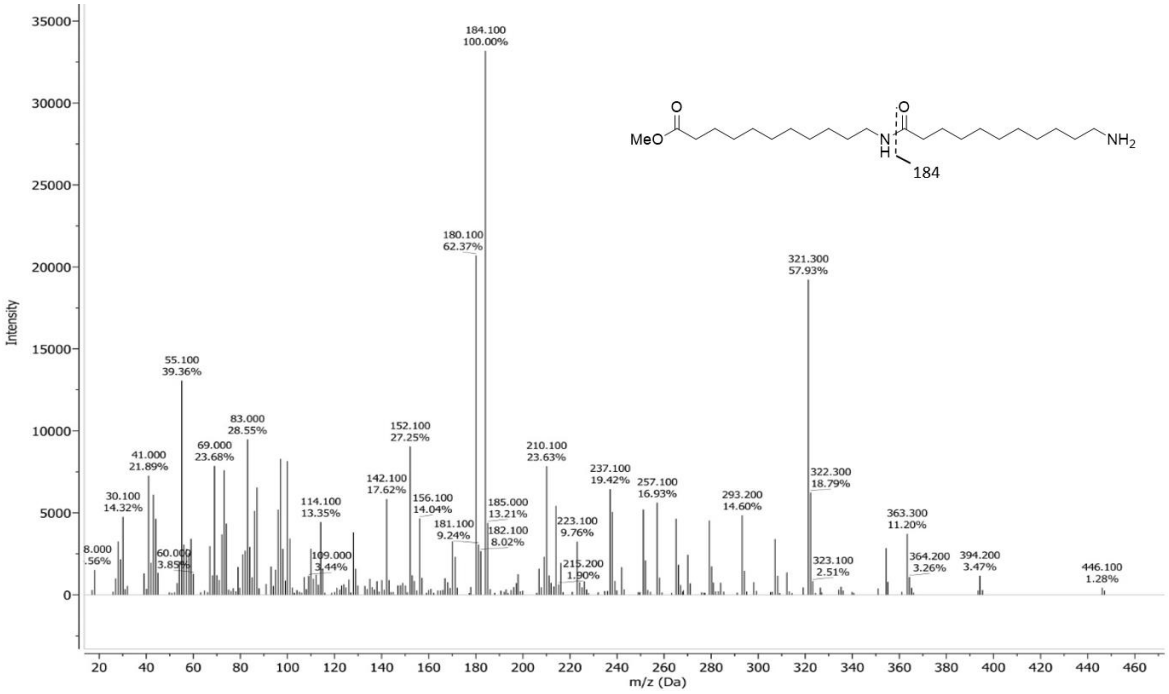

Figure 4-2. Mass spectrum and fragmentation pattern of dimer ester amine at 26 min.

4.4.1.2 *Influence of UNE11 concentration*

No influence of the concentration of UNE11 was observed as the conversion of UNE11 to AE11 remained between 92-95% (**Table 4-6**).

Trials	UNE11 wt %	H_2 bar	NH_3/UNE11 (mol/mol)	AE11 %	UNE11 cis %	SNE11 %	I_2 %	A_2 %	Dimer %
1	31 (1.25)	60	1.10	93	-	2.2	0.1	3.7	-
2	40 (1.9)	60	0.90	92	-	0.2	0.1	6.1	0.1
3	52 (2.15)	60	1.10	95	-	0.1	0.03	3.7	0.3

Table 4-6. the influence of UNE11 concentration on the hydrogenation reaction rate. **AE11:** methyl-11-aminoundecanoate, **UNE11:** (*9Z*)-10-cyano-9-decenoate, **SNE11:** methyl-10-cyanodecanoate, **A_2:** Secondary amine. UNE11 molecular weight (209.29 g/mole) –molar concentration in parenthesis.

4.4.1.3 *Influence of ammonia on the conversion of UNE11*

In terms of mechanism [21], AE11 (methyl-11-aminoundecanoate) and the primary imine (aldimine), are adsorbed on the catalyst surface, but the imine is not detected in the product's solution. The secondary amine is formed by the reaction of amino-ester and the primary imine, and then desorbs from the catalyst into the solution (**Scheme 4-6**).

The results of the experiments reported in **Table 4-7** agree with those carried out by Von Braun on catalysed nitrile derivatives [25]. In his experiments, it was observed that the formation of secondary amines was minimized by carrying out the hydrogenation in the presence of ammonia. The primary imine formed then had less of an opportunity to undergo the reaction (Scheme 4-6 a pathway to form secondary amine A_2) once ammonia was also added to the primary imine in a competitive reaction forming the *gem*-diamine (**Scheme 4-7**).

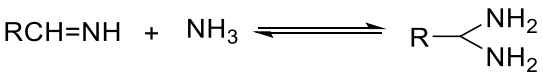

Scheme 4-7. Formation of gem-diamine.

Under hydrogenolysis, the primary amine is formed (**Scheme 4-8**).

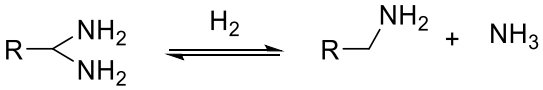

Scheme 4-8. Formation of primary amine from hydrogenolysis of the gem-diamine.

In the presence of NH_3, the condensation-reaction equilibrium is shifted to suppress the formation of the secondary imine, and thus the secondary and tertiary amines. The concentration of the secondary amine is reduced together with the reaction with the primary amine. Other possible explanations could be: the selective poisoning in the catalyst or the modification of the electronic properties of the catalytic metal [45]. Another base, such as NaOH or KOH, is sometimes used instead of ammonia to reduce the formation of secondary amines. However here this option was not selected, as those bases can also affect the catalyst as described in the introduction of the chapter, and it can also interfere with the ester function.

The influence of the NH_3 equivalents on the conversion of UNE11 to AE11 is illustrated in **Table 4-7**. The lowest conversion of UNE11 was obtained in the experiment with the lowest number of NH_3 equivalents (**trial 1**). Surprisingly, it was also found that a higher number of NH_3 equivalents

(**trial 2**) gave a conversion that was 22% lower than the conversion obtained in **trial 3** with 1.1 eq. A higher secondary imine percentage was achieved in **trial 2** (12%) than in **trial 1** (0.55%). One possibility for this result is that higher concentration of NH_3 may inhibits Raney®-nickel, while a too low ammonia concentration favours formation of heavier side products. The fact that 12% secondary imine was detected in the bulk solution corroborates this hypothesis. High ammonia concentration (partial pressure) also means a lower H_2 partial pressure **(Table 4-7).**

trials	NH_3/UNE11 (mol/mol)	AE11 %	UNE11 cis %	SNE11 %	I_2 %	A_2 %
1	0.70	73	3.9	21	0.55	0.5
2	1.38	75	-	8	12	0.3
3	1.10	93	-	2.2	0.07	3.7

Table 4-7. Influence of equivalents of ammonia on the conversion of UNE11 to AE11. AE11: methyl-11-aminoundecanoate, UNE11: (9Z)-10-cyano-9-decenoate, SNE11: methyl-10-cyanodecanoate, I2: Secondary imine, A2: secondary amine.

4.4.1.4 *Solvent influence on the conversion of UNE11*

The application of toluene or methyl-cyclohexane was found to have no significant difference on the conversion of UNE11 to AE11 (**Table 4-8**).

Trials	AE11 %	UNE11 %	SNE11 %	I2 %	A2 %
1	91	-	2.80	0.02	4.8
2	93	-	2.18	0.10	3.7

Table 4-8. Influence of the solvent on the conversion of UNE11 to AE11. Trial 1: hydrogenation of UNE11 with toluene, Trial 2: hydrogenation of UNE11 with methyl-cyclohexane. AE11: methyl-11-aminoundecanoate, UNE11- SNE11: methyl-10-cyanodecanoate. I_2: secondary imine and A_2: Secondary amine.

4.4.2 Catalyst reactivation

Three different methods were tested for the study of catalyst reactivation: a) catalyst washing with methanol and with the reaction solvent; b and c) catalyst regeneration under sonication and d) catalyst regeneration under hydrogen atmosphere.

a) <u>Catalyst washed with methanol and reaction solvent</u>

After the reaction, the catalyst was washed with 3x 10 mL MeOH and 3x10 mL toluene or only 3x 10 mL toluene and reused for a new cycle of UNE11 hydrogenation.

Trial	NH_3	AE11 %	UNE11 %	SNE11 %	I_2 %	A_2 %	Deactivation (loss of conversion)
1	1.12	91	-	2.8	0.02	4.8	-
2	1.15	44	-	54	0.57	1.17	47
3	1.1	47	-	50	0.19	0.91	44

Table 4-9. Trial 1: hydrogenation of UNE11 first cycle catalyst, **Trial 2:** hydrogenation of UNE11 second cycle catalyst, catalyst washed with MeOH, **Trial 3:** hydrogenation of UNE11 second cycle catalyst, catalyst washed with toluene. H_2 pressure: 60 bars. **AE11:** methyl-11-aminoundecanoate, **UNE11:** (9Z)-10-cyano-9-decenoate, **SNE11:** methyl-10-cyanodecanoate. **I_2:** Secondary imine, **A_2:** Secondary amine, Dimer: dimer of AE11. (See **Scheme 4-6.** Hydrogenation of UNE11 to AE11 and corresponding side-reactions. Formation of a secondary amine and tertiary amine: (a) via condensation between two primary

Trials **2** and **3** prove that the catalyst is deactivated after only a single reaction cycle.
No catalyst reactivation was observed after catalyst treatment with MeOH or toluene.

b) Catalyst reactivation under sonication

The catalyst was recovered from the reactor and poured into a solution of MeOH.

The catalyst used in **trial 3** and **trial 4** (**Table 4-10**) was immersed in MeOH and sonicated at 120 kHz (input power 100 and 200W). Nevertheless, the conversion of UNE11 to AE11 after catalyst sonication at 100W and 200W was respectively 10 and 16 points lower than that achieved after the washing procedure with MeOH and toluene.

GC analysis of the MeOH washing solution after sonication showed AE11, SNE11 and traces of secondary imine and the secondary amine.

trial	AE11 %	UNE11 cis %	SNE11 %	Imine %	A_2 %	Dimer %	Deactivation %
1	91	-	2.8	0.02	4.80	-	-
2	44	-	54	0.57	1.17	0.02	47
3	34	-	65	0.53	0.41	0.02	57
4	29	0.26	71	0.32	0.39	-	62

Table 4-10. Trial 1: first cycle hydrogenation of UNE11, **Trial 2:** hydrogenation of UNE11 with catalyst from 1 recovered and washed with 3x MeOH and 3x toluene, **Trial 3:** hydrogenation of UNE11 with the catalyst (from trial 2) reactivated in MeOH solution under 120 kHz, 100W input power, **Trial 4:** hydrogenation of UNE11 with the catalyst (from trial 2) reactivated in MeOH solution under 120 kHz, 200W input power. **AE11:** methyl-11-aminoundecanoate, UNE11: (9Z)-10-cyano-9-decenoate, **SNE11:** methyl-10-cyanodecanoate. **I_2:** Secondary imine, **A_2:** Secondary amine, Dimer: dimer of AE11. (See **Scheme 4-6** for molecular structure). Percentages of the reaction species were measured by GC-FID relative peak area.

The fact that a higher percentage of SNE11 (62% and 50%) than of AE11 (36 and 47%) (**Table 4-11**) was detected is an indication that more intermediate nitrile than amine remains on the deactivated catalysts (desorbed by the ultrasonic treatment in methanol).

Method	AE11 %	UNE11 cis %	SNE11 %	I_2 %	A_2 %	Other species (higher retention time species) %
2	18.7	-	44	2.0	14.7	20.5
3	36	-	62	2.39	-	-
4	47	-	50	0.2	0.9	1.1

Table 4-11. Method 2: Solution of catalyst reactivation under MeOH and silent conditions, **method 3:** solution of catalyst reactivation under MeOH, sonication treatment at 120 kHz and 100W, method 4: solution of catalyst reactivation under MeOH, sonication treatment at 120 kHz and 200W. **AE11:** methyl-11-aminoundecanoate, **UNE11:** (9Z)-10-cyano-9-decenoate, **SNE11:** methyl-10-cyanodecanoate, **I_2:** Secondary imine, **A_2:** Secondary amine, Dimer: dimer of AE11. (See Scheme 4-6 for molecular structure). Percentages of the reaction species were measured by GC-FID relative peak area.

Higher ultrasonic power (200 W) was deleterious because it totally dispersed the catalyst into the liquid phase. For this reason, only catalyst sonicated at 100 W was considered for the following reactivation tests.

c) Caustic treatment

The catalyst from the first cycle was unloaded from the reactor, divided in two fractions and each used for different reactivation tests, and treated with a NaOH 0.05 N solution for sonication at a frequency of 120 kHz and 100W of input power for 1h (**Table 4-12**).

Method	AE11 %	UNE11 cis %	SNE11 %	Imine %	A2 %	Dimer %	Deactivation (loss of conversion)
1	44	-	54	0.6	1.2	0.02	47
2	44	0.14	54	0.2	0.6	-	47
3	34	-	65	0.5	0.4	0.02	57
4	60	-	39	0.7	0.9	-	31

Table 4-12. Method 1: silent conditions (without ultrasounds) in MeOH solution, **method 2:** silent conditions in NaOH solution, **method 3:** hydrogenation of UNE11 with catalyst reactivated under sonication, 120 kHz, 100W in a MeOH solution, **method 4:** hydrogenation of UNE11 with catalyst reactivated under 120 kHz, 100W in a NaOH solution. **AE11:** methyl-11-aminoundecanoate, **UNE11:** (9Z)-10-cyano-9-decenoate, **SNE11:** methyl-10-cyanodecanoate. **I_2:** Secondary imine, **A_2:** Secondary amine, **Dimer:** dimer of AE11. **(**See **Scheme 4-6** for molecular structure). Percentages of the reaction species were measured by GC-FID relative peak area.

Higher amount of AE11 (60%) was obtained in the experiment in which the catalyst was sonicated in the NaOH 0.05 N solution than in the experiment with no sonication (44%) and the experiment in which the catalyst was sonicated in a methanol solution (34%).

Through ICP analysis of the solution of **1)** the catalyst treated under 0.025 M NaOH at room temperature and with mechanical agitation, and **2)** the catalyst treated under caustic conditions under sonication it was observed a loss of 3% Ni from catalyst and only 0.2% of aluminium (**Table 4-13**). The lose of metal in this kind of treatment is significant.

Method	Ni mg/ 100g	Ni %	Lost in Ni total mass	Al mg/100g	Al %	Lost in Al total mass (mg)
1) NaOH (silent)	328.7	3	0.3287	19.0	0.2	0.019
2) US	342.7	3	0.3427	20.8	0.2	0.0234

Table 4-13. Quantification of Nickel and aluminium lost in the catalyst treated under caustic treatment at silent conditions and under sonication, at 120 kHz with 100 W of input power.

d) Catalyst reactivation under H_2 pressure

Raney®-nickel was saturated with hydrogen during its preparation, and one of the hypothesis of catalyst deactivation is the desorption of the hydrogen species present in the active sites of the catalyst.

Pierre Fouilloux described, in his review [46], the existence of a variety of hydrogen species in Raney®-nickel catalysts. Using thermal desorption experiments, he found that H_2 adsorbs onto the catalyst in reversible and irreversible forms. The two species may correspond to the bridged and linear adsorptions observed for hydrogenation using the neutron inelastic scattering technique. The strongly adsorbed hydrogen seems to be inactive in benzene, acetone and acetonitrile hydrogenations, but the presence of weakly adsorbed linear hydrogen is crucial to the success of the reaction.

F. Hochard [12], used Temperature Programmed Desorption (TPD) and inelastic neutron scattering techniques to detect the presence of weakly and strongly adsorbed hydrogen on the catalyst. In his paper, he claims that only weakly adsorbed hydrogen is active for hydrogenation. He observed that the nitrile molecule and hydrogen compete for the same active site, during the reduction of acetonitrile, while the primary amine products of the reaction compete for several active sites on the catalyst. Although the desorption of the amines from the catalyst should be fast, they may be associated with the active sites that result from the presence of alumina when reabsorption occurs [12]. In his experiments, he found that 70 % of the total hydrogen adsorbed in the solid has been consumed by the reaction at 373 K and that the residual is adsorbed onto the (110) and (111) nickel faces. The linear hydrogens were only detected after the re-adsorption of hydrogen at higher pressure. Multi-bonded species at low coverage are more strongly adsorbed than hydrogen to linear sites.

The formation of oligomeric/polymeric species on the surface of the Raney®-nickel catalyst can be an important factor in catalyst deactivation. These species can result from the reaction between amino esters that are adsorbed onto the catalyst surface, thus blocking the active sites of the catalyst. Raney catalysts deactivates more slowly in the hydrogenation of fatty nitriles and dinitriles, where these oligomerization reactions cannot take place, compared to the present case, so it is quite likely that oligomers adsorbed on the surface, suffer hydrolysis during the reactivation under hydrogen (**Scheme 4-9)**.

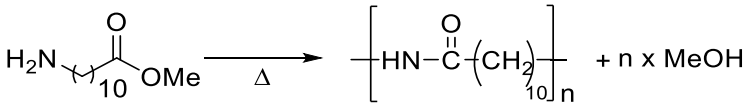

Scheme 4-9. Polymerisation of 11-aminoundecanoate with formation of n MeOH.

Reactivation assay	Temperature (°C)	H_2 (bar)	Reactivation time
a	90	30	60
b	150	30	60
c	200	70-80	60
d	200	70-80	120
e	200	0	60

Table 4-14. Assays of catalyst regeneration at 90, 150 and 200°C, with/without a hydrogen atmosphere.

Trial	Reactivation assay	AE11 %
blank	-	91
1	-	44
2	a	48
3	b	91
4	c	90
5	d	62
6	e	15

Table 4-15. Efficiency of the reactivation experiments tested in a second cycle hydrogenation of UNE11. AE11: methyl-11-aminoundecanoate.

The catalyst completely recovered its activity after treatment under 70-80 bar at 200 °C, and at pilot conditions 150 °C and 30 H_2 bar (trials **4** and **3**). The regeneration treatment time is also an important factor, as a higher treatment time led to the catalyst recovering only 22 points of AE11 conversion (trial 5) compared to no treatment (trial 1). Moreover, no reactivity was achieved in the absence of hydrogen (trial **6**), and higher catalyst deactivation was observed.

4.4.3 Reaction Kinetics study

In order to measure the kinetics of the reaction and to find the best conditions to achieve the highest AE11 conversion, the reaction was pursued with different catalysts concentrations.

The experiments were pursued under constant H_2 pressure of 40 bars. The H_2 pressure was kept constant, by adding minute amounts of H_2 which was carefully monitored. The H_2 moles number was calculated taking in account that the gas dead volume in the reactor did not change during the reaction. (**Equation 4-2**).

$$n = \frac{PV}{RT}$$

Equation 4-2. n: H_2 moles number in the reaction media, P: hydrogen pressure added to the system, **V:** dead volume in the reactor, **R:** gas constant (0.082 bar. mol^{-1}. K^{-1}) and **T:** reaction temperature (K).

To precise the moles number of H_2 consumed over time, we took in account the variation of temperature and pressure over the reaction time. The H_2 consumption was obtained by the difference of moles number measured over time (**Equation 4-3**).

$$n_{H_2}\ consummed\ over\ time = \frac{\Delta PV}{R\Delta T} = n_{tx} - n_{t(x+1)}$$

Equation 4-3. n: H_2 moles consumption over time. tx: time x, t (x+1): following time measurement.

In **Figure 4-3** The number of moles consumed during the reaction with different catalyst loading (wt %) is illustrated.

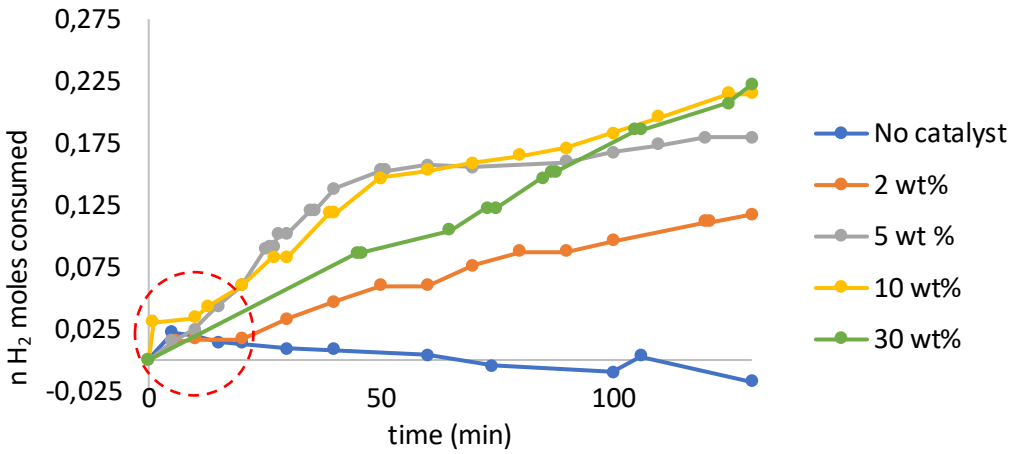

Figure 4-3. H_2 moles consumption over reaction time for different catalyst concentration. Reaction time: 130 min, T=90°C, P=40 bars.

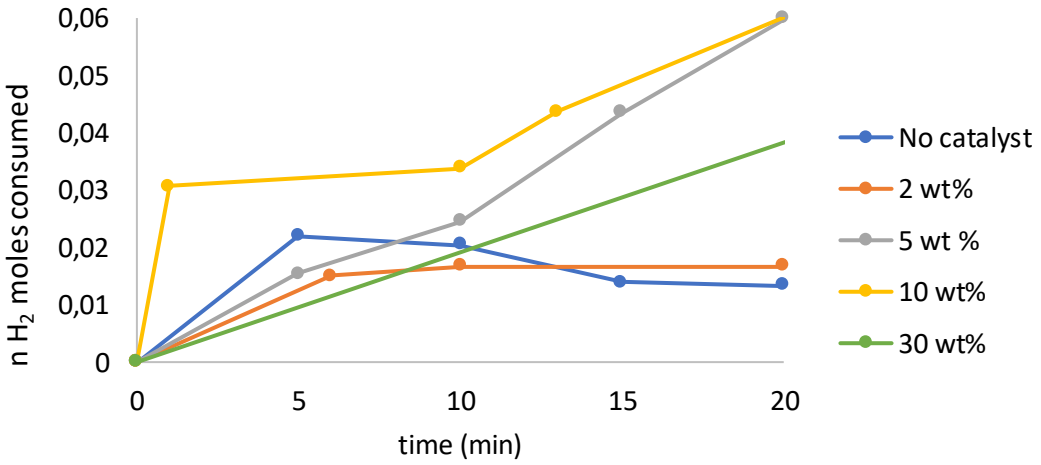

Figure 4-4. Zoom-in H_2 moles consumption over reaction time for different catalyst concentration at low residence time, first 20 minutes.

In the first 10 minutes, the consumption of H_2 was similar in the experiments with 2, 5 and 30 wt %. In **Figure 4-3** it is possible to observe that, in the first 10 minutes, the reaction is not limited by the quantity of catalyst loading. It is also possible to observe that 0.021 H_2 moles were consumed even in the absence of a catalyst. The first minutes are limited by equilibrium in H_2 dissolution and ammonia vaporisation.

Through these results we can conclude that the rate of the reaction, at more than 10 wt % catalyst, is limited by the hydrogen diffusion from the gas phase to the liquid phase and consequently the reaction is slower.

In our experiments we started to increase the temperature gradually until achieve the 90°C desired, however these results proved that the temperature is crucial to gas absorption as it sets the solubility of the gas in the medium. Differently, after 10 minutes with different wt %, the H_2 consumption is lower. There is enough H_2 dissolved in the liquid medium to proceed the reaction and the wt % catalyst is important as mentioned before.

The H_2 consumption in the experiment with 30 wt % catalyst demonstrates that the reaction medium is depleted in H_2 by increasing catalyst loading and so higher mass transfer limitation is observed. Alternatively, with higher catalyst concentration, the local temperature in the catalyst is so high that side reactions such as production of A_2 and oligomerisation are privileged, and the catalyst is deactivated faster. In this case the deposition of species in the catalyst should be directly proportional to the surface area available in the catalyst.

Due to these results we decided to apply higher pressure in the reaction media (60 bar) where higher AE11 was obtained compared with the results obtained at 40 bar pressure.

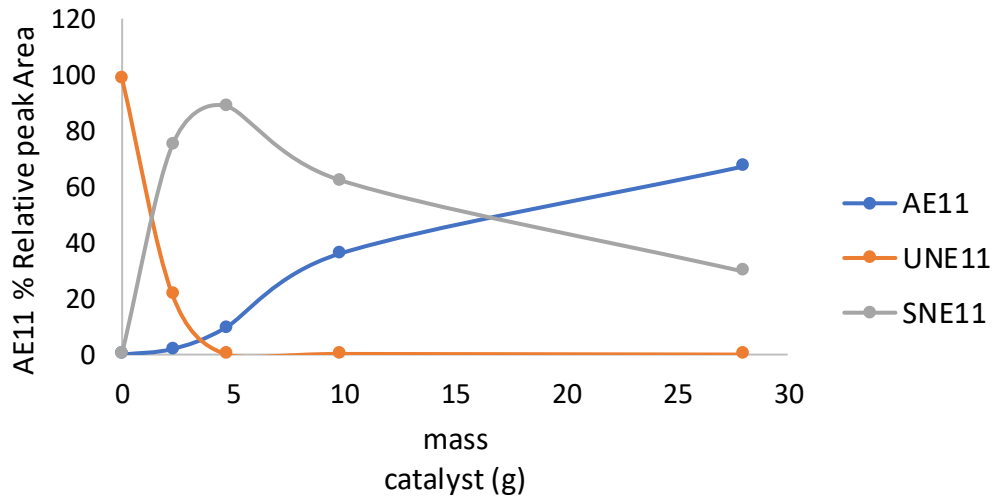

Figure 4-5. % Relative peak area compared with catalyst weight.

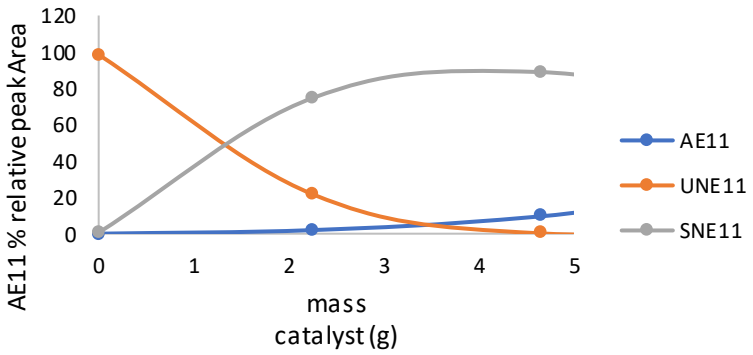

Figure 4-6. Zoom-in from Figure 8. % Relative peak area compared with catalyst weight of 2.26 and 4.65 g.

In **Figure 4-5** it is possible to observe that the conversion of UNE11 in AE11 is higher by increasing the catalyst's loading. As depicted in **Figure 4-6**, from 4.65 wt % catalyst UNE11 was 100% consumed after 3 h of reaction. With 2 wt % catalyst there are not enough active sites to proceed to full conversion.

Under 40 bars the consumption of H_2 is lower than at 60 bars of H_2 (**Figure 4-7**). This result show that at 40 bars the reaction is limited by the diffusion of H_2 in the liquid phase. By increasing the hydrogen pressure, this limitation is overcome, and the reaction rate is higher.

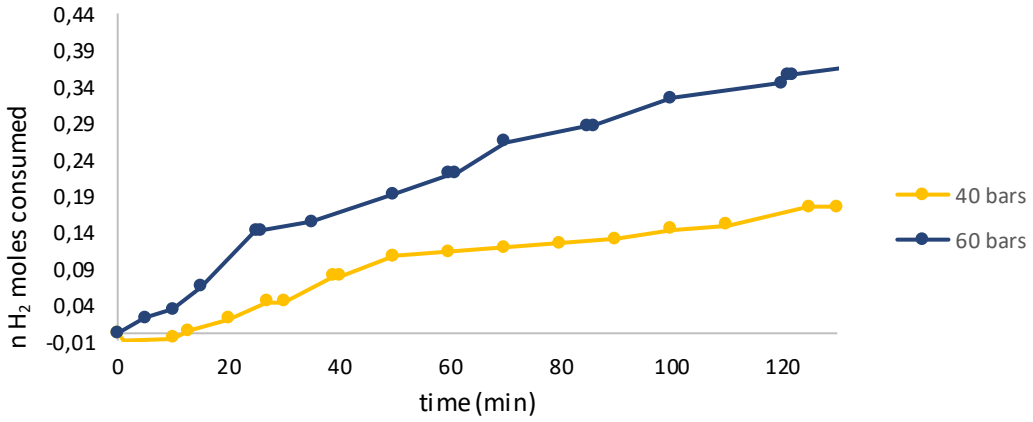

Figure 4-7. H_2 moles consumed profile in the hydrogenation of UNE11 at 40 and 60 bars. Reaction conditions: 10 wt % catalyst loading, 30 wt% UNE11 at 90°C for 130 minutes.

In gas chromatography analysis coupled with flame ionisation detector the concentration of hydrocarbons is measured. In this case the relative peak area (RPA) is the % of carbon quantified.

Being the relative peak area (RPA):

$$RPA_1 = \frac{a_1}{a_1 + a_2 + 2a_3 + 2a_4 + a_5}$$

Equation 4-4. Relative peak areas. a_1: moles number of methyl-aminoundecanoate (AE11), a_2: moles number of 10-cyano-9-decanoate (SNE11), a_3: moles number of secondary amine(A_2), a_4: moles number of secondary imine (I_2), a_5: moles number of 9 (Z)-10-cyano-9-decenoate (UNE11) not reacted.

As described previously there are two possible pathways to produce secondary amine (A_2) and the secondary imine (I_2). Through reaction between two primary imines or one primary amine and one primary imine for this reason the moles number of A_2 and I_2 corresponds to 2 a_3 and 2 a_4.

Being:

$a_1 = RPA_1 \times (a_1 + a_2 + 2a_3 + 2a_4 + a_5)$

$a_2 = RPA_2 \times (a_1 + a_2 + 2a_3 + 2a_4 + a_5)$

$a_3 = RPA_3 \times (a_1 + a_2 + 2a_3 + 2a_4 + a_5)$

$a_4 = RPA_4 \times (a_1 + a_2 + 2a_3 + 2a_4 + a_5)$

Assuming that:

$$(UNE11)^{\circ} = a_1 + a_2 + 2a_3 + 2a_4 + a_5 + a_6$$

Equation 4-5. Constitution of UNE11. **a_1:** moles number of methyl-aminoundecanoate (AE11), **a_2:** moles number of 10-cyano-9-decanoate (SNE11), **a_3:** moles number of secondary amine(A_2), **a_4:** moles number of secondary imine (I_2), **a_5:** moles number of 9 (Z)-10-cyano-9-decenoate (UNE11) not reacted, **a_6:** moles number of species not identified in the chromatographic analysis.

The total H_2 moles consumed during the reaction is dependent on the pression variation (ΔP), on the volume (we considered the dead volume in the reactor for the calculations) and on the temperature variation (ΔT).

$$total\ H_2\ moles\ consummed = \sum \Delta \left(\frac{PV}{RT}\right)$$

Equation 4-6. Total H_2 moles consumed during the hydrogenation of UNE11 to AE11. $\Delta \boldsymbol{P}$: pressure variation, V: dead volume of the reactor (gas volume), R: gas constant, $\Delta \boldsymbol{T}$: reaction temperature variation.

Through the **Scheme 4-10:**

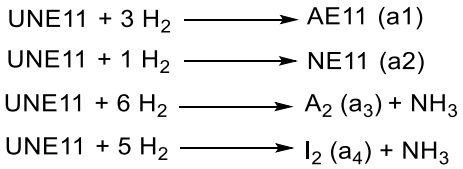

Scheme 4-10. Hydrogen balance for the production of the products and intermediate species of the reaction.

To simplify, we considered that the NH_3 is kept in the liquid phase.

Nevertheless, as observed in **Scheme 4-6** for the production of secondary imine (I_2) and secondary amine (A_2), one molecule of NH_3 is formed so for the hydrogen atoms balance:

$$\sum \Delta\left(\frac{PV}{RT}\right) = 3\,a_1 + a_2 + 4\,a_3 + 3\,a_4 + 0\,a_5 + 3\,a_6 \Leftrightarrow$$

$$\Leftrightarrow \sum \Delta\left(\frac{PV}{RT}\right) = \left(3\,RPA_1 + RPA_2 + \frac{6}{2}RPA_3 + \frac{5}{2}RPA_4\right) x\,(a_1 + a_2 + 2a_3 + 2a_4 + a_5) + na_6$$

Equation 4-7. Total consumption of H_2 moles during the reaction.

Being:

$$(UNE11)^{\circ} = a_1 + a_2 + 2a_3 + 2a_4 + a_5 + a_6$$

Equation 4-8. Consumption of UNE11 regarding the products and the intermediate species in the reaction media.

The total H_2 number moles calculated is represented in **Equation 4-9** :

$$\frac{\sum \Delta PV}{RT} = \left(3\,RPA_1 + RPA_2 + \frac{6}{2}RPA_3 + \frac{5}{2}RPA_4\right) x\,((UNE11)^{\circ} - a_6) + na_6 \Leftrightarrow \frac{\frac{\sum \Delta PV}{RT} - na_6}{\left(3\,RPA_1 + RPA_2 + \frac{6}{2}RPA_3 + \frac{5}{2}RPA_4\right)} - a_6 =$$

$$(UNE11)^{\circ} \Leftrightarrow \frac{\frac{\sum \Delta PV}{RT}}{\left(3\,RPA_1 + RPA_2 + \frac{6}{2}RPA_3 + \frac{5}{2}RPA_4\right)} + a_6\,x\left(1 - \frac{n}{\left(3\,RPA_1 + RPA_2 + \frac{6}{2}RPA_3 + \frac{5}{2}RPA_4\right)}\right) \Leftrightarrow$$

$$\Leftrightarrow a_6 = \frac{(UNE11)^{\circ} - \dfrac{\frac{\sum \Delta PV}{RT}}{3\,RPA_1 + RPA_2 + \frac{6}{2}RPA_3 + \frac{5}{2}RPA_4}}{1 - \dfrac{n}{\left(3\,RPA_1 + RPA_2 + \frac{6}{2}RPA_3 + \frac{5}{2}RPA_4\right)}}$$

Equation 4-9. Moles number of reaction species not detected by GC-FID.

Reaction	AE11	SNE11	Imine	NE11 cis	A_2	Ums	AE10	AE11	SNE11	NE11 cis	Imine
catalyst free	0	0.61	0	98.46	-	-	-	0	0.0013	0.21	0
2 wt %	2	74.78	0.02	21.51	-	-	0.02	0.004	0.165	0.047	4.41×10^{-4}
5 wt %	9.52	88.88	0.07	0.17	-	-	0.05	0.021	0.20	3.7×10^{-4}	1.53×10^{-4}
10 wt %	36.03	62.38	0.28	0.23	0.27	-	0.17	0.078	0.14	5.0×10^{-4}	6.07×10^{-4}
30 wt %	67.2	29.68	0.66	0	0.25	0.04	0.28	0.15	0.064	0	1.4×10^{-4}

Table 4-16. Relative peak area (%) of the different product and intermediate species detected by GC-FID.

Reaction	$(\boldsymbol{UNE11})^{\circ}$	$\frac{\sum \Delta \boldsymbol{PV}}{\boldsymbol{RT}}$	$\boldsymbol{a_6}$	$\frac{\boldsymbol{a_6}}{(UNE11)^{\circ}}\%$	$\left(\boldsymbol{1-\frac{a_6}{(UNE11)^{\circ}}\%}\right)$
catalyst free	0.22	0	0	0%	100%
2 % wt	0.22	0.117	0.075	34%	66%
5 % wt	0.22	0.180	0.066	30%	70%
10% wt	0.22	0.193	0.104	48%	52%
30% wt	0.22	0.223	0.120	56%	44%

Table 4-17. Catalyst free: no catalyst applied in the reaction medium, **$(UNE11)^{\circ}$:** initial moles of UNE11; $\boldsymbol{a_6}$= no identified molecules by GC-FID, $\frac{\boldsymbol{a_6}}{\boldsymbol{n(UNE11)^{\circ}}}$ % = fraction of molecules no identified.

Through the analysis of the **Table 4-17** it is possible to observe that the number of moles of unidentified molecules ($\boldsymbol{a_6}$), increases with higher catalyst loading. Such results suggest that higher the concentration of the catalyst applied in the reaction medium, higher will be the uncertainty of the products detected by the gas chromatographic method applied. In the following table it is described the quantification of molecules not detected by GC-FID (a_6) assuming:

- n=0, the molecules not identified by the analytical method are not hydrogenated.
- n=0.5 (partial hydrogenation), the molecules not identified by the analytical method are hydrogenated.

n=0			n=0.5		
a_6	$\frac{a_6}{(UNE11)^\circ}\%$	$\left(1-\frac{a_6}{(UNE11)^\circ}\%\right)$	a_6	$\frac{a_6}{(UNE11)^\circ}\%$	$\left(1-\frac{a_6}{(UNE11)^\circ}\%\right)$
0	0%	100%	0	0%	100%
0.075	34%	66%	0.20	89%	11%
0.066	30%	70%	0.12	53%	47%
0.073	48%	52%	0.10	48%	52%
0.120	56%	44%	0.15	71%	29%

Table 4-18. a_6: number of moles of species not detected by the chromatographic method applied. $\frac{a_6}{n\,UNE_{11}}\%$: % of a_6 in a total moles number of UNE11, $1-\frac{a_6}{nNE_{11}}\%$: % of species detected by the chromatographic method taking in account the moles of the products not detected. n is represented in **Equation 4-9**.

According the graph represented on **Figure 4-8**, even at lower catalyst loading (2.26 g) products that were not identified by the analytical method were quantified. The linearity of the curve shows that by increasing the catalyst loading the production of molecules not identified is increased.

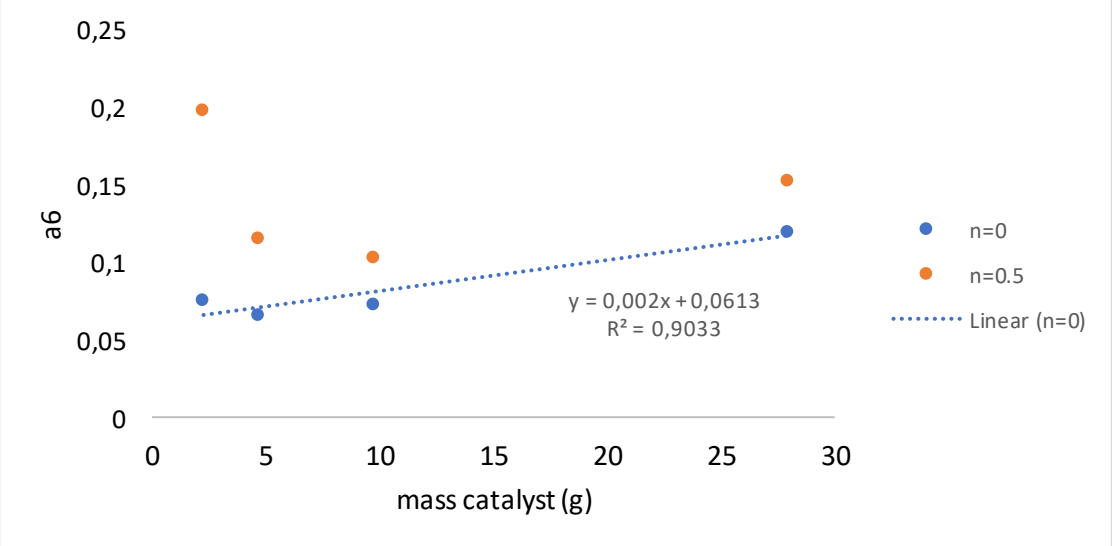

Figure 4-8. variation of moles number of products not identified by the analytical method (a6) with the catalyst loading in the reaction medium. n=0: a6 not hydrogenated, n=0.5: a6 hydrogenated.

These tests reflect the uncertainties in the chromatographic method applied the variation as well of H_2 pressure measured during the reaction time.

The results obtained for n=0 can support the supposition that non-determined reactions can take place with no hydrogen consumption such as polymerisation of AE11 covering the surface of the catalyst.

These results allied to the analysis of the solvent catalyst after regeneration with hot Hydrogen suggest that under catalyst reactivation treatment, the polymeric species are hydrogenolysed giving place to methyl-undecanoate (**Figure 4-9**) and amino-ester, released to the solvent uncovering the catalyst surface. The species such as NE11, AE11, UNE11 detected in the solution after catalyst treatment under hydrogen atmosphere suggest as well that these molecules would be trapped, during a first cycle reaction, in the catalyst cavities which would be blocked by polymerised molecules (**Figure 4-10**). After unblocking the catalyst cavities by hot hydrogen treatment, the molecules would be released to the medium and detected in the solution.

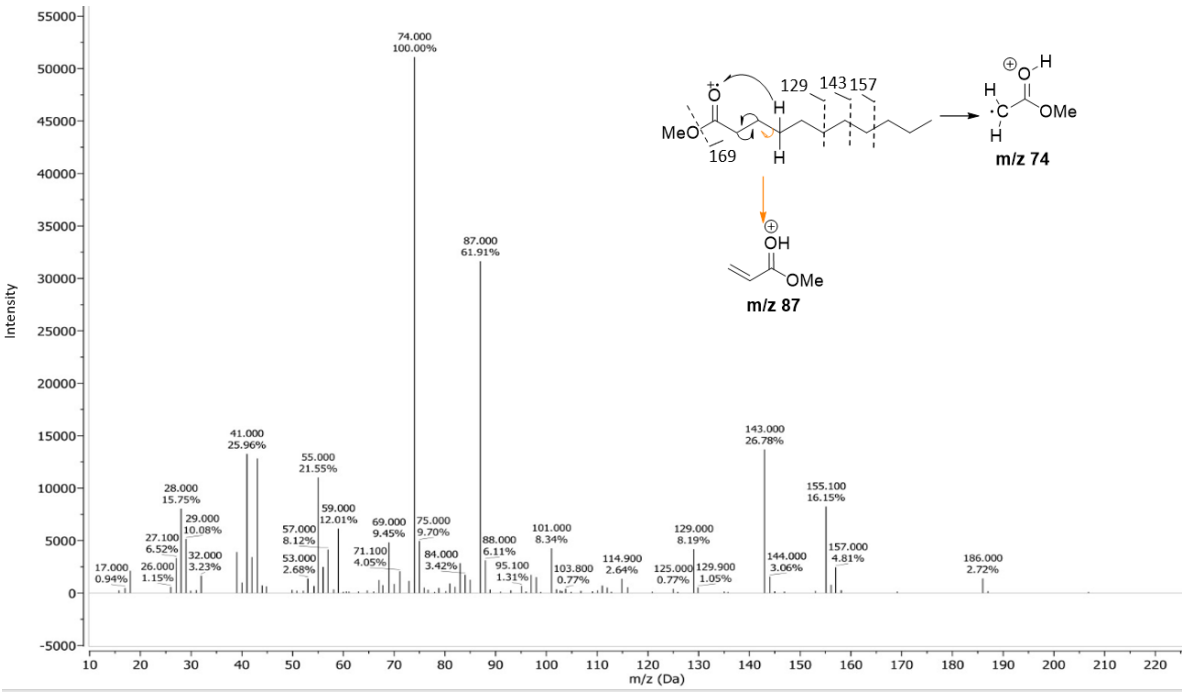

Figure 4-9. Mass spectrum and fragmentation pattern of methyl-undecanoate at 26.32 min retention time.

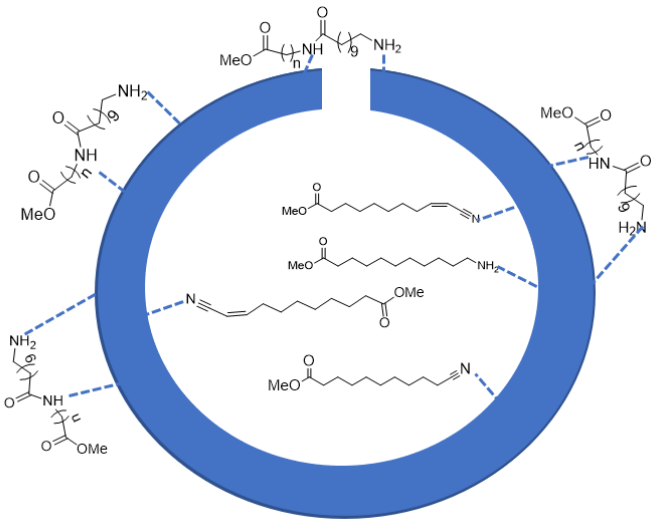

Figure 4-10. Catalyst deactivation by polymer adsorption in the catalyst surface and adsorption of UNE11, SNE11 and AE11 in the cavity of the catalyst.

4.4.4 Theorical Kinetic model

A mathematical kinetic model was developed according the hydrogenation of UNE11.

The following assumptions were made for its production:

- The products of side-reactions were not taken in account.
- H_2 pressure was constant during the reaction time (H_2 diffusional limitations in the reaction media were not take in account).

$$\underset{\mathbf{A}}{\text{UNE11}} \xrightarrow{k_1} \underset{\mathbf{B}}{\text{SNE11}} \xrightarrow{k_2} \underset{\mathbf{C}}{\text{AE11}}$$

Evaluation of A:

$$\frac{dx}{dt} = k_1(A^0 - x) \Leftrightarrow (A^0 - x) \quad = A^0.e^{-k_1 t}$$

Equation 4-10. Concentration of AE11.

Evaluation of B:

$$[B] = \frac{k_1.a}{k_1 - k_2}[e^{-k_2 t} - e^{-k_1 t}]$$

Equation 4-11. Concentration of SNE11.

Evaluation of C:

$$[C] = [A]^0 - [A] - [B]$$

Equation 4-12. Concentration of AE11.

H_2 consumption:

$$H_2 consumption = [B] + 3[C]$$

Equation 4-13. Consumption of H_2.

To test the kinetic model with our data we applied the relative peak area % obtained by GC-FID analysis for the species UNE, SNE_{11} and AE_{11}. Unknown products are assumed to be side products of consecutive minor reactions that do not affect the main reactions mechanisms.

	A	100-A	B	C
Starting material	100	0	0	0
0 wt% catalyst	98.46	1.54	0.61	0
2 wt% catalyst	21.51	78.49	74.78	2
5 wt% catalyst	0.17	99.83	88.88	9.52
10 wt% catalyst	0	99.77	62.38	36.03
30 wt% catalyst	0	100	29.68	67.2

Table 4-19. Relative peak area % of species UNE11 (A), consumption of UNE11 (100-A), formation of SNE11 (B) and formation of AE11 (C) after 3 hr reaction time, P=40 bars and T=90°C.

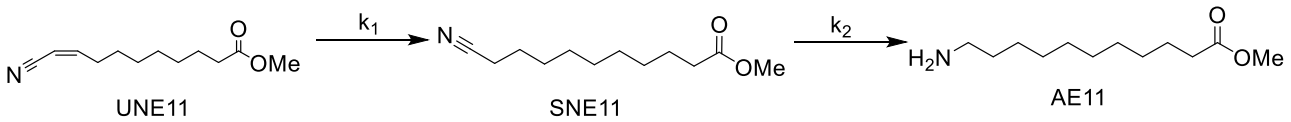

UNE11 SNE11 AE11

Scheme 4-11. Hydrogenation of UNE11 to AE11.

The graphic from **Figure 4-11** shows the experimental data fitting on the theoretical model. The experimental data were fitted with:

- k_1= 0.15
- k_1/k_2= 22.76
- $= \frac{t\,(h)}{m\,Catalyst}$

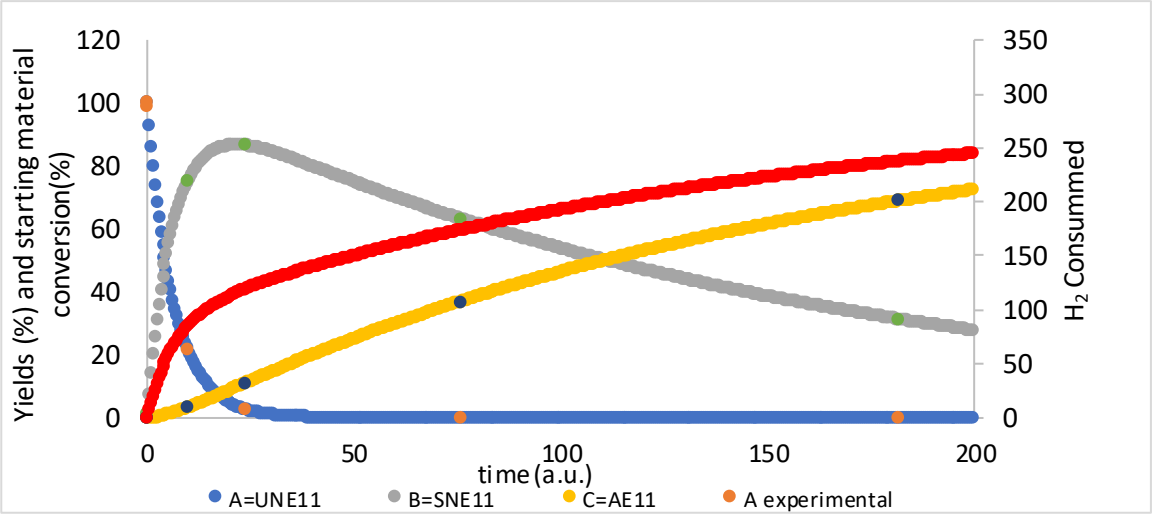

Figure 4-11. Experimental data fitted in the kinetic model prediction.

The fact that the data fits in the model demonstrates that the reduction of the unsaturated carbon bond (C=C) is 22 times faster than the reduction of the nitrile. The graph also demonstrates the fast consumption of H_2 in the initial stages of the reaction which can lead to mass transfer limitation (H_2 depletion).

4.4.5 Catalyst deactivation by reaction products/side-products adsorption

The AE11 production (yield) in a second reaction cycle proves that the catalyst is highly deactivated after only one reaction cycle. We applied the techniques of FTIR and CO adsorption to detect the species adsorbed in the catalyst surface after 1 cycle reaction that can influence the catalyst deactivation and to dose the exposed metal of the exhausted catalyst.

FTIR (Fourier-transform infrared spectroscopy)

In order to detect the molecules adsorbed in the catalyst surface we analysed the catalyst after a first reaction cycle and after reactivation, under hot hydrogen, as it was the method with the best result attaint in the catalyst activity recovery.

Through the analysis of FTIR absorbance spectrum of the catalyst after one reaction cycle it was possible to observe the absorption of O-H (3408 cm^{-1}) stretching, axial aliphatic deformation C-H (2920 and 2836 cm^{-1}), axial deformation C=O (1608 cm^{-1}), stretching C-O-H (1296 cm^{-1}) bending and C-O (1180 cm^{-1}) stretching bands corresponding to methanol and the N-H (3246 cm^{-1}) stretching and C-N (1245 cm^{-1}) bending bands corresponding to amine function.

No dimer species or saturated nitrile species were detected in the catalyst surface once the adsorption bands corresponding to amide functions (-RCON)- between 1680-1640 cm^{-1}, or nitrile function (R-CN) between 2260 and 2240 cm^{-1} are absent in the IR spectrum of the deactivated catalyst (**Figure 4-12**).

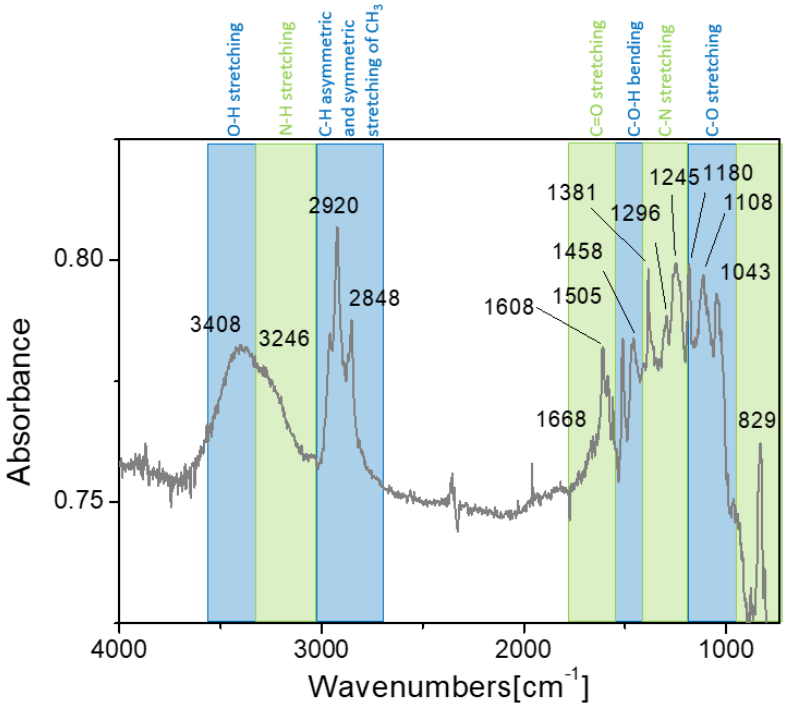

Figure 4-12. FTIR absorbance spectrum of the 1st cycle recovered catalyst sample under outgassing at 90 K.

On the other hand, the FTIR absorbance spectrum of the catalyst sample after regeneration under hydrogen (**Figure 4-13)** showed a dramatic drop of catalyst transparency. Weakly bands adsorption at 3427, 2920, 2836 and 1505 and 1445 cm^{-1} were observed.

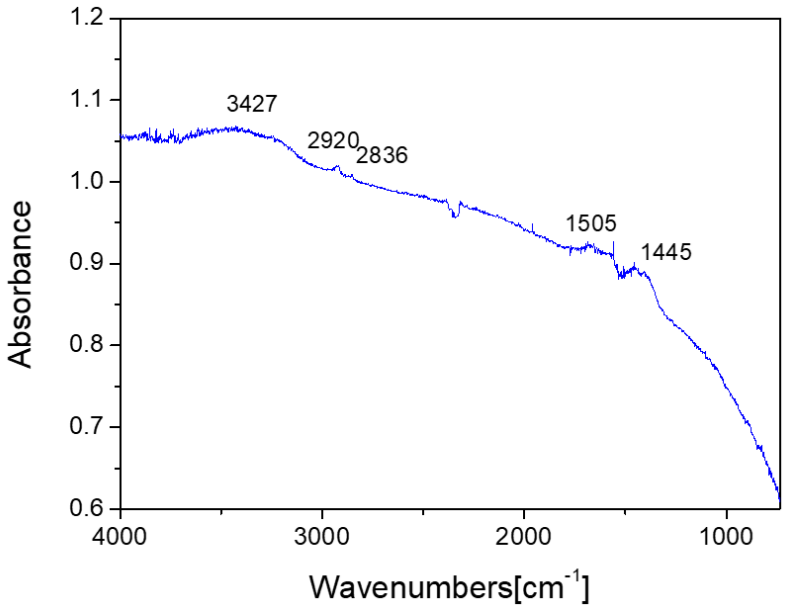

Figure 4-13. FTIR absorbance spectrum of the catalyst recovered from a reactivation under 30 bar of H_2 at 150°C for 1h. Sample under outgassing at 90 K.

GC-MS analysis

In GC-MS analysis of the solvent after catalyst reactivation under hydrogen pressure the following species were detected: NE11, UNE11, AE11, SNE11, A_2 and traces of I_2 , A_2 and of dimerisation product of AE11.

CO adsorption

Raney-Nickel catalyst have high activity in methanation reactions. Furthermore, CO is a perfect probe molecule to study adsorption by vibrational spectroscopy. Since CO can adopt different adsorption geometries (terminal, 2 folding bridging, 3-fold hollow) we used this probe to obtain information about the surface site distribution of the Raney-Nickel catalyst before and after catalyst regeneration with hot hydrogen (**Figure 4-14**).

The spectrum of gaseous CO shows no probe adsorption at the catalyst surface. This sustains the statement that the catalyst is deactivated, no access to catalyst sites, after the first cycle.

The deactivation can be associated to:

(i) Coverage of the surface sites by the reaction products of the above reaction, showing catalyst deactivation,

(ii) Low catalyst surface area, implying a low number of sites, i.e. Under the detection limit of the spectroscopic technique,

(iii) catalyst leaching (metal lost).

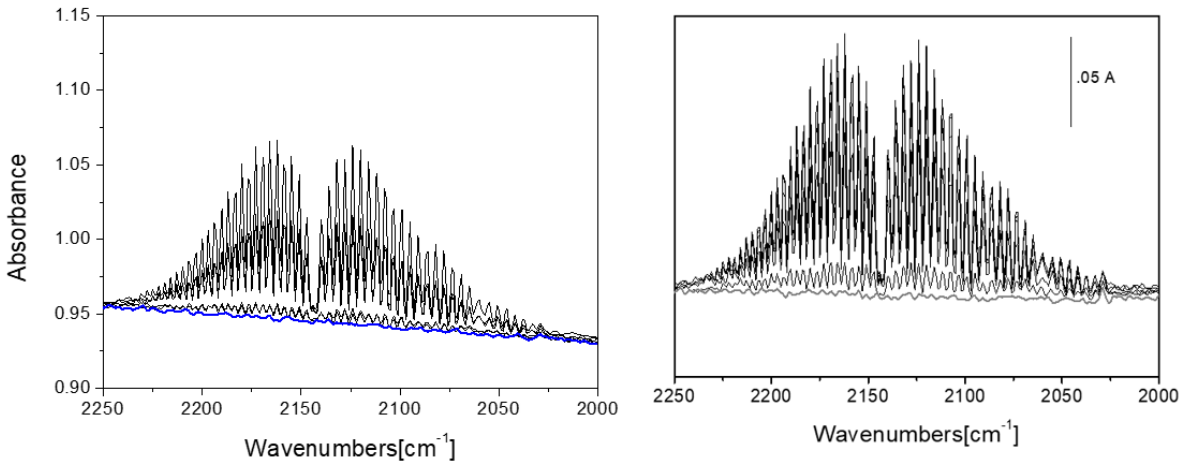

Figure 4-14. CO adsorption spectrum at 90K. **a)** on regenerated catalyst, **b)** catalyst after first reaction cycle.

The supposition **ii** and **iii** are not vailable once the surface area calculated was 40 m^2 and the catalyst activity after regeneration under hydrogen atmosphere is recovered.

4.4.6 Observations and some considerations

The initial purpose study was the study of catalyst reactivation under different methods. However, for the reaction and kinetics study, which were derived from the experiments done for the catalyst deactivation study, some major reaction and analysis conditions should have been taken in account such as:

- Use of a buffer hydrogen bottle in order to keep constant H_2 addition in the autoclave, (the hydrogen pressure variation was not constant for the different experiments).
- Use of internal standards for GC-FID reaction species quantification.
- Experiments at different temperatures and UNE11 concentrations and lower catalyst loading (in order to avoid mass-transfer limitation) for **correct** initial kinetics study.

4.4.7 Complementary experiments

We studied the reactivation of Ru SiC pellet catalyst used in a continuous flow hydrogenation of UNE11 to AE11 under sonication at 25, 40 and 120 kHz, and in-situ solvent wash (methylcyclohexane and ethanol) at 110°C.

4.4.7.1 *Catalyst treatment under sonication*

In order to find the best frequencies that fitted the exigence of low catalyst degradation under sonication, the degradation of catalyst was tested at different frequencies and input power loading.

In **Table 4-20** is possible to observe that by decreasing the frequency and at higher input power higher is the degradation of the catalyst under the sonication treatment. Therefore, the best frequency to apply in the catalyst reactivation treatment is 120 kHz. The results are in accordance with the physical phenomenon's described in the literature, whereby decreasing the frequency, higher will be the cavitation bubble radius and so the implosion energy (hot spot). This high energy release gives place to more aggressive phenomenon's such as shockwaves or microjects contributing to a higher erosion of the catalyst and so higher catalyst weight loss during treatment.

	40kHz		**80kHz**		**120kHz**	
Input Power	50%	100%	50%	100%	50%	100%
catalyst mass weight	1.20	1.10	0.72	1.15	1.42	1.35
m organic (mg)	3.70	4.80	3.23	2.1	6.5	1
m inorganic (mg)	4.20	6.90	6.90	7.2	0.1	0.002

Table 4-20. Catalyst weight lost after treatment at different frequencies.

Catalyst treatment in-situ with ethanol at 100°C was found to have the highest effect on the catalyst reactivation. Surprisingly under sonication the highest catalyst reactivation was found when methylcyclohexane was used as the treatment solvent.

Solvent	**100°C *in-situ***	**40 kHz (25°C)**	**120 kHz (25°C)**
EtOH	15%	11%	4%
MCH	0%	7%	14%

Table 4-21. Catalyst reactivation % after treatment in-situ or ex-situ under sonication at 40 and 120 kHz.

4.5 Conclusions

Amino esters are the perfect building blocks for the production of polyamides. These monomers can be obtained through the reduction of unsaturated nitrile esters. The hydrogenation of nitrile compounds to the corresponding amines can be carried out smoothly and in excellent yields using Raney®-nickel catalysts. However, the quick loss of activity, after only a single reaction cycle, makes this process unattractive for industrial applications. In this chapter, we have described the best conditions, 60 bar H_2, 90°C, ammonia and 10 wt % catalyst, for a 92 % yield of the methyl-11-aminoundecanoate. Kinetics studies with different catalyst loading shows that higher catalyst loading affords higher conversion of UNE11 to AE11. However, the H_2 diffusion in the reaction media is limited reducing the rate of the reaction. Through calculation studies based on the H_2 moles consumption over the reaction time at 40 bars, it was observed that side-molecules not identified by GC-FID were formed with no hydrogen consumption suggesting the catalyst deactivation by polymers of secondary/tertiary amine between two NE11 molecules which are trapped in the catalyst porosity. Moreover, among the tested methodologies for catalyst reactivation: 1) via washing with methanol or reaction solvent; 2) via sonication with either a MeOH or NaOH solution at a frequency of 120 kHz and input power of 100 W or 200 W ; and 3) under a hydrogen atmosphere at either 30 or 60 bar and at 150 or 200°C respectively; only the latter catalyst reactivation method with hydrogen proved to be efficient. The *in-pot* catalyst reactivation under a hydrogen atmosphere and under pilot conditions (150°C, 30 bar) was described. Some promising results were also obtained by reactivation under ultrasound by catalyst dispersion in NaOH 0.05 N and sonication at 120 kHz (100W input power). Catalyst activity was recovered by 22 points of yield of methyl-11-aminoundecanoate in comparison with no catalyst treatment. Catalyst deactivation mechanism was proved through analysis of the catalyst surface by FTIR and CO adsorption techniques where the molecules adsorbed on the exhausted catalyst, were detected as well proved their desorption after treatment under hot hydrogen. The analysis of the solvent solution after catalyst reactivation under hydrogenation as well the quantification of molecules not detected by GC-FID, suggest catalyst deactivation through catalyst cavities blocking by non-hydrogenated molecules such as polymers and reaction species trapped inside of catalyst cavities not allowing the reaction progress.

4.6 References

[1] J. M.Lyons, N. K. Singh, X. Shen, Functional MBS modifiers for using in egeneering resins, 2014. PCT patent US 2014/0364541 A1.

[2] D.C. Sherrington, Polymer technology dictionary, React. Polym. 23 (1994) 107. doi:10.1016/0923-1137(94)90029-9.

[3] M.P. Shandura, Y.P. Kovtun, V.P. Yakubovskyi, Y.P. Piryatinski, P.M. Lutsyk, R.J. Perminov, A.B. Verbitsky, A. Rozhin, Dehydr oacetic acid based dioxaborine styryl dye: Effective fluorescent probe for ammonia and amine detection, Key Eng. Mater. 605 (2014) 159–162. doi:10.4028/www.scientific.net/KEM.605.159.

[4] J. Lipp, Possible mechanisms of morphine analgesia, Clin. Neuropharmacol. 14 (1991) 131–147. doi:10.1097/00002826-199104000-00003.

[5] L. Liu, X. Pu, Y. Zhou, J. Zhou, D. Luo, Z. Ren, Smart Pickering Water-in-Oil Emulsion by Manipulating Interactions between Nanoparticles and Surfactant as Potential Oil-Based Drilling Fluid, Colloids Surfaces A Physicochem. Eng. Asp. 586 (2020) 124246. doi:10.1016/j.colsurfa.2019.124246.

[6] C. Matthieu, E. Dietrich, H. Delmas, J. Jenck, Hydrogenation of adiponitrile catalyzed by raney nickel use of intrinsic kinetics to measure gas-liquid mass transfer in a gas induced stirred slurry reactor, Chem. Eng. Sci. 47 (1992) 2289–2294. doi:10.1016/0009-2509(92)87049-V.

[7] W. Huber, Hydrogenation of Basic Nitriles with Raney Nickel, J. Am. Chem. Soc. 66 (1944) 876–879. doi:10.1021/ja01234a009.

[8] D.J. Segobia, A.F. Trasarti, C.R. Apesteguía, Chemoselective hydrogenation of unsaturated nitriles to unsaturated primary amines: Conversion of cinnamonitrile on metal-supported catalysts, Appl. Catal. A Gen. 494 (2015) 41–47. doi:10.1016/j.apcata.2015.01.028.

[9] P. Sabatier, E.E. Reid, Catalysis in Organic Chemistry, D. Van Nostrand Company (Michigan), 1922.

[10] H. Greenfield, Catalytic hydrogenation of butyronitrile, Eng. Chem. Prod. Res. Dev. 6 (1967) 142–144.doi: 10.1021/i360022a014.

[11] J. Volf, J. Pašek, Hydrogenation of Nitriles, Stud. Surf. Sci. Catal. 27 (1986) 105–144. doi:10.1016/S0167-2991(08)65350-1.

[12] F. Hochard, H. Jobic, J. Massardier, A.J. Renouprez, Gas phase hydrogenation of acetonitrile on Raney nickel catalysts: reactive hydrogen, J. Mol. Catal. A. Chem. 95 (1995) 165–172. doi:10.1016/1381-1169(94)00010-7.

[13] F.. Von Braun, J.; Blessing, G.; Zobel, Catalytic hydrogenations under pressure in the presence of nickel salts. VI. Nitriles, Chem. Ber. 36 (1923) 1988–2001.

[14] D.J. Segobia, A.F. Trasarti, C.R. Apesteguía, Chemoselective hydrogenation of unsaturated nitriles to unsaturated primary amines: Conversion of cinnamonitrile on metal-supported catalysts, Appl. Catal. A Gen. (2015). doi:10.1016/j.apcata.2015.01.028.

[15] G. Sparrow, Nickel, Benchmark Books/Marshall Cavendish, 2005.

[16] K. Wilhelm, Nickel: An Element with Wide Application in Industrial Homogeneous Catalysis, Angew. Chemie Int. Ed. English. 29 (2003) 235–244. doi:10.1002/anie.199002351.

[17] T. Ben Halima, J. Masson-Makdissi, S.G. Newman, Nickel-Catalyzed Amide Bond Formation from Methyl Esters, Angew. Chemie - Int. Ed. 57 (2018) 12925–12929. doi:10.1002/anie.201808560.

[18] A. Chen, T. Miyao, K. Higashiyama, H. Yamashita, M. Watanabe, High catalytic performance of ruthenium-doped mesoporous nickel-aluminum oxides for selective CO methanation, Angew. Chemie - Int. Ed. 49 (2010) 9895–9898. doi:10.1002/anie.201005650.

[19] J. Martínez, E. Hernández, S. Alfaro, R. López Medina, G. Valverde Aguilar, E. Albiter, M. Valenzuela, High Selectivity and Stability of Nickel Catalysts for CO2 Methanation: Support Effects, Catalysts. 9 (2018) 24. doi:10.3390/catal9010024.

[20] I. L. Simakova, A. V. Simakov, D. Yu. Murzin, Valorization of Biomass Derived Terpene Compounds by Catalytic Amination, Catalysts. 8 (2018) 365. doi:10.3390/catal8090365.

[21] L.C. Dresch, C.H. Junges, O. de L. Casagrande, R. Stieler, Nickel complexes supported by selenium-based tridentate ligands and their use as effective catalyst systems for ethylene dimerisation, J. Organomet. Chem. 856 (2018) 34–40. doi:10.1016/j.jorganchem.2017.12.025.

[22] N. Savjani, K. Singh, G.A. Solan, Bis(iminopyridyl)phthalazine as a sterically hindered compartmental ligand for an M<inf>2</inf> (M = Co, Ni, Fe, Zn) centre; Applications in ethylene oligomerisation, Inorganica Chim. Acta. 436 (2015) 184–194. doi:10.1016/j.ica.2015.08.004.

[23] C. Carriel Schmitt, M. Gagliardi Reolon, M. Zimmermann, K. Raffelt, J.-D. Grunwaldt, N. Dahmen, Synthesis and Regeneration of Nickel-Based Catalysts for Hydrodeoxygenation of Beech Wood Fast Pyrolysis Bio-Oil, Catalysts. 8 (2018) 449. doi:10.3390/catal8100449.

[24] H. Reaction, T. Xiao, Y. Zhao, Tuning Selectivity of Maleic Anhydride, (2019) 1–18.

[25] M. Raney, Method of producing finely-divided Nickel, 1628190, 1927.

[26] J.I. Macnab, R.B. Anderson, The Structure of Raney Nickel VIII. Magnetic Properties Related to Particle Size and Hydrogen Evolution, 1973.

[27] R.L. Augustine, Heterogeneous Catalysis for the Synthetic Chemist, Taylor & Francis, 1995.

[28] H. Adkins, H.R. Billica, The Preparation of Raney Nickel Catalysts and their Use Under Conditions Comparable with Those for Platinum and Palladium Catalysts, J. Am. Chem. Soc. 70 (1948) 695–698. doi:10.1021/ja01182a080.

[29] F. Devred, A.H. Gieske, N. Adkins, U. Dahlborg, C.M. Bao, M. Calvo-Dahlborg, J.W. Bakker, B.E. Nieuwenhuys, Influence of phase composition and particle size of atomised Ni-Al alloy samples on the catalytic performance of Raney-type nickel catalysts, Appl. Catal. A Gen. (2009). doi:10.1016/j.apcata.2008.12.039.

[30] C.H. Bartholomew, R.J. Farrauto, Fundamentals of Industrial Catalytic Processes, Wiley, 2011.

[31] W. Gerhartz, F. Ullmann, B. Elvers, Ullmann's encyclopedia of industrial chemistry, VCH, 1989.

[32] J.-F. Briffaud, Thierry, Couturier, Jean-Luc, Dubois, Jean-Luc, Devaux, Composition made of amino acid or ester with polymer quality and methods for obtaining same, 2017. PCT patent: WO2017/0555745A1. https://patentimages.storage.googleapis.com/b1/c1/b3/1ba99c207092cc/WO2017055745A1.pdf (accessed August 24, 2019).

[33] Bio-based Renewable Solutions, (2019). https://www.extrememateriels-arkema.com/en/product-families/rilsan-polyamide-11-family/bio-based-renewable-solutions/ (accessed April 14, 2019).

[34] Z. Saedi, S. Tangestaninejad, M. Moghadam, V. Mirkhani, I. Mohammadpoor-Baltork, MIL-101 metal-organic framework: A highly efficient heterogeneous catalyst for oxidative cleavage of alkenes with H 2O 2, Catal. Commun. 17 (2012) 18–22. doi:10.1016/j.catcom.2011.10.005.

[35] D. Shi, R. Wojcieszak, S. Paul, E. Marceau, Ni promotion by fe: What benefits for catalytic hydrogenation?, Catalysts. 9 (2019). doi:10.3390/catal9050451.

[36] H. Jiang, S. Lu, X. Zhang, B. Tian, H. Peng, W. Dai, J. Qiao, Effect of polyamide on selectivity of its supported Raney Ni catalyst, Sci. China Chem. 59 (2016) 776–780. doi:10.1007/s11426-015-5541-4.

[37] J. Bidange, J.L. Dubois, J.L. Couturier, C. Fischmeister, C. Bruneau, Ruthenium catalyzed ethenolysis of renewable oleonitrile, Eur. J. Lipid Sci. Technol. 116 (2014) 1583–1589. doi:10.1002/ejlt.201400184.

[38] J. Bidange, C. Fischmeister, C. Bruneau, J.L. Dubois, J.L. Couturier, Cross metathesis of bio-sourced fatty nitriles with acrylonitrile, Monatshefte Fur Chemie. 146 (2015) 1107–1113. doi:10.1007/s00706-015-1480-1.

[39] J.K. Hollmann, Estimate accuracy: Dealing with reality, AACE Int. Trans. 3 (2012) 1753–1771. https://www.validest.com/index_htm_files/Hollmann_Accuracy.pdf (accessed August 17, 2019).
[40] J.-L. Dubois, Method for the synthesis of omega-amino-alkanoic acids, US 8,642,792 B2, 2014.
[41] J.-L. Dubois, J.-L. Couturier, Cross methathesis process, 2015. PCT patent US 2015/0344416 A1.
[42] J.-L. Dubois, 3D Printing for intensified catalytic processes. A case study from the PrintCr3Dit project, 2019.
[43] P. Kukula, K. Koprivova, Structure-selectivity relationship in the chemoselective hydrogenation of unsaturated nitriles, J. Catal. 234 (2005) 161–171. doi:10.1016/j.jcat.2005.06.011.
[44] J. Krupka, Nitrile Hydrogenation on Solid Catalysts – New Insights into the Reaction, Curr. Org. Chem. 16 (2012) 988–1004. doi:10.2174/138527212800194692.
[45] C. Bartholomew, M. Argyle, Advances in Catalyst Deactivation and Regeneration, Catalysts. 5 (2015) 949–954. doi:10.3390/catal5020949.
[46] P. Fouilloux, The nature of raney nickel, its adsorbed hydrogen and its catalytic activity for hydrogenation reactions (review), Appl. Catal. 8 (1983) 1–42. doi:10.1016/0166-9834(83)80051-7.

Conclusions and perspectives

Over the years, the oxidative cleavage of fatty acids and derivatives, proved to be an attractive way to obtain bi-functional monomers that can be used for polycondensation reactions to obtain specialty polymers.

In our studies of economic risk assessment for the Novamont's process, we conclude that the composition of the vegetable oil has higher economic impact than the price of the raw material. Therefore, by using an oil rich in mono-unsaturated fatty acids (sunflower oil) the initial capital cost is highly reduced and the probability of generating a profit is increased.

Mono-Unsaturated fatty nitriles from MUFAs have been selected by Arkema as precursor of a new synthetic route to obtain monomers for PA11 and PA12 using H_2O_2.

H_2O_2 is an oxidant easier to handle than ozone, but the kinetics of the catalyzed reactions are still slow. The time-consuming reaction (24h) requires high temperatures (85-95°C) to cleave C-C bonds (347-356 kJ/mole, at 298 K) and achieve the desired products. In addition, several studies highlighted major limitations in mass transfer leading to undesired by-products and lack of reproducibility at larger scale.

The need for an emergent technology that could solve the problems associated to this type of reaction led us to the sonochemistry.

Since 1927 ultrasound technology confirmed its potential in a variety of catalytic processes. It has been also proved that mass transfer across the phase boundary of a multiphasic system is substantially enhanced through acoustic emulsification.

The aim of our work was to exploit sonochemical methods to overcome mass transfer and time limitation of conventional oxidative cleavage reaction in MUFAs and derivatives.

Significant results were obtained with an ultrasonic horn, working at frequency of 25 kHz and 100 W of input power. With this system we were not only able to reduce **1)** the reaction time from 24h to 5h, **2)** the concentration of H_2O_2 from 70% to 35%, **3)** reduce the working temperature from 90°C to 60°C but also **4)** to achieve the desirable monomers in the absence of an emulsifier.

Besides the safer alternative of using lower concentration of oxidant and no need of emulsifier, with this new technology, the monomers could be obtained with the same yields than in conventional in more aggressive conditions (45%) .

However, the production of high molecular weight molecules due to the acidity of the medium, demonstrates that the catalytic system is not the most appropriate, exposing its sensibility, and for this reason higher monomer yield is difficult to obtain.

With the experiments pursued, we can conclude that a process should be done in two steps where the hydrogen peroxide is only added for synthesize the diol intermediate. To proceed the cleavage, the pH of the medium should be increased and another oxidant such as O_2 should be added.

Nevertheless, the production of estolides and acetals with high molecular weight in our catalytic system was an important discovery. Estolides can be applied in the cosmetic market, and so this catalytic system in ultrasonic conditions can be exploited to synthesize these high value molecules. Also, by isolation of the acetals formed by acetalization between the diol intermediate and the aldehydes can be high of interest. The concomitant hydrolysis of these species can afford the aldehydes which can posteriorly separate, and which have much higher market value than the corresponding carboxylic acids.

The ultrasound technology was also applied in the reactivation of a commercial catalyst, Raney-Nickel used in the hydrogenation of mono-unsaturated fatty ester-nitriles to afford amino-ester. We demonstrated a gain on the catalyst activity of 20% compared with no treatment, however, by treating the exhaustive catalyst (*in-situ*) under hydrogen atmosphere proved that the major catalyst deactivation mechanism was related to the loss of active adsorbed hydrogen and to the molecules adsorbed on the catalyst surface.

Finally, our experiments demonstrated that 100% gain of catalyst activity is possible with *in-situ* regeneration under hydrogen atmosphere after at least two catalytic cycles. Such process can be easily applied industrially in the hydrogenation of ester-nitriles to obtain amino-esters high value monomers for the polymer industry.

Ultrasound technology has demonstrated its industrial applicability in different areas such as food cutting, welding and cleaning. Besides the major success stories in the application of ultrasound in sonochemistry the uncertainty of locally high temperatures formed due cavitation implosions (hot-spots) it is still a major concern to up-scale the technology for synthesis purpose in exception of crystallization (continuous mode) or emulsifications processes.

Poster Comunications

Maria, A.L., Couturier, J.L., Dubois, J.L., Cravotto, G., *New process to synthesize polyamides monomers by oxidative cleavage of fatty nitriles,* 4th International Congress For Biorrefineries (CatBiorg), Lyon – France, 11-15th December, **2017**

Maria, A.L., Couturier, J.L., Dubois, J.L., Cravotto, G., *New Process to Make Polyamides Monomers by Oxidative Cleavage of Fatty Nitriles,* 15th Euro Fed Lipid Congress, Uppsala – Sweden, 27-31th August, **2017**

Maria, A.L., Couturier, J.L., Dubois, J.L., Cravotto, G., *Ultrasound oxidative cleavage of fatty acids and derivatives,* 6th Meeting of European Society of Sonochemistry, Besançon– France, 15-19th April, **2018 (Winner best poster presentation)**

Maria, A.L., Couturier, J.L., Dubois, J.L., Cravotto, G., *Ultrasound oxidative cleavage of functionalized fatty acids,* Ultrasonics 2018, Costa da Caparica– Portugal, 10-13th June, **2018**

Maria, A.L., Couturier, J.L., Dubois, J.L., Cravotto, G., *Specialty monomer synthesis by ultrasound assisted oxidative cleavage ,* 2nd international Process Intensification Conference (IPIC), Leuven– Belgium, 27-29th May, **2019**

Oral Communications

Maria, A.L., Couturier, J.L., Dubois, J.L., Cravotto, G., *Ultrasound oxidative cleavage of fatty nitriles,* 6th Meeting of European Society of Sonochemistry, Besançon– France, 15-19th April, **2018**

Maria, A.L., Couturier, J.L., Dubois, J.L., Cravotto, G., *US oxidative cleavage,* Ultrasonics 2018, Costa da Caparica– Portugal, 10-13th June, **2018 (Shot-gun presentation)**

Maria, A.L., Couturier, J.L., Dubois, J.L., Cravotto, G., *Coupure oxydante en monomères bi-fonctionnels biosourcés sous ultrasons*, Biomolécules Lipidiques du pole IAR, Canéjan – France, 5th Mars, **2019**

Maria, A.L., Couturier, J.L., Dubois, J.L., Cravotto, G., *Assisted Synthesis of Value building-block for the Industry*, Plant Based Summit (PBS 2019), Lyon – France, 22-24th May, Lyon-France, **2019**

Maria, A.L., Couturier, J.L., Dubois, J.L., Cravotto, G., *Oxidative cleavage of fatty acids/esters/nitriles to bi-functional bio-sourced monomers under ultrasounds,* 1st International Congress on Unconventional catalysis, Reactors and Applications (UCRA), Zaragossa – Spain, 16-18th October, **2019**

Publications

Soutelo-Maria, A., Dubois, J.-L., Couturier, J.-L., Cravotto, G., 2018. Oxidative Cleavage of Fatty Acid Derivatives for Monomer Synthesis. Catalysts 8, 464. https://doi.org/10.3390/catal8100464

Soutelo-Maria, A., Dubois, J.-L., Couturier, J.-L., Brebion Magali, Cravotto, G., 2020 – Efficient Synthesis of high value monomers with Raney®-Nickel catalyst recycling. Catalysts 10, 229. https://www.mdpi.com/2073-4344/10/2/229

Izeppi, G., Dubois, J.-L., Balle, A., Soutelo-Maria, A. - Economic Risk Assessment Using Monte Carlo Simulation For The Production Of Azelaic Acid And Pelargonic Acid From Vegetable Oils (Wating for approval) (Colaboration avec Microinnova, Allerheiligen bei Wildon, Áustria) - https://doi.org/10.1016/j.indcrop.2020.112411

SUPPLEMENTARY DATA

[Document subtitle]

S.1 Economic Risk Assessment using Monte Carlo Simulation for the production of azelaic acid and pelargonic acid from vegetable oils

S.1.1. Correlation matrix

a)

	Palm Oil	*Methanol*	*H2O2 100%*	*Tungstic Acid*	*Cobalt Acetate*	*Azelaic acid*	*Crude glycerol*	*Pelargonic acid*	*C16:0*	*C18:0*	*C20:0*	*C3,DC3 in water*	*C6*	*C7*	*C8*	*DC8*
Palm Oil	1															
Methanol	0,49	1														
H2O2 100%	-0,4	0,05	1													
Tungstic Acid	0,1	0,44	0,05	1												
Cobalt Acetate	0,45	0,39	0,05	-0,2	1											
Azelaic acid	-0,1	-0,4	0,27	0,05	0,05	1										
Crude glycerol	0,39	0,45	-0,1	0,09	0,45	-0,4	1									
Pelargonic acid	0,24	0,07	0,01	0,19	-0,5	-0,1	0,36	1								
C16:0	0,45	0,45	-0,5	0,5	-0,5	0,45	0,45	-0,5	1							
C18:0	0,5	-0	0,17	-0,5	0,5	0,45	-0,1	-0,5	0,45	1						
C20:0	0,05	0,05	0,05	0,05	0,05	0,05	0,05	0,05	0,05	0,05	1					
C3,DC3 in water	0,05	0,05	0,05	0,05	0,05	0,05	0,05	0,05	0,05	0,05	0,05	1				
C6	-0,5	-0,1	0,5	0,05	0,05	-0,5	0,37	0,45	-0,5	-0,5	0,05	0,05	1			
C7	0,05	0,05	0,05	0,05	0,05	0,05	0,05	0,05	0,05	0,05	0,05	0,05	0,05	1		
C8	0,17	0,11	0,5	-0,5	0,5	-0,5	0,15	0,5	0,31	0,03	0,05	0,05	0,5	0,05	1	
DC8	0,05	0,05	0,05	0,05	0,05	0,05	0,05	0,05	0,05	0,05	0,05	0,05	0,05	0,05	0,05	1

b)

	Palm Oil	*Methanol*	*H2O2 100%*	*Tungstic Acid*	*Cobalt Acetate*	*Azelaic acid*	*Crude glycerol*	*Pelargonic acid*	*C16:0*	*C18:0*	*C20:0*	*C3,DC3 in water*	*C6*	*C7*	*C8*	*DC8*
Palm Oil	1															
Methanol	0,5	1														
H2O2 100%	-0,4	0,05	1													
Tungstic Acid	0,1	0,5	0,05	1												
Cobalt Acetate	0,4	0,4	0,05	0	1											
Azelaic acid	0	0	0,3	0,05	0,05	1										
Crude glycerol	0,3	0,4	0	0	0,01	-0,3	1									
Pelargonic acid	0,3	0,05	0	0,1	0,05	-0,4	0,1	1								
C16:0	0,6	0,4	0,1	0,1	-0,1	0,4	0,1	0,1	1							
C18:0	0,5	0,4	0,1	0,1	0,01	0,4	-0,1	0,1	0,7	1						
C20:0	0	0,05	0,05	0,05	0,05	0,05	0,05	0,05	0,1	0,1	1					
C3,DC3 in water	0,05	0,05	0,05	0,05	0,05	0,05	0,05	0,05	0,05	0,05	0,05	1				
C6	0	0	0,05	0,05	0,05	-0,2	0,1	0,45	0	0,1	0,05	0,05	1			
C7	0,05	0,05	0,05	0,05	0,05	-0,2	0,05	0,45	0,05	0,05	0,05	0,05	0,7	1		
C8	0,2	0,1	0,05	0,05	0,05	-0,5	0,1	0,8	0,1	0,05	0,05	0,05	0,5	0,7	1	
DC8	0,05	0,05	0,05	0,05	0,05	0,05	0,05	0,05	0,05	0,05	0,05	0,05	0,05	0,05	0,05	1

Fig. 1. Correlation matrix for palm oil a) Based on historical data b) Based on historical data and expert judgement

a)

	Palm Oil	Methanol	H2O2 100%	Tungstic Acid	Cobalt Acetate	Azelaic acid	Crude glycerol	Pelargonic acid	C16:0	C18:0	C20:0	C3,DC3 in water	C6	C7	C8	DC8
Palm Oil	1															
Methanol	0,49	1														
H2O2 100%	-0,4	0,05	1													
Tungstic Acid	0,1	0,44	0,05	1												
Cobalt Acetate	0,45	0,39	0,05	-0,2	1											
Azelaic acid	-0,1	-0,4	0,27	0,05	0,05	1										
Crude glycerol	0,39	0,45	-0,1	0,09	0,45	-0,4	1									
Pelargonic acid	0,24	0,07	0,01	0,19	-0,5	-0,1	0,36	1								
C16:0	0,45	0,45	-0,5	0,5	-0,5	0,45	0,45	-0,5	1							
C18:0	0,5	-0	0,17	-0,5	0,5	0,45	-0,1	-0,5	0,45	1						
C20:0	0,05	0,05	0,05	0,05	0,05	0,05	0,05	0,05	0,05	0,05	1					
C3,DC3 in water	0,05	0,05	0,05	0,05	0,05	0,05	0,05	0,05	0,05	0,05	0,05	1				
C6	-0,5	-0,1	0,5	0,05	0,05	-0,5	0,37	0,45	-0,5	-0,5	0,05	0,05	1			
C7	0,05	0,05	0,05	0,05	0,05	0,05	0,05	0,05	0,05	0,05	0,05	0,05	0,05	1		
C8	0,17	0,11	0,5	-0,5	0,5	-0,5	0,15	0,5	0,31	0,03	0,05	0,05	0,5	0,05	1	
DC8	0,05	0,05	0,05	0,05	0,05	0,05	0,05	0,05	0,05	0,05	0,05	0,05	0,05	0,05	0,05	1

b)

	HOSO Oil	Methanol	H2O2 100%	Tungstic Acid	Cobalt Acetate	Azelaic acid	Crude glycerol	Pelargonic acid	C16:0	C18:0	C20:0	C3,DC3 in water	C6	C7	C8	DC8
HOSO Oil	1															
Methanol	0,5	1														
H2O2 100%	-0,4	0,05	1													
Tungstic Acid	0,1	0,5	0,05	1												
Cobalt Acetate	0,4	0,4	0,05	0	1											
Azelaic acid	0	0	0,3	0,05	0,05	1										
Crude glycerol	0,3	0,4	0	0	0,01	-0,3	1									
Pelargonic acid	0,3	0,05	0	0,1	0,05	-0,4	0,1	1								
C16:0	0,6	0,4	0,1	0,1	-0,1	0,4	0,1	0,1	1							
C18:0	0,5	0,4	0,1	0,1	0,01	0,4	-0,1	0,1	0,7	1						
C20:0	0	0,05	0,05	0,05	0,05	0,05	0,05	0,05	0,1	0,1	1					
C3,DC3 in water	0,05	0,05	0,05	0,05	0,05	0,05	0,05	0,05	0,05	0,05	0,05	1				
C6	0	0	0,05	0,05	0,05	-0,2	0,1	0,45	0	0,1	0,05	0,05	1			
C7	0,05	0,05	0,05	0,05	0,05	-0,2	0,05	0,45	0,05	0,05	0,05	0,05	0,7	1		
C8	0,2	0,1	0,05	0,05	0,05	-0,5	0,1	0,8	0,1	0,05	0,05	0,05	0,5	0,7	1	
DC8	0,05	0,05	0,05	0,05	0,05	0,05	0,05	0,05	0,05	0,05	0,05	0,05	0,05	0,05	0,05	1

Fig. 2. Correlation matrix for high oleic sunflower oil oil a) Based on historical data b) Based on historical data and expert judgement

S.1.2. Products and Raw Materials prices distributions

Methanol	**H_2O_2 100%**
5% to 95% probability range: [201, 542] US$/ton	**5% to 95% probability range:** [823, 1126] US$/ton
Distribution type: Log-Normal	**Distribution type:** Gaussian,
mean:5.8, **σ:**0.302	**mean:**975, **σ:**92
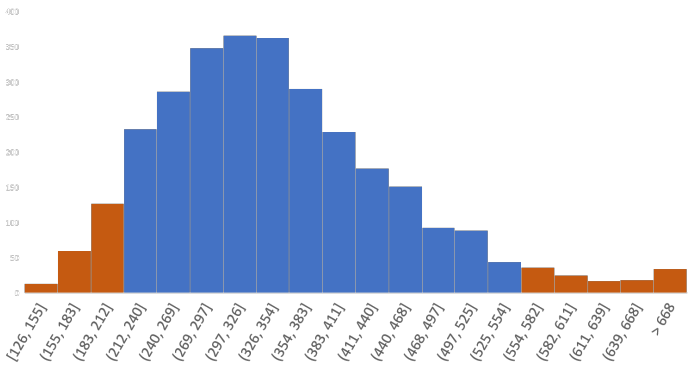	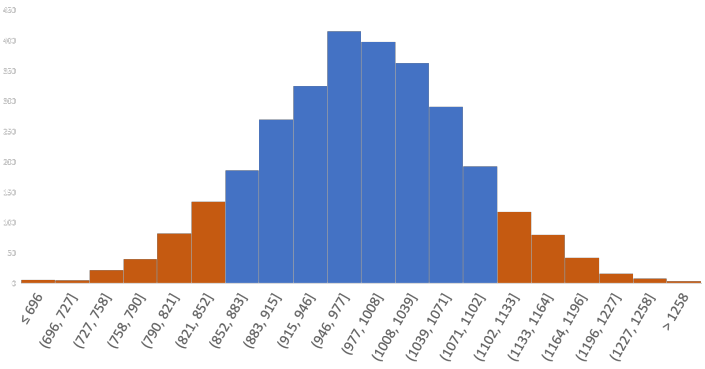
Tungstic acid	**Cobalt Acetate**
5% to 95% probability range: [31355, 34644] US$/ton	**5% to 95% probability range:** [10095, 11740] US$/ton
Distribution type: Log-Normal	**Distribution type:** Gaussian,
mean:33000, **σ:**1000	**mean:**10918, **σ:**500
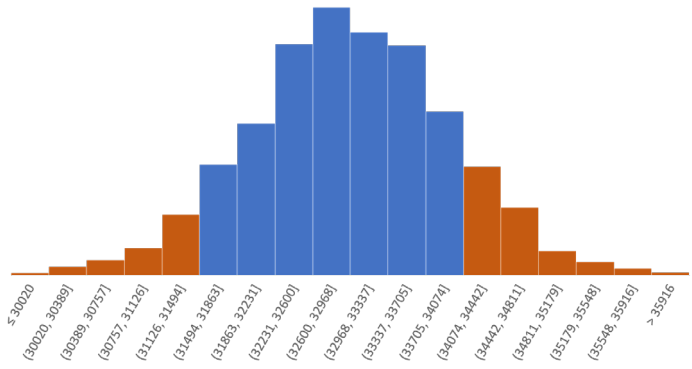	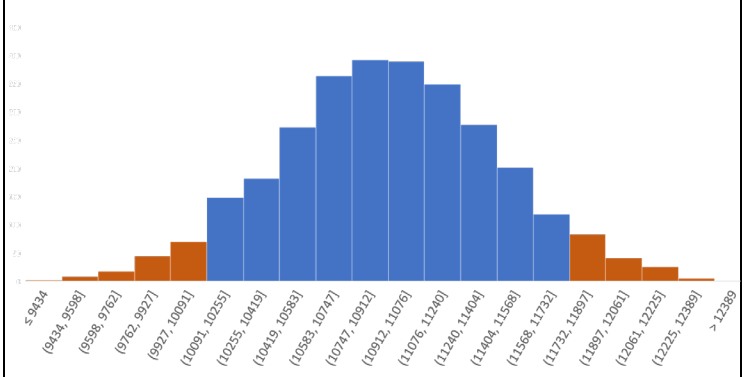

Fig.S.1.3. Fitted future price distribution of the raw materials: methanol, H_2O_2, Tungstic acid and Cobalt acetate based on historical price.

Azelaic Acid	Crude Glycerol
5% to 95% probability range: [5648, 8110] US$/ton	**5% to 95% probability range:** [143, 422] US$/ton
Distribution type: Log-Normal	**Distribution type:** Triangular
mean:8.82, **σ:**0.11	**a:**100, **b:**500 and **c:**200
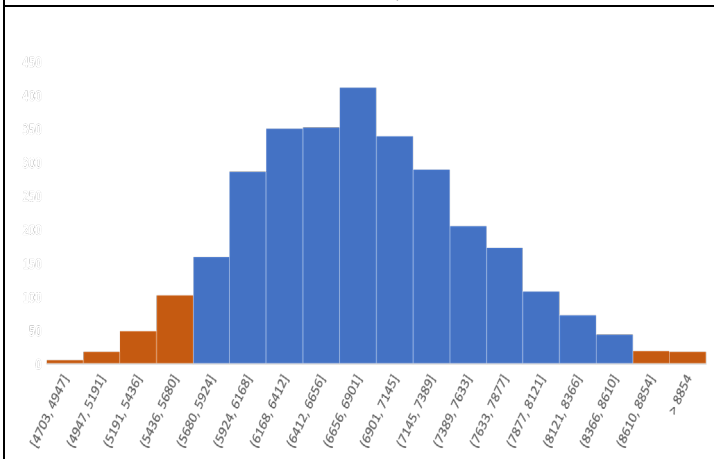	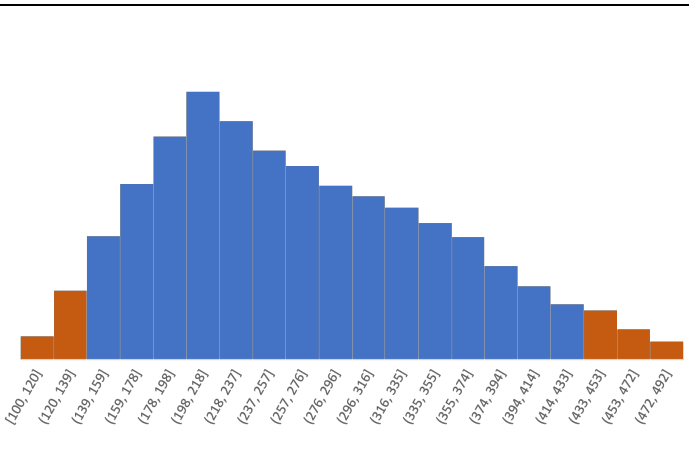
Pelargonic Acid	**C16:0**
5% to 95% probability range: [2620, 5059] US$/ton	**5% to 95% probability range:** [548, 1471] US$/ton
Distribution type: Log-Normal	**Distribution type:** Log-Normal
mean:8.2, **σ:**0.2	**mean:**6.8, **σ:**0.3
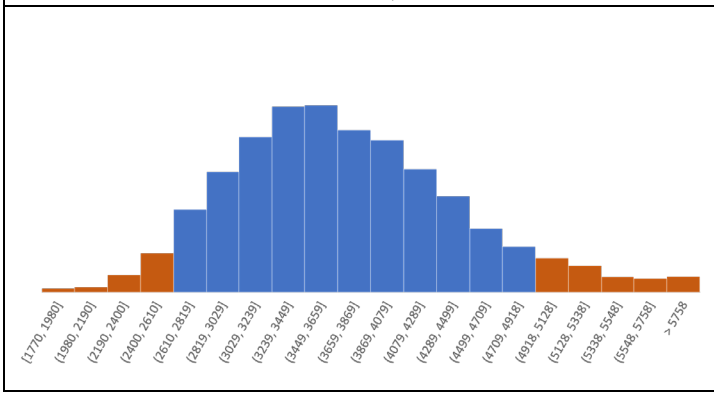	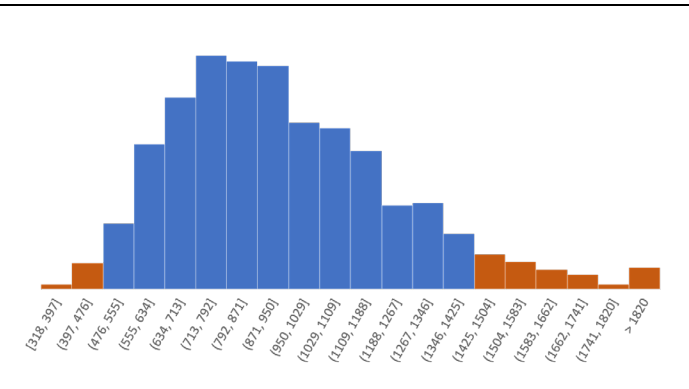

Fig.S.1.4. Fitted future price distribution of the products azelaic acid, crude glycerol, pelargonic acid and C16/0, based on historical price.

C18:0	C20:0
5% to 95% probability range: [630, 17313] US$/ton	**5% to 95% probability range:** [568, 2117] US$/ton
Distribution type: Log-Normal	**Distribution type:** Log-Normal
mean:6.946, **σ:**0.304	**mean:**7, **σ:**0.4
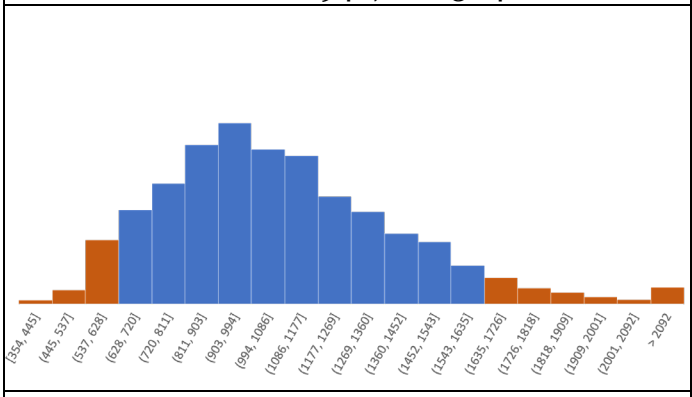	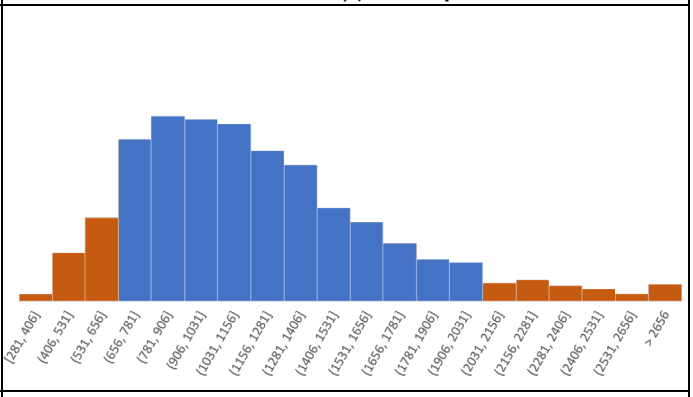
C3,DC3	**C6**
5% to 95% probability range: [571, 1229] US$/ton	**5% to 95% probability range:** [1471, 2129] US$/ton
Distribution type: GAUSSIAN	**Distribution type:** Log-Normal
mean:900, **σ:**200	**mean:**1800, **σ:**200
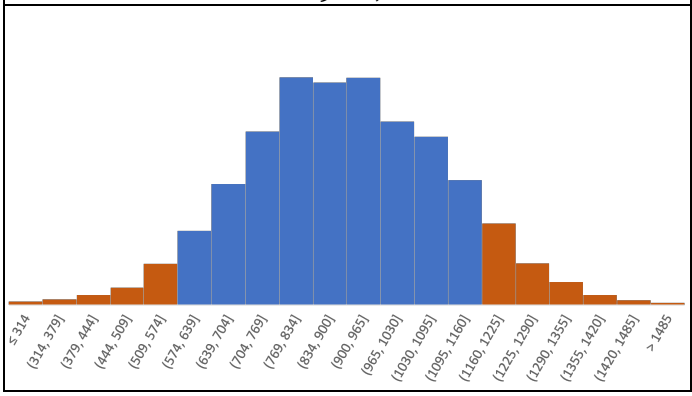	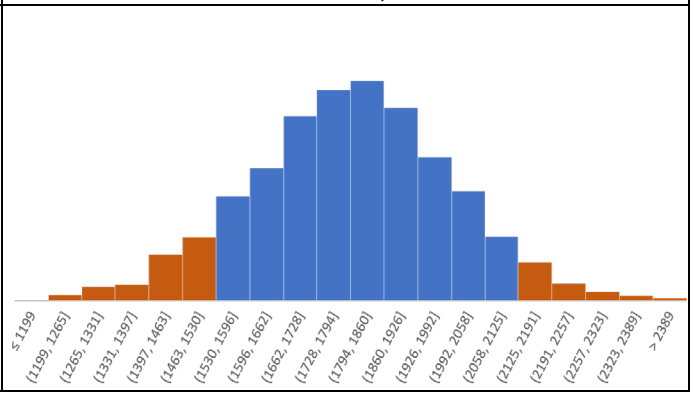

Fig.S1.5. Fitted future price distribution of products: C18:0, C20:0, C3, D3, C6, based on historical price.

C7	C8
5% to 95% probability range: [2419, 3960] US$/ton	**5% to 95% probability range:** [1355, 4644] US$/ton
Distribution type: GAMMA	**Distribution type:** Log-Normal
mean:45, **σ:**70	**mean:**3000, **σ:**1000
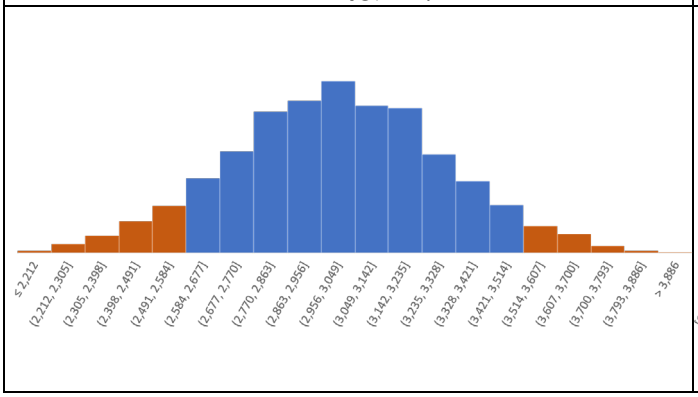	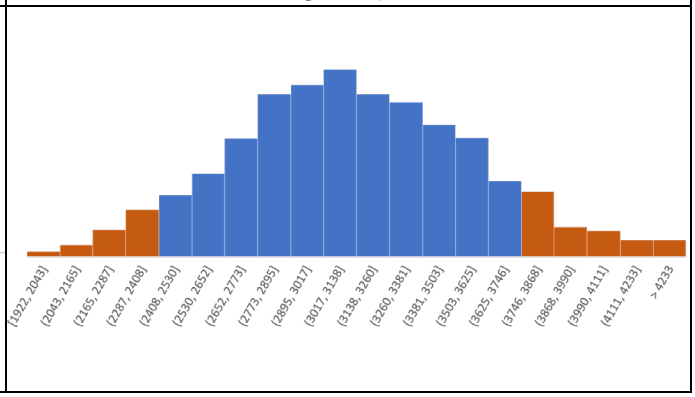

Fig.6. Fitted future price distribution of products: C7and C8, based on historical price.

S.1.3. Summary of the investment costs, yearly costs and yearly sales

Table 1. Information for the generation of tornado plot for the production of azelaic from high oleic sunflower oil and palm oil

	High oleic sunflower oil	palm oil
	investment costs	
total capital costs	81 Million $	106 Million $
	yearly costs	
Total Raw materials costs	26 Million $	30 Million $
labor costs (operators, administration, plant overhead, laboratory, supervisors)	3.2 Million $	3.2 Million $
utilities	2.6 Million $	3 Million $
Distribution and selling	11.4 Million $	12.7 Million $
Research and Development	5.7 Million $	6.4 Million $
Royalties	3.4 Million $	3.8 Million $
Maintenance and repairs	1.2 Million $	1.6 Million $
Operating Supplies	0.6 Million $	0.8 Million $

Property taxes	1.2 Million $	1.6 Million $
Insurance	1.2 Million $	1.6 Million $
Financing interest	1.2 Million $	1.6 Million $
	yearly sales	
products	114 Million $	127 Million $

S.2 Ultrasound-assisted oxidative cleavage of unsaturated fatty compounds

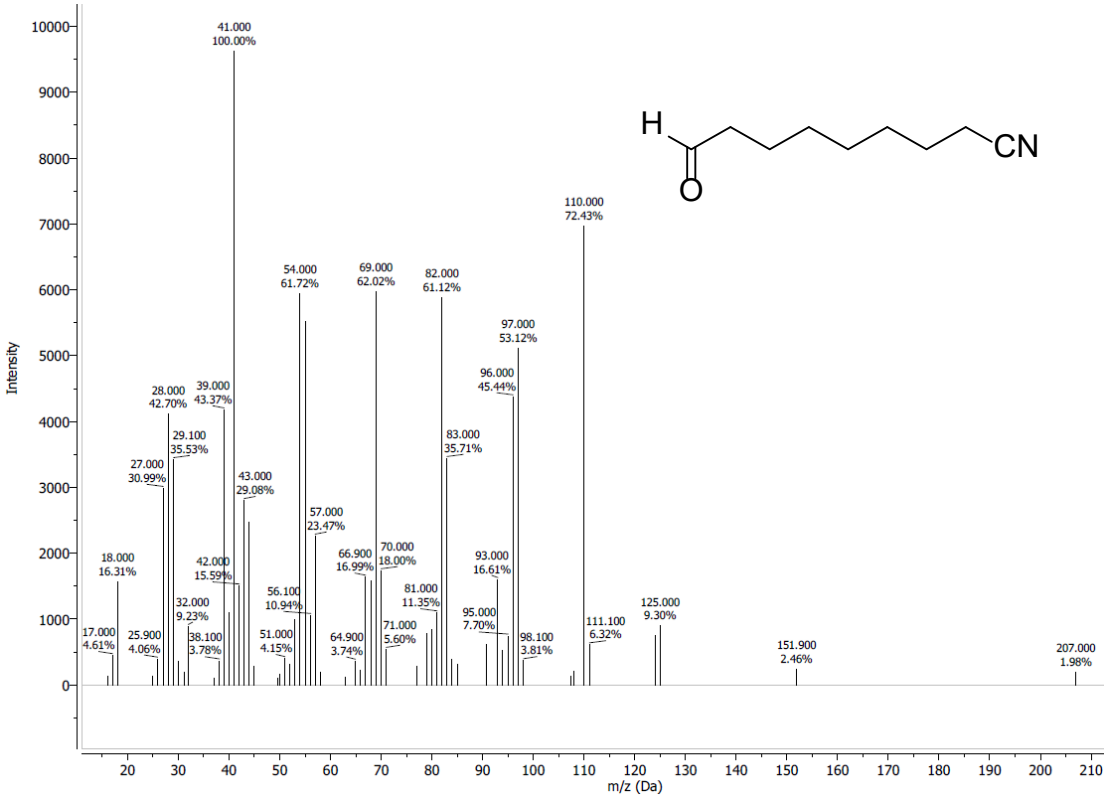

Figure 2-1. Mass spectrum of 10-oxodecanenitrile.

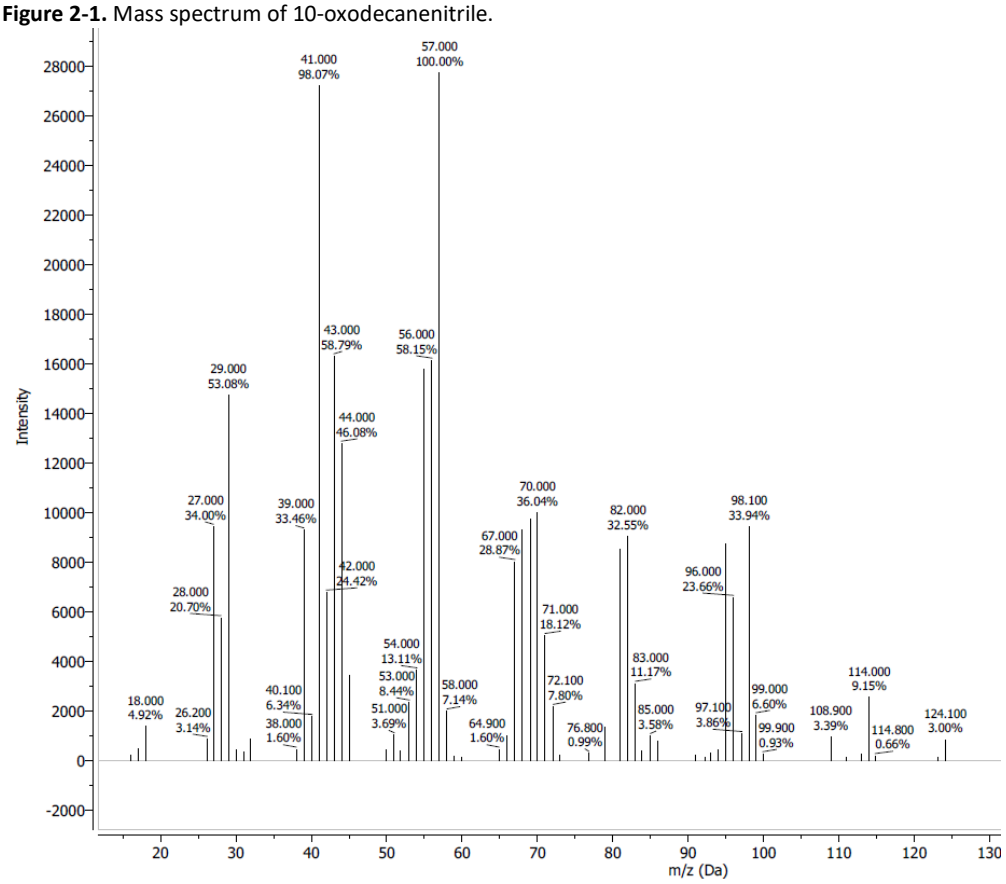

Figure 2-2. Mass spectrum of nonanal.

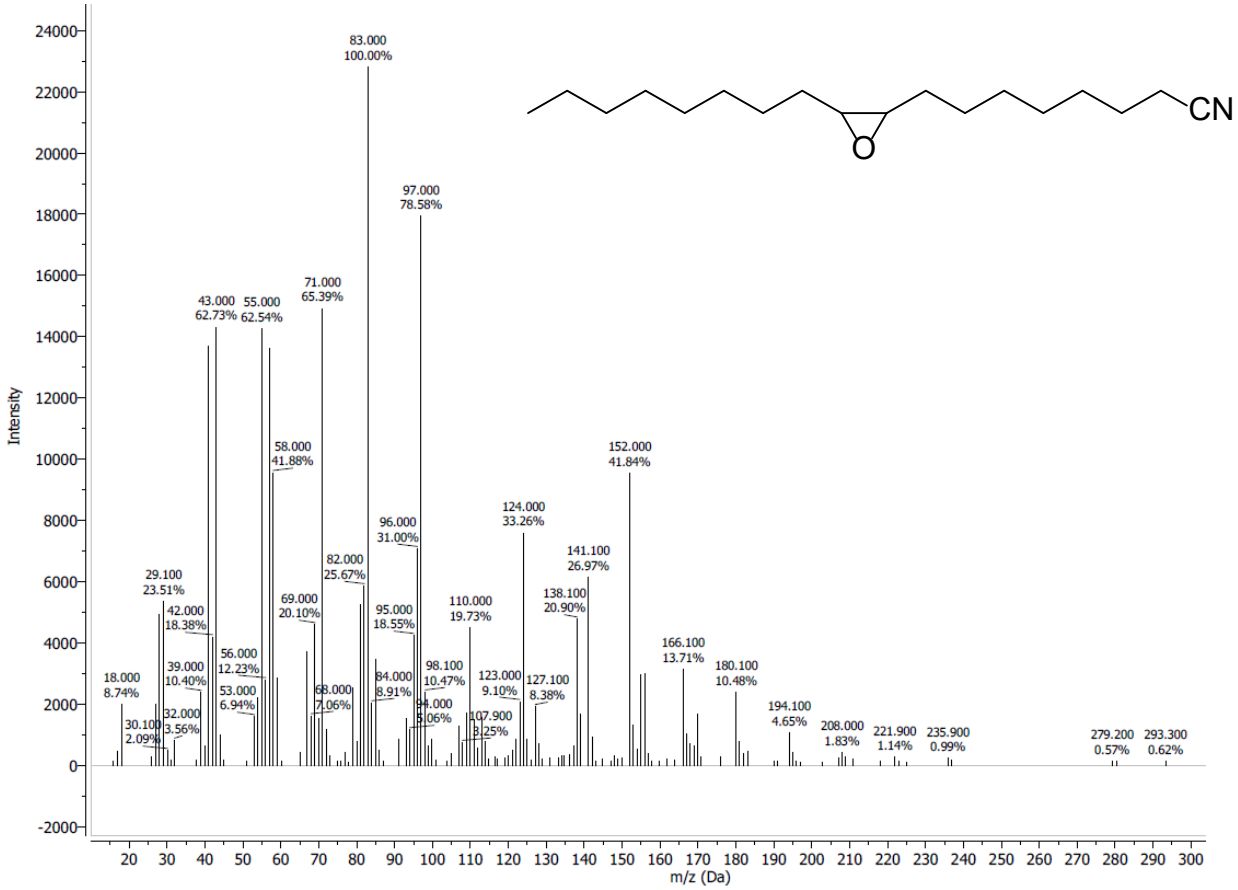

Figure 2-3. Mass spectrum of 8-(3-octyloxiran-2-yl)octanenitrile.

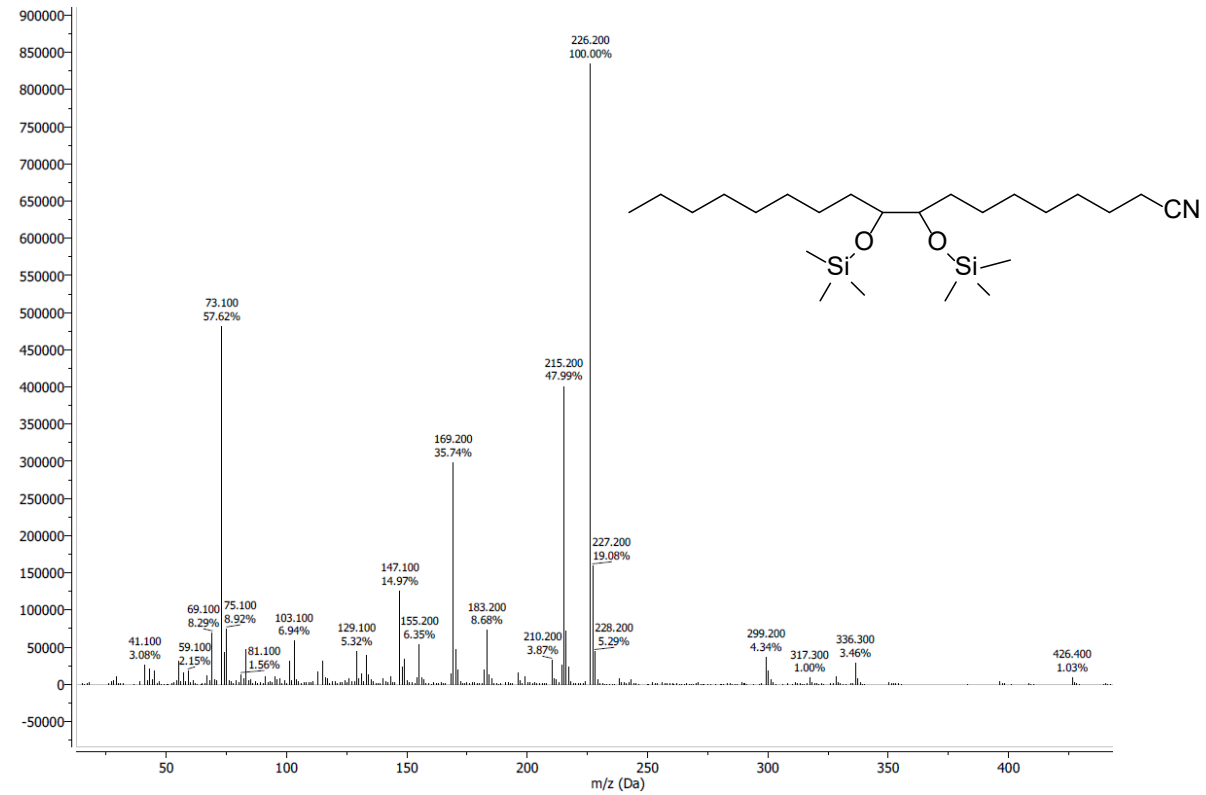

Figure 2-4. Mass spectrum of 9,10-dihydroxyoctadecanenitrile.

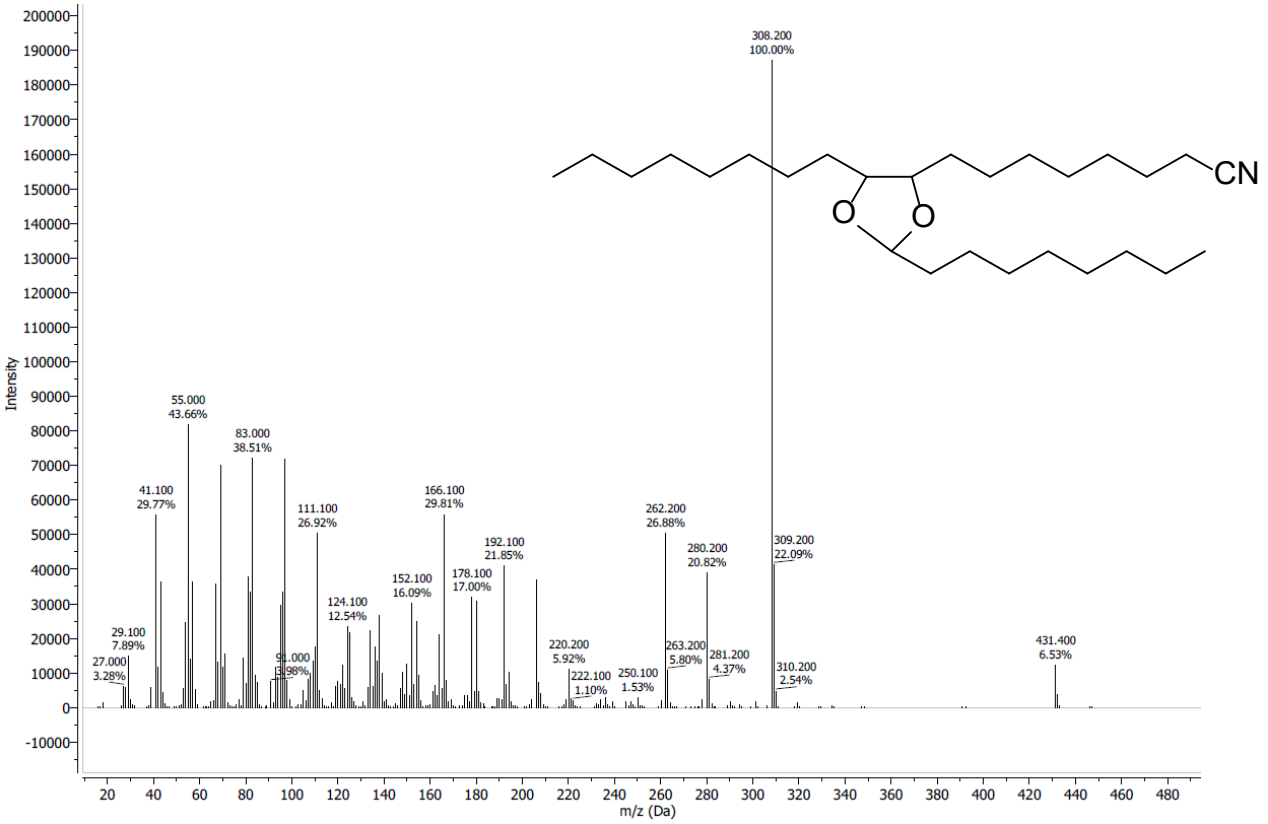

Figure 2-5. 8-(2,5-dioctyl-1,3-dioxolan-4-yl)dioctanenitrile mass spectrum.

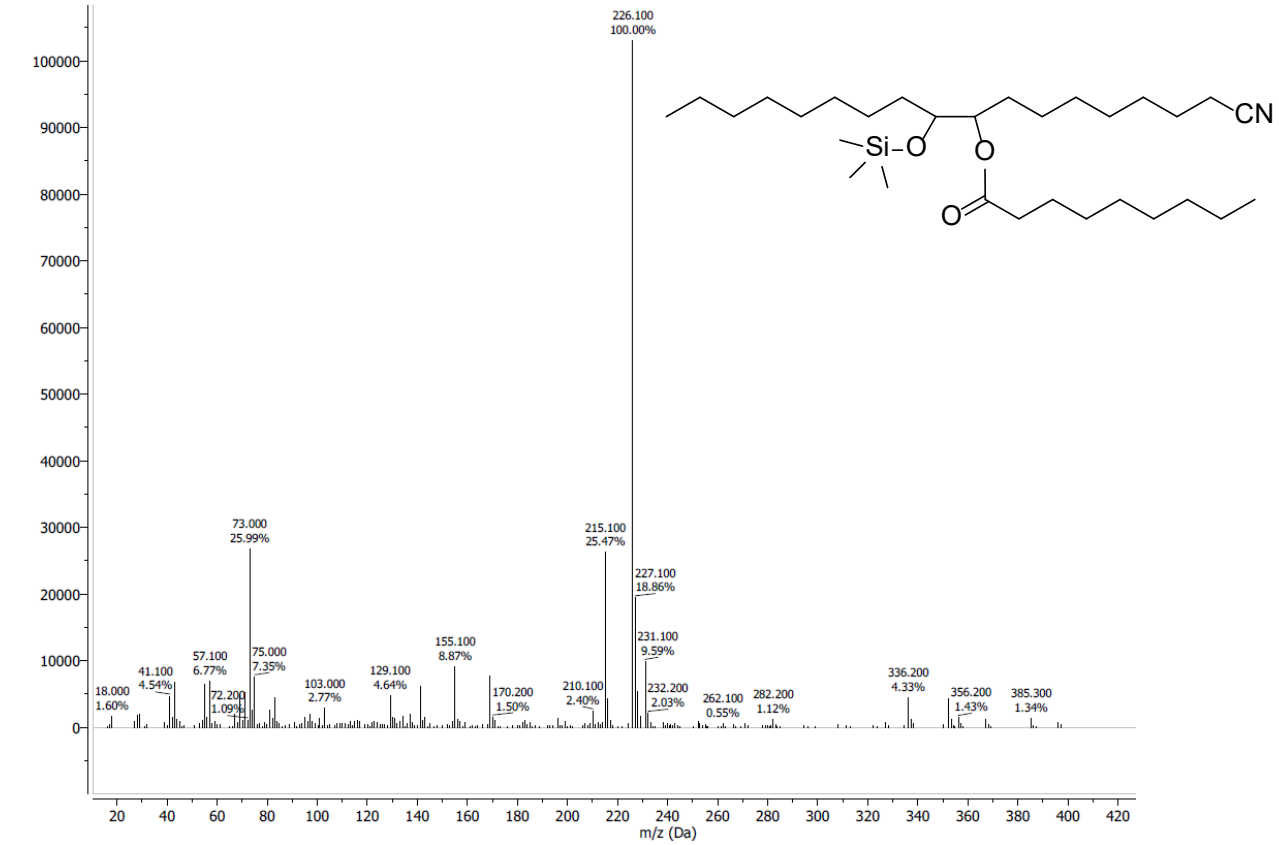

Figure 2-6. 1- Mass spectrum of cyano-8-hydroxyheptadecn-9-yl nonanoate.

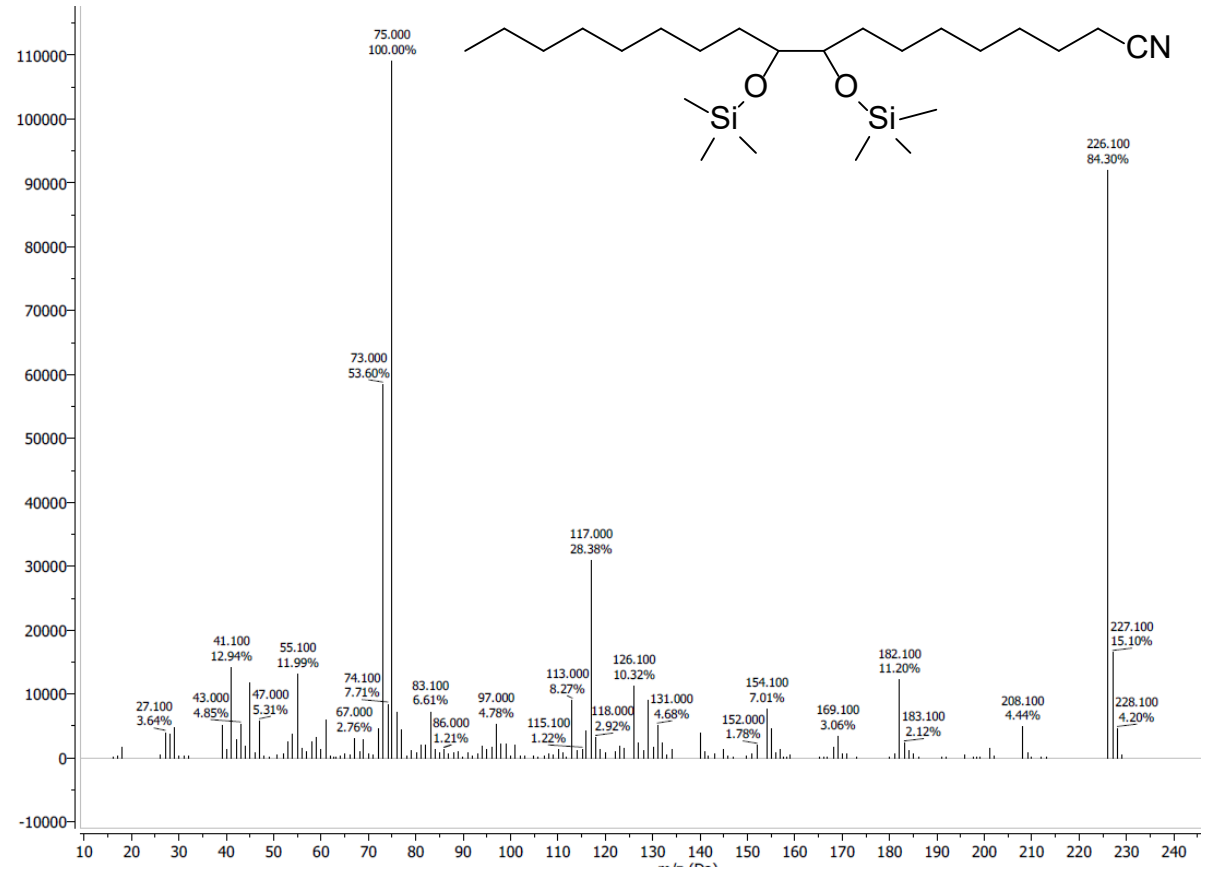

Figure 2-7. Mass spectrum of 9.10-dihydroxyoctadecanenitrile sililated.

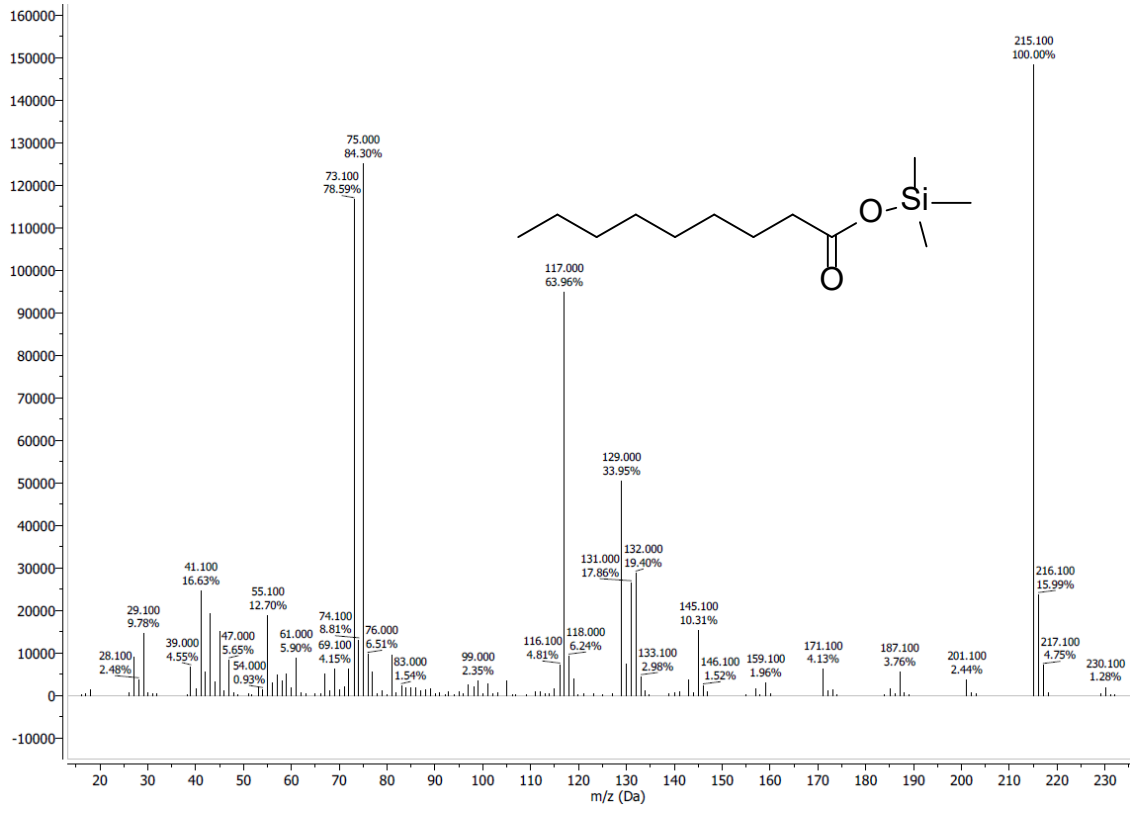

Figure 2-8. Mass spectrum of nonanoic acid.

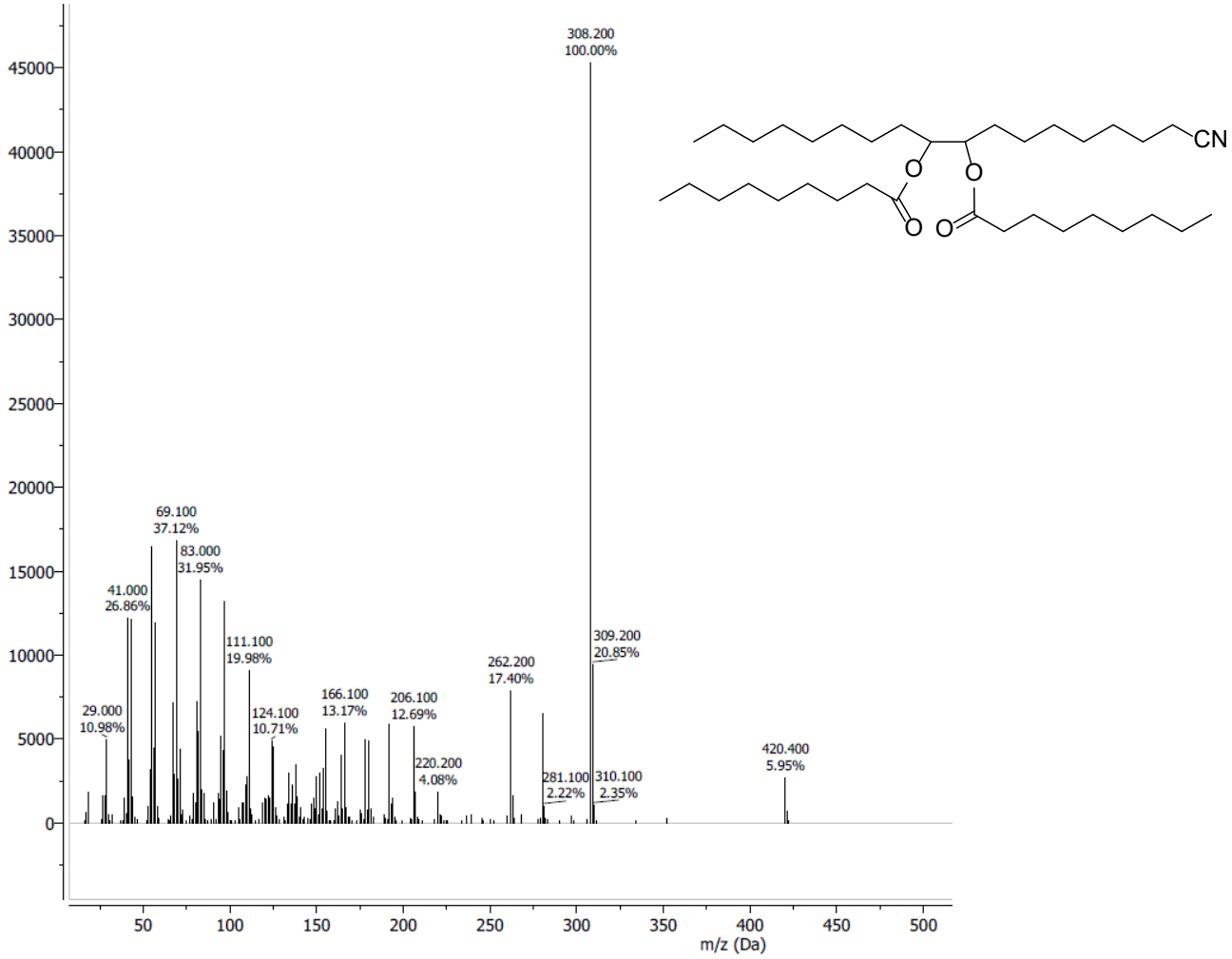

Figure 2-9. 1-cyanoheptadecane-8.9-diyl dinonanoate

S.3 Raney-Nickel catalyst recycling for the obtention of high-value amino-esters

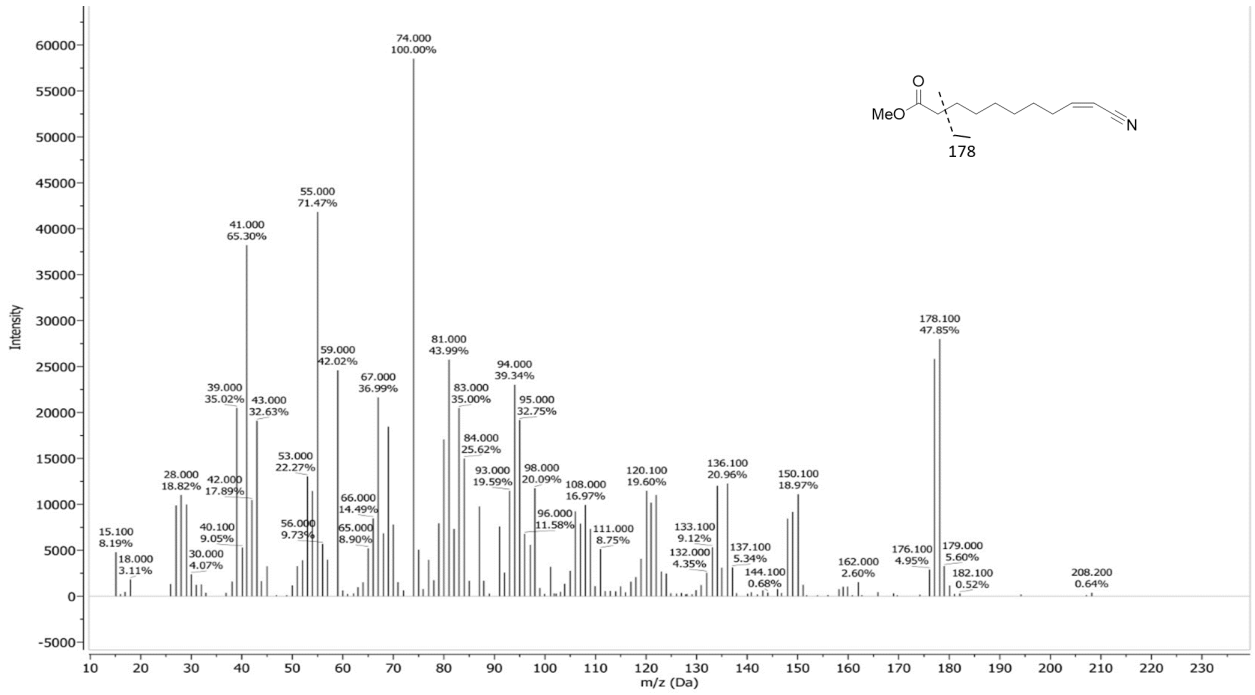

Figure 3-1. Mass Spectrum of Methyl (Z)-10-cyano-9-decenoate.

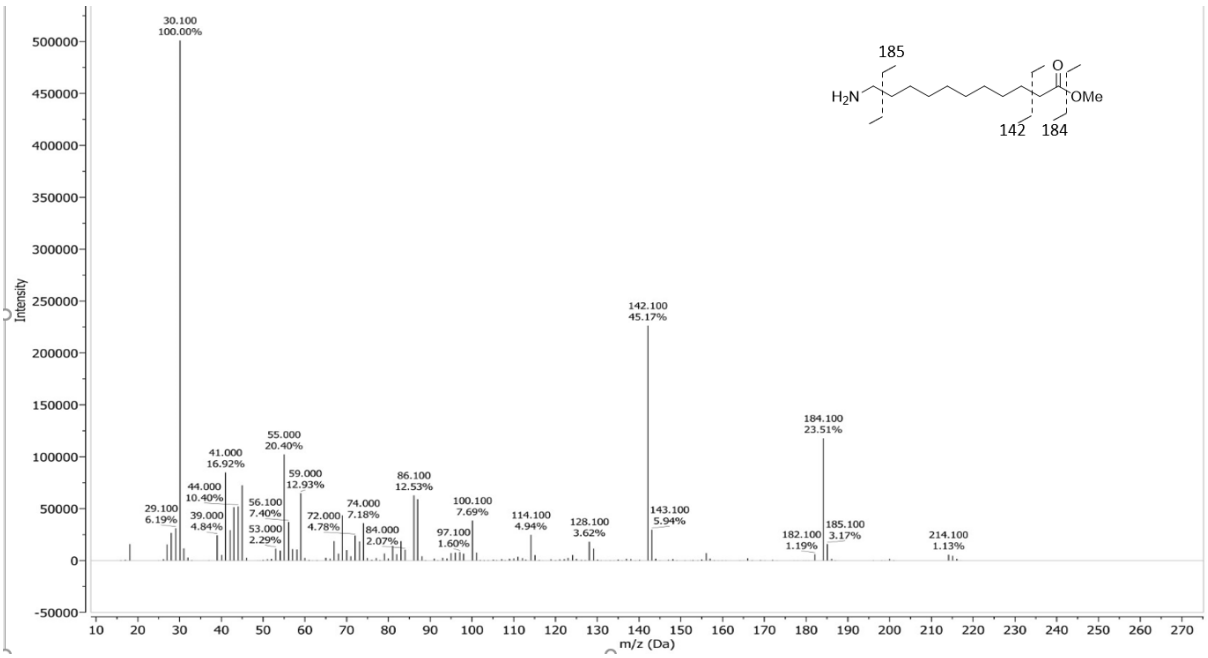

Figure 3-2. Mass Spectrum of methyl-11-aminoundecanoate.

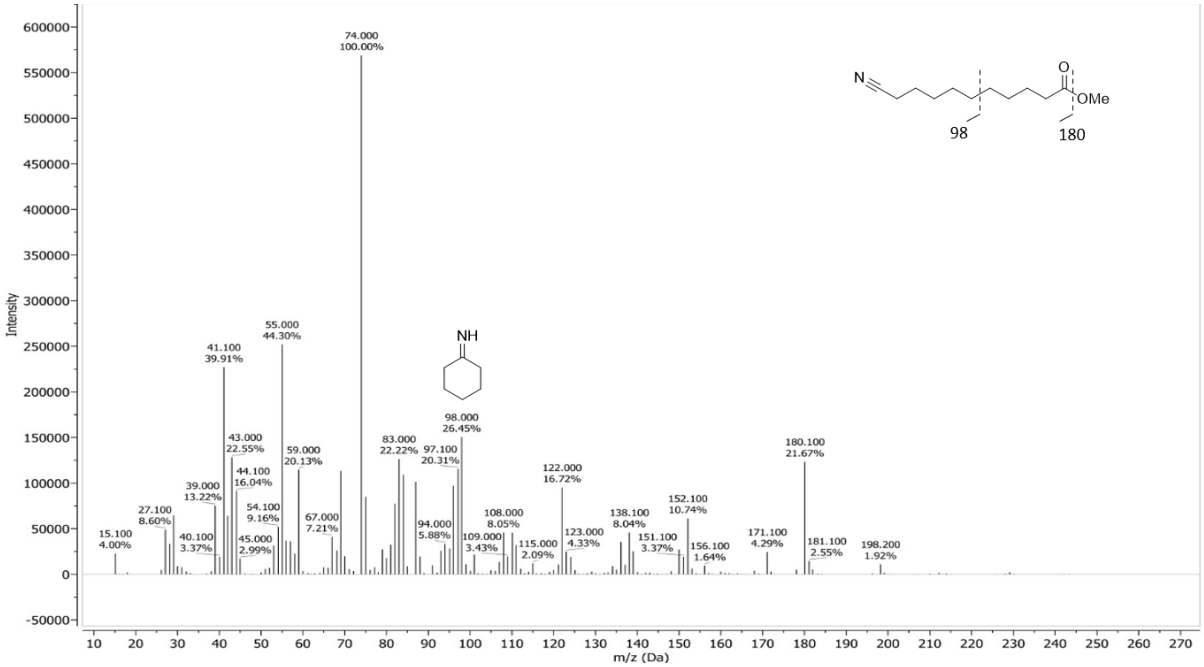

Figure 3-3. Methyl-10-cyanodecanoate.

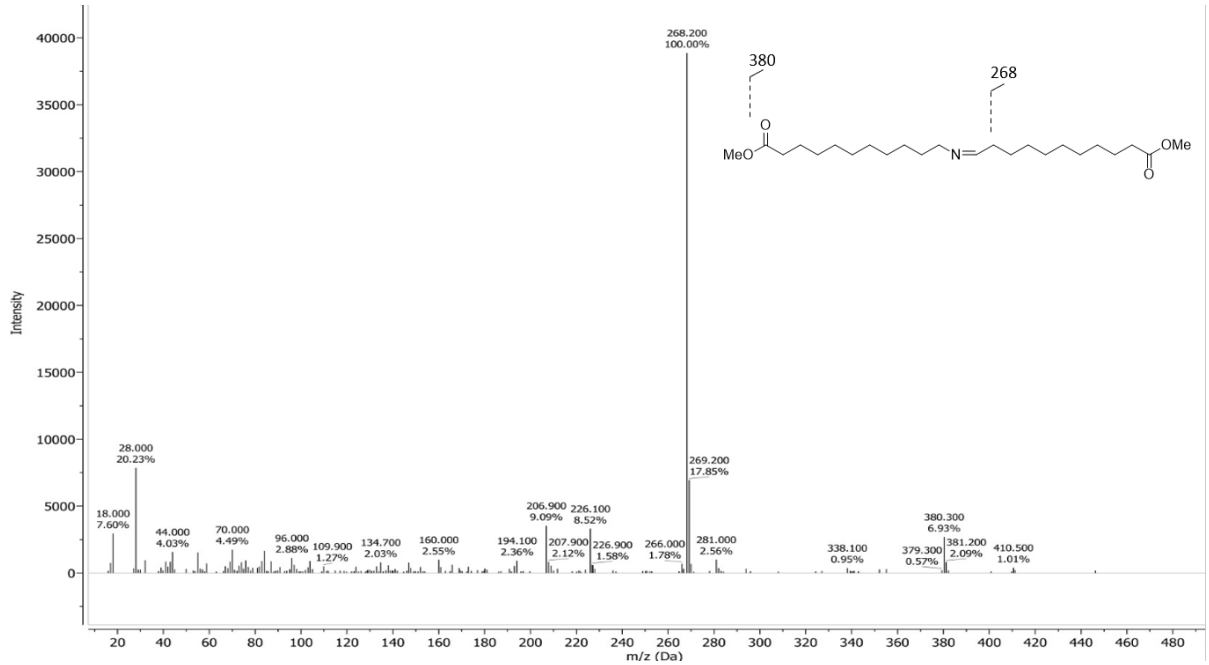

Figure 3-4. Mass spectrum of Secondary imine (I_2).

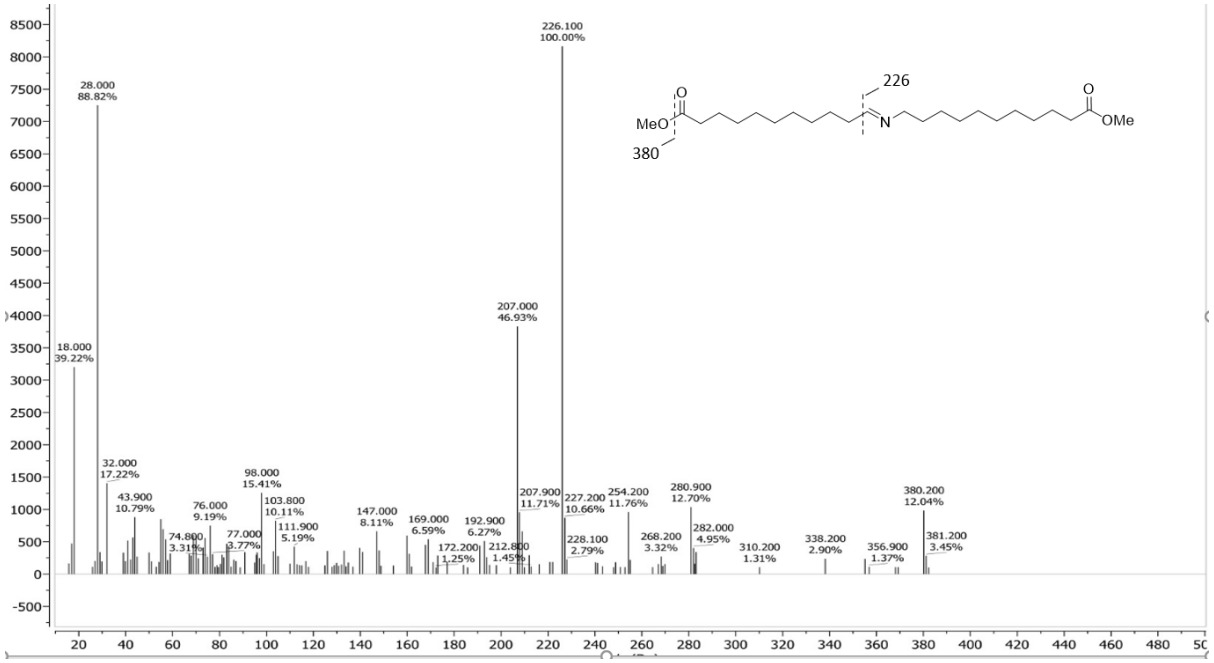

Figure 3-5. Mass spectrum of trans-Secondary imine (I_2).

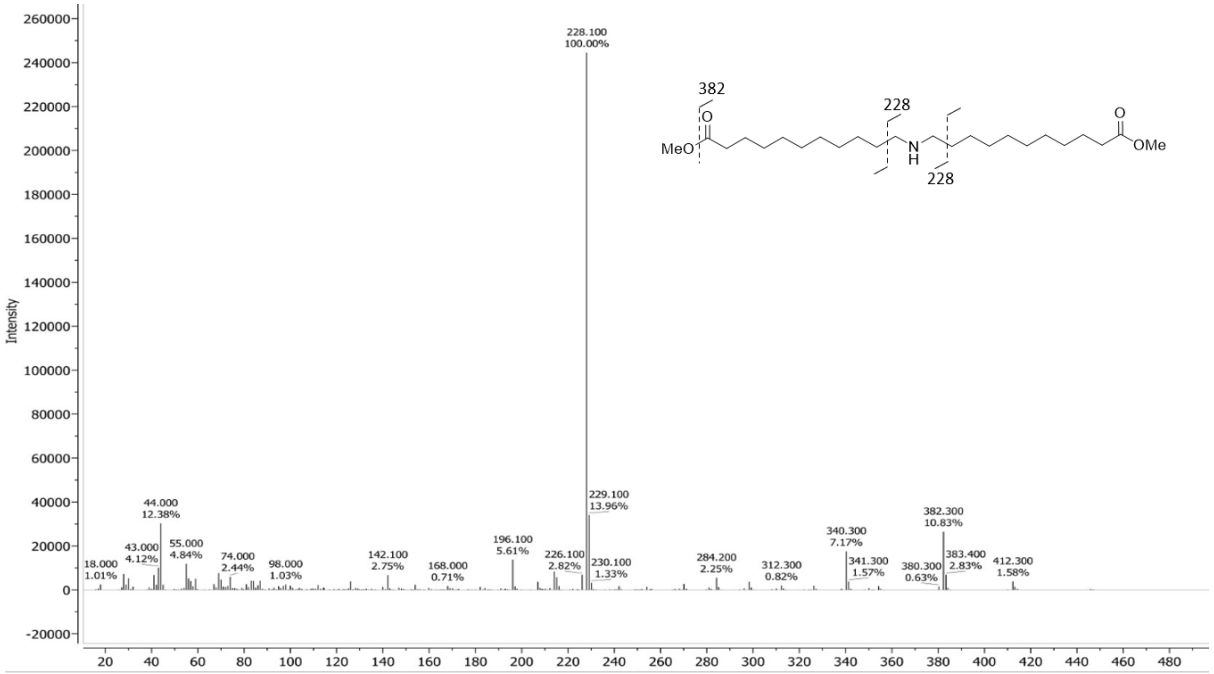

Figure 3-6. Mass spectrum of Secondary amine (A_2).

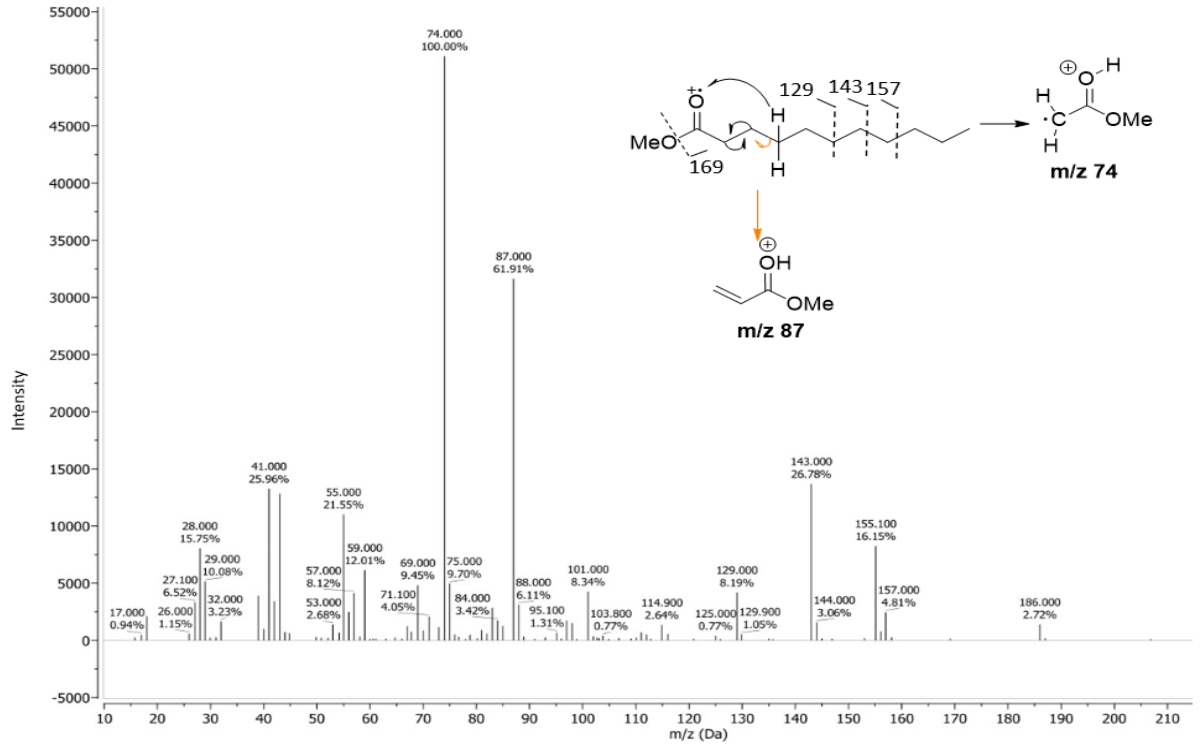

Figure 2-6. Mass spectrum of methyl-undecanoate at 6 minutes retention time.

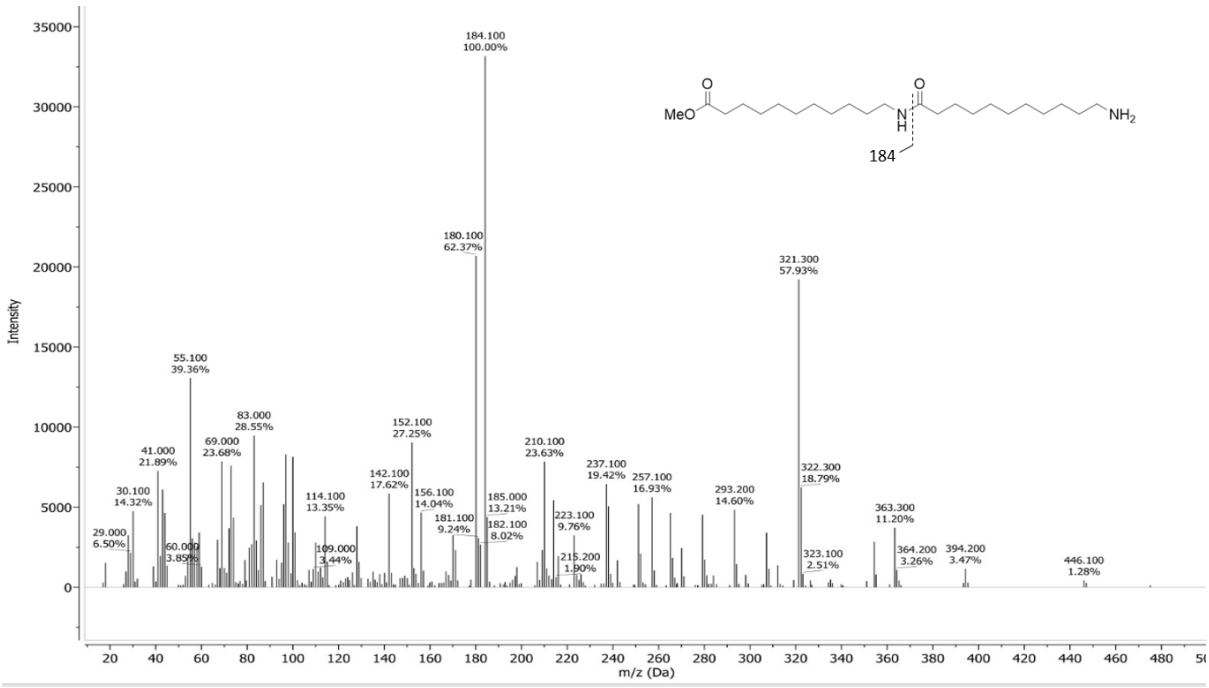

Figure 2-7. Mass spectrum of amino ester dimer at 25.95 minutes retention time.